Understanding Atypical Kinases as Essential Factors for the Biosynthesis and Cellular Distribution of Coenzyme Q

By

Zachary A. Kemmerer

A dissertation submitted in partial fulfillment

of the requirements for the degree of

Doctor of Philosophy

(Biochemistry)

at the

UNIVERSITY OF WISCONSIN–MADISON

2020

Date of final oral examination: 12/17/2020

This dissertation is approved by the following members of the Final Oral Committee:
David J. Pagliarini, Professor, Washington University, Cell Biology & Physiology
Brian G. Fox, Chair, Biochemistry
John M. Denu, Professor, Biomolecular Chemistry
Katherine A. Henzler-Wildman, Professor, Biochemistry
Edwin R. Chapman, Professor, Neuroscience

Understanding Atypical Kinases as Essential Factors for the Biosynthesis and Cellular Distribution of Coenzyme Q

Zachary A. Kemmerer

Under the supervision of Professor David J. Pagliarini

At the University of Wisconsin-Madison

Abstract

UbiB family proteins are widespread and highly conserved across all three domains of life. A subset of UbiB proteins (Coq8 in yeast, COQ8A/COQ8B in human) are essential for coenzyme Q (CoQ) biosynthesis, but a mechanistic understanding is lacking. All five human homologs been connected to human disease, yet most of these proteins are completely uncharacterized. Here, I present work addressing (1) COQ8's biochemical function by characterizing robust ATPase activity that is regulated by endogenous and synthetic small-molecule modulators and (2) characterizing UbiB yeast homologs Ypl109c (Cqd1) and Ylr253w (Cqd2) as reciprocal regulators of cellular CoQ distribution.

Chapter 1 summarizes the biosynthesis of CoQ and its various roles in cell biology. I introduce the UbiB family of protein-kinase like genes, highlighting important unanswered questions and the significance of studying these proteins. Chapter 2 describes our identification of small-molecule regulators that enhance COQ8 ATPase activity. We find two alkylphenols (CoQ mimics) and cardiolipin (CL) stimulate robust ATPase activity in the presence of COQ8's N-terminal transmembrane domain. Further, I generate an analog-sensitive COQ8 (Coq8-*AS*) tool to investigate the effects of acute inhibition on respiratory growth and CoQ abundance *in vivo*. Chapter 3 summarizes literature describing CoQ mobilization and uptake, highlighting the many gaps in our current understanding. In Chapter 4, I design a genome-wide screen to identify

mitochondrial machinery involved in CoQ distribution. Using a combination of yeast genetics, biochemical fractionation, and lipid profiling, I identify two highly conserved but poorly characterized mitochondrial proteins, Ypl109c (Cqd1) and Ylr253w (Cqd2), that reciprocally regulate this process. Loss of Cqd1 skews cellular CoQ distribution away from mitochondria, resulting in markedly enhanced resistance to oxidative stress caused by exogenous polyunsaturated fatty acids (PUFAs), whereas loss of Cqd2 promotes the opposite effects. The activities of both proteins rely on their atypical kinase/ATPase domains, which they share with Coq8. Chapter 5 summarizes my findings and provides future directions for the continued investigation of UbiB proteins. Together, this work suggests that UbiB family proteins may function more broadly in the management of CoQ biology. This work provides a host of new tools for the continued exploration of UbiB molecular function.

Acknowledgments

The greatest part of coming to graduate school is knowing that my life will be forever changed. I came here on the recommendation of a former alum and mentor, but against the grain of my former situation. Madison has given me so much—a new home, outstanding colleagues, dependable friends, scientific expertise, and even a fiancé. I am forever grateful to have walked these halls with giants, and I must recognize the people that contributed to my journey.

I thank Professor Dave Pagliarini for his unwavering guidance and mentorship throughout my graduate career. When Dave welcomed me into the lab, he took a chance on me—someone having limited experience in the field of science and have no pedigree for higher education. I thank Dave for seeing potential that I did not always see in myself and having steadfast confidence in my abilities. Dave did an excellent job of creating a work environment that emphasized collaboration, respect, and intellectual rigor. Dave is a thoughtful leader and a tremendous role model who has inspired me in many ways. I am thankful for this opportunity to learn from one of the best.

I would like to thank my lab mates, old and new, for being my toughest critics and the biggest scientific supporters. Your generosity in lending your time and thoughts helped me to grow as a scientist and improve as a communicator. Success is never achieved alone, and these conversations certainly influenced the direction I went and the perspectives I held. I offer a special thanks to the original members of the Q branch: Jon Stefely, Andrew Reidenbach, and Danielle Lohman. Great leaders recruit great talent, and after rotating in Q branch, I knew who I wanted to be in the trenches with during my PhD. I admire you all dearly, and I thank you for the wealth of scientific, professional, and emotional support you've given me. More recently, I had the privilege of collaborating with pun master Kyle Robinson, fighting the uphill battle in the year of COVID.

Mateusz Manicki, Natalie Niemi, and Mike Veling were also essential pillars in navigating the challenges of my PhD.

Thank you to our wonderful collaborators that helped elevate our studies on the UbiB proteins: Joshua Coon and the many talented mass spectrometry experts from his lab, especially Brett Paulson and Paul Hutchins; Craig Bingman and Bob Smith; Deniz Aydin and Matteo Dal Perraro; Jamie Stark and John Markley. Thank you to those collaborators that shared critical reagents and insight that enabled work describe in Chapter 4: Jared Rutter and Jodi Nunnari for yeast cell lines; Nora Vogtle and Oleh Khalimonchuk for yeast antibodies; Adam Frost for the GFP nanobody construct; and Steven Claypool for consultation on SMALP generation. Collaboration is one of the sweetest fruits of science, and I am thankful to have been part of these interdisciplinary projects. I am grateful for your contributions and I am fortunate to have been exposed to so many different areas of science. I also thank my thesis committee for constantly challenging my interpretation and understanding of these data. You have offered great insight for improving my work, all of which has culminated in this defense. I thank my committee for their commitment to making my science and my graduate experience so memorable.

I thank my friends for providing the entertainment that kept me grounded during my graduate career. Samantha Anderson in particular has been a very important influence during this time. November Project gave me an active community to hang out with, even during the colder months in Wisconsin. And most importantly, Fred Bartman has been my best friend in Madison. When COVID cancelled our ninja workouts, we transitioned to virtual WODs, but we have continued to “embrace the grind” together. Fred and his family have been important structures for my physical and mental well-being. My friends beyond Madison have also provided continued

support, Jake Hunter and Bryan Ortenzio in particular. I also thank my mother for sending me Wawa coffee multiple times a year, which helped keep me focused when long hours were needed.

Finally, I thank my loving, exceptional fiancé Mimi Nora (and her amazing family). My partner in crime since 2016, Mimi is my rock in every way. She has been an unconditional supporter of my scientific journey. She motivates me during the difficult times and celebrates the moments of success. She inspires me to be the best version of myself, and I can't imagine going through graduate school, or anything else without her. As an accomplished emergency veterinarian, an Ironman finisher, and the most adventurous person I know, she is an inspiration for how to lead my own life. In the past five years, we've gone through a prelim exam, American Ninja Warrior, 18 months of distance, one dog adoption, 200 miles of backcountry hiking in Colorado, a proposal and wedding planning together. And on December 17th, we will hopefully add thesis defense to that list!

Table of Contents

Chapter 1: Introduction

Author Contributions: Zachary A. Kemmerer wrote this chapter.

Overview of Coenzyme Q

Discovery of Coenzyme Q and its Biological Roles

Fueled by key advancements in cellular bioenergetics, the discovery of coenzyme Q (CoQ, ubiquinone) was part of a concerted effort to identify and understand the mechanism of biological energy conservation. Biochemists in the 1950s sought to understand how the oxidation of metabolic substrates was connected to the production of adenosine triphosphate (ATP). Technical advancements allowed proteinaceous components of the mitochondrial oxidative phosphorylation (OxPhos) pathway to be isolated. However, in isolation, these proteinaceous components were insufficient to fully reconstitute mitochondrial OxPhos.

In 1957, CoQ was discovered in the laboratory of David Green by Frederick Crane and others at the Enzyme Institute at the University of Wisconsin–Madison[1]. Understanding that lipids may play a critical role in OxPhos, Crane extracted lipids from beef heart mitochondria to isolate a distinctly yellow compound. Interestingly, CoQ had been independently isolated two years prior, but its quinone structure was unknown and its biological role remained a mystery[2]. Benzoquinones were believed to be rare in animals, but Crane explored whether this yellow lipid had quinone-like properties. Successful manipulation of the lipid, then referred to as Q275, supported this hypothesis. Subsequent studies at Merck helped elucidate CoQ's chemical structure[3], revealing two major features—a decorated quinone head group and a long polyisoprenoid lipid tail (Figure 1A). In the following years, CoQ was isolated from a diverse collection of organisms, including

prokaryotes like *E. coli*, plants and animals[4], and cellular CoQ distribution was found to be widespread[5], raising important questions about CoQ biosynthesis, cellular distribution, and functions outside of mitochondria.

As a redox-active lipid, the canonical role of CoQ is to facilitate electron and proton transfer (Figure 1B) between OxPhos complexes in the electron transport chain (ETC, Figure 1C). The polyisoprene tail length of CoQ varies by organism; human, *S. cerevisiae*, and *E. coli* CoQ contains ten (CoQ_{10}), six (CoQ_6), and eight (CoQ_8) isoprene units, respectively[4]. It is this extremely hydrophobic tail moiety (Figure 1A) that anchors CoQ within the membrane bilayer. The redox-active quinone head group enables the reduction-oxidation chemistry required for OxPhos (Figure 1B). Briefly, complexes I (NADH-CoQ oxidoreductase) and II (succinate-CoQ oxidoreductase) accept electrons from NADH or $FADH_2$, respectively. Within the IMM, CoQ relays electrons from complex I and II to complex III (CoQ-cytochrome c oxidoreductase). Importantly, electron transfer is coupled with complex-dependent (I, III, and IV) proton pumping across the IMM and into the mitochondrial inner membrane space (IMS). This proton gradient is harnessed by ATP synthase (complex V) to synthesize ATP within the mitochondrial matrix[5].

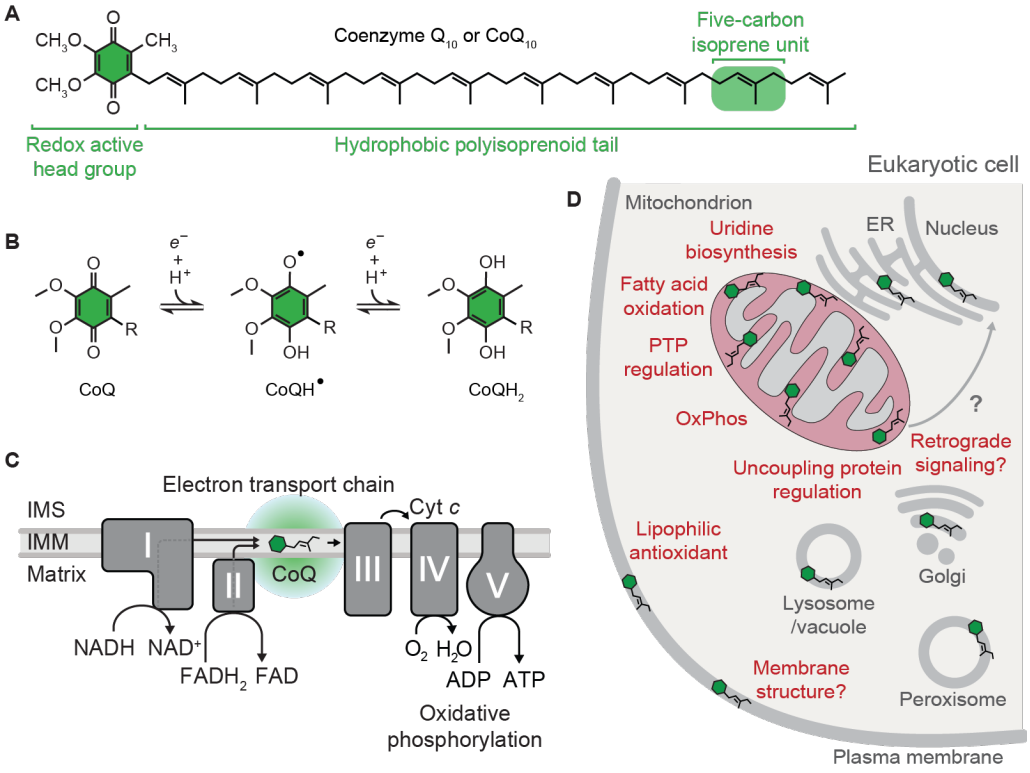

Figure 1. CoQ Structure and Function in Oxidative Phosphorylation and Other Pathways. Figure adapted from Stefely and Pagliarini, 2017[6]. **A,** Structure of coenzyme Q_{10} (CoQ_{10}). **B,** Single electron transfer reactions of the CoQ quinone head group. Oxidized quinone (CoQ), semiquinone ($CoQH^{\bullet}$), and reduced quinol ($CoQH_2$). **C,** CoQ is a requisite component of the electron transport chain, shuttling electrons from complexes I and II to complex III to enable ATP production. **D,** CoQ is localized across the cell and participates in a variety of cellular pathways; PTP, permeability transition pore.

Beyond this fundamental role, which is performed across all domains of life[4], a broader set of cellular functions are being increasingly recognized for CoQ (Figure 1D). Within mitochondria, CoQ accepts electrons from glycerol 3-phosphate dehydrogenase (GPDH)[7], electron-transferring-flavoprotein dehydrogenase (ETFDH) dehydrogenase[8], and dihydroorotate dehydrogenase

(DHODH)[9,10], supporting CoQ's role in glycerol metabolism, fatty acid oxidation, and uridine biosynthesis, respectively. CoQ is also believed to function as a lipophilic antioxidant[11-14] and influence membrane fluidity[15] around the cell, although the findings from Sevin et al. have been challenged recently[16] and conflicting reports exist regarding its *in vivo* antioxidant properties[17]. Recently though, plasma membrane FSP1 (*H.s.*) showed CoQ-dependent activity in mitigating toxic lipid peroxide species[18,19], a key step in preventing a type of regulated cell death called ferroptosis[20]. Additional roles for CoQ have been demonstrated (Figure 1D) but our understanding of CoQ function, especially in extra-mitochondrial biology, is still incomplete.

Biosynthesis of CoQ

Across all domains of life, CoQ is synthesize endogenously at the membrane surface (matrix side of the IMM in eukaryotes; at the cell membrane in prokaryotes, due to their lacking mitochondria). Synthesis likely occurs in proximity to the respiration machinery where it can fulfill its role in OxPhos. CoQ biosynthesis can generally be separated into four phases: 1) head group production 2) polyisoprene tail production, 3) attachment of the head group to the polyisoprene tail, and 4) headgroup modification to produce mature CoQ (Figures 2). This scheme is consistent amongst eukaryotic and prokaryotic CoQ production. Exogenously supplied CoQ is poorly absorbed by cells and tissues, likely due to its extreme hydrophobicity, poor solubility, and large size[21], supporting endogenous synthesis as the predominant source.

In eukaryotes, CoQ biosynthesis requires at least 11 proteins, including Coq1-9, Yah1, and Arh1[22] (Figure 2). [Note: Coq(#), yeast protein; COQ(#), human protein; collectively COQ(#) moving forward]. More recently, Coq10 and Coq11 have been connected to CoQ biosynthesis. Coq10 contains a lipid binding domain and is hypothesized to bind mature CoQ, potentially

escorting it to OxPhos complexes[23], while the function of Coq11 remains unknown[23-25]. In bacteria, UbiA-K and UbiX[26] are required under aerobic conditions. More recently, it was discovered that *E.coli* and other bacterial pathogens continue producing CoQ even under anaerobic conditions. This anaerobic pathway requires UbiU and UbiV (heterodimeric hydroxylase), as well as UbiT (possible lipid binding protein)[27,28], but the physiological relevance of this pathway is still unclear. Although CoQ biosynthesis is generally conserved between eukaryotes and prokaryotes, important differences exist—in the derivation of precursors molecules, early steps in head group modification, and supramolecular organization of the biosynthetic enzymes. These differences will be the focus of the following sections.

CoQ Precursors

The two basic building blocks of CoQ biosynthesis—isoprenes and 4-hydroxybenzoate (4-HB)—have different origins in eukaryotic (Figure 2) and prokaryotic systems. Eukaryotes derive isoprene from the mevalonate pathway, the same pathway responsible for cholesterol synthesis[29,30]. Within the matrix, two isoprene diphosphate molecules (isopentyl and dimethylallyl pyrophosphate; IPP and DMAPP) are stitched together by the polyprenyl synthase enzyme COQ1 (PDSS1/PDSS2 in humans)[31]. Interestingly, the CoQ tail length is also dictated by this step for different organisms[32], but the biological rationale for these differences is still unclear. In *E. coli*, isoprenes are derived from the methylerythritol pathway (MEP) and are connected by COQ1 homolog, IspB[33]. Aromatic amino acid tyrosine (or phenylalanine via phenylalanine hydroxylase[34,35]) is converted to 4-HB by a series of steps in eukaryotes[36], most of which have yet to be elucidated[37,38]. Bacteria leverage the more direct shikimate pathway to produce chorismate, which is converted to 4-HB via chorismate pyruvate lyase (UbiC)[39-41]. Yeast are unique in their

ability produce head group precursor via both the shikimate and tyrosine pathways[36], having a preference for the former. Yeast can also use *para*-amino benzoic acid (*p*ABA) as an alternative head group precursor[42,43], but this *p*ABA pathway does not exist elsewhere[42,44,45]. Condensation of these two precursors is performed by homologous prenyltransferases COQ2 (in eukaryotes) or UbiA (in prokaryotes)[46], producing a polyprenyl hydroxybenzoate (PPHB) molecule ready for head group modification.

Complex Q and a UbiB Complex

In eukaryotes, CoQ biosynthesis is achieved by an organized collection of subunits called complex Q [47-49]. Genetic studies demonstrated higher molecular weight species containing various combinations of Coq proteins (Coq3-9) in yeast[48]. Deletion of a single *Coq* gene (*Coq3-9*) led to the accumulation of PPHB, the earliest intermediate of the head group modification phase[50-52]. *Coq* gene deletion also consistently decreased the steady state level of other genes in the pathway[48]. Multi-omic (protein, lipid, and metabolite) mass spectrometry profiling of a 174 single gene knockout yeast strains[38] corroborated these effects. Further, affinity purification mass spectrometry (APMS) using two mammalian cell lines highlighted a highly interconnected network of COQ protein interactions[53]. Most recently, submitochondrial fluorescent co-localization efforts have demonstrated Coq proteins form discrete domains in yeast and human cells[54], supporting the conserved existence of supramolecular assemblies.

Interestingly, evidence for a prokaryotic biosynthetic complex was lacking. Unlike eukaryotes, deletion of individual genes in the *E.coli* CoQ biosynthesis pathway results in predictable accumulation of the nearest upstream intermediate[55], suggesting lower co-dependence amongst the bacterial subunits. However, recent work has identified a 1 MDa Ubi complex

consisting of seven proteins, UbiE-K, that exists in the soluble fraction of *E.coli* extracts[56]. This supramolecular assembly includes 5 enzymes and 2 auxiliary proteins, similar to the eukaryotic complex Q.

For decades, there has been a growing appreciation for the existence and benefit of "metabolons" in multi-step biosynthetic pathways[57,58]. A metabolon is defined as a transient assembly of multiple (often sequential) enzymes that mediate substrate channeling[57,59]. This is especially true of challenging lipid biochemistry, where a CoQ metabolon may help to overcome hydrophobic barriers, enhance biosynthesis flux, protect from toxic intermediates, sequester promiscuous enzymes, or enable better regulation. Both prokaryotic and eukaryotic organism appear to leverage this approach; however, a key difference exists. Eukaryotic complex Q has a tight and constant association with the IMM where the Ubi complex is separated and must transport intermediates to and from the membrane[26]. In both cases, major question remain concerning the access and movement of hydrophobic intermediates. Investigations into the composition, structure, and regulation of these supramolecular structures should improve our understanding of how these multimeric protein complexes overcome this biophysical barrier.

Headgroup Modification in Eukaryotes

A great deal of effort has been dedicated to defining nearly all of the enzymatic steps needed to convert PPHB to mature CoQ (Figure 2). Headgroup modification involves a decarboxylation, and a series of hydroxylations (three) and methylations (two *O*-methyl, one *C*-methyl). Hydroxyl groups are derived from molecular O_2 and methyl groups from *S*-adenosylmethionine (SAM)[60-62]. The reaction order is predicted to follow electrophilic aromatic substitution (EAS) chemical logic and be influenced by enzyme active site structure, but these

hypotheses remain untested[6]. Of note, several enzymatic and transport steps have no assigned enzyme, and multiple proteins essential for CoQ production are still lacking characterization (COQ4/8/9). Significant progress has been made on understanding the auxiliary roles of COQ8 and COQ9[6], but more work is needed to understand their mechanistic functions in CoQ biosynthesis.

In eukaryotes, head group modification begins with COQ6 hydroxylation of the C5 ring position[63]. COQ6 is a flavin-containing monooxygenase that uses both FAD and NAD(P)H. In yeast, mitochondria electron transfer proteins Yah1 and Arh1 may assist this transformation[43,63], but human orthologs have yet to be confirmed. Next, COQ3 *O*-methylates PPDHB[64]. COQ3 is a class 1 methyltransferase that contains a divalent cation in addition to SAM[64-66]. PPVA is then decarboxylated and hydroxylated at C1, but no enzyme has yet been identified for these steps. It is unclear whether this involves two enzyme or just one performing successive reactions. These steps produce DDMQ, which is then *C*-methylated at C2 by COQ5[67], another SAM-dependent methyltransferase. *In vitro* data for yeast Coq5 suggests that the reaction may require NADH as well[68,69]. DMQ is then hydroxylated by diiron hydroxylase COQ7 at the C6 position[70-74]. And lastly, this C6 hydroxyl group is *O*-methylated by COQ3 (its second reaction) to produce mature CoQ[64].

In addition to enzymatic components of the CoQ biosynthesis pathway, there are also auxiliary proteins essential for the pathway with unknown functions (COQ4/8/9). COQ4 is believed to serve a scaffolding or regulatory role because it co-purifies with complex Q, but does not share homology with a known enzyme[47,75-77]. COQ4 contains a putative metal binding site and it is plausible that COQ4 has a yet to be defined enzymatic role[75]. COQ9 is a lipid binding protein that physically interacts with COQ7 to enable its hydroxylation activity[52,78,79]. Importantly, COQ9

appears to assist with CoQ intermediate presentation, especially for the COQ7 reaction. COQ8 (Coq8, COQ8A/ADCK3) belongs to the UbiB family of protein kinase-like genes and is considered an atypical kinase. Recent *in vitro* work from our lab has helped us to define characteristic structural motifs[80] and demonstrate ATPase for COQ8[81]. COQ8 has been proposed to regulate CoQ biosynthesis through COQ protein phosphorylation, but these effects are indirect and do not align with *in vitro* observations, namely the lack of trans phosphoryl transfer activity[81]. Currently, COQ8 is thought to function as a small molecule kinase or ATPase, but these hypotheses need to be tested more thoroughly. Further, it is unclear what role either of these activities would have in CoQ biosynthesis. COQ8 and other UbiB proteins are the focus of this thesis and will be discuss in detail below.

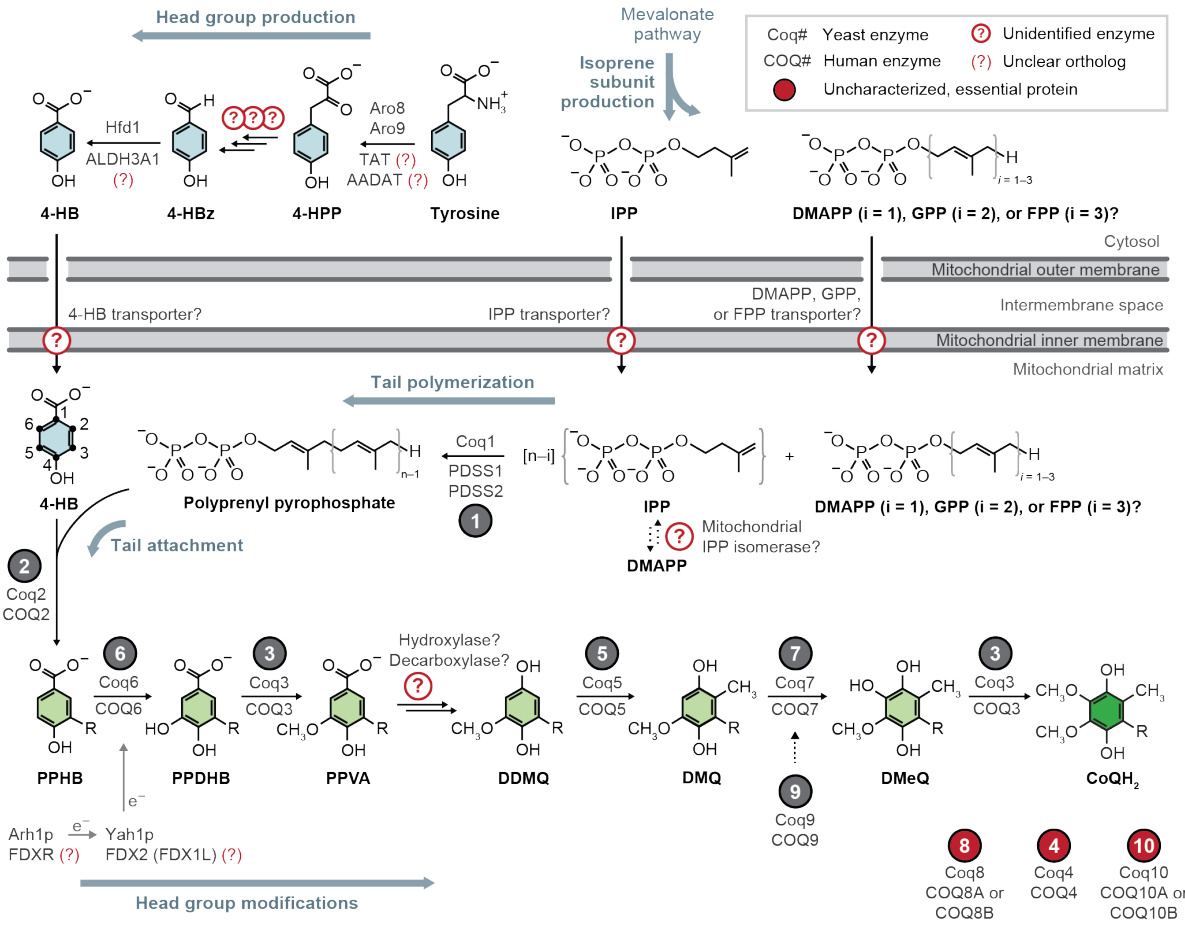

Figure 2. CoQ Biosynthesis Pathway in Eukaryotes (Yeast and Humans). Figure adapted from Stefely and Pagliarini, 2017[6]. Scheme of eukaryotic CoQ biosynthesis with predicted human orthologs (question marks), currently unassigned enzyme steps (circled question marks), and essential genes with undefined functions (red circles). Pathway intermediate abbreviations: 4-HB, 4-hydroxybenzoate; 4-HBz, 4-hydroxybenzaldehyde; 4-HPP, 4-hydroxyphenolpyruvate; IPP, isopentenyl pyrophosphate; DMAPP, dimethylallyl pyrophosphate; GPP, geranyl pyrophosphate; FPP, farnesyl pyrophosphate; PPHB polyprenyl-hydroxybenzoate; PPDHB, polyprenyl-dihydroxybenzoate; PPVA, polyprenyl-vanillic acid; DDMQ dimethyl-demethoxy-coenzyme Q; DMQ dimethoxy-coenzyme Q; DeMQ, dimethyl-coenzyme Q.

Headgroup Modification in Bacteria

Using similar strategies, much of the bacterial CoQ pathway mirrors the eukaryotic pathway outlined above. One of the major differences comes in the first step. Unlike in eukaryotes, the decarboxylation of PPHB in *E.coli* is well defined. UbiX is a flavin mononucleotide (FMN)-containing prenyltransferase that synthesizes a unique prenylated flavin cofactor[82]. This cofactor is then used by UbiD, a Mn^{2+} containing carboxy-lyase, to decarboxylate the C1 ring position[83]. Mitochondrial orthologs of UbiX and D have not been found in eukaryotes, suggesting other mechanisms likely exist. Next, OPP is hydroxylated at C5 by UbiI (COQ6 ortholog), a FAD-binding monooxygenase[84]. Notably, in *ΔubiI* cells, UbiF (COQ7 ortholog) can perform this reaction[84], demonstrating that *E. coli* hydroxylases have greater substrate flexibility than eukaryotes. UbiG (COQ3 ortholog), a SAM-dependent methyltransferase, *O*-methylates the C5 hydroxyl group[85]. UbiH then produces DDMQ by hydroxylating C1[86,87]. Next, UbiE (COQ5 ortholog), another SAM-dependent methyltransferase, *C*-methylates C2 to produce DMQ. A third flavin-containing monooxygenase UbiF hydroxylates C6 in the penultimate step[88]. Lastly, UbiG generates mature CoQ by *O*-methylating the C6 hydroxyl moiety[88,89].

Similar to eukaryotes, there are several auxiliary proteins in bacteria whose functions remain unclear but have recently emerged as key factors for overcoming hydrophobic barriers in CoQ biosynthesis. UbiJ and UbiK are two recently discovered factors that significantly reduce CoQ levels upon deletion[90,91], but only under aerobic conditions. Interestingly, purified UbiJ and UbiK interact to form a complex[91] and UbiJ contains a lipid binding domain that binds CoQ intermediates[56]. These proteins are components of the soluble Ubi complex, and are predicted to assist in presenting CoQ intermediates to other enzymes[56]. Although its function is still unclear, UbiT has a this same lipid binding domain[92] and has recently been demonstrated to bind CoQ,

recognizing the polyprenyl tail moiety[27]. This suggest that UbiT may substitute for UbiJ/K complex under anoxic conditions. Finally, UbiB is the founding member of the UbiB family (COQ8 ortholog). Like other proteins in this family, it shares primary sequence motifs with eukaryotic protein kinases, but how it functions in CoQ biosynthesis remains unclear[93].

Despite significant progress in understanding CoQ biosynthesis, many questions about enzyme mechanism, missing steps, contributions of auxiliary protein, and multi-protein complex dynamics remain. Continued investigation of this pathway will be critical for developing new treatments to combat CoQ deficiency and metabolically-related diseases[94].

The UbiB Family of Atypical Kinases

The UbiB family of protein kinase-like (PKL) genes represent an expansive group of atypical kinases found in all domains of life, having little to no characterization. Mutagenesis work done in *E.coli* during the 1960s led to the initial identification of *ubiB* as a gene involved in CoQ (or ubiquinone) biosynthesis. Many years later, sequencing efforts of existing and new bacterial and archaeal genomes[95,96] would highlight the extraordinary prevalence of UbiB genes (Figure 3A), as well as unique motifs common to this family. Through the early 2000s, genetic and molecular biology studies definitively showed UbiB and yeast Coq8 to be essential genes for CoQ biosynthesis. Further, perturbing Coq8 levels via gene deletion or overexpression impacts the stability of other CoQ pathway genes[49,97]. During this time, five human homologs (ADCK1-5) were identified[98] and a growing list of human diseases have been associated with these genese (discussed in section below). Yet, the molecular functions of UbiB family proteins remain a mystery.

In a recent breakthrough, COQ8A (ADCK3) was purified, crystalized, and examined for *in vitro* activity[80] (Figure 3B), representing the first mechanistic study of any UbiB family protein. The following year, a COQ8A knockout mouse was generated to explore its pathophsyiology, and follow-up biochemical efforts determined COQ8 is an atypical kinase[81]. There are still many outstanding questions conerning COQ8's enigmatic function *in vivo*, and importantly, many other UbiB proteins remain completely uncharacterized. Efforts to fill in these gaps across yeast, human, and plant sytems have accelerated in recent years and are the focus of this thesis.

Discovery and Early History of UbiB

Originally discovered in 1968, the *ubiB* (*yigR*) gene was identified after performing chemical mutagenesis on *E. coli* and selecting respiratory deficient strains—strains that could use glucose and not malate as the sole carbon source[99]. Named for its apparent involvement in ubiquinone (or CoQ) production, the *ubiB* gene was the second (or B) CoQ biosynthesis gene discovered. Characterization of isolated *ubiB* mutant strains (AN59 and others) showed an accumulation of octaprenyl phenol (OPP)[100], an early prenylated intermediate. Decades later, superior sequencing tools showed the AN59 strain had defects affecting the entire *ubiB* operon (*ubiE/ubiJ/ubiB*)[93]. Transformation of AN59 with a plasmid containing the whole operon was needed to restore CoQ levels—*ubiB* alone did not rescue CoQ production. To date, no *in vitro* biochemistry has been done with UbiB and our understanding of its role in CoQ biosynthesis remains unclear.

Understanding the role of eukaryotic homologs (yeast Coq8 and human COQ8A/ADCK3; collectively COQ8) first began with the systematic cataloging and investigation of nuclear petite (pet-) genes[101]. Nuclear petite strains are defined as having an intact mitochondrial genome and a

nuclear-derived allelic mutation that confers a respiratory-deficient phenotype (petite colony size). Analysis of this collection revealed that several pet- strains have reduced CoQ (named COQ1-8), but the genetic identities of each of the eight mutations were not known.

Later, the gene coding for Coq8 was identified as a multicopy suppressor of respiratory defect due a mutation in *Cbs2*, a complex III subunit (cytochrome bc1 complex)[102]. The authors called this gene *Abc1*, for activity of bc1 complex. Other work has referred to this gene *Cabc1*, or chaperone activity of bc1 complex[103]. Interestingly, in yet another sequencing mistake, the complex III defect suppression phenotype was due to a neighboring $tRNA^{Trp}$ gene located downstream of *Abc1/Coq8*[104]. In 2001, new evidence definitively showed Coq8 is an essential gene for CoQ biosynthesis[105]. *Coq8* and *Abc1* were found to be the same gene, and a fresh Δ*coq8* strain was generated. Deletion of *coq8* led to the accumulation early intermediate PPHB, and complete ablation of mature CoQ. Further, Δ*coq8* was partially rescued by supplementing with CoQ. It was later demonstrated that introduction of human COQ8A could rescue Δ*coq8* yeast after 10 days of growth on glycerol containing media[106], suggesting possible functional conservation. Additional studies will be needed to determine the differences amongst UbiB protein function in the CoQ biosynthesis pathway.

UbiB Family are Highly Conserved, Atypical Kinases

UbiB family proteins are highly conserved and ubiquitous across domains of life[96,98]. This was first appreciated in 1998 when sequencing efforts in bacteria and archaea revealed four previously unidentified protein kinase-like (PKL) families, including the "ABC1 family"[95]. A decade later, the Global Oceanic Sampling expedition significantly expanded the number of known UbiB genes[96,107], highlighting that UbiB proteins represent roughly 25% of the ocean microbial

kinome (Figure 3A). Additional sequences have been identified, including 3 in yeast (*S. cerevisiae*), 5 in humans[98] (Figure 3C), and 17 in plants (*A. thaliana*)[108]. Importantly, the abundance of available UbiB sequences has enabled detailed structural analyses of UbiB proteins[80,81,96], helping to classify UbiB proteins as atypical kinases. More recently, two crystal structures of human COQ8A have been solved[80,81], providing deeper insight into the atypical nature of these proteins.

Based on primary sequence and secondary structure predictions, UbiB proteins are predicted protein kinases. Structure analyses of eukaryotic protein kinases (ePKs) have identified twelve conserved motifs (subdomains) that form the protein kinase catalytic domain[109]. Although UbiB proteins share many of these features, it was unclear whether they would adopted this same fold *in vivo*. COQ8A apo[80] and substrate (nucleotide)-bound[81] structures revealed a PKL fold with the presence of a large N-terminal extension, positioned directly above the canonical substrate pocket (Figure 3B). Interestingly, the UbiB-specific and invariant KxGQ motif (Figure 3D) is oriented towards the putative active site, suggesting this fold is important for protein function. This may be a conserved feature of UbiB family proteins, but structural analyses will be needed to confirm. Several other unique structural features were observed[80]. Notably, the predominantly glycine-rich nucleotide binding loop is replaced with an alanine-rich loop, altering its nucleotide binding preference (to ADP over ATP)[80]. Using a non-hydrolyzable ATP analog, COQ8A substrate-bound structure was determined to be largely similar to the apo form. However, two small, hydrophobic pockets in COQ8A's core were identified in the nucleotide-bound structure[81]. Two modest rearrangements (Q switch 1 and 2) produced a small channel near the putative active site, large enough to accommodate a small-molecule kinase substrate. Although the KxGQ motif still occluded the active site, molecular simulations determined that these rearrangements

positioned catalytic residue D488 in the active conformation and K276 of the KxGQ motif proximal to the terminal phosphate of ATP. The second pocket is partially formed by the 'x' of this motif and may serve as a site of allosteric regulation. Together, this suggested that despite the occluded active site, COQ8A could adopt a conformation capable of kinase activity, likely facilitated by the atypical positioning of the KxGQ motif.

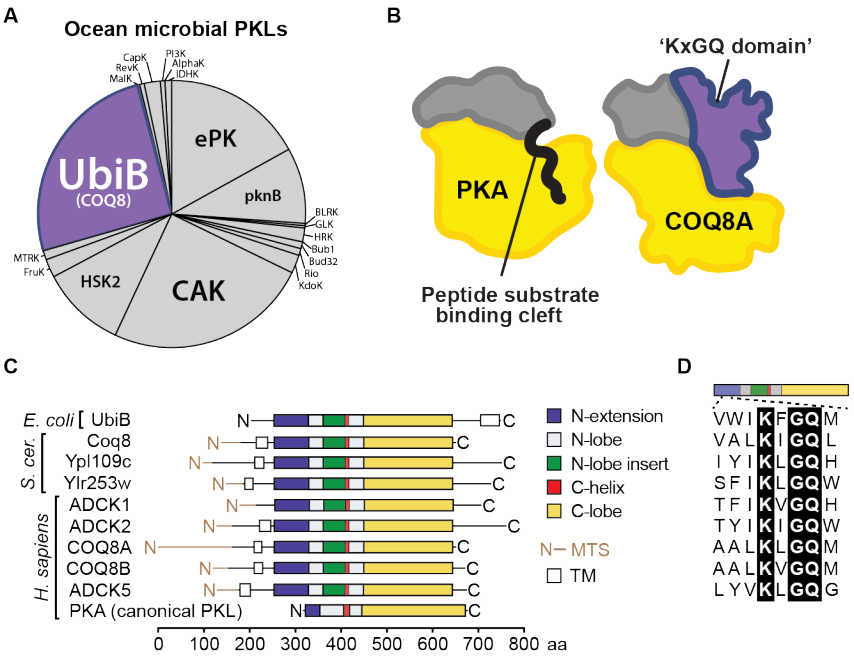

Figure 3.UbiB Proteins are Abundant and Highly Conserved Atypical Kinases. A, UbiB proteins represent a large portion of the oceanic microbial kinome. This figure was generated using data from Kannan et. al., 2007[96]. **B,** Cartoon depiction of canonical protein kinase A (PKA, PDB: 1ATP) and COQ8A (PDB: 4PED). **C** and **D,** Figures modified from Stefely et al., 2015[80]. **C,** Domain structure of UbiB family proteins (bacteria, yeast, and human) and PKA (human). MTS, mitochondrial targeting sequence; TM, transmembrane domain. **D,** Alignment of the 'KxGQ' motif within the N-terminal extension of UbiB proteins. This motif is invariant across the family.

COQ8 Influence over CoQ Biosynthesis and Complex Q

In 2001, yeast *COQ8* (formerly *ABC1*) was definitive identified, localized to mitochondria, and implicated as an essential gene for CoQ biosynthesis[105]. Human UbiB proteins were also localized to mitochondrial a few years later[110]. Similar to other *coq* deletion strains, Δ*coq8* yeast are deficient in mature CoQ and instead accumulate early precursor PPHB, supporting the existence of a CoQ biosynthetic metabolon (complex Q)[22]. This structure appears to exist in humans as well[53,54]. Further, *COQ8* deletion reduces the steady state levels of other Coq proteins[22,38]. Interestingly, Coq1, 2, 5, and 8 are unaffected by other *coq* deletion strains. A recent integrated multi-omic analysis in single gene yeast deletion strains showed similar proteomic phenotypes for the Coq proteins[38]. However, it remains unclear how complex Q is maintained and what role COQ8 might plays in this maintenance.

COQ8 has been associated with the matrix face of the IMM[49,111,112], and contains a transmembrane domain that enables protein dimerization[113]. At the membrane interface, COQ8 physically interacts with COQ5 and other COQ proteins[53,81]. Further, Coq8 overexpression in yeast has been shown to stabilize subcomplexes and diagnostic intermediates in different *coq* deletion strains[114], serving as an important tool for dissecting the complicated pathway. Taken together, the prevailing hypothesis for how COQ8 contributed to CoQ biosynthesis and/or stabilized complex Q was through protein kinase activity within the CoQ pathway. Previous work leaned heavily on indirect assays to demonstrate *COQ8*-dependent phosphorylation of Coq3, Coq5, and Coq7[106,112]. This work was never validated *in vitro* with purified proteins. In a recent study using yeast and mice systems, 12,000 phosphopeptides were detected[81], yet no phosphorylation was identified for

these Coq proteins. Importantly, Coq8 was shown to lack activity *in trans*[81], casting serious doubt on this original hypothesis

Recent studies demand the exploration of alternative models for how COQ8 might support CoQ biosynthesis, namely via small-molecule kinase or ATPase activity. In support of small-molecule kinase activity, Coq8 was shown to co-purify with early intermediates in the CoQ synthesis pathway (octaprenyl hydroxybenzoate, OHB and octaprenyl phenol, OPP). Low level ATPase activity was also demonstrated for recombinant Coq8 *in vitro*, and both of these observations were dependent on the integrity of catalytic or UbiB-specific residues[81]. Collectively, COQ8 appears to possess unorthodox kinase-like activity that is essential for supporting CoQ biosynthesis and the stability of complex Q.

Human UbiB Proteins and Disease

Five UbiB family proteins have been identified in humans (ADCK1-5), and each has been associated with human disease. Of these, COQ8A (ADCK3) and COQ8B (ADCK4) have been studied most and have established connections to CoQ biosynthesis[81,115,116]. Dysfunction or deletion of these proteins results in primary CoQ deficiency, manifesting in cerebellar ataxia and kidney disease, respectively. Meanwhile, the biological roles of other ADCK proteins remain elusive. Genome-wide knockdown studies have implicated these uncharacterized *ADCK* genes in several cancer disease states, including glioblastoma multiform[117], estrogen receptor-positive breast tumors[118], altered epithelial cell migration[119], and lung cancer[120]. Interestingly, a recent study reported that haploinsufficiency of *ADCK2* led to aberrant mitochondrial lipid oxidation and myopathy associated with CoQ deficiency[121], suggesting that other UbiB proteins may also have a connection to CoQ biology.

As novel targets for human disease intervention, significant efforts will be needed to determine ADCK protein functions and their specific pathway associations. Historically, kinase inhibitors have been successful chemotherapeutic agents. Notably, small-molecule modulators have been developed for Coq8[122] and COQ8A[123], indicating that UbiB proteins are promising druggable targets whose manipulation could provide therapeutic benefit for an array of different disease states.

Yeast UbiB Family Members

Yeast (*S. cerevisiae*) contain three UbiB proteins—Coq8, Ylr253w (Mcp2), and Ypl109c. All three genes have been localized to mitochondria; however, unlike matrix-facing Coq8, Ylr253w and Ypl109c are embedded in the IMM facing the IMS (outer face)[124-126]. Targeted investigations employing salt, carbonate, and detergent treatments of purified mitochondria determined Ylr253w is an integral IMM protein[124]. More recently, a pair of studies combined heavy labeling and submitochondrial fractionation approaches with quantitative mass spectrometry profiling to localize the yeast mitochondrial proteome[125,126]. This work confirmed Ylr253w localization and determined Ypl109c was also an integral IMM protein facing the IMS.

Although yeast have been used extensively to study Coq8, Ylr253w and Ypl109c have no assigned function and remain relatively uncharacterized. Previous work identified an array of genetic interactions for Ylr253w and Ypl109c with lipid biosynthesis and homeostasis genes[127,128]. Notably, Ylr253w has negative genetic interactions with all five subunits of the ER-mitochondrial encounter structure (ERMES), a key protein tether connecting ER and mitochondria for essential lipid and metabolite transfer. Further, Ypl109c and Ylr253w have inverse genetic relationships with Psd1 and Ups1, two key mitochondrial enzymes involved in phosphatidylethanolamine (PE)

and cardiolipin (CL) biosynthesis, respectively[129]. Indeed, Ylr253w was previously identified as a high-copy suppressor of a growth defect caused by loss of the mitochondrial ERMES subunit Mdm10[124]. More recently, three conserved Ylr253w active site residues were shown to mitigate rescue of Δ*mdm10* yeast growth[130].

In contrast, Ypl109c is completely uncharacterized. In 2010, Ypl109c was associated with isoprenoid biosynthesis as one of 59 genes identified as having an inverse response to lovastatin (HMG-CoA reductase, Hmg1) and zaragozic acid (squalene synthase, Erg9) inhibitors[131]. Ypl109c expression was elevated during zaragozic acid treatment and diminished during lovastatin treatment. A few years later, Ypl109c was identified as one of 93 genes that when knocked out caused increased respiratory growth in copper supplemented media[132]. However, Ypl109c's relationship to isoprenoid biosynthesis and copper homeostasis remains unclear.

Collectively, Ylr253w and Ypl109c appear to have intriguing associations with mitochondrial lipid homeostasis, suggesting a conserved role of the UbiB family in lipid maintenance. Future studies will be needed to associate these genes with a specific mitochondrial pathway and to better understand how they might help maintain lipid homeostasis.

The UbiB Family in Plants (ABC1K)

In plants (*Arabidopsis thaliana*), the number of UbiB proteins (ABC1K) has greatly expanded. 17 ABC1K proteins are found in *Arabidopsis* and these are found in either plastids or mitochondria[108]. Within plastids, six ABC1K proteins are predominantly localized to plastoglobules (PGs), thylakoid-associated monolayer lipoprotein particles containing prenyl and neutral lipids and a small, rather uncharacterized proteome[133]. These plant "lipid droplets" are believed to be key sites of prenyl lipid (α-tocopherol, plastoquinol-9 (PQ-9), and phylloquinone

(Vitamin K_1)) metabolism, functioning in both their biosynthesis and storage[108,134], but the metabolic purpose of these PGs is still unclear. Further, PGs have been implicated in stress and energy regulation processes, making them important structures for plant health and survival[135].

Previous proteomic analyses revealed that PG isolated from *Arabidopsis* contain just 30 proteins[136,137]. Six ABCIK proteins (ABC1K1, 3,5,6,7, and 9) are among these, constituting 20% of the protein diversity of this compartment. Interestingly, these proteins are evolutionarily distinct from the ABC1K found in plant mitochondria (ABC1K10-15), suggesting their function is likely specific to plastid metabolism. Of note, ABC1K13 (*AtAbc1*) functionally complimented Δ*coq8* yeast growth on glycerol plates[138], but CoQ levels were not investigated. Other protein identified in PG have been proposed to play roles in the trafficking and biosynthesis of prenyl lipids. The most abundant proteins in PGs are Fibrillin (FBN) proteins (7 proteins, 53% protein mass)[136], and they are beleived to bind and transport hydrophobic small-molecules[139]. VTE1 (tocopherol cylase) and VTE3 (UbiE-like methyltransferase) are biosynthetic enzymes required for the production of both α-tocopherol and plastochromanol-8 (a PQ-9 derivative)[140]. In *E.coli*, it is worth noting that *ubiE* and *ubiB* are found within the same operon. Here, PGs also contain orthologs of COQ5 and COQ8, suggesting that a conserved functional relationship between the two proteins may exist.

Our understanding of ABC1K function in plant biology are currently limited, relying heavily on gene deletion experiments. Several studies have suggested that VTE1 is regulated by ABC1K-mediated phosphorylation, but there is no direct evidence[141,142]. An *in vitro* phosphorylation assay using radiolabeled ATP with purified ABC1K1 and VTE1 showed very little VTE1 phosphorylation[143]. Additionally, this experiment lacked the proper activity-dead ABC1K1 control, making data interpretation challenging. Previous phenotypic work demonstrated that the plant double knockout of ABC1K1 and ABC1K3 (Δ*k1*Δ*k3)* had reduced stress resistance

and significant changes in the prenyl lipid compositions[141]. This was especially apparent with the distribution of PQ-9 between PGs and thylakoid membrane. More recently, continued efforts suggest ABC1K1 and ABC1K3 may affect the mobility and exchange of subcellular PG-9 pools to protect against certain exogenous stress[144,145]. Additional studies will be needed to understand how these atypical kinases might be involved in sensing and mobilizing prenyl lipids within PGs.

Do UbiB Proteins Broadly Support Quinone Homeostasis?

Over the past 5 years, our understanding of UbiB proteins has substantially matured[6]; however, we are still in the nascent stages of understanding the diverse roles these proteins might play and fundamentally how they operate to achieve these functions. COQ8 has been established as an essential gene in CoQ biosynthesis, but its mechanism of action and how it is regulated are still unknown. A major challenge in studying UbiB proteins is the absence of *in vitro* biochemistry—many UbiB proteins are recalcitrant to recombinant protein purification, stifling our ability to investigate protein activity and small-molecule regulators. UbiB proteins often have transmembrane domains and are likely membrane associated, complicating attempts to truncate proteins and maintain solubility[80].

Moving forward, two critical questions must be addressed to advance our understanding of UbiB protein biology. First, as an atypical kinase, how does COQ8 support CoQ biosynthesis? As a member of the ePK superfamily, an intuitive explanation for COQ8 function would be protein phosphorylation of other biosynthetic enzymes, thus tuning pathway flux through post-translational modifications. However, convincing evidence to support this model is absent. Moreover, recent work suggests that COQ8 is unlikely to function as a protein kinase[80] and new models are needed to explain its role in CoQ biosynthesis[81] (Figure 4). One alternative function is

small-molecule kinase activity (lipid or cofactor). Chemical rational suggests that phosphorylation of CoQ intermediates (e.g., DDMQ) may enhance subsequent reactions, but no such intermediate has yet been identified, possibly due to product lability. Another possibility is COQ8 could act as an ATPase (water kinase), coupling ATP hydrolysis to some mechanical output. An intriguing possibility is that COQ8 ATPase activity could drive complex Q assembly and/or the extraction of CoQ intermediates from the IMM. Finally, it is worth noting that COQ8 is unlikely a pseudokinase. Despite the growing interest in pseudokinase biology and their non-catalytic functions[146], UbiB proteins have all the necessary catalytic residues for phosphoryl transfer and *in vitro* activity has been demonstrated for COQ8[81].

The second question relates to functional conservation within the UbiB family. Specifically, do UbiB proteins broadly support and/or regulate quinone homeostasis? It is well-established that COQ8 orthologs support quinone production across domains of life. However, despite our limited understanding of other UbiB homologs, there are a growing number of interconnected clues supporting their role in lipid homeostasis. Genetic interaction profiles and phenotypic observations[124,127,128] for yeast homologs make an interesting, yet tangential case for their involvement in CoQ biology. Predicted to be structural similar to COQ8 (Figure 3C), these proteins are intriguingly located on the other side of the IMM[125,126], positioning them for post-production handling and submitochondrial transport of CoQ. Recent work in *Arabidopsis* implicated ABC1K proteins in proper PQ-9 distribution[144,145], further supporting this hypothesis. In yeast and humans, UbiB homologs facing the IMS physically interact with subunits of the mitochondrial contact site and cristae organization system (MICOS)[53,147], an essential structure for mitochondrial lipid trafficking. Collectively, these observations support investigating what role(s) UbiB proteins have in supporting quinone production, trafficking, and degradation.

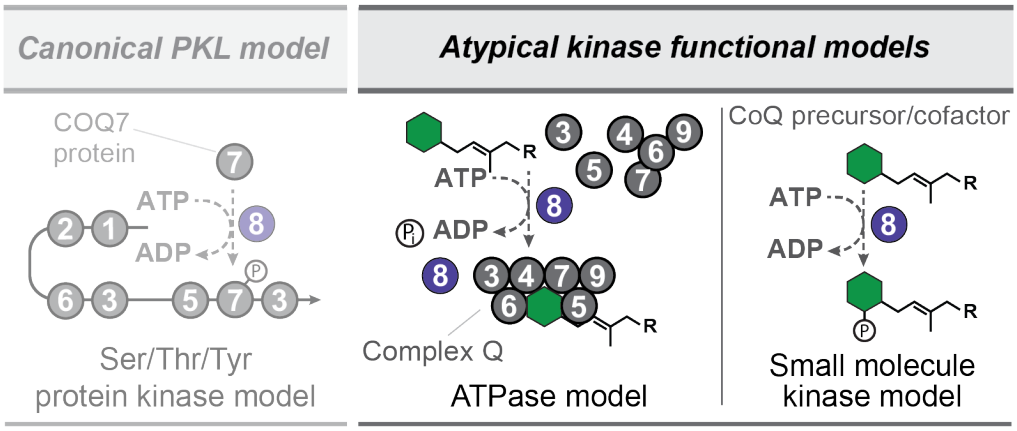

Figure 4. Alternative Models for how COQ8 Supports CoQ Biosynthesis. Figure modified from Stefely et al., 2016[81]. Direct evidence for COQ8 protein kinase activity is lacking, with structure and *in vitro* data arguing against it. Alternatively, COQ8 could have atypical kinase activity, functioning as an ATPase or small-molecule kinase to support CoQ production. ATPase activity could seed the formation of complex Q, while phosphorylation of CoQ intermediates could enhance biosynthetic flux.

Significance of Studying the UbiB Family

Despite having clear associations with a diverse spectrum of human disease, UbiB family proteins remain poorly understood and our knowledge of biochemical function is extremely limited. Mutations in COQ8A and COQ8B result in cerebellar ataxia[81,115] and steroid- resistant nephrotic syndrome[116], respectively. Efforts to treat these conditions with CoQ supplementation have failed to fully alleviate symptoms[115,148,149]. More broadly, other UbiB homologs have a growing number of connections to cancer[117-120], highlighting them as potential therapuetic targets. Collectively, there is a strong human health incentive to determine the mechanistic underpinnings and pathway associations of the UbiB protein family.

Our understanding of COQ8 serves as a model for exploring the function of other UbiB proteins. Paired with genetic interactions data[127,128], phenotypic observations[124], and defined interaction partners[53,147], one or more UbiB proteins may participate in other aspects of CoQ biology, such as CoQ transport. Currently, our knowledge of CoQ mobilization is exceptionally limited and required mitochondrial machinery has yet to be identified (discussed in Chapter 3). An intriguing possibility is that UbiB proteins participate in this pathway to regulate cellular CoQ distribution. If so, targeting these proteins would enable chemical and genetic control over cellular CoQ distribution, a significant asset in treating CoQ-deficient disease states.

Finally, elucidation of UbiB protein function will have important implications for ongoing efforts to broaden our understanding of PKL superfamily genes, especially those with atypical functions and those that remain uncharacterized[98,150]. UbiB proteins may represent a novel class of enzyme that supports proper lipid homeostasis across the cell.

References

1. Crane, F.L., Hatefi, Y., Lester, R.L. & Widmer, C. Isolation of a quinone from beef heart mitochondria. *Biochim Biophys Acta* **25**, 220-1 (1957).

2. Festenstein, G.N., Heaton, F.W., Lowe, J.S. & Morton, R.A. A constituent of the unsaponifiable portion of animal tissue lipids (lambda max. 272 m mu). *Biochem J* **59**, 558-66 (1955).

3. Wolf, D.E.H. et al. Coenzyme Q. I. Structure Studies on the Coenzyme Q Group. *J. Am. Chem. Soc* **80**, 4752 (1958).

4. Lester, R.L. & Crane, F.L. The natural occurrence of coenzyme Q and related compounds. *J Biol Chem* **234**, 2169-75 (1959).

5. Sastry, P.S., Jayaraman, J. & Ramasarma, T. Distribution of coenzyme Q in rat liver cell fractions. *Nature* **189**, 577 (1961).

6. Stefely, J.A. & Pagliarini, D.J. Biochemistry of Mitochondrial Coenzyme Q Biosynthesis. *Trends Biochem Sci* **42**, 824-843 (2017).

7. Mracek, T., Drahota, Z. & Houstek, J. The function and the role of the mitochondrial glycerol-3-phosphate dehydrogenase in mammalian tissues. *Biochim Biophys Acta* **1827**, 401-10 (2013).

8. Frerman, F.E. Acyl-CoA dehydrogenases, electron transfer flavoprotein and electron transfer flavoprotein dehydrogenase. *Biochem Soc Trans* **16**, 416-8 (1988).

9. Jones, M.E. Pyrimidine nucleotide biosynthesis in animals: genes, enzymes, and regulation of UMP biosynthesis. *Annu Rev Biochem* **49**, 253-79 (1980).

10. Rawls, J., Knecht, W., Diekert, K., Lill, R. & Loffler, M. Requirements for the mitochondrial import and localization of dihydroorotate dehydrogenase. *Eur J Biochem* **267**, 2079-87 (2000).

11. Do, T.Q., Schultz, J.R. & Clarke, C.F. Enhanced sensitivity of ubiquinone-deficient mutants of Saccharomyces cerevisiae to products of autoxidized polyunsaturated fatty acids. *Proc Natl Acad Sci U S A* **93**, 7534-9 (1996).

12. Stocker, R., Bowry, V.W. & Frei, B. Ubiquinol-10 protects human low density lipoprotein more efficiently against lipid peroxidation than does alpha-tocopherol. *Proc Natl Acad Sci U S A* **88**, 1646-50 (1991).

13. Frei, B., Kim, M.C. & Ames, B.N. Ubiquinol-10 is an effective lipid-soluble antioxidant at physiological concentrations. *Proc Natl Acad Sci U S A* **87**, 4879-83 (1990).

14. Navas, P., Villalba, J.M. & de Cabo, R. The importance of plasma membrane coenzyme Q in aging and stress responses. *Mitochondrion* **7 Suppl**, S34-40 (2007).

15. Sevin, D.C. & Sauer, U. Ubiquinone accumulation improves osmotic-stress tolerance in Escherichia coli. *Nat Chem Biol* **10**, 266-72 (2014).

16. Tempelhagen, L., Ayer, A., Culham, D.E., Stocker, R. & Wood, J.M. Cultivation at high osmotic pressure confers ubiquinone 8-independent protection of respiration on Escherichia coli. *J Biol Chem* **295**, 981-993 (2020).

17. Wang, Y. & Hekimi, S. Understanding Ubiquinone. *Trends Cell Biol* **26**, 367-378 (2016).

18. Bersuker, K. et al. The CoQ oxidoreductase FSP1 acts parallel to GPX4 to inhibit ferroptosis. *Nature* **575**, 688-692 (2019).

19. Doll, S. et al. FSP1 is a glutathione-independent ferroptosis suppressor. *Nature* **575**, 693-698 (2019).

20. Dixon, S.J. et al. Ferroptosis: an iron-dependent form of nonapoptotic cell death. *Cell* **149**, 1060-72 (2012).

21. Miles, M.V. The uptake and distribution of coenzyme Q10. *Mitochondrion* **7 Suppl**, S72-7 (2007).

22. Tran, U.C. & Clarke, C.F. Endogenous synthesis of coenzyme Q in eukaryotes. *Mitochondrion* **7 Suppl**, S62-71 (2007).

23. Barros, M.H. et al. The Saccharomyces cerevisiae COQ10 gene encodes a START domain protein required for function of coenzyme Q in respiration. *J Biol Chem* **280**, 42627-35 (2005).

24. Allan, C.M. et al. A conserved START domain coenzyme Q-binding polypeptide is required for efficient Q biosynthesis, respiratory electron transport, and antioxidant function in Saccharomyces cerevisiae. *Biochim Biophys Acta* **1831**, 776-791 (2013).

25. Allan, C.M. et al. Identification of Coq11, a new coenzyme Q biosynthetic protein in the CoQ-synthome in Saccharomyces cerevisiae. *J Biol Chem* **290**, 7517-34 (2015).

26. Abby, S.S., Kazemzadeh, K., Vragniau, C., Pelosi, L. & Pierrel, F. Advances in bacterial pathways for the biosynthesis of ubiquinone. *Biochim Biophys Acta Bioenerg* **1861**, 148259 (2020).

27. Vo, C.D. et al. The O2-independent pathway of ubiquinone biosynthesis is essential for denitrification in Pseudomonas aeruginosa. *J Biol Chem* **295**, 9021-9032 (2020).

28. Pelosi, L. et al. Ubiquinone Biosynthesis over the Entire O2 Range: Characterization of a Conserved O2-Independent Pathway. *mBio* **10**(2019).

29. Bloch, K. The biological synthesis of cholesterol. *Vitam Horm* **15**, 119-50 (1957).

30. Gloor, U. & Wiss, O. On the biosynthesis of ubiquinone (50). *Arch Biochem Biophys* **83**, 216-22 (1959).

31. Ashby, M.N. & Edwards, P.A. Elucidation of the deficiency in two yeast coenzyme Q mutants. Characterization of the structural gene encoding hexaprenyl pyrophosphate synthetase. *J Biol Chem* **265**, 13157-64 (1990).

32. Okada, K. et al. Polyprenyl diphosphate synthase essentially defines the length of the side chain of ubiquinone. *Biochim Biophys Acta* **1302**, 217-23 (1996).

33. Asai, K. et al. The identification of Escherichia coli ispB (cel) gene encoding the octaprenyl diphosphate synthase. *Biochem Biophys Res Commun* **202**, 340-5 (1994).

34. Olson, R.E., Dialamieh, G.H., Bentley, R., Springer, C.M. & Ramsey, V.G. Studies on Coenzyme Q. Pattern of Labeling in Coenzyme Q9 after Administration of Isotopic Acetate and Aromatic Amino Acids to Rats. *J Biol Chem* **240**, 514-23 (1965).

35. Olson, R.E. Biosynthesis of ubiquinones in animals. *Vitam Horm* **24**, 551-74 (1966).

36. Olson, R.E. & Rudney, H. Biosynthesis of ubiquinone. *Vitam Horm* **40**, 1-43 (1983).

37. Payet, L.A. et al. Mechanistic Details of Early Steps in Coenzyme Q Biosynthesis Pathway in Yeast. *Cell Chem Biol* **23**, 1241-1250 (2016).

38. Stefely, J.A. et al. Mitochondrial protein functions elucidated by multi-omic mass spectrometry profiling. *Nat Biotechnol* **34**, 1191-1197 (2016).

39. Olson, R.E. et al. Benzoate Derivatives as Intermediates in the Biosynthesis of Coenzyme Q in the Rat. *J Biol Chem* **238**, 3146-8 (1963).

40. Bentley, R.R., V. G.; Springer, C. M.; Dialameh, G. H.; Olson, R. E. The Origin of the Benzoquinone Ring of Coenzyme Q9 in the Rat. *Biochem Biophys Res Commun* **5**, 443-446 (1961).

41. Cox, G.B. & Gibson, F. Biosynthesis of Vitamin K and Ubiquinone. Relation to the Shikimic Acid Pathway in Escherichia Coli. *Biochim Biophys Acta* **93**, 204-6 (1964).

42. Marbois, B. et al. para-Aminobenzoic acid is a precursor in coenzyme Q6 biosynthesis in Saccharomyces cerevisiae. *J Biol Chem* **285**, 27827-38 (2010).

43. Pierrel, F. et al. Involvement of mitochondrial ferredoxin and para-aminobenzoic acid in yeast coenzyme Q biosynthesis. *Chem Biol* **17**, 449-59 (2010).

44. Hamilton, J.A. & Cox, G.B. Ubiquinone biosynthesis in Escherichia coli K-12. Accumulation of an octaprenol, farnesylfarnesylgeraniol, by a multiple aromatic auxotroph. *Biochem J* **123**, 435-43 (1971).

45. Xie, L.X. et al. Resveratrol and para-coumarate serve as ring precursors for coenzyme Q biosynthesis. *J Lipid Res* **56**, 909-19 (2015).

46. Young, I.G., Leppik, R.A., Hamilton, J.A. & Gibson, F. Biochemical and genetic studies on ubiquinone biosynthesis in Escherichia coli K-12:4-hydroxybenzoate octaprenyltransferase. *J Bacteriol* **110**, 18-25 (1972).

47. Marbois, B. et al. Coq3 and Coq4 define a polypeptide complex in yeast mitochondria for the biosynthesis of coenzyme Q. *J Biol Chem* **280**, 20231-8 (2005).

48. Gonzalez-Mariscal, I. et al. Regulation of coenzyme Q biosynthesis in yeast: a new complex in the block. *IUBMB Life* **66**, 63-70 (2014).

49. He, C.H., Xie, L.X., Allan, C.M., Tran, U.C. & Clarke, C.F. Coenzyme Q supplementation or over-expression of the yeast Coq8 putative kinase stabilizes multi-subunit Coq polypeptide complexes in yeast coq null mutants. *Biochim Biophys Acta* **1841**, 630-44 (2014).

50. Poon, W.W., Do, T.Q., Marbois, B.N. & Clarke, C.F. Sensitivity to treatment with polyunsaturated fatty acids is a general characteristic of the ubiquinone-deficient yeast coq mutants. *Mol Aspects Med* **18 Suppl**, S121-7 (1997).

51. Gin, P. et al. The Saccharomyces cerevisiae COQ6 gene encodes a mitochondrial flavin-dependent monooxygenase required for coenzyme Q biosynthesis. *J Biol Chem* **278**, 25308-16 (2003).

52. Johnson, A. et al. COQ9, a new gene required for the biosynthesis of coenzyme Q in Saccharomyces cerevisiae. *J Biol Chem* **280**, 31397-404 (2005).

53. Floyd, B.J. et al. Mitochondrial Protein Interaction Mapping Identifies Regulators of Respiratory Chain Function. *Mol Cell* **63**, 621-32 (2016).

54. Subramanian, K. et al. Coenzyme Q biosynthetic proteins assemble in a substrate-dependent manner into domains at ER-mitochondria contacts. *J Cell Biol* **218**, 1353-1369 (2019).

55. Aussel, L. et al. Biosynthesis and physiology of coenzyme Q in bacteria. *Biochim Biophys Acta* **1837**, 1004-11 (2014).

56. Hajj Chehade, M. et al. A Soluble Metabolon Synthesizes the Isoprenoid Lipid Ubiquinone. *Cell Chem Biol* **26**, 482-492 e7 (2019).

57. Srere, P.A. Complexes of sequential metabolic enzymes. *Annu Rev Biochem* **56**, 89-124 (1987).

58. Robinson, J.B., Jr. & Srere, P.A. Organization of Krebs tricarboxylic acid cycle enzymes in mitochondria. *J Biol Chem* **260**, 10800-5 (1985).

59. Zhang, Y. & Fernie, A.R. Stable and temporary enzyme complexes and metabolons involved in energy and redox metabolism. *Antioxid Redox Signal* (2020).

60. Ozeir, M. et al. Coq6 is responsible for the C4-deamination reaction in coenzyme Q biosynthesis in Saccharomyces cerevisiae. *J Biol Chem* **290**, 24140-51 (2015).

61. Alexander, K. & Young, I.G. Alternative hydroxylases for the aerobic and anaerobic biosynthesis of ubiquinone in Escherichia coli. *Biochemistry* **17**, 4750-5 (1978).

62. Jackman, L.M., O'Brien, I.G., Cox, G.B. & Gibson, F. Methionine as the source of methyl groups for ubiquinone and vitamin K: a study using nuclear magnetic resonance and mass spectrometry. *Biochim Biophys Acta* **141**, 1-7 (1967).

63. Ozeir, M. et al. Coenzyme Q biosynthesis: Coq6 is required for the C5-hydroxylation reaction and substrate analogs rescue Coq6 deficiency. *Chem Biol* **18**, 1134-42 (2011).

64. Poon, W.W. et al. Yeast and rat Coq3 and Escherichia coli UbiG polypeptides catalyze both O-methyltransferase steps in coenzyme Q biosynthesis. *J Biol Chem* **274**, 21665-72 (1999).

65. Clarke, C.F., Williams, W. & Teruya, J.H. Ubiquinone biosynthesis in Saccharomyces cerevisiae. Isolation and sequence of COQ3, the 3,4-dihydroxy-5-hexaprenylbenzoate methyltransferase gene. *J Biol Chem* **266**, 16636-44 (1991).

66. Jonassen, T. & Clarke, C.F. Isolation and functional expression of human COQ3, a gene encoding a methyltransferase required for ubiquinone biosynthesis. *J Biol Chem* **275**, 12381-7 (2000).

67. Barkovich, R.J. et al. Characterization of the COQ5 gene from Saccharomyces cerevisiae. Evidence for a C-methyltransferase in ubiquinone biosynthesis. *J Biol Chem* **272**, 9182-8 (1997).

68. Dai, Y.N. et al. Crystal structures and catalytic mechanism of the C-methyltransferase Coq5 provide insights into a key step of the yeast coenzyme Q synthesis pathway. *Acta Crystallogr D Biol Crystallogr* **70**, 2085-92 (2014).

69. Nguyen, T.P. et al. Molecular characterization of the human COQ5 C-methyltransferase in coenzyme Q10 biosynthesis. *Biochim Biophys Acta* **1841**, 1628-38 (2014).

70. Jonassen, T. et al. Yeast Clk-1 homologue (Coq7/Cat5) is a mitochondrial protein in coenzyme Q synthesis. *J Biol Chem* **273**, 3351-7 (1998).

71. Behan, R.K. & Lippard, S.J. The aging-associated enzyme CLK-1 is a member of the carboxylate-bridged diiron family of proteins. *Biochemistry* **49**, 9679-81 (2010).

72. Stenmark, P. et al. A new member of the family of di-iron carboxylate proteins. Coq7 (clk-1), a membrane-bound hydroxylase involved in ubiquinone biosynthesis. *J Biol Chem* **276**, 33297-300 (2001).

73. Tran, U.C. et al. Complementation of Saccharomyces cerevisiae coq7 mutants by mitochondrial targeting of the Escherichia coli UbiF polypeptide: two functions of yeast Coq7 polypeptide in coenzyme Q biosynthesis. *J Biol Chem* **281**, 16401-9 (2006).

74. Lu, T.T., Lee, S.J., Apfel, U.P. & Lippard, S.J. Aging-associated enzyme human clock-1: substrate-mediated reduction of the diiron center for 5-demethoxyubiquinone hydroxylation. *Biochemistry* **52**, 2236-44 (2013).

75. Marbois, B., Gin, P., Gulmezian, M. & Clarke, C.F. The yeast Coq4 polypeptide organizes a mitochondrial protein complex essential for coenzyme Q biosynthesis. *Biochim Biophys Acta* **1791**, 69-75 (2009).

76. Belogrudov, G.I. et al. Yeast COQ4 encodes a mitochondrial protein required for coenzyme Q synthesis. *Arch Biochem Biophys* **392**, 48-58 (2001).

77. Casarin, A. et al. Functional characterization of human COQ4, a gene required for Coenzyme Q10 biosynthesis. *Biochem Biophys Res Commun* **372**, 35-9 (2008).

78. Lohman, D.C. et al. Mitochondrial COQ9 is a lipid-binding protein that associates with COQ7 to enable coenzyme Q biosynthesis. *Proc Natl Acad Sci U S A* **111**, E4697-705 (2014).

79. Lohman, D.C. et al. An Isoprene Lipid-Binding Protein Promotes Eukaryotic Coenzyme Q Biosynthesis. *Mol Cell* **73**, 763-774 e10 (2019).

80. Stefely, J.A. et al. Mitochondrial ADCK3 employs an atypical protein kinase-like fold to enable coenzyme Q biosynthesis. *Mol Cell* **57**, 83-94 (2015).

81. Stefely, J.A. et al. Cerebellar Ataxia and Coenzyme Q Deficiency through Loss of Unorthodox Kinase Activity. *Mol Cell* **63**, 608-20 (2016).

82. White, M.D. et al. UbiX is a flavin prenyltransferase required for bacterial ubiquinone biosynthesis. *Nature* **522**, 502-6 (2015).

83. Payne, K.A. et al. New cofactor supports alpha,beta-unsaturated acid decarboxylation via 1,3-dipolar cycloaddition. *Nature* **522**, 497-501 (2015).

84. Hajj Chehade, M. et al. ubiI, a new gene in Escherichia coli coenzyme Q biosynthesis, is involved in aerobic C5-hydroxylation. *J Biol Chem* **288**, 20085-92 (2013).

85. Hsu, A.Y., Poon, W.W., Shepherd, J.A., Myles, D.C. & Clarke, C.F. Complementation of coq3 mutant yeast by mitochondrial targeting of the Escherichia coli UbiG polypeptide: evidence that UbiG catalyzes both O-methylation steps in ubiquinone biosynthesis. *Biochemistry* **35**, 9797-806 (1996).

86. Young, I.G., Stroobant, P., Macdonald, C.G. & Gibson, F. Pathway for ubiquinone biosynthesis in Escherichia coli K-12: gene-enzyme relationships and intermediates. *J Bacteriol* **114**, 42-52 (1973).

87. Nakahigashi, K., Miyamoto, K., Nishimura, K. & Inokuchi, H. Isolation and characterization of a light-sensitive mutant of Escherichia coli K-12 with a mutation in a gene that is required for the biosynthesis of ubiquinone. *J Bacteriol* **174**, 7352-9 (1992).

88. Kwon, O., Kotsakis, A. & Meganathan, R. Ubiquinone (coenzyme Q) biosynthesis in Escherichia coli: identification of the ubiF gene. *FEMS Microbiol Lett* **186**, 157-61 (2000).

89. Young, I.G.M., L. M.; Stroobant, P.; Gibson, F. Characterization and Genetic Analysis of Mutant Strains of *Escherichia coli* K-12 Accumulating the Ubiquinone Precursors 2-Octaprenyl-6-Methoxy-1,4-Benzoquinone and 2-Octaprenyl-3-Methyl-6-Methoxy-1,4-Benzoquinone. *J Bacteriol* **105**, 769-778 (1971).

90. Aussel, L. et al. ubiJ, a new gene required for aerobic growth and proliferation in macrophage, is involved in coenzyme Q biosynthesis in Escherichia coli and Salmonella enterica serovar Typhimurium. *J Bacteriol* **196**, 70-9 (2014).

91. Loiseau, L. et al. The UbiK protein is an accessory factor necessary for bacterial ubiquinone (UQ) biosynthesis and forms a complex with the UQ biogenesis factor UbiJ. *J Biol Chem* **292**, 11937-11950 (2017).

92. Groenewold, M.K. et al. A phosphatidic acid-binding protein is important for lipid homeostasis and adaptation to anaerobic biofilm conditions in Pseudomonas aeruginosa. *Biochem J* **475**, 1885-1907 (2018).

93. Poon, W.W. et al. Identification of Escherichia coli ubiB, a gene required for the first monooxygenase step in ubiquinone biosynthesis. *J Bacteriol* **182**, 5139-46 (2000).

94. Quinzii, C.M. & Hirano, M. Primary and secondary CoQ(10) deficiencies in humans. *Biofactors* **37**, 361-5 (2011).

95. Leonard, C.J., Aravind, L. & Koonin, E.V. Novel families of putative protein kinases in bacteria and archaea: evolution of the "eukaryotic" protein kinase superfamily. *Genome Res* **8**, 1038-47 (1998).

96. Kannan, N., Taylor, S.S., Zhai, Y., Venter, J.C. & Manning, G. Structural and functional diversity of the microbial kinome. *PLoS Biol* **5**, e17 (2007).

97. Hsieh, E.J. et al. Saccharomyces cerevisiae Coq9 polypeptide is a subunit of the mitochondrial coenzyme Q biosynthetic complex. *Arch Biochem Biophys* **463**, 19-26 (2007).

98. Manning, G., Whyte, D.B., Martinez, R., Hunter, T. & Sudarsanam, S. The protein kinase complement of the human genome. *Science* **298**, 1912-34 (2002).

99. Cox, G.B., Gibson, F. & Pittard, J. Mutant strains of Escherichia coli K-12 unable to form ubiquinone. *J Bacteriol* **95**, 1591-8 (1968).

100. Cox, G.B., Young, I.G., McCann, L.M. & Gibson, F. Biosynthesis of ubiquinone in Escherichia coli K-12: location of genes affecting the metabolism of 3-octaprenyl-4-hydroxybenzoic acid and 2-octaprenylphenol. *J Bacteriol* **99**, 450-8 (1969).

101. Tzagoloff, A. & Dieckmann, C.L. PET genes of Saccharomyces cerevisiae. *Microbiol Rev* **54**, 211-25 (1990).

102. Bousquet, I., Dujardin, G. & Slonimski, P.P. ABC1, a novel yeast nuclear gene has a dual function in mitochondria: it suppresses a cytochrome b mRNA translation defect and is essential for the electron transfer in the bc 1 complex. *EMBO J* **10**, 2023-31 (1991).

103. Iiizumi, M., Arakawa, H., Mori, T., Ando, A. & Nakamura, Y. Isolation of a novel gene, CABC1, encoding a mitochondrial protein that is highly homologous to yeast activity of bc1 complex. *Cancer Res* **62**, 1246-50 (2002).

104. Hsieh, E.J., Dinoso, J.B. & Clarke, C.F. A tRNA(TRP) gene mediates the suppression of cbs2-223 previously attributed to ABC1/COQ8. *Biochem Biophys Res Commun* **317**, 648-53 (2004).

105. Do, T.Q., Hsu, A.Y., Jonassen, T., Lee, P.T. & Clarke, C.F. A defect in coenzyme Q biosynthesis is responsible for the respiratory deficiency in Saccharomyces cerevisiae abc1 mutants. *J Biol Chem* **276**, 18161-8 (2001).

106. Xie, L.X. et al. Expression of the human atypical kinase ADCK3 rescues coenzyme Q biosynthesis and phosphorylation of Coq polypeptides in yeast coq8 mutants. *Biochim Biophys Acta* **1811**, 348-60 (2011).

107. Gross, L. Untapped bounty: sampling the seas to survey microbial biodiversity. *PLoS Biol* **5**, e85 (2007).

108. Lundquist, P.K., Davis, J.I. & van Wijk, K.J. ABC1K atypical kinases in plants: filling the organellar kinase void. *Trends Plant Sci* **17**, 546-55 (2012).

109. Hanks, S.K. & Hunter, T. Protein kinases 6. The eukaryotic protein kinase superfamily: kinase (catalytic) domain structure and classification. *FASEB J* **9**, 576-96 (1995).

110. Pagliarini, D.J. et al. A mitochondrial protein compendium elucidates complex I disease biology. *Cell* **134**, 112-23 (2008).

111. Cullen, J.K. et al. AarF Domain Containing Kinase 3 (ADCK3) Mutant Cells Display Signs of Oxidative Stress, Defects in Mitochondrial Homeostasis and Lysosomal Accumulation. *PLoS One* **11**, e0148213 (2016).

112. Tauche, A., Krause-Buchholz, U. & Rodel, G. Ubiquinone biosynthesis in Saccharomyces cerevisiae: the molecular organization of O-methylase Coq3p depends on Abc1p/Coq8p. *FEMS Yeast Res* **8**, 1263-75 (2008).

113. Khadria, A.S. et al. A Gly-zipper motif mediates homodimerization of the transmembrane domain of the mitochondrial kinase ADCK3. *J Am Chem Soc* **136**, 14068-77 (2014).

114. Xie, L.X. et al. Overexpression of the Coq8 kinase in Saccharomyces cerevisiae coq null mutants allows for accumulation of diagnostic intermediates of the coenzyme Q6 biosynthetic pathway. *J Biol Chem* **287**, 23571-81 (2012).

115. Lagier-Tourenne, C. et al. ADCK3, an ancestral kinase, is mutated in a form of recessive ataxia associated with coenzyme Q10 deficiency. *Am J Hum Genet* **82**, 661-72 (2008).

116. Ashraf, S. et al. ADCK4 mutations promote steroid-resistant nephrotic syndrome through CoQ10 biosynthesis disruption. *J Clin Invest* **123**, 5179-89 (2013).

117. Wiedemeyer, W.R. et al. Pattern of retinoblastoma pathway inactivation dictates response to CDK4/6 inhibition in GBM. *Proc Natl Acad Sci U S A* **107**, 11501-6 (2010).

118. Brough, R. et al. Functional viability profiles of breast cancer. *Cancer Discov* **1**, 260-73 (2011).

119. Simpson, K.J. et al. Identification of genes that regulate epithelial cell migration using an siRNA screening approach. *Nat Cell Biol* **10**, 1027-38 (2008).

120. Qiu, M. et al. aarF domain containing kinase 5 gene promotes invasion and migration of lung cancer cells through ADCK5-SOX9-PTTG1 pathway. *Exp Cell Res* **392**, 112002 (2020).

121. Vazquez-Fonseca, L. *et al.* ADCK2 Haploinsufficiency Reduces Mitochondrial Lipid Oxidation and Causes Myopathy Associated with CoQ Deficiency. *J Clin Med* **8** (2019).

122. Reidenbach, A.G. et al. Conserved Lipid and Small-Molecule Modulation of COQ8 Reveals Regulation of the Ancient Kinase-like UbiB Family. *Cell Chem Biol* **25**, 154-165 e11 (2018).

123. Asquith, C.R.M., Murray, N.H. & Pagliarini, D.J. ADCK3/COQ8A: the choice target of the UbiB protein kinase-like family. *Nat Rev Drug Discov* **18**, 815 (2019).

124. Tan, T., Ozbalci, C., Brugger, B., Rapaport, D. & Dimmer, K.S. Mcp1 and Mcp2, two novel proteins involved in mitochondrial lipid homeostasis. *J Cell Sci* **126**, 3563-74 (2013).

125. Vogtle, F.N. et al. Landscape of submitochondrial protein distribution. *Nat Commun* **8**, 290 (2017).

126. Morgenstern, M. et al. Definition of a High-Confidence Mitochondrial Proteome at Quantitative Scale. *Cell Rep* **19**, 2836-2852 (2017).

127. Costanzo, M. et al. A global genetic interaction network maps a wiring diagram of cellular function. *Science* **353**(2016).

128. Hoppins, S. et al. A mitochondrial-focused genetic interaction map reveals a scaffold-like complex required for inner membrane organization in mitochondria. *J Cell Biol* **195**, 323-40 (2011).

129. Tatsuta, T. & Langer, T. Intramitochondrial phospholipid trafficking. *Biochim Biophys Acta Mol Cell Biol Lipids* **1862**, 81-89 (2017).

130. Odendall, F. et al. The mitochondrial intermembrane space-facing proteins Mcp2 and Tgl2 are involved in yeast lipid metabolism. *Mol Biol Cell* **30**, 2681-2694 (2019).

131. Kuranda, K., Francois, J. & Palamarczyk, G. The isoprenoid pathway and transcriptional response to its inhibitors in the yeast Saccharomyces cerevisiae. *FEMS Yeast Res* **10**, 14-27 (2010).

132. Schlecht, U. et al. A functional screen for copper homeostasis genes identifies a pharmacologically tractable cellular system. *BMC Genomics* **15**, 263 (2014).

133. Eugeni Piller, L., Abraham, M., Dormann, P., Kessler, F. & Besagni, C. Plastid lipid droplets at the crossroads of prenylquinone metabolism. *J Exp Bot* **63**, 1609-18 (2012).

134. Jasinski, M. et al. AtOSA1, a member of the Abc1-like family, as a new factor in cadmium and oxidative stress response. *Plant Physiol* **147**, 719-31 (2008).

135. van Wijk, K.J. & Kessler, F. Plastoglobuli: Plastid Microcompartments with Integrated Functions in Metabolism, Plastid Developmental Transitions, and Environmental Adaptation. *Annu Rev Plant Biol* **68**, 253-289 (2017).

136. Lundquist, P.K. et al. The functional network of the Arabidopsis plastoglobule proteome based on quantitative proteomics and genome-wide coexpression analysis. *Plant Physiol* **158**, 1172-92 (2012).

137. Ytterberg, A.J., Peltier, J.B. & van Wijk, K.J. Protein profiling of plastoglobules in chloroplasts and chromoplasts. A surprising site for differential accumulation of metabolic enzymes. *Plant Physiol* **140**, 984-97 (2006).

138. Cardazzo, B., Hamel, P., Sakamoto, W., Wintz, H. & Dujardin, G. Isolation of an Arabidopsis thaliana cDNA by complementation of a yeast abc1 deletion mutant deficient in complex III respiratory activity. *Gene* **221**, 117-25 (1998).

139. Singh, D.K. & McNellis, T.W. Fibrillin protein function: the tip of the iceberg? *Trends Plant Sci* **16**, 432-41 (2011).

140. Havaux, M. Plastoquinone In and Beyond Photosynthesis. *Trends Plant Sci* **25**, 1252-1265 (2020).

141. Lundquist, P.K. et al. Loss of plastoglobule kinases ABC1K1 and ABC1K3 causes conditional degreening, modified prenyl-lipids, and recruitment of the jasmonic acid pathway. *Plant Cell* **25**, 1818-39 (2013).

142. Martinis, J., Glauser, G., Valimareanu, S. & Kessler, F. A chloroplast ABC1-like kinase regulates vitamin E metabolism in Arabidopsis. *Plant Physiol* **162**, 652-62 (2013).

143. Martinis, J. et al. ABC1K1/PGR6 kinase: a regulatory link between photosynthetic activity and chloroplast metabolism. *Plant J* **77**, 269-83 (2014).

144. Pralon, T. et al. Plastoquinone homoeostasis by Arabidopsis proton gradient regulation 6 is essential for photosynthetic efficiency. *Commun Biol* **2**, 220 (2019).

145. Pralon, T. et al. Mutation of the Atypical Kinase ABC1K3 Partially Rescues the PROTON GRADIENT REGULATION 6 Phenotype in Arabidopsis thaliana. *Front Plant Sci* **11**, 337 (2020).

146. Kung, J.E. & Jura, N. Prospects for pharmacological targeting of pseudokinases. *Nat Rev Drug Discov* **18**, 501-526 (2019).

147. von der Malsburg, K. et al. Dual role of mitofilin in mitochondrial membrane organization and protein biogenesis. *Dev Cell* **21**, 694-707 (2011).

148. Atmaca, M. et al. Follow-up results of patients with ADCK4 mutations and the efficacy of CoQ10 treatment. *Pediatr Nephrol* **32**, 1369-1375 (2017).

149. Mollet, J. et al. CABC1 gene mutations cause ubiquinone deficiency with cerebellar ataxia and seizures. *Am J Hum Genet* **82**, 623-30 (2008).

150. Kanev, G.K. et al. The Landscape of Atypical and Eukaryotic Protein Kinases. *Trends Pharmacol Sci* **40**, 818-832 (2019).

Chapter 2: Conserved Lipid and Small Molecule Modulation of COQ8 Reveals Regulation of the Ancient Kinase-like UbiB Family

Andrew G. Reidenbach, Zachary A. Kemmerer, Deniz Aydin, Adam Jochem, Molly T. McDevitt, Paul D. Hutchins, Jaime L. Stark, Jonathan A. Stefely, Thiru Reddy, Alex S. Hebert, Emily M. Wilkerson, Isabel E. Johnson, Craig A. Bingman, John L. Markley, Joshua J. Coon, Matteo Dal Peraro, and David J. Pagliarini

This chapter was published as an article in *Cell Chemical Biology* (2018, vol. 25 no. 2 pp 154-165.e11) by the authors listed above.

Author Contributions

A.G.R. and D.J.P. conceived of the project and its design. A.G.R., Z.A.K., D.A., A.J., M.T.M., P.D.H., J.L.S., J.A.S., T.R., A.S.H., E.M.W., I.E.J., C.A.B., and M.D.P. performed experiments and data analysis. D.A. and M.D.P designed and performed molecular modeling and simulation that supported the experimental design. J.L.M., J.J.C., M.D.P., and D.J.P. provided key experimental resources and/or aided in experimental design. A.G.R. and D.J.P. wrote the manuscript.

Summary

Human COQ8A (ADCK3) and *Saccharomyces cerevisiae* Coq8p (collectively COQ8) are UbiB family proteins essential for mitochondrial coenzyme Q (CoQ) biosynthesis. However, the biochemical activity of COQ8 and its direct role in CoQ production remain unclear, in part due to lack of known endogenous regulators of COQ8 function and of effective small molecules for probing its activity *in vivo.* Here we demonstrate that COQ8 possesses evolutionarily conserved ATPase activity that is activated by binding to membranes containing cardiolipin and by phenolic compounds that resemble CoQ pathway intermediates. We further create an analog-sensitive version of Coq8p and reveal that acute chemical inhibition of its endogenous activity in yeast is sufficient to cause respiratory deficiency concomitant with CoQ depletion. Collectively, this work defines lipid and small molecule modulators of an ancient family of atypical kinase-like proteins and establishes a chemical genetic system for further exploring the mechanistic role of COQ8 in CoQ biosynthesis.

Introduction

The UbiB family of atypical protein kinase-like (PKL) genes is conserved across all three domains of life[1]. In eukaryotes, UbiB proteins are found exclusively in mitochondria and plastids where they have been linked to diverse processes involving cell migration, tumor cell viability, and lipid metabolism[2-4]. An orthologous subset of UbiB proteins, including *Escherichia coli* UbiB, *S. cerevisiae* Coq8p, and human COQ8A (ADCK3) and COQ8B (ADCK4), support the biosynthesis of coenzyme Q (ubiquinone, CoQ)[5,6], and mutations in COQ8A and COQ8B give rise to CoQ-related neurologic and kidney disorders, respectively[7-11]. Despite these connections, the specific biochemical activities, regulation, and direct roles of UbiB proteins in cellular processes remain largely unclear, in part because effective tools for addressing these questions have been lacking.

To date, the only biochemical activities observed for UbiB family proteins are COQ8 *cis* autophosphorylation, which is seemingly spurious, and a low-level COQ8 ATPase activity[11,12]. Additionally, structural analyses revealed that the COQ8 active site is likely sterically inaccessible to proteinaceous substrates, suggesting that this family possesses unorthodox kinase functionality in lieu of canonical protein kinase activity. However, many members of the protein kinase-like (PKL) superfamily are subject to activation by lipids and small molecules, including AMPK (AMP)[13], PKA (cAMP)[14], PKC (diacylglycerol)[15,16], and AKT (phosphoinositides)[17,18], indicating that COQ8 activity may be altered or enhanced in a similar manner. Consistently, we recently found that Coq8p copurifies with intermediates in the CoQ pathway[11], and have shown that the single-pass transmembrane domain of COQ8A can induce dimerization[19], together suggesting that COQ8 activity may particularly be regulated by interactions at the membrane; however, this remains unexplored.

A second limitation for defining the functions of UbiB proteins has been the lack of specific inhibitors that can be used to disrupt protein activity. While the use of COQ8 active site point mutants in growth assays has implied the importance of COQ8 catalytic activity for CoQ production[12,20], this has not been tested directly by chemical inhibition *in vivo*. Chemical-genetic strategies have proven effective for kinase inhibition when specific inhibitors for the wild type kinase are lacking. This approach involves mutating a "gatekeeper" residue in the ATP binding pocket to create a larger space capable of accommodating custom, cell-permeable inhibitors that are too bulky to bind to other kinases[21]. Additionally, to enable covalent, irreversible inhibition, a conserved valine near the active site can be mutated to a cysteine[22-24]. When successful, this technique enables acute and selective inhibition of kinase activity *in vivo,* thereby overcoming the caveats associated with long-term adaptions that can arise from genetic manipulation. Although this approach has been used for various classes of kinases[22-27], it has never been attempted for the much more divergent and atypical UbiB family, nor for a mitochondria-localized kinase in general.

To address these limitations in investigating the UbiB family, we combined biophysical, biochemical, computational, and chemical genetic analyses to explore the activity and regulation of COQ8. We found that ATPase activity is an evolutionarily conserved feature of COQ8 orthologs from *E. coli* to humans that is enhanced by phenolic compounds resembling CoQ biosynthetic precursors. Remarkably, we also find that mature COQ8 specifically associates with, and is activated by, cardiolipin-containing liposomes. Finally, we establish an analog-sensitive version of COQ8 in yeast and show that acute inhibition of endogenous COQ8 activity is sufficient to disrupt CoQ production and cause respiratory deficiency. Overall, our work reveals lipid and small molecule modulators of this ancient kinase-like protein, and establishes a chemical genetic tool for the further exploration of its direct role in CoQ biosynthesis.

Results

UbiB family ATPase activity is enhanced by phenols

To explore the ability of UbiB proteins to bind lipids and small molecules, we purified a maltose binding protein (MBP)-tagged version of *E. coli* UbiB that lacks its predicted C-terminal transmembrane (TM) domains (UbiB$^{C\Delta47}$) and analyzed copurifying lipids by mass spectrometry (Figure S1A). We found that MBP-UbiB$^{C\Delta47}$ preferentially copurifies with *E. coli* CoQ biosynthesis intermediates octaprenylphenol (OPP) and octaprenylhydroxybenzoate (OHB) and that this copurification depends on the integrity of active site residues (Figures 1A, S1B–E, and Table S1). These data are highly consistent with our previous lipid-binding data for Coq8p, indicating that the binding of CoQ precursors to UbiB family members is conserved from bacteria to eukaryotes[11].

As an orthogonal approach to assessing protein-small molecule interactions, we next performed a one-dimensional (1D) ^{1}H NMR ligand-affinity screen of a diverse 417 compound library using COQ8A$^{N\Delta250}$ (COQ8A lacking its mitochondrial targeting sequence and TM domain). To do so, we introduced COQ8A$^{N\Delta250}$ to mixtures of 3-5 compounds and analyzed the resulting line broadening and/or chemical shift changes of the ^{1}H peaks for compounds interacting with COQ8A$^{N\Delta250}$. In addition to its expected binding to adenosine, COQ8A$^{N\Delta250}$ interacted with a total of 25 compounds including multiple that, like OPP and OHB, are phenol derivatives (Figures 1B and S1F and Table S2). Collectively, these data establish that COQ8 possesses an evolutionarily conserved capacity to bind CoQ precursor-like molecules, suggesting that these molecules are potential regulators or direct substrates of COQ8.

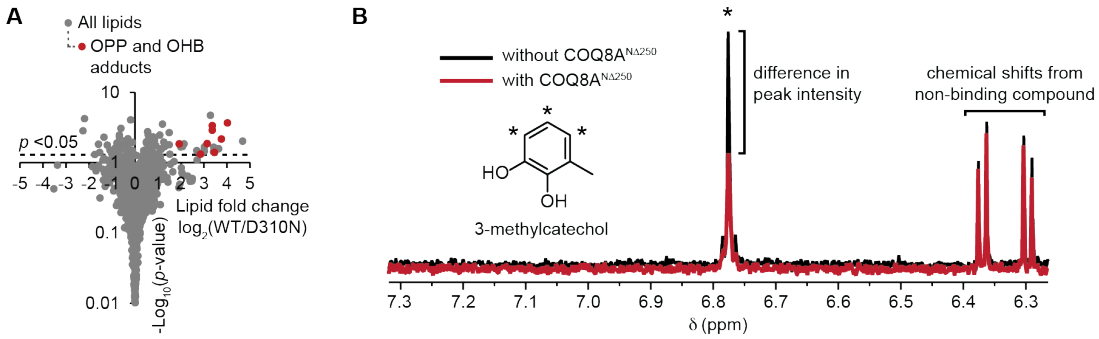

Figure 1. UbiB Family Members Bind CoQ Precursor-like Lipids and Small Molecules. (A) Fold changes in the abundances of lipids copurifying with UbiB protein variants (log_2[MBP-UbiB$^{C\Delta47}$/ MBP-UbiB$^{C\Delta47}$ D310N], n = 3) as quantified by LC-MS/MS versus statistical significance. Different OPP and OHB adducts (e.g., OPP $[M-H]^-$ and OPP $[M+Cl]^-$) are shown in red. (B) A selected region of the ^{1}H NMR spectra for a mixture containing 3-methylcatechol (3-MC) with and without COQ8A$^{N\Delta250}$. Asterisk (*) indicates the three benzyl hydrogens on the 3-MC peak that exhibit line-broadening. The peaks shown around 6.3 - 6.4 ppm belong to another compound (*cis*-3-chloroacrylic acid) in the mixture that is not interacting with COQ8A$^{N\Delta250}$. See also Figure S1 and Tables S1–S3.

The CoQ precursors that copurify with Coq8p and UbiB are difficult to synthesize and are not commercially available; as such, to explore the functional ramifications of these COQ8-ligand interactions, we opted to screen a variety of CoQ headgroup-like analogs (phenols and hydroquinones) for their effect on COQ8 activity. To monitor ATP consuming activity, we used the ADP-Glo assay, which measures ADP produced as a proxy for phosphoryl transfer activity. We included the nonionic detergent Triton X-100 in our screens, as it has been shown to activate certain membrane bound or membrane associated proteins[28,29]. We found that 2-alkylphenols (2-allylphenol and 2-propylphenol), which are structurally similar to OPP, strongly activated UbiB

family members when in the presence of Triton X-100 (Figures 2A and S2A). This increase in activity was seen both for wild type (WT) and the A339G (A-to-G) nucleotide-binding loop (P-loop) mutant, which has a higher baseline ATPase and *cis* autophosphorylation activity likely due to enhanced ATP binding[11] (See Table S3 and Figure S2F for explanations of mutants used in this study). The negative control D507N (D-to-N) mutant, which lacks ATP binding ability, showed no activity (Figures 2A and S2A).

Our previous structure of COQ8 revealed the presence of a water molecule in the active site bound by the glutamine (Q) of the invariant KxGQ motif that could serve as the nucleophile for an ATPase reaction[12]. As such, we hypothesized that the majority of our observed ADP production was due to ATP hydrolysis with water, which could be detected by the production of free phosphate using a malachite green assay. Indeed, we found a clear correlation between the amount of activity observed in the ADP-Glo assay and the malachite green assay, demonstrating that 2-alkylphenols with Triton X-100 increase the ATPase activity of UbiB family members (Figures 2B and S2B). Consistently, COQ8 KxGQ domain mutations that possess markedly enhanced *cis* autophosphorylation (e.g., the double A-to-G, K-to-H mutant)[11,12] show little ATPase activity, are unable grow in respiratory media, and fail to enable CoQ_6 production *in vivo* (Figures 2C, 2D, S2C, and S2D). This further demonstrates that ATPase activity, and not protein kinase-related activity, tracks most closely with the endogenous function of COQ8.

Notably, compounds that more closely mimic the mature CoQ headgroup, such as 2,6-dimethoxyhydroquinone or CoQ_1, did not greatly enhance COQ8 activity, in agreement with our CoQ precursor binding data (Figure S2E)[11]. Furthermore, the activation by 2-alkylphenols with Triton X-100 is conserved in UbiB, Coq8p, and COQ8A, mirroring the conservation of CoQ

precursor binding (Figure 2E). Overall, these data suggest that COQ8 possesses an evolutionarily conserved ability to bind early CoQ intermediates and to be activated by 2-alkylphenols.

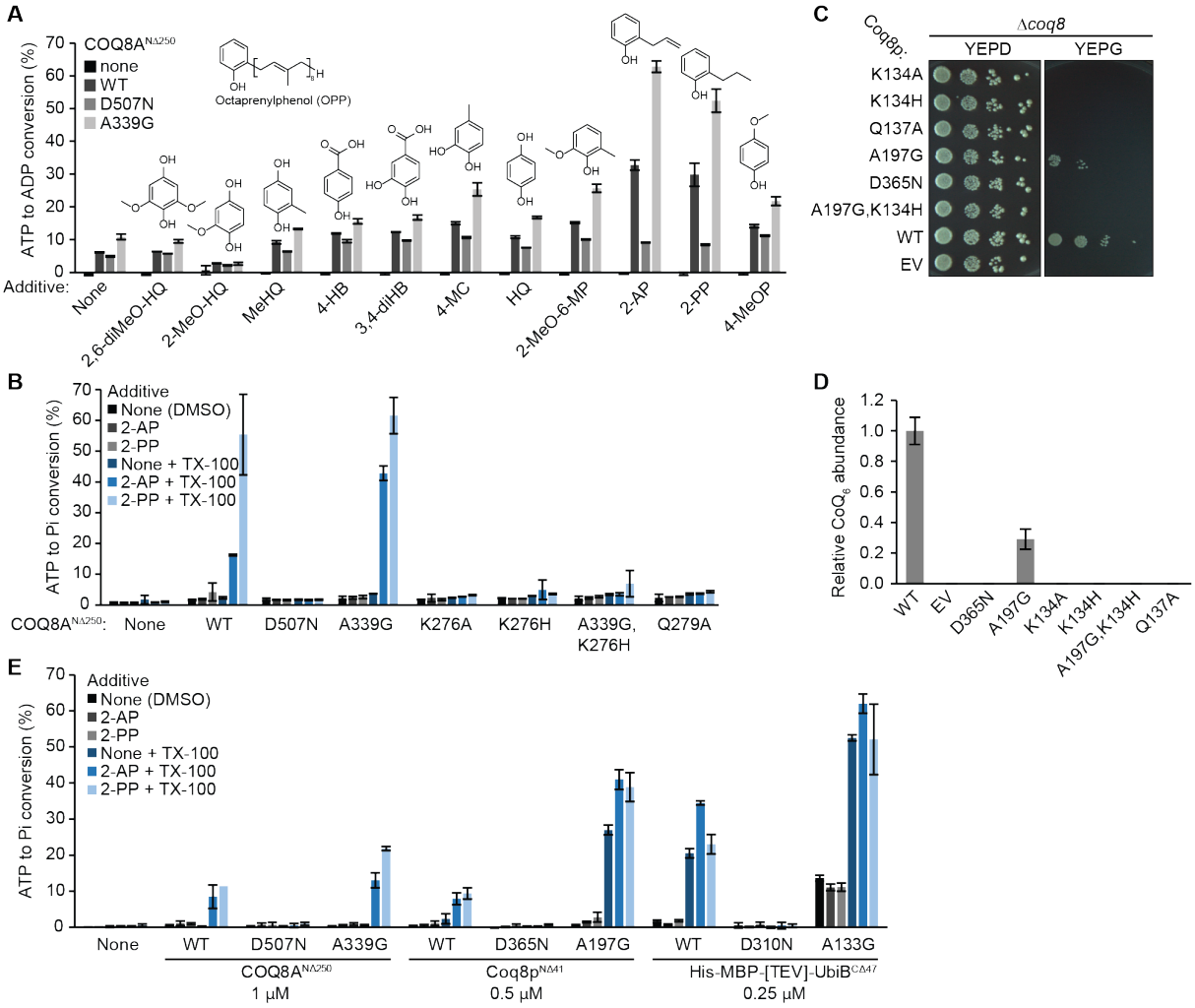

Figure 2. UbiB Family Members Are Activated by Triton X-100 and 2-Alkylphenols. (A) Screen of CoQ intermediate-like compounds with Triton X-100 in an ADP-Glo assay. 2,6-diMeO-HQ, 2,6-dimethoxyhydroquinone; 2-MeO-HQ, 2-methoxyhydroquinone; MeHQ, methylhydroquinone; 4-HB, 4-hydroxybenzoic acid; 3,4-diHB, 3,4-dihydroxybenzoic acid; 4-MC, 4-methylcatechol; HQ, hydroquinone; 2-MeO-6-MP, 2-methoxy-6-methylphenol; 2-AP, 2-allylphenol; 2-PP, 2-propylphenol; 4-MeOP, 4-methoxyphenol. (B) Malachite green ATPase assay

with COQ8A$^{N\Delta250}$ KxGQ mutants, Triton X-100, and 2-alkylphenols. Pi, inorganic phosphate. (C) Drop assay of Δ*coq8* transformed with KxGQ mutants. (D) Relative CoQ abundance from Δ*coq8* transformed with Coq8p variants. Error bars represent SD of three independent experiments. (E) Malachite green ATPase assay of UbiB family members from human, yeast, and *E. coli* with 2-alkylphenols and Triton X-100. Concentration of protein used is listed under the protein name, and reactions were incubated at 30 °C for 10 minutes rather than 45 minutes. For ATPase assays, error bars represent SD of technical triplicate measurements. See also Figure S2 and Table S3.

Mature COQ8 is activated by liposomes

Endogenous COQ8 contains a TM domain that anchors it to the inner mitochondrial membrane (IMM) facing the matrix where the other complex Q proteins reside and where it can potentially interact with CoQ intermediates[30-32]. This suggests that membrane association might be another important modulator of its activity, as has been shown for other membrane-bound kinases[33]. The mature N-termini of COQ8A and Coq8p (i.e., the N-termini present after cleavage of the mitochondrial sequences) begin 163 residues and 42 residues from the unprocessed N-terminus, respectively[12,30,34,35]. To test the effect of an intact TM domain on COQ8 membrane association and activity, we purified recombinant versions of the mature forms of COQ8A (COQ8A$^{N\Delta162}$) and Coq8p (Coq8p$^{N\Delta41}$) (Figure S3A).

Given that mature COQ8 resides on the IMM, we reasoned that mixing the protein with liposomes that contain IMM-enriched lipids, such as cardiolipin (CL) and phosphatidylethanolamine (PE)[36-38], along with the abundant membrane lipid phosphatidylcholine (PC), could have an effect on COQ8 membrane binding and activity. To test this, we first used a liposome flotation assay to determine how effectively COQ8 binds to liposomes (Figure 3A).

Without the TM domain, COQ8A$^{N\Delta250}$ exhibited moderate affinity for PC/PE/CL liposomes; however, the addition of the TM domain enabled near complete COQ8A$^{N\Delta162}$ and Coq8p$^{N\Delta41}$ liposome binding (Figures 3B). Strikingly, this association markedly enhanced the ATPase activity of COQ8A$^{N\Delta162}$ and Coq8p$^{N\Delta41}$ (Figure 3C), which is several orders of magnitude higher than autophosphorylation (Figure S3B). Similar to the results observed with phenols and Triton X-100, KxGQ mutants were not activated by liposomes (Figure S3C). These data imply that UbiB proteins, like other PKL family members, may be activated endogenously by binding to particular membrane environments.

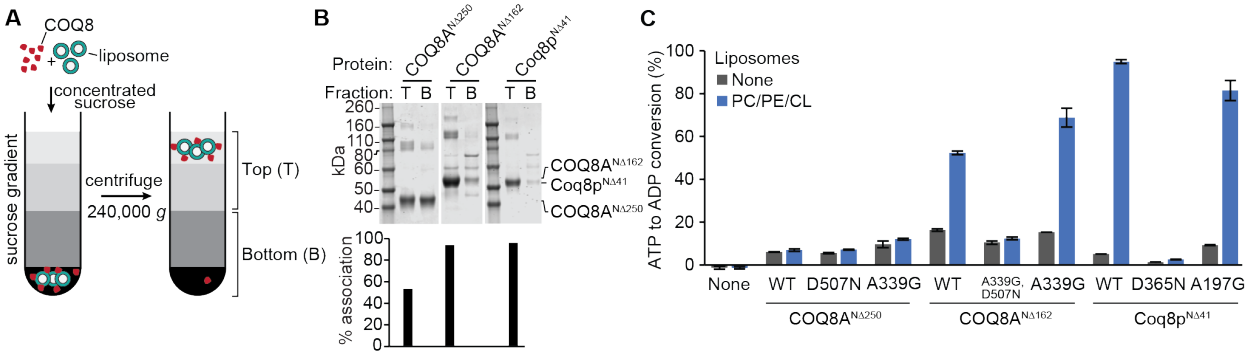

Figure 3. COQ8 Binds to Liposomes. (A) Schematic of a liposome flotation assay. (B) Coomassie stained SDS-PAGE from a liposome flotation assay with COQ8 and PC/PE/CL liposomes. T; top fraction, B, bottom fraction. (C) ADP-Glo assay with COQ8 variants and PC/PE/CL liposomes. Error bars represent SD of two independent experiments performed in technical triplicate. See also Figure S3.

Cardiolipin specifically increases COQ8 membrane interaction and ATPase activity

To determine whether the COQ8 membrane binding and activity is driven by a particular membrane component, we tested the ability of multiple individual lipids to activate COQ8 when

reconstituted in PC carrier liposomes. Remarkably, from amongst the eight individual species tested, only CL was able to activate COQ8 (Figure 4A). This increase in activity was matched by the superior ability of CL to facilitate binding of COQ8 to liposomes, indicating that CL activation of COQ8 is directly linked to its ability to mediate COQ8-membrane interactions (Figures 4B and S4A). Interestingly, COQ8 lacking its TM still preferentially bound to CL-containing liposomes (Figure S4B), but was not activated by them (Figure 3C), suggesting that the TM domain itself is a regulatory feature of COQ8.

To test whether liposome/CL binding specifically enhances the ATPase activity of COQ8, we performed [γ-^{32}P]ATP kinase reactions with liposomes to follow the location of the gamma phosphate. We also assessed autophosphorylation using SDS-PAGE and potential phosphorylation of copurifying lipid substrates or CL using thin-layer chromatography. Consistent with the activation of COQ8 by phenols, no autophosphorylation or lipid phosphorylation was observed (data not shown), further supporting the hypothesis that COQ8 acts as an ATPase (Figures S4C). Additionally, liposome activation of COQ8 did not alter its inability to phosphorylate purified protein substrates, including complex Q proteins and myelin basic protein (Figures S4D and S4E). Collectively, these data demonstrate that CL enables COQ8 membrane binding and enhances COQ8 ATPase activity.

COQ8 interacts with the membrane through its signature KxGQ domain

To further explore the nature of COQ8 membrane binding and activation, we used molecular dynamics to simulate the binding of COQ8A to membranes. Examination of the electrostatic surface potential of the soluble domain of COQ8A revealed an extensive positive patch generated primarily by the GQα1 and GQα4 helices that likely interacts with negatively charged

phospholipids found in the IMM, such as the CL used in our liposomes (Figures 4C and S4F). We then used coarse-grained molecular dynamics (CG-MD) simulations to investigate the binding of COQ8A to PC/PE/CL, mimicking the IMM-like membranes used in our liposome flotation assays, or to PC alone, mimicking a non-IMM membrane model. Invariably, the presence of CL at physiological concentration[36] was required to induce rapid (within the first microsecond) membrane association (Figure 4D and Movies S1 and S2) mediated by the GQα1 and GQα4 helices (Figures 4F), providing independent validation of our liposome flotation assay results. Interestingly, anchoring of COQ8A at the IMM is associated with local reorganization of lipids, featuring a strong segregation of CL species to the COQ8A interface (Figure 4E).

Our CG-MD simulations further predicted three positively charged residues of the GQα1 helix (R262, R265, and K269) as the key anchor points driving initial encounter of the soluble domain with the membrane via electrostatic interactions with cardiolipin phosphate heads (Figures S4G and S4H). To validate the importance of these residues, we purified a triple mutant of $COQ8A^{N\Delta 250}$ (R262A,R265A,K269A; Triple A) and measured its ability to bind liposomes. Indeed, this mutant demonstrated a large decrease in liposome association (Figures 4G and S4I). When the corresponding mutations were introduced into *COQ8,* its ability to rescue Δ*coq8* respiratory deficiency was significantly diminished, suggesting that these residues may have important ramifications for membrane binding and/or orientation *in vivo* (Figures 4H, S4J and S4K). Altogether, these simulations reinforce the importance of CL for COQ8 membrane association and suggest that the COQ8–CL interaction is driven by conserved residues in the signature KxGQ domain.

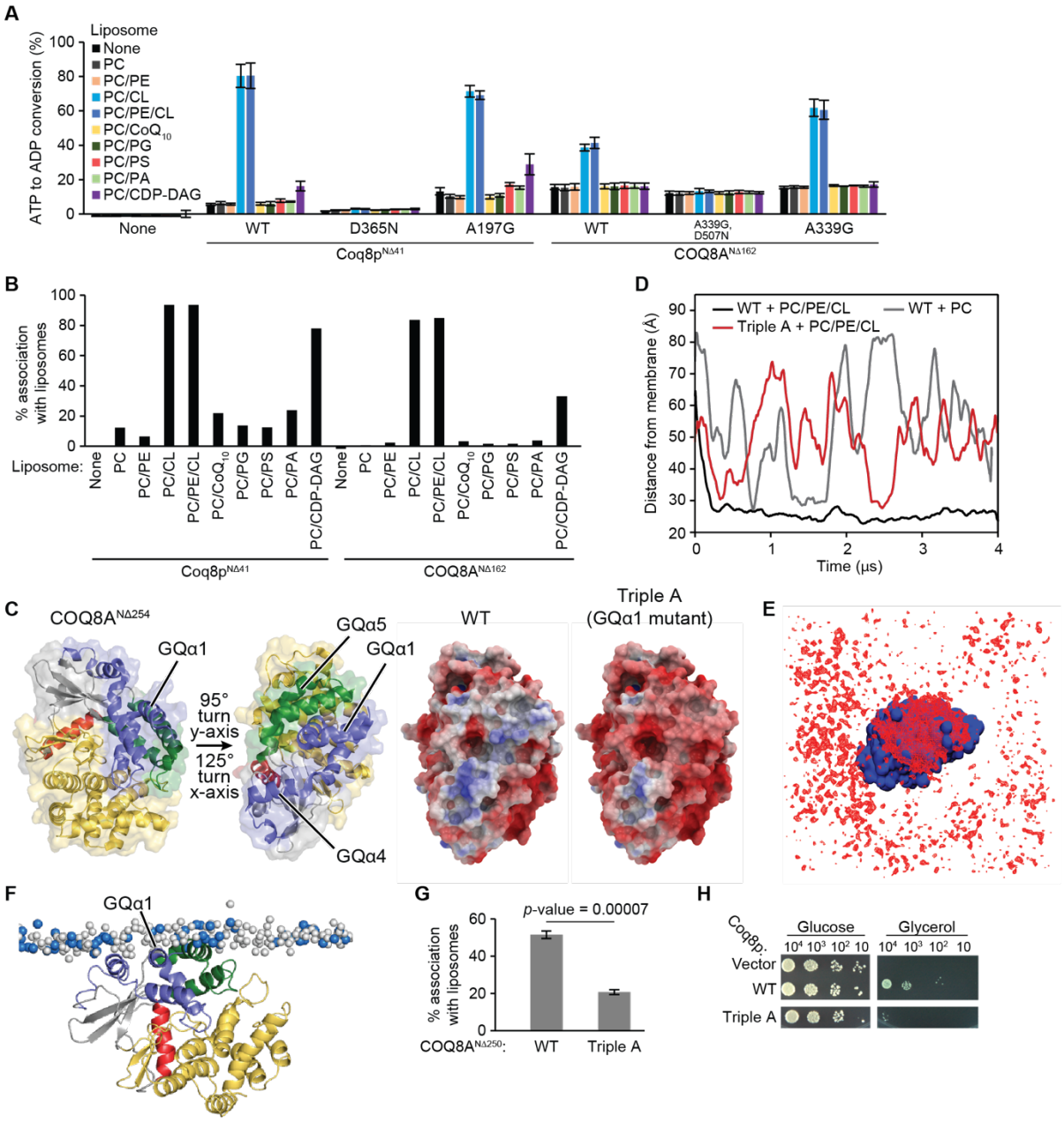

Figure 4. CL Enhances the ATPase Activity of COQ8 and Liposome Binding. (A) ADP-Glo assay with a panel of liposomes and TM domain-containing COQ8. Error bars represent SD of two independent experiments performed in technical duplicate. (B) Liposome flotation assay with a panel of PC based liposomes and TM domain-containing COQ8. (C) The two structures of COQ8A$^{N\Delta254}$ on the left are colored as described previously[12] and turned to show the orientation of the electrostatic maps. The KxGQ domain is colored in purple and green in the structures on the

left. On the right, there are electrostatic maps of COQ8A$^{N\Delta254}$ showing the positively charged region spanning GQα1, GQα4, and GQα5 (negative [−5 kcal/(mol•e) charge]: red, via white, to positive [+5 kcal/(mol•e) charge]: blue). (D) Time evolution of the distance between the center of mass of the protein and the center of mass of the phosphate heads of the leaflet it interacts with for CG-MD simulations of COQ8A$^{N\Delta254}$ with PC or PC/PE/CL liposomes or of the Triple A mutant with PC/PE/CL liposomes. (E) Average occupancy of CL phosphate heads (red) when COQ8A$^{N\Delta254}$ (blue) is centered throughout the trajectory. (F) Snapshot from a CG-MD simulation (t ~ 4 μs) showing the interaction of COQ8A$^{N\Delta254}$ with a PC/PE/CL membrane. CL phosphate heads are shown in blue, and PC/PE phosphate heads are shown in white. (G) Percent protein associating with liposomes from a liposome flotation assay with COQ8A$^{N\Delta250}$ WT and the Triple A mutant (R262A,R265A,K269A). Error bars represent SD of three independent experiments. (H) Serial dilutions of Δ*coq8* transformed with Coq8p WT or the Triple A mutant (R120A,K124A,K127A) on synthetic complete glucose (2% w/v) or glycerol (3% w/v) containing media. See also Figure S4.

Inhibition of Coq8p-*AS* activity disrupts CoQ biosynthesis

Our analyses above suggest that COQ8 is a conserved ATPase that is activated by lipids found in its native environment on the mitochondrial inner membrane. We next sought to determine whether acute chemical inhibition of COQ8 activity in this native environment would be sufficient to disrupt CoQ biosynthesis and respiratory function in yeast. To do so, we attempted to generate an analog-sensitive (*AS*) version of Coq8p (Coq8p-*AS*) that could be covalently modified by halomethyl ketone inhibitors[21,22,24].

To create Coq8p-*AS*, we first identified the putative Coq8p gatekeeper and conserved valine residues by performing sequence and structural alignments of Coq8p with RSK2, a kinase amenable to covalent inhibition by halomethyl ketone inhibitors (Figures 5A and 5B)[22]. These analyses suggested that methionine 303 (M303) is the Coq8p gatekeeper residue and that V202 occupies the position of a nonconserved cysteine present in mammalian p90 RSK family kinases. To further test this *in silico*, we mutated the gatekeeper to a smaller residue (M303C), and mutated V202 to a cysteine to enable reactivity with halomethyl ketone inhibitors (Figure 5C). Our models indicated that the WT Coq8p nucleotide-binding pocket was incapable of accepting CMK—a halomethyl ketone inhibitor designed specifically for kinases with a small gatekeeper and a cysteine on ß-strand 2 in place of a conserved valine—due to steric clashes with the methionine side chain (Figures 5D and S5A). However, the M303C and V202C mutations alleviated these steric clashes and enabled covalent modification by CMK, respectively (Figures 5E and 5F).

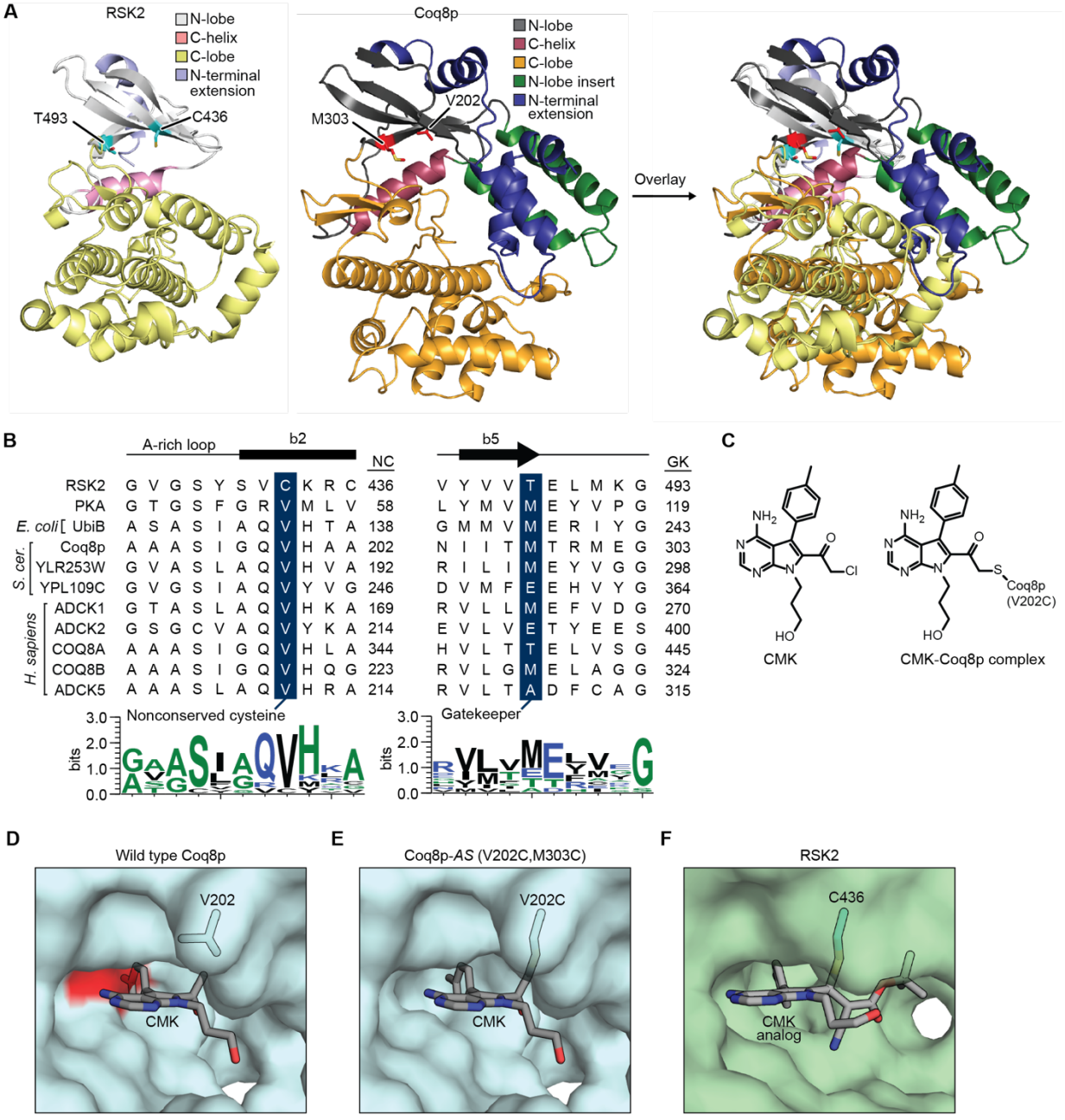

Figure 5. Creation of Analog-Sensitive Coq8p. (A) Structural alignment of a Coq8p homology model based on COQ8A (PDB: 5I35) with RSK2 (PDB: 4D9U). The nonconserved cysteine C436 and gatekeeper T493 residues of RSK2 are shown in cyan. The V202 and gatekeeper M303 residues of Coq8p are shown in red. (B) Primary sequence alignment of the nonconserved cysteine and gatekeeper residues from human RSK2, human PKA, and the UbiB family. Sequence logos

are shown for the displayed amino acid sequences. NC, nonconserved cysteine; GK, gatekeeper. (C) Structure of CMK and its covalent adduct with Coq8p. (D) Modeling of CMK (lacking the chlorine atom) in the active site of the homology model of Coq8p. The surface of M303 is colored in red demonstrating a steric clash with CMK. (E) Mutation of valine 202 and methionine 303 to cysteine (V202C,M303C) creates a binding pocket for, and allows covalent modification by, CMK. (E) Structure of RSK2 (PDB: 4D9U) with a cyanoacrylate CMK analog[39]. See also Figure S5.

To generate this putative Coq8p-*AS*, we expressed and purified Coq8p$^{N\Delta41}$ V202C,M303C from *E. coli* (Figure S5B). Using differential scanning fluorimetry[40], we tested the ability of Coq8p$^{N\Delta41}$ V202C,M303C to bind CMK. Consistent with the modeling predictions, only the V202C,M303C mutant was able to bind to the inhibitor CMK, which increased the melting temperature of the mutant by a remarkable 15 °C (Figures 6A and 6B). LC-MS/MS of an *in vitro* reaction containing Coq8p-*AS* and CMK revealed selective covalent modification of residue C202 by CMK (Figure S6A). The V202C,M303C mutant was able to rescue Δ*coq8* respiratory function (Figure 6C), demonstrating that the endogenous function of the protein is intact. Accordingly, in an *in vitro* ATPase assay, Coq8p$^{N\Delta41}$ V202C,M303C had activity in the presence of PC/CL liposomes, but was completely inactivated by CMK (Figure 6D).

To determine the effects of endogenous Coq8p inhibition, we treated Δ*coq8* yeast expressing Coq8p V202C,M303C with CMK and measured respiratory function and the *de novo* production of CoQ. Treatment of Coq8p-*AS* yeast with CMK caused a marked decrease in respiratory function, as indicated by severely delayed growth in liquid culture, whereas this treatment had very little effect on WT or empty vector (EV)-transformed yeast (Figure 6C). To

assess *de novo* CoQ biosynthesis, yeast were grown first in glucose-based media, and were then swapped into glycerol-based media containing heavy isotope labeled 4-hydroxybenzoic acid ($^{13}C_6$-4-HB), a precursor of the CoQ head group, and CMK (Figures 6E and S6B). Both media lacked *para*-amino benzoate (*p*ABA), an alternative CoQ precursor. Treatment of the V202C,M303C strain with CMK caused a rapid and near complete inhibition of *de novo* CoQ biosynthesis concomitant with an increase in the CoQ precursor, polyprenyl-hydroxybenzoate (PPHB) (Figures 6F and 6G). These data reveal that CMK added to yeast liquid culture is capable of accessing and inhibiting Coq8p-*AS* in its proper endogenous location within the mitochondrial matrix, and that COQ8 catalytic activity is required for CoQ precursor processing downstream of PPHB, consistent with earlier analyses of Δ*coq8* yeast and of strains harboring *COQ8* mutations. Collectively, our work defines lipid and small molecule modulators—both endogenous and custom *AS*-compounds—of an ancient atypical kinase-like protein. Additionally, our establishment of a chemical genetic system for acutely inactivating COQ8 will enable further dissection of the precise mechanistic role of COQ8 in CoQ biosynthesis.

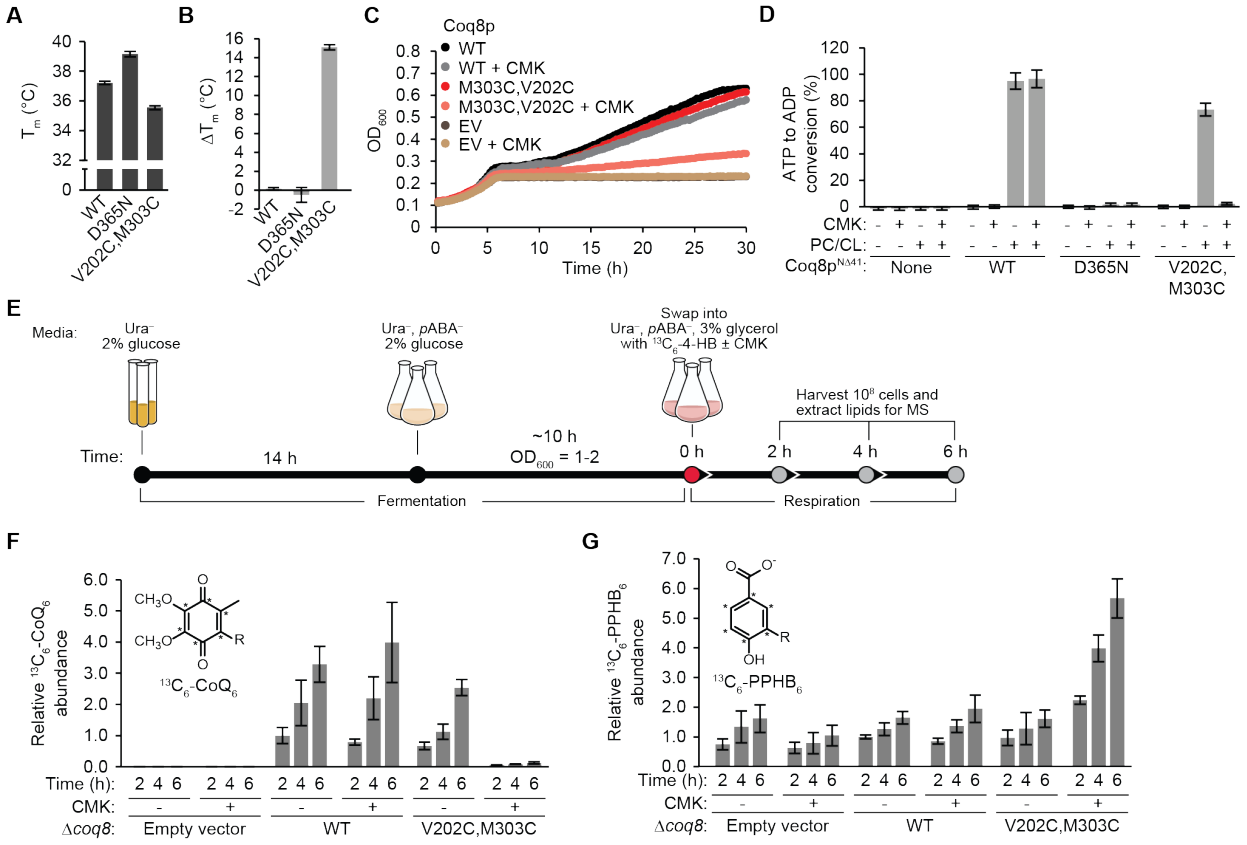

Figure 6. Acute Inhibition of Coq8p-AS (V202C,M303C) with CMK Decreases De Novo CoQ Biosynthesis. (A) Melting temperature of Coq8p variants measured with DSF. (B) ΔT_m for COQ8 variants with the inhibitor CMK. Error bars represent SD of three independent experiments performed in technical triplicate. (C) Growth curve of Δ*coq8* yeast transformed with Coq8p-*AS* and treated with CMK (20 μM) in Ura⁻, *p*ABA⁻ glucose (0.1% w/v) and glycerol (3% w/v) media. EV, empty vector. (D) ADP-Glo assay with Coq8p variants, PC/CL liposomes and the inhibitor CMK. Error bars represent SD of three independent experiments performed in technical triplicate. (E) Experimental scheme for heavy isotope labeling of CoQ_6 and $PPHB_6$ using $^{13}C_6$-4HB. (F) and (G) Relative abundance of $^{13}C_6$-CoQ_6 (*de novo* synthesized CoQ_6) and $^{13}C_6$-$PPHB_6$ from Δ*coq8* yeast transformed with Coq8p-*AS* and treated with $^{13}C_6$-4HB (50 μM) and CMK (20 μM) after 2, 4, and 6 hours in Ura⁻, *p*ABA⁻ glycerol (3% w/v) media measured using targeted LC-MS/MS.

Asterisk (*) indicates ^{13}C atoms; R, six isoprene units. Error bars represent SD from three biological replicates normalized to a CoQ_{10} internal standard. See also Figure S6.

Discussion

Coenzyme Q was discovered 60 years ago as a key component of the mitochondrial electron transport chain, yet multiple aspects of its biosynthesis remain obscure. One such aspect is the unexplained need for multiple auxiliary proteins that have no clear catalytic role in the pathway, including COQ8—a highly conserved member of the large protein kinase-like (PKL) superfamily. Given its PKL membership, COQ8 has been proposed to fill a regulatory gap in CoQ biosynthesis by phosphorylating other proteins in the CoQ pathway[20]. However, to date, no COQ8 *trans* protein kinase activity has been observed, demanding that other models for its activity be explored.

To further investigate the biochemical function of COQ8, we sought to study it in its native environment and to establish new tools to modulate its function. Multiple members of the PKL superfamily become activated by binding to endogenous molecules found at their sites of cellular activity, such as the activation of PKC or Akt by diacylglycerol and phosphatidylinositol 3,4,5-trisphosphate, respectively, at the plasma membrane[17,18,41]. Furthermore, protein-lipid interactions in general are becoming increasingly recognized as regulatory and structural features of proteins[42-44], indicating that it may be important to identify the full set of molecules that interact with COQ8 in order to elucidate its biochemical function.

Consistent with our recent results using Coq8p, our binding assays point to a conserved and selective interaction between COQ8 and precursors in the CoQ biosynthesis pathway. Curiously, these interactions seem to rely on the integrity of the COQ8 active site and result in an increase in COQ8 ATPase activity without affecting its inability to phosphorylate proteinaceous

substrates. In mitochondria, these precursors would most likely be found buried between the leaflets of the inner mitochondrial membrane (IMM) due to their extreme hydrophobicity. These data might suggest that COQ8 is poised to sense CoQ precursors within the membrane and to then couple the hydrolysis of ATP to the partial extraction of these lipids into the aqueous matrix environment where they could be modified by other CoQ biosynthesis enzymes. Alternatively, it remains possible that the observed ATPase activity is a proxy for small molecule kinase activity *in vivo*; however, as COQ8-dependent small molecule phosphorylation was not observed in our assays, these data indicate that endogenous small molecule substrate(s) would likely be distinct from the free hydroxyl group(s) of CoQ intermediates, the most intuitive candidate substrates.

Similar to PKC and Akt, our data also indicate that COQ8 is activated via interaction with a specific lipid—cardiolipin (CL). CL is a unique anionic, four-tailed lipid found at particularly high concentrations in the IMM where it influences the activity and stability of various mitochondrial membrane proteins[45-48], and promotes the formation of respiratory chain supercomplexes[49]. In addition to mere binding, our CG-MD simulations indicate that CL also directs the orientation of the soluble COQ8 domain along the membrane surface, perhaps thereby enabling COQ8's known interactions with other COQ proteins[30,50] and/or with membrane-embedded CoQ precursors. Furthermore, CL is thought to be distributed non-uniformly throughout the IMM[51], suggesting that the interaction of COQ8 with CL might seed complex Q formation at strategic sub-mitochondrial locations. These observations suggest models whereby the proper positioning of COQ8 at CL-rich domains on the mitochondrial inner membrane activates its ATPase activity as a requisite first step in enabling complex Q assembly and/or CoQ biosynthesis, and that exposure to CoQ intermediates at those sites can further enhance COQ8 function (Figure

7). Within this context, CG-MD shows once more to be a powerful resource to understand the molecular determinants underlying protein-lipid interplay.

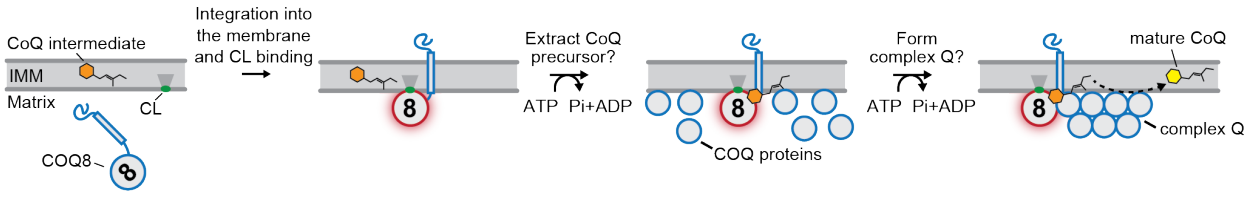

Figure 7. Model for How COQ8 ATPase Ability Could Facilitate CoQ Biosynthesis.

First, COQ8 is imported into the matrix. Binding to CL then facilitates COQ8's association with, and insertion into, the IMM with its soluble domain properly oriented along the membrane surface. Next, the CL-induced activation of COQ8 (red glow) allows it to advance CoQ biosynthesis by coupling the hydrolysis of ATP to the extraction of CoQ precursors out of the IMM and/or to the formation of complex Q.

More broadly, these results suggest an important and underappreciated connection between CoQ and CL—two quintessential mitochondrial lipids that enable oxidative phosphorylation (OxPhos). Indeed, CL has long been known to enable electron transfer between CI and CIII[52], and in plants, CL was found to have a positive effect on the electron transfer rate from CoQ to the photosynthetic reaction center[53]. Similarly, CL enhances electron transport from Complex I to CoQ in *Drosophila* mitochondrial lysate[54], and the CL remodeling phospholipase Cld1p was shown to rescue *coq7* hypomorphs in *S. cerevisiae* harboring mutations in Coq7p's hydrophobic α-helix that is predicted to bind the IMM[55]. These observations in conjunction with our data suggest a model whereby enhanced CL biosynthesis may augment OxPhos function in part by enabling the biosynthesis of CoQ via COQ8.

Testing these and other models of COQ8 function require new tools to modulate COQ8 activity in its endogenous setting where these activating molecules are present. To that end, we developed an analog-sensitive (*AS*) version of yeast Coq8p (Coq8p-*AS*). This chemical genetic strategy has proven to be highly effective for elucidating the functions of other PKL family members, but has never been attempted for the highly divergent UbiB family. Furthermore, this approach has not been attempted for kinases that reside within organelles where they would potentially be inaccessible to inhibitors. Our work demonstrates that endogenous chemical inhibition of COQ8 is sufficient to rapidly disrupt *de novo* CoQ biosynthesis, further suggesting that the catalytic activity of COQ8 is important for this pathway. Moreover, our demonstration that a UbiB family member is amenable to a chemical genetic system suggests that this tool can likewise be used to interrogate the functions of other family members, including Ypl109c and Ylr253w (Mcp2p) in yeast, the ABC1Ks in plants, and ADCK1, 2 & 5 in humans. These proteins have been implicated in diverse biological functions in cell migration[4], tumor cell viability[3,56], and lipid metabolism[2,57,58], each through unclear means. A chemical genetic approach would offer the opportunity to identify functions for these proteins without the added complexity of compensatory changes that accompany full gene knockouts.

Significance

UbiB proteins comprise a large and ancient family of protein kinase-like (PKL) molecules that spans all three domains of life. These proteins have been implicated in diverse cellular processes and are mutated in human diseases; however, little is known about their direct biochemical roles and activities. The main orthologous UbiB proteins investigated in this work—*S. cerevisiae* Coq8p and human COQ8A (jointly referred to as COQ8)—exemplify this problem: they are known to enable the biosynthesis of the key mitochondrial lipid, coenzyme Q (CoQ), but the mechanism is unclear. Investigations into the functions of other PKL family members have benefitted greatly from the identification of activating lipids and small molecules, and from the use of custom inhibitors, suggesting that such tools may likewise be beneficial in elucidating how UbiB proteins operate; however, such resources have not been established for this family. Our work helps to address these deficiencies by defining lipid and small molecule modulators of COQ8. We demonstrate that COQ8 exhibits a conserved ATPase activity that is activated by CoQ-like precursors and by binding to membranes that contain cardiolipin—a prevalent mitochondrial lipid enriched at the IMM where COQ8 resides. We also establish an "analog-sensitive" version of Coq8p that can be inhibited by small molecules *in vivo* and use this tool to demonstrate that acute inhibition of Coq8p is sufficient to cause CoQ deficiency and respiratory dysfunction. Collectively, our work advances our understanding of the core COQ8 biochemical function across evolution (ATPase activity), reveals how the positioning of COQ8 on the IMM is key to its activation, and provides effective new tools for the further investigation of the role of COQ8 in CoQ biosynthesis.

STAR Methods

Key Resource Table

REAGENT or RESOURCE	SOURCE	IDENTIFIER
Antibodies		
Coq8p antiserum	Catherine Clarke	NA
Anti-beta actin	Abcam	Cat#ab8224; RRID: AB_449644
Goat anti-rabbit secondary antibody	LI-COR	Cat#925-32211; RRID: AB_2651127
Goat anti-mouse secondary antibody	LI-COR	Cat#925-68070; RRID: AB_2651128
Bacterial and Virus Strains		
E. coli strain BL21-CodonPlus(DE3)-RIPL	Agilent	Cat#230280
E. coli strain DH5α	NEB	Cat#C2987I
Chemicals, Peptides, and Recombinant Proteins		
2,6-diMeO-HQ, 2,6-dimethoxyhydroquinone; 1,4-Dihydroxy-2,6-dimethoxybenzene	Sigma Aldrich	Cat#565032
2-MeO-HQ, 2-methoxyhydroquinone	Sigma Aldrich	Cat#176893
4-HB, 4-hydroxybenzoic acid	Sigma Aldrich	Cat#H20059
3,4-diHB, 3,4-dihydroxybenzoic acid	Sigma Aldrich	Cat#37580
4-MC, 4-methylcatechol	Sigma Aldrich	Cat#M34200
HQ, hydroquinone	Sigma Aldrich	Cat#H9003
2-MeO-6-MP, 2-methoxy-6-methylphenol	Sigma Aldrich	Cat#L167932
2-AP, 2-allylphenol	Sigma Aldrich	Cat#A34805
2-PP, 2-propylphenol	Sigma Aldrich	Cat#W352209
4-MeOP, 4-methoxyphenol	Sigma Aldrich	Cat#54050
MeHQ, methylhydroquinone	Sigma Aldrich	Cat#112968
L-α-phosphatidylcholine (Egg, Chicken); PC (Egg)	Avanti Polar Lipids	Cat#840051C
1,2-dioleoyl-sn-glycero-3-phosphoethanolamine-N-(7-nitro-2-1,3-benzoxadiazol-4-yl) (ammonium salt); NBD-PE 18:1	Avanti Polar Lipids	Cat#810145
1,2-dioleoyl-sn-glycero-3-phosphoethanolamine; PE 18:1	Avanti Polar Lipids	Cat#850725
1',3'-bis[1,2-dioleoyl-sn-glycero-3-phospho]-sn-glycerol (sodium salt); CL 18:1	Avanti Polar Lipids	Cat#710335C
Coenzyme Q_{10}; CoQ_{10}	Sigma Aldrich	Cat#C9538
1,2-dioleoyl-sn-glycero-3-phospho-(1'-rac-glycerol) (sodium salt); PG 18:1	Avanti Polar Lipids	Cat#840475C
1,2-dioleoyl-sn-glycero-3-phospho-L-serine (sodium salt); PS 18:1	Avanti Polar Lipids	Cat#840035C
1,2-dioleoyl-sn-glycero-3-(cytidine diphosphate) (ammonium salt); CDP-DAG	Avanti Polar Lipids	Cat#870520
PA 16:0 1,2-dipalmitoyl-sn-glycero-3-phosphate (sodium salt)	Avanti Polar Lipids	Cat#830855P
Triton X-100	Sigma Aldrich	Cat#T9284
Triton X-100 reduced	Sigma Aldrich	Cat#282103

CMK	MedChem Express	Cat#HY-52101 CAS: 821794-90-5
Coenzyme Q_6; CoQ_6	Avanti Polar Lipids	Cat#900150
CoQ_1	Sigma Aldrich	Cat#C7956
Ultra Pure ATP (for enzyme assays, comes with ADP-Glo kit)	Promega	Cat#V9102
SYPRO® Orange Protein Gel Stain	Invitrogen	Cat#S6651
ATP (for DSF)	Sigma Aldrich	Cat#A2383
ADP (for DSF)	Sigma Aldrich	Cat#A2754
[γ-^{32}P]ATP	Perkin Elmer	Cat#BLU002A001MCI
S. cerevisiae Coq8p$^{N\Delta41}$	Stefely et al., 2016	N/A
S. cerevisiae Coq8p$^{N\Delta41}$ K134H	Stefely et al., 2016	N/A
S. cerevisiae Coq8p$^{N\Delta41}$ A197G	Stefely et al., 2016	N/A
S. cerevisiae Coq8p$^{N\Delta41}$ A197G,K134H	Stefely et al., 2016	N/A
S. cerevisiae Coq8p$^{N\Delta41}$ V202C,M303C	This work	N/A
S. cerevisiae Coq8p$^{N\Delta41}$ D365N	Stefely et al., 2016	N/A
E. coli MBP-UbiB$^{C\Delta47}$ (8His-MBP-TEV-UbiB$^{C\Delta47}$)	This work	N/A
E. coli MBP-UbiB$^{C\Delta47}$ K70A (8His-MBP-TEV-UbiB$^{C\Delta47}$)	This work	N/A
E. coli MBP-UbiB$^{C\Delta47}$ A133G (8His-MBP-TEV-UbiB$^{C\Delta47}$)	This work	N/A
E. coli MBP-UbiB$^{C\Delta47}$ D310N (8His-MBP-TEV-UbiB$^{C\Delta47}$)	This work	N/A
E. coli MBP (8His-MBP-TEV-)	This work	N/A
H. sapiens COQ8A$^{N\Delta250}$	Stefely et al., 2015	N/A
H. sapiens COQ8A$^{N\Delta250}$ R262A,R265A,K269A (Triple A)	Stefely et al., 2015	N/A
H. sapiens COQ8A$^{N\Delta250}$ K276A	Stefely et al., 2015	N/A
H. sapiens COQ8A$^{N\Delta250}$ K276H	Stefely et al., 2015	N/A
H. sapiens COQ8A$^{N\Delta250}$ Q279A	Stefely et al., 2015	N/A
H. sapiens COQ8A$^{N\Delta250}$ A339G	Stefely et al., 2015	N/A
H. sapiens COQ8A$^{N\Delta250}$ A339G,K276H	Stefely et al., 2015	N/A
H. sapiens COQ8A$^{N\Delta250}$ D507N	Stefely et al., 2015	N/A
H. sapiens COQ8A$^{N\Delta162}$	This work	N/A
H. sapiens COQ8A$^{N\Delta162}$ A339G	This work	N/A
H. sapiens COQ8A$^{N\Delta162}$ A339G,D507N	This work	N/A
Cell-free COQ protein mix	Stefely et al., 2016	N/A
M. Musculus PKA	Stefely et al., 2016	N/A
CIP	NEB	Cat#M0290S
Myelin basic protein, dephosphorylated	Millipore/Fisher	Cat#NC9871399
Critical Commercial Assays		
CytoPhos Endpoint Phosphate Assay	Cytoskeleton Inc	Cat#BK054
ADP-Glo™ Kinase Assay	Promega	Cat#V9102
Experimental Models: Organisms/Strains		
S. cerevisiae strain W303	Jared Rutter lab	N/A
S. cerevisiae WT background strain BY4742 (*MAT*alpha his3Δ1 leu2Δ0 lys2Δ0 ura3Δ0)	Thermo	Cat#YSC1049
S. cerevisiae strain W303 Δ*coq8*	Stefely et al., 2015	N/A
S. cerevisiae BY4742 Δ*coq8*	Stefely et al., 2016	N/A
Oligonucleotides		
For all primers, see Table S4	This paper	N/A
Recombinant DNA		

pVP68K	Blommel et al. 2009	N/A
p426 GPD	Mumberg et al. 1995	N/A
pVP68K *S. cerevisiae* 8His-MBP-[TEV]-Coq8p$^{N\Delta41}$	Stefely et al., 2016	N/A
pVP68K *S. cerevisiae* 8His-MBP-[TEV]-Coq8p$^{N\Delta41}$ K134H	Stefely et al., 2016	N/A
pVP68K *S. cerevisiae* 8His-MBP-[TEV]-Coq8p$^{N\Delta41}$ A197G	Stefely et al., 2016	N/A
pVP68K *S. cerevisiae* 8His-MBP-[TEV]-Coq8p$^{N\Delta41}$ A197G,K134H	Stefely et al., 2016	N/A
pVP68K *S. cerevisiae* 8His-MBP-[TEV]-Coq8p$^{N\Delta41}$ V202C,M303C	This work	N/A
pVP68K *S. cerevisiae* 8His-MBP-[TEV]-Coq8p$^{N\Delta41}$ D365N	Stefely et al., 2016	N/A
pVP68K *E. coli* 8His-MBP-[TEV]-UbiB$^{C\Delta47}$	This work	N/A
pVP68K *E. coli* 8His-MBP-[TEV]-UbiB$^{C\Delta47}$ K70A	This work	N/A
pVP68K *E. coli* 8His-MBP-[TEV]-UbiB$^{C\Delta47}$ A133G	This work	N/A
pVP68K *E. coli* 8His-MBP-[TEV]-UbiB$^{C\Delta47}$ D310N	This work	N/A
pVP68K *H. sapiens* 8His-MBP-[TEV]-COQ8A$^{N\Delta250}$	Stefely et al., 2015	N/A
pVP68K *H. sapiens* 8His-MBP-[TEV]-COQ8A$^{N\Delta250}$ R262A,R265A,K269A (Triple A)	This work	N/A
pVP68K *H. sapiens* 8His-MBP-[TEV]-COQ8A$^{N\Delta250}$ K276A	Stefely et al., 2015	N/A
pVP68K *H. sapiens* 8His-MBP-[TEV]-COQ8A$^{N\Delta250}$ K276H	Stefely et al., 2015	N/A
pVP68K *H. sapiens* 8His-MBP-[TEV]-COQ8A$^{N\Delta250}$ Q279A	Stefely et al., 2015	N/A
pVP68K *H. sapiens* 8His-MBP-[TEV]-COQ8A$^{N\Delta250}$ A339G	Stefely et al., 2015	N/A
pVP68K *H. sapiens* 8His-MBP-[TEV]-COQ8A$^{N\Delta250}$ A339G,K276H	Stefely et al., 2015	N/A
pVP68K *H. sapiens* 8His-MBP-[TEV]-COQ8A$^{N\Delta250}$ D507N	Stefely et al., 2015	N/A
pVP68K *H. sapiens* 8His-MBP-[TEV]-COQ8A$^{N\Delta162}$	This work	N/A
pVP68K *H. sapiens* 8His-MBP-[TEV]-COQ8A$^{N\Delta162}$ A339G	This work	N/A
pVP68K *H. sapiens* 8His-MBP-[TEV]-COQ8A$^{N\Delta162}$ A339G,D507N	This work	N/A
p426 GPD *S. cerevisiae COQ8*	Stefely et al., 2015	N/A
p426 GPD *S. cerevisiae COQ8* R120A,K124A,K127A	This work	N/A
p426 GPD *S. cerevisiae COQ8* K134A	Stefely et al., 2015	N/A
p426 GPD *S. cerevisiae COQ8* K134H	Stefely et al., 2015	N/A
p426 GPD *S. cerevisiae COQ8* Q137A	Stefely et al., 2015	N/A
p426 GPD *S. cerevisiae COQ8* A197G	Stefely et al., 2015	N/A
p426 GPD *S. cerevisiae COQ8* A197G,K134H	This work	N/A
p426 GPD *S. cerevisiae COQ8* V202C,M303C	This work	N/A
p426 GPD *S. cerevisiae COQ8* D365N	Stefely et al., 2015	N/A
Software and Algorithms		
Topspin	Bruker	N/A
NMRbot	Clos et al., 2013	N/A
NMRmix	Stark et al., 2016	N/A
MestReNova	Mestrelab Research	N/A

SWISS-MODEL	Biasini, et al., 2014	https://swissmodel.expasy.org/
PyMOL	Schrödinger, LLC (Version 1.8)	https://sourceforge.net/projects/pymol/
UCSF Chimera	Pettersen et al., 2004	https://www.cgl.ucsf.edu/chimera/
GROMACS v. 5 and above	Pronk et al., 2013; Abraham et al., 2015	http://www.gromacs.org/Downloads
VMD	Humphrey et al., 1996	http://www.ks.uiuc.edu/Development/Download/download.cgi?PackageName=VMD
ICM	Abagyan et al., 1994	http://www.molsoft.com/download.html
Image Studio v5.2 software	LI-COR	https://www.licor.com/bio/products/software/image_studio/?gclid=CjwKEAjw_PfGBRDW_sutqMbQsmMSJAAMpUapnCbeDQSTBAWjOLZv7FuyOMGKZxDTzL0XUOTKhqx6_RoCFMrw_wcB
SigmaPlot v13.0	SYSTAT Software	http://www.sigmaplot.co.uk/products/sigmaplot/sigmaplot-details.php
COMPASS	Wenger et al., 2011	http://www.mybiosoftware.com/omssa-2-1-9-msms-peptide-spectra-identification.html
Martini force field	Marrink et al., 2007	http://cgmartini.nl/index.php/force-field-parameters
Other		
Silica TLC	Fisher Scientific	Cat#M1057210001
TLC PEI Cellulose F, 25 Plastic sheets 20 x 20 cm	VWR	Cat#1.05579.0001

Contact for Reagent and Resource Sharing

Further information and requests for resources and reagents should be directed to and will be fulfilled by the Lead Contact, Dave Pagliarini (dpagliairini@morgridge.wisc.edu).

Experimental Model and Subject Details

Escherichia coli strain DH5α (NEB) was used for all cloning applications and grown at 37 °C in LB media [tryptone (10 g/L), yeast extract (5 g/L), NaCl (5 g/L)] with antibiotics. *Escherichia coli* strain BL21-CodonPlus (DE3)-RIPL (Agilent) was used for all protein expression and purification purposes and grown in autoinduction media (900 mL TB+G, 100 mL PO_4^- mix, 50 mL 20× 80155, 25 mL 15% aspartate buffer, 2 mL 1M $MgSO_4$, 2 mL 15 mg/mL chloramphenicol stock (in ethanol), and 2 mL 60.6 mg/mL kanamycin stock). TB+G: tryptone (12 g/L), yeast extract (24 g/L), 10% (w/v) glycerol (40 mL/L) and autoclaved to sterilize. PO_4^- mix: KH_2PO_4 (23.1 g/L), K_2HPO_4 (125.4 g/L) and autoclaved to sterilize. 15% aspartate buffer: aspartate (150 g/L) and NaOH (44.6 g/L) pH 6.5-7.0 and autoclaved to sterilize. 20× 80155: glucose (3 g/L), α-lactose monohydrate (100 g/L), glycerol (160 g/L) and autoclaved to sterilize. 1M $MgSO_4$, 15 mg/mL chloramphenicol, and 60.6 mg/mL kanamycin stocks were sterilized by filtration (0.22 μm pore size). 1 x 10^{11} *E.coli* cells (grown in LB with antibiotics) were seeded in 500 mL of autoinduction media and incubated for 3 h at 37 °C and 19 h at 21 °C (230 rpm). See the following method below for more details: Recombinant Protein Expression and Purification. For yeast rescue assays in Figures 2C, 2D, 4H, S4J and S4K, *Saccharomyces cerevisiae* strain W303 was used. For the analog-sensitive experiments (Figure 6C, 6F and 6G), *Saccharomyces cerevisiae* strain BY4742 was used. Ura^- media contained Ura^- drop-out mix (1.92 g/L), yeast nitrogen base (6.7 g/L, with ammonium sulfate and without amino acids), and a carbon source of glucose and/or glycerol. Ura^- media contained Ura^-, *p*ABA^- drop-out mix (770 mg/L), yeast nitrogen base (6.7 g/L, with ammonium sulfate and without amino acids), and a carbon source of glucose and/or glycerol. Synthetic Ura^- media were sterilized by filtration (0.22 μm pore size). See the following methods

below for more details: Yeast Drop Assay and Growth Curves, Growth of Yeast and Extraction of Yeast CoQ_6 for LC-MS Quantitation, and Immunoblotting of Yeast Coq8p.

Method Details

NMR screening

One dimensional (1D) NMR ligand-affinity screens provide a quick and effective approach to identify small molecules from a large library of compounds that interact with a protein[59-61]. We used a 1D ^{1}H NMR ligand affinity screen to identify interacting small molecules from a library of 417 compounds, which consists primarily of metabolites, substrates, inhibitors, etc (Table S2). To minimize the materials required to evaluate every compound with $COQ8A^{N\Delta250}$, the compounds were combined into 89 mixtures of 3-5 compounds each. The mixtures were designed to minimize ^{1}H peak signal overlap between the compounds using NMRmix[62]. Two sets of NMR samples were created for each mixture: one with $COQ8A^{N\Delta250}$ and one without $COQ8A^{N\Delta250}$. The NMR samples were prepared in 15 mM bis-Tris-d_{19} buffer at pH 7.4 with 250 μM NaCl, 0.04% NaN_3, and 15 μM DSS in in 99.99% D_2O and placed in 3 mm SampleJet NMR tubes. Each NMR sample had a 75 μM final concentration for each compound in the mixture and a final $COQ8A^{N\Delta250}$ concentration of 6 μM in the set of samples containing protein. The NMR spectra were collected on a Bruker Avance III 600 MHz spectrometer equipped with a 5 mM cryoprobe and a SampleJet sample changer set at 25 °C, and Topspin v3 (Bruker) and NMRbot were used to automate the data collection process[63]. The 1D ^{1}H spectra were collected for all samples using a Carr-Purcell-Meiboom-Gill (CPMG) pulse sequence with f_1 presaturation and 128 averaged transients consisting of 16,384 time-domain points and a sweep width of 12 ppm.

The 1D ^{1}H spectra were phased, baseline corrected, referenced to DSS, and analyzed using MestReNova 11 (Mestrelab Research). The spectra of the mixtures with COQ8A$^{N\Delta250}$ were visually compared to the spectra of the mixtures without COQ8A$^{N\Delta250}$. If the peak intensities of a compound in a mixture showed a substantial decrease (typically >50%) in the presence of COQ8A$^{N\Delta250}$, the compound would be considered a "hit" or interacting compound. The screen of the compound library with COQ8A$^{N\Delta250}$ identified 25 interacting compounds (Table S2).

Computational Modeling and Coarse-Grained Molecular Dynamics Simulations

All simulations were performed using the GROMACS[64,65] simulation package version 5.0.4. The systems were described with the MARTINI[66] CG force field, together with the ElNeDyn[67] approach to maintain the secondary and tertiary structure of the protein. CG-MD simulations based on the MARTINI force field have been previously used with success for different systems to investigate protein-lipid interactions[68-71].

The systems were built with center of mass of COQ8A (PDB: 4PED) 70 Å away from the surface of the membrane and checked for whether the protein approaches and interacts with the membrane. Inner mitochondrial membrane (IMM) models were built according to the experimental molecular ratio of CL observed for bovine heart mitochondria, namely 15 to 20% of the phosphorus content[72]. Therefore, IMM mimics were featuring a lipid concentration of 16% CL/41% POPC/37% POPE/6% DSPC, while generic membrane models featuring 100% POPC lipids were built as control. Lipid bilayers of 130 × 130 Å^2 were generated using the insane (INSert membrANE)[73] method of MARTINI. Systems were solvated with polarizable CG water and counter ions were added to neutralize the system. Following solvation, systems were energy minimized with a timestep of 5 fs. Successive equilibrations with decreasing restraints were

performed in order to obtain a fully equilibrated system (force constants of 1000, 500, 250 and 0 kJ/mol applied on protein particles, 10 ns of run with a timestep of 10 fs for each). In the production phase, which is 4 μs for all simulations, the protein, membrane and the aqueous phase (water and ions) were coupled independently to an external bath at 310 K and 1 bar. Three MD repeats with randomized initial velocities were performed for each membrane system and they yielded consistent results. Average occupancy of cardiolipins was calculated using VMD's VolMap plugin[74].

Atomistic models of the different GQα mutated COQ8A proteins were built in PyMOL by mutating the following residues to alanine: R262, R265, K269 for ΔGQα1; K310, K314 for ΔGQα4; R262, R265, K269, K310, K314 for ΔGQα1α4; Q366, S367, N369, S370, N373, N374 for ΔGQα5. The effect of these mutations on the electrostatic potential surface of the protein was visualized through the ICM-REBEL module of the ICM program[75]. CG-MD simulations were performed for these four mutants following the procedure explained above, where the residues listed for each mutant were altered by the removal of charges of the polarizable CG beads, to knockout Coulomb interactions without changing the residue types.

Modeling of Coq8p-*AS* with CMK

A homology model of Coq8p-*AS* was generated by SWISS-MODEL using the nucleotide-bound form of COQ8A (PDB: 5I35) as a template (RMSD 0.35 Å over 2264 of 2590 aligned atoms)[76]. To understand the likely position of the bulky analog CMK bound to Coq8p-*AS*, CMK was superposed on the adenine ring and C1' atoms of the nucleotide in 5I35 (RMSD 0.064 Å over 11 paired atoms.) Clashes were relieved in UCSF Chimera by a small rigid body displacement of CMK, adjusting torsion angles of CMK[77]. The cealign PyMOL command was used to overlay the

Coq8p homology model and RSK2 (PDB: 4D9U) (RMSD of 4.75 Å over 120 residues). Sequence logos were created with WebLogo3[78].

DNA Constructs and Cloning

Cloning of COQ8A$^{N\Delta250}$, Coq8p$^{N\Delta41}$, PKA, and p426 GPD *COQ8* plasmids was previously described[11,12]. For MBP-UbiB$^{C\Delta47}$ and COQ8A$^{N\Delta162}$ standard PIPE cloning methods[79] were used. PIPE reactions were DpnI digested and transformed into DH5α competent *E. coli* cells. Plasmids were isolated from transformants and DNA sequencing was used to identify those containing the correct constructs. pVP68K, a plasmid for expression of recombinant proteins in bacteria [8His-cytoplasmically-targeted maltose-binding protein (MBP) with a linker including a tobacco etch virus (TEV) protease recognition site fused to the protein construct (8His-MBP-[TEV]-Protein)], has been described previously[80]. Oligonucleotides were purchased from IDT (Coralville, IA, USA). For yeast rescue experiments, *COQ8* was cloned into the p426 GPD vector[81]. Point mutations were introduced by PCR-based mutagenesis and confirmed by DNA sequencing.

Recombinant Protein Expression and Purification

Human COQ8A$^{N\Delta162}$ and COQ8A$^{N\Delta250}$. Method adapted from[11,12]. COQ8A constructs were overexpressed in *E. coli* by autoinduction (Fox and Blommel, 2009). Cells were isolated and frozen at –80 °C until further use. For protein purification, cells were thawed, resuspended in Lysis Buffer [20 mM HEPES (pH 7.2), 300 mM NaCl, 10% glycerol, 5 mM 2-mercaptoethanol (BME) or 0.5 mM tris(2-carboxyethyl)phosphine (TCEP), 0.25 mM phenylmethylsulfonyl fluoride (PMSF)] (4 °C). The cells were lysed by sonication (4 °C, 75% amplitude, 10 s × 3). The lysate was clarified by centrifugation (15,000 *g*, 30 min, 4 °C). The cleared lysate was mixed with cobalt IMAC resin

(Talon resin) and incubated (4 °C, 1 h). The resin was pelleted by centrifugation (700 *g*, 2 min, 4 °C) and washed four times with Wash Buffer [50 mM HEPES (pH 7.2), 300 mM NaCl, 10% glycerol, 5 mM BME, 0.25 mM PMSF, 10 mM imidazole]. His-tagged protein was eluted with Elution Buffer [20 mM HEPES (pH 7.2), 300 mM NaCl, 10% glycerol, 5 mM BME or 0.5 mM TCEP, 0.25 mM PMSF, 100 mM imidazole]. The eluted protein was concentrated with a MW-cutoff spin filter (50 kDa MWCO) and exchanged into Storage Buffer [20 mM HEPES (pH 7.2), 300 mM NaCl, 10% glycerol, 5 mM BME or 0.5 mM TCEP]. The concentration of 8His-MBP-[TEV]-COQ8A$^{N\Delta250}$ was determined by its absorbance at 280 nm (ε = 96,720 M^{-1} cm^{-1}) (MW = 89.9 kDa) and 8His-MBP-[TEV]-COQ8A$^{N\Delta162}$ (ε = 96,720 M^{-1} cm^{-1}) (MW = 99.26 kDa). The fusion protein was incubated with Δ238TEV protease (1:50, TEV/fusion protein, mass/mass) (1 h, 20 °C). The TEV protease reaction mixture was mixed with cobalt IMAC resin (Talon resin), incubated (4 °C, 1 h). The resin was pelleted by centrifugation (700 *g*, 3 min, 4 °C). The unbound COQ8A was collected and concentrated with a MW-cutoff spin filter (30 kDa MWCO) and exchanged into storage buffer. The concentration of COQ8A$^{N\Delta250}$ was determined by its absorbance at 280 nm (ε = 28,880 M^{-1} cm^{-1}) (MW = 45.6 kDa). The concentration of COQ8A$^{N\Delta162}$ was determined by its absorbance at 280 nm (ε = 28,880 M^{-1} cm^{-1}) (MW = 54.99 kDa). The protein was aliquoted, frozen in $N_{2(l)}$, and stored at –80 °C. Fractions from the protein preparation were analyzed by SDS-PAGE.

Yeast Coq8p$^{N\Delta41}$. Coq8p$^{N\Delta41}$ plasmid constructs were transformed into RIPL competent *E. coli* cells for protein expression. 8His-MBP-[TEV]-Coq8p$^{N\Delta41}$ was overexpressed in *E. coli* by autoinduction. Cells were isolated by centrifugation, frozen in $N_{2(l)}$, and stored at –80 °C until further use. For protein purification, cells were thawed on ice, resuspended in Lysis Buffer [50

mM HEPES (pH 7.5), 150 mM NaCl, 5% glycerol, 1 mM BME, 0.25 mM PMSF, 1 mg/mL lysozyme, pH 7.5] and incubated (1 h, 4 °C). The cells were lysed by sonication (4 °C, 6 V, 60 s × 4). The lysate was clarified by centrifugation (15,000 *g*, 30 min, 4 °C). The cleared lysate was mixed with cobalt IMAC resin (Talon resin) and incubated (4 °C, 1 h). The resin was pelleted by centrifugation (700 *g*, 5 min, 4 °C) and washed four times with Wash Buffer [50 mM HEPES (pH 7.5), 150 mM NaCl, 5% glycerol, 1 mM BME, 0.25 mM PMSF, 10 mM imidazole, pH 7.5] (10 resin bed volumes). His-tagged protein was eluted with Elution Buffer [50 mM HEPES (pH 7.5), 150 mM NaCl, 5% glycerol, 1 mM BME, 100 mM imidazole, pH 7.5]. The eluted protein was concentrated with a MW-cutoff spin filter (50 kDa MWCO) and exchanged into storage buffer [50 mM HEPES (pH 7.5), 150 mM NaCl, 5% glycerol, 1 mM BME, pH 7.5]. The concentration of 8His-MBP-[TEV]-Coq8p$^{N\Delta41}$ was determined by its absorbance at 280 nm (ε = 109,210 M^{-1} cm^{-1}) (MW = 96.2 kDa). The fusion protein was incubated with Δ238TEV protease (1:50, TEV/fusion protein, mass/mass) (1 h, 20 °C). The TEV protease reaction mixture was mixed with cobalt IMAC resin (Talon resin) and incubated (4 °C, 1 h). The unbound Coq8p$^{N\Delta41}$ was isolated and concentrated with a MW-cutoff spin filter (30 kDa MWCO) and exchanged into Storage Buffer. The concentration of Coq8p$^{N\Delta41}$ was determined by its absorbance at 280 nm (ε = 41,370 M^{-1} cm^{-1}) (MW = 52 kDa). The protein was aliquoted, frozen in $N_{2(l)}$, and stored at –80 °C. Fractions from the protein preparation were analyzed by SDS-PAGE.

Mouse PKA. 8-His-MBP-PKA and PKA (mouse PKA, Prkaca) were isolated as described above for Coq8p$^{N\Delta41}$. The concentration of 8His-MBP-[TEV]-PKA was determined by its absorbance at 280 nm (ε = 121,700 M^{-1} cm^{-1}) (MW = 84.8 kDa). The concentration of PKA was determined by its absorbance at 280 nm (ε = 53,860 M^{-1} cm^{-1}) (MW = 40.5 kDa).

E. coli MBP-UbiB$^{C\Delta47}$ and MBP. 8His-MBP-[TEV]-UbiB$^{C\Delta47}$ and 8His-MBP-[TEV]- were overexpressed in *E. coli* by autoinduction. Cells were isolated and frozen at –80 °C until further use. For protein purification, cells were thawed, resuspended in Lysis Buffer [50 mM HEPES (pH 7.2), 300 mM NaCl, 10% glycerol (w/v), 5 mM BME, 0.25 mM PMSF] (4 °C). The cells were lysed by sonication (4 °C, 75% amplitude, 20 s × 2). The lysate was clarified by centrifugation (15,000 *g*, 30 min, 4 °C). The cleared lysate was mixed with cobalt IMAC resin (Talon resin) and incubated (4 °C, 1 h). The resin was pelleted by centrifugation (700 *g*, 5 min, 4 °C) and washed four times with Wash Buffer [20 mM HEPES (pH 7.2), 300 mM NaCl, 10% glycerol, 5 mM BME or 0.5 mM TCEP, 0.25 mM PMSF, 10 mM imidazole]. His-tagged protein was eluted with Elution Buffer [50 mM HEPES (pH 7.2), 300 mM NaCl, 10% glycerol, 5 mM BME, 0.25 mM PMSF, 100 mM imidazole]. The eluted protein was concentrated with a MW-cutoff spin filter (50 kDa MWCO) and exchanged into storage buffer [50 mM HEPES (pH 7.2), 300 mM NaCl, 10% glycerol, 5 mM BME]. The concentration of 8His-MBP-[TEV]-MBP-UbiB$^{C\Delta47}$ was determined by its absorbance at 280 nm (ε = 142,670 M^{-1} cm^{-1}) (MW = 102.1 kDa). 8His-MBP-[TEV]- (ε = 67,840 M^{-1} cm^{-1}) (MW = 44.284 kDa). The protein was aliquoted, frozen in $N_{2(l)}$, and stored at –80 °C. Fractions from the protein preparation were analyzed by SDS-PAGE.

Nucleotide Binding

The general differential scanning fluorimetry (DSF) method (thermal shift assay) has been described previously[40]. Mixtures (20 μL total volume) of Coq8p$^{N\Delta41}$ (2 μM) were prepared with SYPRO Orange dye (Life Tech.) (2×), NaCl (150 mM), HEPES (100 mM, pH 7.5), and ligands (e.g. MgATP). Otherwise, the general DSF method, ligand screen, and dissociation constant

experiments were conducted for $COQ8A^{N\Delta250}$ as previously described[12]. $Coq8p^{N\Delta41}$ proteins used for DSF analysis were prepared as described.

ADP-Glo Assay

ADP-Glo (Promega) was performed according to the manufacturer's instruction with the following modifications. All solutions were diluted in HBS (150 mM NaCl, 20 mM HEPES pH 7.5). $Coq8p^{N\Delta41}$ (1 μM), $COQ8A^{N\Delta250}$ (2 or 4 μM), $COQ8A^{N\Delta162}$ (2 μM), or MBP-$UbiB^{C\Delta47}$ (0.5 μM) were mixed with liposomes (~3.33 mM), ATP (100 μM), $MgCl_2$ (4 mM), CMK (20 μM) or DMSO (0.2% v/v), Triton X-100 (1 mM) or reduced Triton X-100 (1 mM) (Sigma Aldrich), and CoQ headgroup analogs (Sigma Aldrich) dissolved as 200 mM stock solutions in DMSO (2-PP, 2-propylphenol; 2-MeO-6-MP, 2-methoxy-6-methylphenol; 4-methylcatechol; 4-HB, 4-hydroxybenzoic acid; 2-MeO-HQ, 2-methoxyhydroquinone; 4-MeOP, 4-methoxyphenol; 2-AP, 2-allylphenol; HQ, hydroquinone; 3,4-di-HB, 3,4-dihydroxybenzoic acid; MeHQ, methylhydroquinone; 2,6-diMeO-HQ, 2,6-dimethoxyhydroquinone) (1 mM) (final concentrations for reaction components). Reactions were incubated (30 °C, 45 min). Then ADP-Glo Reagent (5 μL) was added and incubated (40 min, r.t. [~21 °C], covered). Kinase Detection Reagent was added (10 μL) and incubated (40 min, r.t., covered). Luminescence was read using default values on a Biotek Cytation 3 plate reader. An ADP/ATP standard curve was made according to the manufacturer's instructions. Error bars represent SD of technical triplicate measurements unless otherwise specified.

Cytophos ATPase Assay

The Cytophos ATPase assay (Malachite green) was performed according to the manufacturer's instruction with the following modifications. All solutions were diluted in HBS (150 mM NaCl, 20 mM HEPES pH 7.5). COQ8A$^{N\Delta250}$ (1 μM final), Coq8p$^{N\Delta41}$ (1 μM final), COQ8A$^{N\Delta162}$ (1 μM final) or MBP-UbiB$^{C\Delta47}$ (0.25 μM final) with 100 μM ATP, 4 mM $MgCl_2$, 1 mM 2-alkylphenol, 0.5 mM CoQ_1, 1 mM Triton X-100 or reduced Triton X-100. CoQ_1 was reduced by adding 1.2 fold molar excess of $NaBH_4$ (Sigma) (10 min, r.t.). Reactions were incubated (30 °C, 45 min) and 35 μL of Cytophos reagent was added and incubated (10 min, r.t.). Absorbance was measured at 650 nm. Reactions in Figure 2E were incubated for 10 min rather than 45 min and [Coq8p$^{N\Delta41}$] was 0.5 μM. The standard curve ranged from 0–50 μM phosphate. Error bars represent SD of technical triplicate measurements unless otherwise specified.

In Vitro [γ-^{32}P] Autophosphorylation and ATPase Comparison Assay

Method for Figure S3B. Coq8p$^{N\Delta41}$ (4 μM) was mixed with [γ-^{32}P]ATP (0.25 μCi/μL, 100 μM $[ATP]_{total}$) and $MgCl_2$ (4 mM) in an aqueous buffer (20 mM HEPES, 150 mM NaCl, pH 7.5) and incubated (30 °C, 45 min, 20 μL total reaction volume) (final concentrations for reaction components). 10 μL of reaction was quenched with 10 μL 0.75 M potassium phosphate pH 3.3, 1 μL of quenched reaction was spotted on a PEI-cellulose TLC plate and developed using the method above. The other 10 μL of the reaction was quenched with 4 μL 4× LDS buffer and 10 μL was loaded onto an SDS-PAGE gel. [γ-^{32}P]ATP was separated from Coq8p$^{N\Delta41}$ by SDS-PAGE (10% Bis-Tris gel, MES buffer, 150 V, 80 min). The gel was stained with Coomassie Brilliant Blue, dried under vacuum, and imaged by digital photography. The same storage phosphor screen was exposed to the TLC plate and the SDS-PAGE gel (1 hr) and then imaged with a Typhoon (GE) to generate the phosphorimages used for quantification of Pi and autophosphorylation.

In Vitro [γ-^{32}P]ATP ATPase Assay

Method for Figure S4C. Unless otherwise indicated, COQ8A$^{N\Delta162}$ (2 μM) or Coq8p$^{N\Delta41}$ (1 μM) was mixed with liposomes (~3.33 mM), [γ-^{32}P]ATP (0.01 μCi/μL, 100 μM $[ATP]_{total}$), and $MgCl_2$ (4 mM) in an aqueous buffer (20 mM HEPES, 150 mM NaCl, pH 7.5) and incubated (20 μL total volume, 30 °C, 45 min, 700 rpm) (final concentrations for reaction components). Reactions were quenched with 0.75 M potassium phosphate pH 3.3 (20 μL, 4 °C). 1 μL of quenched reaction was spotted on PEI-cellulose TLC (Millipore) and developed with 0.5 M LiCl in 1 M formic $acid_{(aq)}$. After drying, a storage phosphor screen was exposed to the PEI-cellulose TLC plate (~5 hours) and then imaged with a Typhoon (GE) to generate the phosphorimages.

In Vitro [γ-^{32}P]ATP Kinase Assay

Method for Figures S4D-S4F. Unless otherwise indicated, COQ8A$^{N\Delta162}$, Coq8p$^{N\Delta41}$ (4 μM), or PKA (0.2 μM) was mixed with [γ-^{32}P]ATP (0.25 μCi/μL, 100 μM $[ATP]_{total}$) and $MgCl_2$ (4 mM) in an aqueous buffer (20 mM HEPES, 150 mM NaCl, pH 7.5) and incubated (30 °C, 45 min, 700 rpm) (final concentrations for reaction components). Myelin basic protein (1 μM) and a cell-free expressed COQ protein complex consisting of COQ3, COQ4, COQ5, COQ6, COQ7-strep, and COQ9 (~1.5–0.1 μM). Half (10 μL) of each reaction was quenched with 4× LDS buffer. [γ-^{32}P]ATP was separated from COQ8 by SDS-PAGE (10% Bis-Tris gel, MES buffer, 150 V, 1.5 h). The gel was stained with Coomassie Brilliant Blue, dried under vacuum, and imaged by digital photography. The other half (10 μL) of the reaction was quenched with 1:1 $CHCl_3$:MeOH (50 μL, 4 °C) and 1 M HCl (12.5 μL, 4 °C). Reactions were mixed by vortexing (3 × 10 s), centrifuged (3000 *g*, 1 min, 4 °C) and the aqueous layer was discarded. 10 μL of the organic layer was spotted

on silica TLC and lipids were separated with $CHCl_3$/MeOH/30% $NH_4OH_{(aq)}$/H_2O (50:40:8:2, v/v/v/v). A storage phosphor screen was exposed to the gel or TLC plate (~5 days) and then imaged with a Typhoon (GE) to generate the phosphorimages.

Yeast Drop Assay and Growth Curves

Yeast cultures for drop assays. *S. cerevisiae* (BY4742) Δ*coq8* yeast were transformed as previously described[82] with p426 GPD plasmids encoding Coq8p variants and grown on uracil drop-out (Ura^-) synthetic media plates containing glucose (2%, w/v). Individual colonies of yeast were used to inoculate Ura^- media (2% glucose, w/v) starter cultures, which were incubated (30 °C, ~18 h, 230 rpm). Serial dilutions of yeast (10^4, 10^3, 10^2, or 10 yeast cells) were dropped onto Ura^- agar media plates containing either glucose (2%, w/v) or glycerol (3%, w/v) and incubated (30 °C, 2 d). To assay yeast growth in liquid media, yeast from a starter culture were swapped into Ura^- media with glucose (0.1%, w/v) and glycerol (3%, w/v) at an initial density of 5×10^6 cells/mL. The cultures were incubated in a sterile 96 well plate with an optical, breathable cover seal (shaking at 1140 rpm). Optical density readings were obtained every 10 min. For Coq8p-*AS* experiments, individual colonies of *S. cerevisiae* (BY4742) were used to inoculate Ura^- media (20 g/L glucose) starter cultures, which were incubated (30 °C, ~12 h, 230 rpm). Yeast were diluted to 2.5×10^4 cells/mL in Ura^-, *p*ABA^- media (20 g/L glucose) and incubated until early log phase (30 °C, 16 h, 230 rpm). Yeast were swapped into Ura^-, *p*ABA^- media with glucose (0.1%, w/v) and glycerol (3%, w/v) at an initial density of 5×10^6 cells/mL with or without 20 μM CMK. The cultures were incubated in a sterile 96 well plate with an optical, breathable cover seal (shaking at 1140 rpm). Optical density readings were obtained every 10 min.

Growth of Yeast and Extraction of Yeast CoQ_6 for LC-MS Quantitation

Method for Figure 2D adapted from[12]. 2.5×10^6 yeast cells (as determined by OD_{600} of a starter culture) were used to inoculate a 25 mL culture of Ura$^-$ media (10 g/L glucose), which was incubated (30 °C, 230 rpm) for 23 h. At 23 h, the yeast cultures were ~4 h past the diauxic shift and the media was depleted of glucose. The OD_{600} of the culture was measured and used to determine the volume of culture needed to isolate 1×10^8 yeast cells. 1×10^8 yeast cells were pelleted by centrifugation in 15 mL conical tubes (4,000 *g*, 3 min, 4 °C) and transferred to 1.5 mL tubes and spun again (16,000 *g*, 0.5 min, 4 °C), the supernatant was discarded, and the yeast pellet was flash frozen in liquid N_2 and stored at –80 °C. A frozen pellet of yeast (10^8 yeast cells) was thawed on ice and mixed with phosphate buffered saline (200 µL) and glass beads (0.5 mm diameter, 100 µL). The yeast were lysed by vortexing with the glass beads (30 s). Coenzyme Q_{10} (CoQ_{10}) was added as an internal standard (10 µM, 10 µL), and the lysate was vortexed (30 s). Hexanes/2-propanol (10:1, v/v) (500 µL) was added and vortexed (2 × 30 s). The samples were centrifuged (3,000 *g*, 1 min, 4 °C) to complete phase separation. 400 µL of the organic phase was transferred to a clean tube and dried under $Ar_{(g)}$. The organic residue was reconstituted in ACN/IPA/H_2O (65:30:5, v/v/v) (100 µL) by vortexing (30 s) and transferred to a glass vial for LC-MS analysis. Samples were stored at –80 °C.

For analog-sensitive *COQ8* experiments (Figure 6), 3 mL starter cultures in Ura$^-$ (2% glucose, w/v) were inoculated with a single colony of yeast and incubated (30 °C, 14 h). Next, 50 mL cultures in Ura$^-$ *p*ABA$^-$ (2% glucose, w/v) were inoculated with 2.5×10^7 cells and incubated (30 °C, 230 rpm) until reaching an OD_{600} between 1-2. Then, 1×10^8 cells were centrifuged (3220 *g*, 3 min, r.t.). The cells were resuspended in Ura$^-$, *p*ABA$^-$ media (3% glycerol, w/v) containing $^{13}C_6$-4HB (50 µM) and either CMK (20 µM) or DMSO (0.2%, v/v) and incubated (30 °C, 230

rpm). At 2, 4 and 6 h after the media swap, the OD_{600} of the culture was measured and used to determine the volume of culture needed to isolate 1×10^8 yeast cells. 1×10^8 yeast cells were pelleted by centrifugation in 15 mL conical tubes (3,000 *g*, 3 min, 4 °C) and transferred to 1.5 mL tubes and spun again (16,000 *g*, 0.5 min, 4 °C), the supernatant was discarded, and the yeast pellet was flash frozen in liquid N_2 and stored at –80 °C. A frozen pellet of yeast (1×10^8 yeast cells) was thawed on ice and mixed with water (200 µL), coenzyme Q_{10} (CoQ_{10}) was added as an internal standard (20 µM, 10 µL), and glass beads (0.5 mm diameter, 100 µL). The yeast were lysed by vortexing with the glass beads (2×30 s), and the lysate was vortexed (30 s). Cold $CHCl_3$/MeOH (2:1, v/v) (900 µL) was added and vortexed (2 × 30 s). Samples were acidified with HCl (1 M, 200 µL) and vortexed (2 × 30 s). The samples were centrifuged (5,000 *g*, 2 min, 4 °C) to complete phase separation. 400 µL of the organic phase was transferred to a clean tube and dried under $Ar_{(g)}$. The organic residue was reconstituted in ACN/IPA/H_2O (65:30:5, v/v/v) (100 µL) by vortexing (2 × 30 s) and transferred to a glass vial for LC-MS analysis. Samples were stored at –80 °C.

Targeted LC-MS for Yeast CoQ_6

Method for Figure 2D. LC-MS analysis was performed on an Acquity CSH C18 column held at 50 °C (100 mm x 2.1 mm x 1.7 µL particle size; Waters) using (400 µL/min flow rate; Thermo Scientific). Mobile phase A consisted of 10 mM ammonium acetate in ACN/H_2O (70:30, v/v) containing 250 µL/L acetic acid. Mobile phase B consisted of 10 mM ammonium acetate in IPA/ACN (90:10, v/v) with the same additives. Initially, mobile phase B was held at 40% for 6 min and then increased to 60% over 3 min followed by an increase to 85% over 15 s. Mobile phase B was then increased to 99% over 75 s where it was held for 30 s. The column was re-equilibrated for 4 min before the next injection. 10 µL of sample was injected for each sample. The LC system

was coupled to a Q Exactive mass spectrometer (Build 2.3 SP2) by a HESI II heated ESI source kept at 300 °C. The inlet capillary was kept at 300 °C, sheath gas was set to 25 units, and auxiliary gas to 10 units. For identification of CoQ_6 and CoQ_{10} species, the MS was operated in positive mode (5 kV) and masses (591.44 and 880.71, respectively) were targeted for fragmentation. AGC target was set to $1x10^6$ and resolving power was set to 140,000. Quantitation was performed in Xcalibur (Thermo) by monitoring the product ion 197.08 Th, corresponding to the Q headgroup, for each targeted mass. Error bars represent SD of three biological replicates.

For Coq8p-*AS* lipid samples (Figure 6D), LC-MS analysis was performed on an Acquity CSH C18 column held at 50 °C (100 mm × 2.1 mm × 1.7 µL particle size; Waters) using an Vanquish Binary Pump (400 µL/min flow rate; Thermo Scientific). Mobile phase A consisted of 10 mM ammonium acetate in ACN/H_2O (70:30, v/v) containing 250 µL/L acetic acid. Mobile phase B consisted of 10 mM ammonium acetate in IPA/ACN (90:10, v/v) with the same additives. Mobile phase B was held at 50% for 1.5 min and then increased to 99% over 7.5 min where it was held for 2 min. The column was then reequilibrated for 2.5 min before the next injection. 10 µL of sample were injected by a Vanquish Split Sampler HT autosampler (Thermo Scientific). The LC system was coupled to a Q Exactive mass spectrometer by a HESI II heated ESI source kept at 300 °C (Thermo Scientific). The inlet capillary was kept at 300 °C, sheath gas was set to 25 units, auxiliary gas to 10 units, and the spray voltage was set to 4,000 V. The MS was operated in positive mode and masses (597.46, 591.44 and 880.71, respectively) were targeted for fragmentation. Automatic gain control (AGC) target was set to $5x10^5$ and resolving power was set to 120,000. Quantification was performed in Xcalibur (Thermo Scientific) by monitoring the product ion 203.10 Th (heavy CoQ_6) and 197.08 Th (light CoQ_6 and CoQ_{10}), corresponding to the Q headgroup, for each targeted mass. The MS was operated in negative mode and masses (551.42,

550.44, 545.40 and 544.42, respectively) were targeted to quantify heavy and light CoQ intermediates, $PPHB_6$. The resulting LC-MS data were processed using TraceFinder 3.3 (Thermo Scientific). Metabolite signals were integrated and normalized to the CoQ_{10} internal standard. Error bars represent SD of three biological replicates.

AP-MS Lipidomics of 8His-MBP-[TEV]-MBP-UbiB$^{C\Delta47}$

8His-MBP-[TEV]-MBP-UbiB$^{C\Delta47}$ protein purifications were performed in biological triplicate according to the method used above. Eq/S buffer (50 mM HEPES [pH 7.2], 300 mM NaCl, 10% glycerol [w/v]) was added to 25 nmol of 8His-MBP-[TEV]-MBP-UbiB$^{C\Delta47}$ to bring total sample volume to 682 µL. 20 µL of 25 µM CoQ_6 internal standard (in $CHCl_3$:MeOH, 1:1, v/v) (Avanti Polar Lipids) was added to each sample and vortex 10 s (500 pmols) (protein precipitated upon mixing). Cold CH_3Cl:MeOH (1:1, v/v, 4.3 mL) was added to each sample and mixed to form one phase by vortexing (1 × 30 s, 4 °C). Samples were acidified by adding HCl (1 M, 30 µL) and vortexing (2 × 30 s). Phase separation was induced by addition of saturated $NaCl_{(aq)}$ (100 µL) and mixed by vortexing (10 s). Phase separation was completed by centrifugation (3000 *g*, 1 min, 4 °C). Aqueous layer was discarded and 2.9 mL of the organic layer was transferred to new glass tube and dry under $Ar_{(g)}$ (r.t., ~2 hr). The organic residue was reconstituted in ACN/IPA/ H_2O (65:30:5, v/v/v) (200 µL) by vortexing (30 s, 4 °C), bath sonication (60 s, 4 °C), and vortexing (30 s, 4 °C). Transfer 180 µL to an autosampler vial labeled, stored under $Ar_{(g)}$ at –80 °C.

LC-MS Discovery and Targeted Methods for AP-MS

Both targeted and discovery-based lipidomics of UbiB were done using the instrumentation, column, and mobile phases described in Targeted LC-MS for yeast CoQ_6.

Discovery Lipidomics. Mobile phase B started at 2% and increased to 85% over 20 min, then increased to 99% over 1 min, where it was held for 7 min. The column was then reequilibrated for 2 min before the next injection. The LC system was coupled to a Q Exactive mass spectrometer by a HESI II heated ESI source kept at 300 °C (Thermo Scientific). The inlet capillary was kept at 300 °C, sheath gas was set to 25 units, auxiliary gas to 10 units, and the spray voltage was set to 3,000 V. The MS was operated in polarity switching mode, acquiring both positive mode and negative mode MS^1 and MS^2 spectra. The AGC target was set to $1x10^6$ and resolving power to 17,500. Ions from 200-1600 m/z were isolated (Top 2) and fragmented by stepped HCD collision energy (20, 30, 40). The resulting LC-MS/MS data were processed using Compound Discoverer 2.0 (Thermo Fisher) and an in-house-developed software suite. Briefly, all m/z peaks were aggregated into distinct chromatographic profiles (i.e., compound groups) using a 10 p.p.m. mass tolerance. These chromatographic profiles were then aligned across all LC-MS/MS experiments using a 0.2 min retention time tolerance. All compound groups were compared against a matrix run and only compound groups whose intensity was 5-fold greater were retained. MS/MS spectra were searched against an in-silico generated lipid spectral library containing 35,000 unique molecular compositions representing 31 distinct lipid classes. Spectral matches with a dot product score greater than 650 and a reverse dot product score greater than 750 were retained for further analysis. Identifications were further filtered using precursor mass, MS/MS spectral purity, retention time, and chromatographic profile. Lipid MS/MS spectra which contained no significant interference (<75%) from co-eluting isobaric lipids were identified at the individual fatty acid substituent level of structural resolution. Otherwise, lipid identifications were made with the sum of the fatty acid substituents. All lipid intensities were normalized to the total intensity of all lipids

in the chromatogram following the void volume. Intensities of each individual lipid were divided by the sum of the intensities for each sample and averaged across all three biological replicates. These normalized intensities were then divided to determine fold enrichment in one condition versus another (i.e. MBP-UbiB$^{C\Delta47}$/ MBP-UbiB$^{C\Delta47}$ D310N). Student's *t*-test was used to determine statistical significance. Nomenclature for lipid acyl chains is from [83].

Targeted Lipidomics for CoQ and its Intermediates. LC-MS analysis was performed on an Acquity CSH C18 column held at 50 °C (100 mm x 2.1 mm x 1.7 µL particle size; Waters) using an Ultimate 3000 RSLC Binary Pump (400 µL/min flow rate; Thermo Scientific). Mobile phase A consisted of 10 mM ammonium acetate in ACN/H_2O (70:30, v/v) containing 250 µL/L acetic acid. Mobile phase B consisted of 10 mM ammonium acetate in IPA/ACN (90:10, v/v) with the same additives. Mobile phase B was held at 50% for 1.5 min and then increased to 95% over 6.5 min where it was held for 2 min. The column was then reequilibrated for 3.5 min before the next injection. 10 µL of sample were injected by an Ultimate 3000 RSLC autosampler (Thermo Scientific). The LC system was coupled to a Q Exactive mass spectrometer by a HESI II heated ESI source kept at 300 °C (Thermo Scientific). The inlet capillary was kept at 300 °C, sheath gas was set to 25 units, auxiliary gas to 10 units, and the spray voltage was set to 4,000 V and 5,000 V for positive and negative mode respectively. CoQ and its intermediates were targeted for quantification. The MS was operated in positive or negative mode depending on the intermediate being targeted. Metabolite signals were integrated and normalized to a CoQ_6 internal standard. Error bars represent SD of biological triplicate measurements. See Table S1 for targeted CoQ species.

Liposomes

Liposomes were made by drying down lipids in a 5 mL plastic tube under $Ar_{(g)}$ at room temperature until a film was left. Liposomes were made of the following lipid (Avanti Polar Lipids) compositions: PC, PC/NBD-PE 99.9/0.1; PC/PE, PC/PE/NBD-PE 89.9/10/0.1; PC/CL, PC/CL/NBD-PE 89.9/10/0.1; PC/PE/CL, PC/PE/CL/NBD-PE 79.9/10/10/0.1; PC/CoQ_{10}, PC/CoQ_{10}/NBD-PE 97.9/2/0.1; PC/PG, PC/PG/NBD-PE 89.9/10/0.1; PC/PS, PC/PS/NBD-PE 89.9/10/0.1; PC/PA, PC/PA/NBD-PE 89.9/10/0.1; PC/CDP-DAG, PC/CDP-DAG/NBD-PE 89.9/10/0.1; all mol %. The lipids were dried in a vacuum chamber overnight at 25-30 inHg vacuum. The dry lipid film was reconstituted in HBS buffer (20 mM HEPES pH 7.5, 150 mM NaCl) at 30–35 °C for one hour with occasional pipetting to resuspend the lipid film. The total concentration of lipids in solution was 10 mM. 2 μL of the liposomes were taken before and after extrusion and diluted with 22 μL of HBS to determine how much the liposomes were diluted during extrusion by measuring the fluorescence of NBD-PE (excitation: 460 nm, emission: 535 nm). Liposomes were extruded through 100 nm membranes (Avanti Polar Lipids), 15 passes, 30–35 °C. Liposomes were made fresh before each experiment.

Liposome Flotation Assay

Liposome flotation assay is adapted from[84] with the following modifications. Liposomes (100 μL) were mixed with protein (50 μL 6× COQ8) at 4 °C then incubated (r.t., ~10 min). Final concentrations of reagents are as follows: 2–4 μM protein and 3.33 mM liposomes in HBS (150 mM NaCl, 20 mM HEPES pH 7.5). 2.72 M sucrose (110 μL) was added to the protein liposome mixture (1.15 M [sucrose] final). The sucrose-liposome-protein mixture (250 μL) was added to the ultracentrifuge tube. The sucrose gradient was made by layering 300 μL HBS 0.86 M sucrose,

250 µL HBS 0.29 M sucrose, and 150 µL HBS on top of the sucrose-liposome-protein mix. This gradient was centrifuged (240,000 *g*, 1 h, 4 °C). 450 µL was removed for the top layer and 450 µL for the bottom layer. Liposome location was determined by mixing 8 µL of top or bottom fraction with 16 µL HBS and reading NBD-PE fluorescence for (excitation: 460 nm, emission: 535 nm). To concentrate the protein from the top and bottom fractions, a $CHCl_3$:MeOH precipitation was performed according to[85]. Methanol (1800 µL, 4 volumes) was added to a 450 µL fraction. After thorough mixing chloroform (450 µL, one volume) was added and vortexed. Water (1350 µL, three volumes) was added and the mixture was vortexed again then centrifuged immediately at full speed (~4,200 *g*, 5 min). A white disc of protein should form between the organic layer (bottom) and the aqueous layer (upper). Discard most of the upper aqueous layer, and be careful not to disturb the protein pellet. Methanol was added (1000 µL) to the tube, inverted 3 times, and centrifuged at full speed (5 min, 16,000 *g*). All of the liquid was removed and the pellet was air or vacuum dried. The precipitated protein pellet was resuspend in 30 µL 1× LDS with 10 mM DTT, incubated (95 °C, ~10 min), and analyzed with 4–12% Novex NuPAGE Bis-Tris SDS-PAGE (Invitrogen) gels (1 hr, 150 V). Band quantification was done with imaging and densitometry on a LI-COR Odyssey CLx (700 nm) using Image Studio v5.2 software. Error bars for Figure 4G represent SD of three independent floats. Student's *t*-test was used to determine statistical significance.

Coq8p V202C,M303C with CMK LC-MS/MS

CMK labeling reaction. 20 µL of Coq8p (1 µM final concentration) and 20 µL of CMK (20 µM final concentration) were mixed and incubated (30 °C, 15 min). The samples were then flash frozen in $N_{2(l)}$ and stored at –80 °C.

Sample preparation. Samples were diluted 10× in 100 mM Tris pH 8, 2 M urea, and 40 mM chloroacetamide and digested with trypsin (25:1 protein to enzyme) overnight. Sample cleanup was performed by desalting over a polystyrene-divinylbenzene solid phase extraction (PS-DVB SPE) cartridge (Phenomenex, Torrance, CA).

LC-MS/MS. Peptides were dissolved in 0.2% formic acid and 10% was injected onto the column for each analysis. Separations were performed over in-house fabricated 75 µm inner diameter x 360 µm outer diameter columns with an integrated nano electrospray emitter packed 30 cm long with 1.7 µm C18 bridged ethylene hybrid particles (Waters, Milford, MA). Samples were loaded in 100% A (0.2% formic acid), followed by gradient elution in increasing % B (0.2% formic acid/70% acetonitrile), and re-equilibration times in 100% A. All separations were performed with a Thermo Dionex Ultimate 3000 RSLC-nano liquid chromatography instrument and an in house fabricated column heater to perform separations at 50 °C[86]. Eluted peptides were analyzed on an Orbitrap Lumos Fusion platform. All MS analyses were performed in the Orbitrap with 60,000 resolving power. Following each MS1 survey scan, MS/MS analyses were performed on the most intense precursors for 1 second. Precursors were filtered with the quadrupole using a 2.0 Da isolation window, fragmented with HCD collision energy = 30 NCE, and fragment ions were analyzed in the Orbitrap. Dynamic exclusion was set to 45 seconds, MonoIsotope Precursor Selection (MIPS) was toggled on for all runs and charge states unknown, 1, or > 6 were excluded.

Data analysis. Raw files were converted to text files and scored against theoretical spectra from a target-decoy reference proteome database, using the OMSSA search engine. The database was

generated by downloading the P27697 sequence from Uniprot concatenating a clone of the P27697 sequence but with sites 202 and 303 converted to cysteines. Tryptic peptides were searched with one missed cleavage. Cysteine carbamidomethylation, and CMK modification (+322.1429 Da) and methionine oxidation were set as variable modifications. Peptides were searched with 25 ppm tolerance on the precursor mass and 0.01 Da tolerance on fragment ion masses. The COMPASS software suite was used to filter search results to a 1% unique peptide FDR (based on E-value and ppm mass error)[87].

Immunoblotting of Yeast Coq8p

Single yeast colonies (strain W303) were picked and grown in Ura$^-$ glucose (2% w/v) media (230 rpm, overnight, 30 °C). 50 mL cultures of Ura$^-$ glucose (0.1% w/v) and glycerol (3% w/v) were seeded with 2.5 x 10^6 cells and incubated (30 °C, 25 h, 230 rpm). 1 x 10^8 cells were collected, flash frozen, and stored (–80 °C). The cells were resuspended in 150 µL NaOH/BME (prepared from 1 mL 2 M NaOH + 80 µL ß-mercaptoethanol), and incubated on ice for 10 minutes, mixing every 2 minutes. 150 µL 50% TCA was added to each sample and incubated on ice for an additional 10 minutes, mixing every 2 minutes. Samples were centrifuged (14,000 *g*, 2 min), and the pellet was washed with 1 mL acetone, mixed briefly, and centrifuged (14,000 *g*, 2 min). The supernatant was removed and the pellet allowed to dry. Samples were resuspended in 60 µL 0.1 M NaOH. 25 µL 6× LDS sample buffer with 10 mM DTT was added and samples were incubated (95 °C, ~10 min). Proteins were analyzed with 4–12% Novex NuPAGE Bis-Tris SDS-PAGE (Invitrogen) gels (1 hr, 150 V). The gel was transferred to PVDF membrane at 20 V for 1 h with transfer buffer (192 mM glycine, 25 mM Tris, 20% methanol [v/v]). The membrane was blocked with 5% nonfat dry milk (NFDM) in TBST (20 mM Tris pH 7.4, 150 mM NaCl, 0.05% Tween 20 [v/v]) (1 h with agitation).

Affinity purified Coq8p antibody (1:100) and the ß-actin antibody (1:5000) were diluted in 1% NFDM in TBST and incubated with the PVDF (overnight, 4 °C with agitation). The PVDF was washed three times in TBST and the secondary antibodies were diluted 1:15,000 in 1% NFDM in TBST (1 h, r.t.). The membrane was washed three times in TBST and imaged. Band quantification was done with imaging and densitometry on a LI-COR Odyessey CLx using Image Studio v5.2 software. Error bars for Figure S4K represent SD of three independent experiments.

Coq8p Antibody Affinity Purification

A 4-12% Bis Tris SDS-PAGE gel was loaded with 20 µg $Coq8p^{N\Delta41}$ (5 µg per lane, 4 lanes total). The $Coq8p^{N\Delta41}$ was transferred to PVDF according to the procedure above. The PVDF membrane was stained with 1x Ponceau solution (10-15 min, r.t) and washed several times with water. The Coq8p band was cut out from the membrane. The membrane pieces were blocked with 2% NFDM in TBST (2 h, r.t.) and washed with TBST several times. Coq8p rabbit antisera (Catherine Clarke's lab) was added to the membrane (overnight, 4 °C with agitation then 1 h, r.t.). Membrane pieces were washed 6-7 times TBST. To elute bound antibodies, 600 µL of 0.2 M glycine, pH 3.0 was added to the membrane pieces and mixed (1 min). Extract was transferred to a tube containing 36 µL (can be scaled up depending on the antisera added) of 1 M Tris-HCl pH 8.8 to obtain a neutral pH. Affinity enriched antibody was flash frozen in $N_{2(l)}$ and stored at –80 °C.

Quantification and Statistical Analysis

See each individual method for the associated statistical analysis. In general, *p*-values were calculated using an unpaired, two-tailed, Student's *t*-test. In all cases, n represents independent replicates of an experiment.

Acknowledgements

We thank Professor Kevan Shokat and Flora Rutaganira for useful discussions and reagents. Research reported in this publication was supported by the National Institute of General Medical Sciences of the National Institutes of Health under award numbers R01GM112057 (to D.J.P.), T32GM008505 (to A.G.R.), T32DK007665 (to Z.A.K.), T32HL007899 (to E.M.W.), and R35GM118110 (to J.J.C). This work was further supported by SNSF grants 31003A_170154 and 200021_157217 (to M.D.P.). The content is solely the responsibility of the authors and does not necessarily represent the official views of the National Institutes of Health.

Supplemental Figures, Movies, and Tables

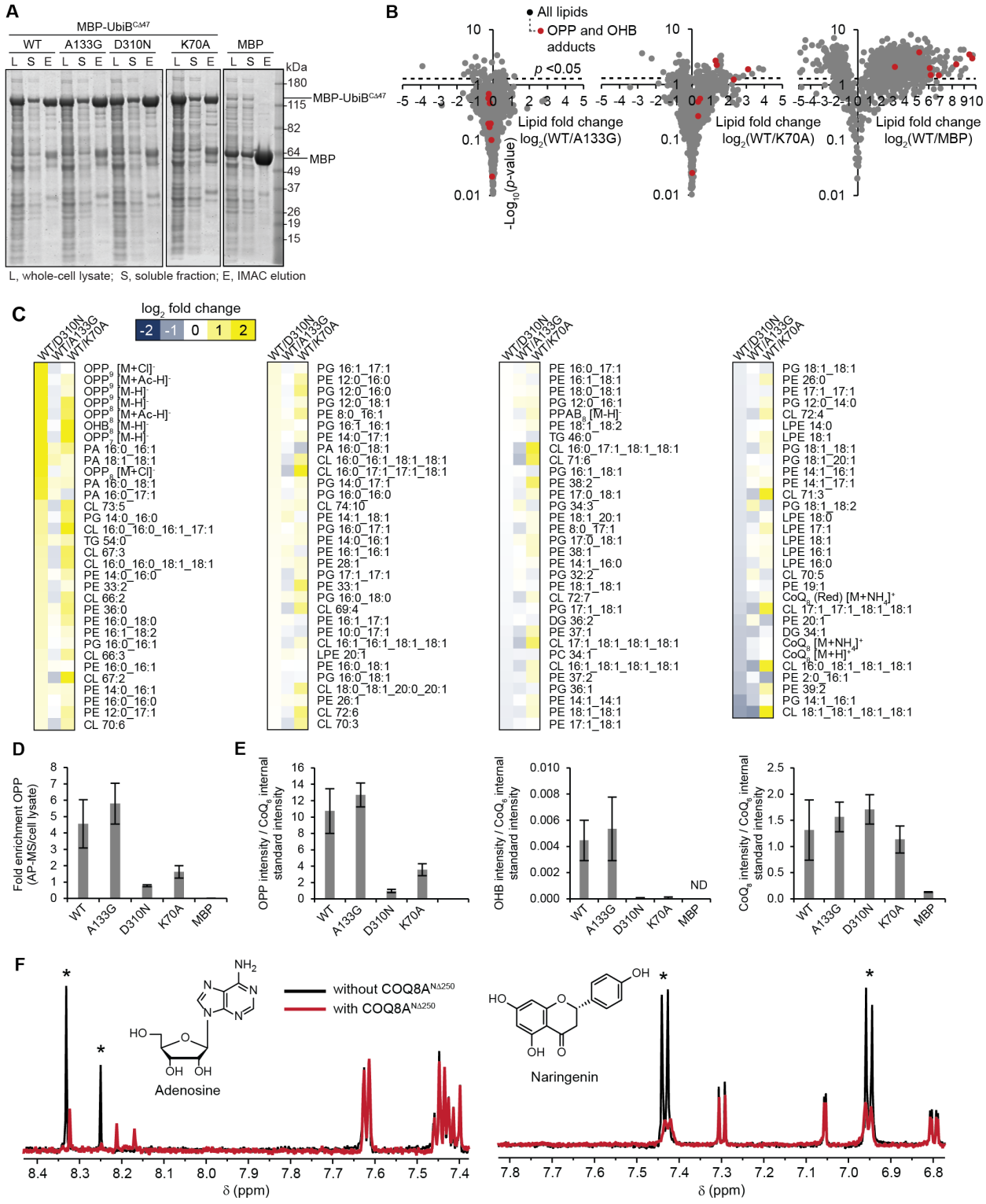

Figure S1, related to Figure 1. UbiB Family Members Bind CoQ Precursor-like Lipids and Small Molecules. (A) Representative Coomassie-stained SDS-PAGE gel from MBP-UbiB$^{C\Delta47}$ protein purification for lipidomics and activity assays. (B) Fold changes in lipid abundances (log_2[(WT MBP-UbiB$^{C\Delta47}$)/(mutant or MBP)], n = 3) versus statistical significance as quantified by LC-MS/MS. (C) Heat map of the fold changes for all identified and quantified lipids comparing WT MBP-UbiB$^{C\Delta47}$ to mutants. (D) Fold enrichment of OPP with purified protein compared to OPP abundance in matched cell lysate samples measured using targeted LC-MS. (E) Amount of copurifying OPP, OHB, and CoQ_8, measured using targeted LC-MS/MS. ND, not determined. Error bars in D and E represent SD of biological triplicate measurements. (F) A selected region of the ^{1}H NMR spectra for mixtures containing adenosine (left) and naringenin (right) with and without COQ8A$^{N\Delta250}$. Asterisks (*) indicate significant peaks for adenosine or naringenin that exhibit line-broadening. Other peaks belong to different compounds in the mixtures that are not interacting with COQ8A$^{N\Delta250}$.

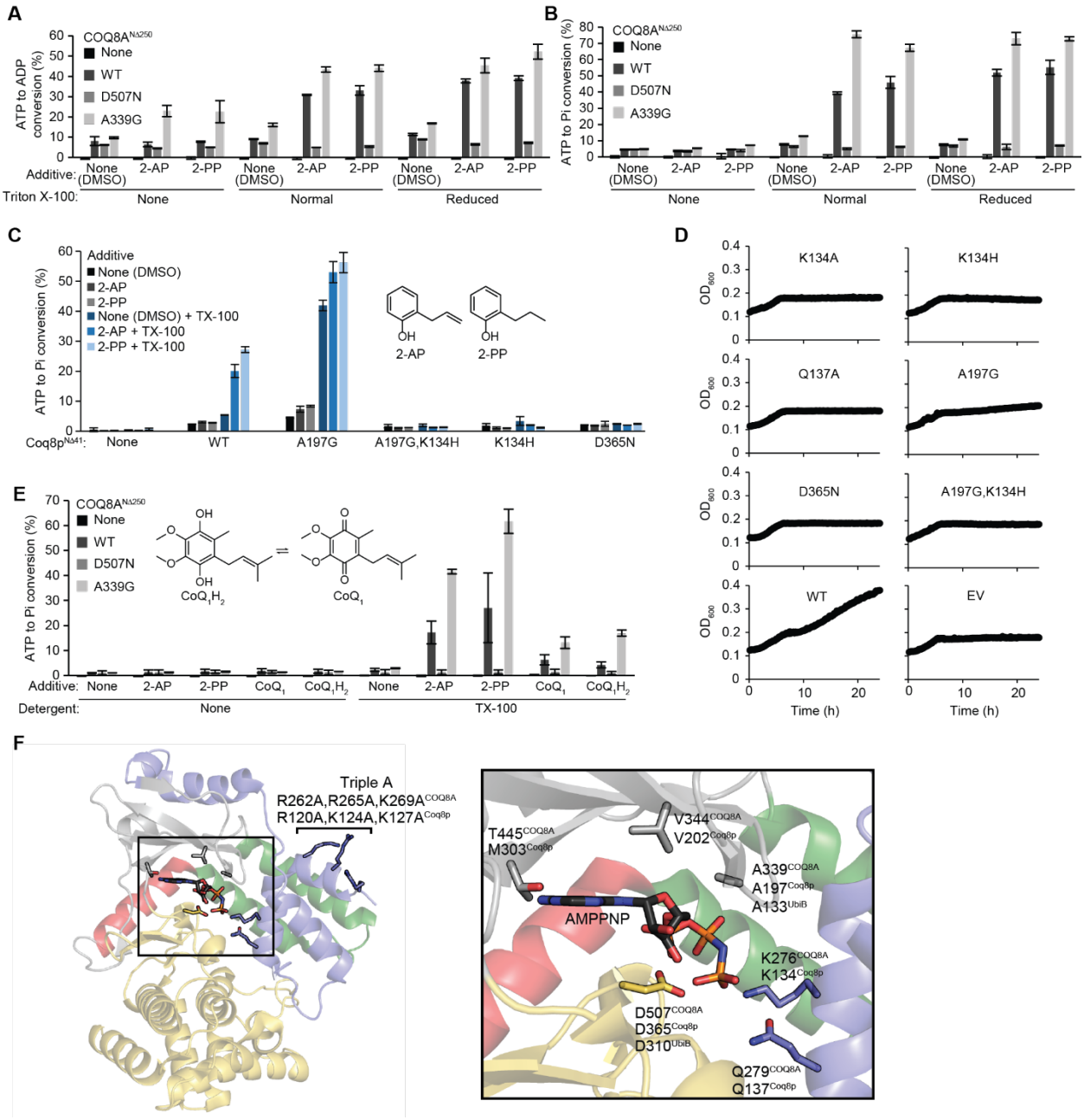

Figure S2, related to Figure 2. UbiB Family Members are Activated by Triton X-100 and 2-Alkylphenols. (A) ADP-Glo assay with COQ8A$^{N\Delta250}$ variants, Triton X-100 (TX-100) or Triton X-100 reduced, and 2-alkylphenols. (B) Malachite green assay with COQ8A$^{N\Delta250}$ variants, Triton X-100 or Triton X-100 reduced, and 2-alkylphenols. Pi, inorganic phosphate. (C) Malachite green ATPase assay with Coq8p$^{N\Delta41}$ KxGQ mutants, 2-alkylphenols and Triton X-

100. (D) Growth curves of Δ*coq8* yeast transformed with KxGQ mutants in Ura^{-}, glucose (0.1% w/v) and glycerol (3% w/v) respiratory media. (E) Malachite green ATPase assay with $COQ8A^{N\Delta250}$, 2-alkylphenols or CoQ_1. For ATPase assays, error bars represent SD of technical triplicate measurements. (F) Structure of COQ8A (PDB: 5I35) with residues highlighted and annotated for COQ8A, Coq8p, and UbiB that are referenced in this manuscript. Black box shows larger view of active site residues.

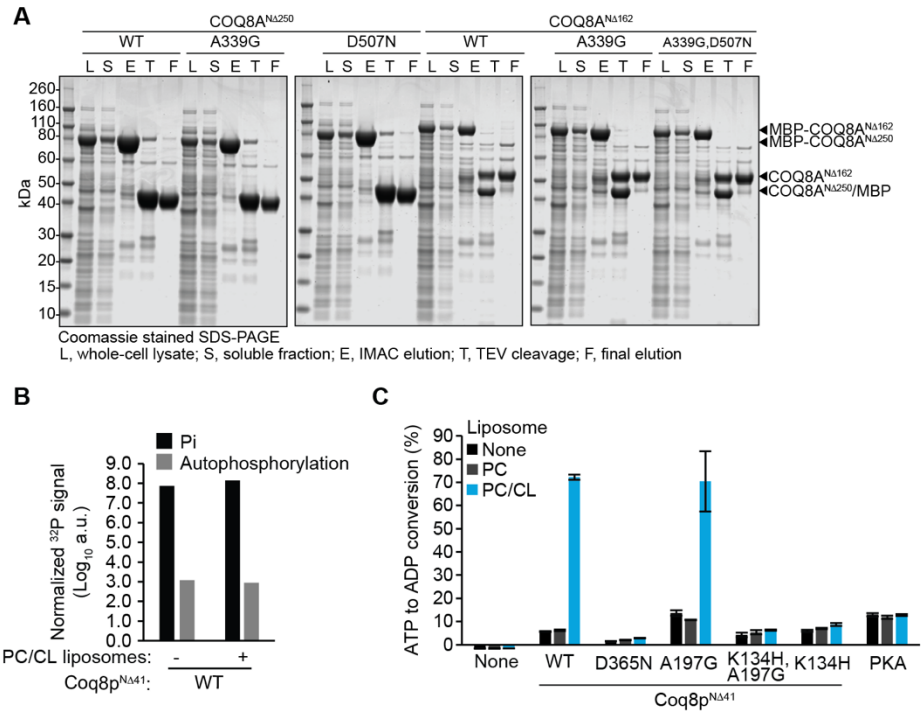

Figure S3, related to Figure 3. Purification of COQ8A$^{N\Delta162}$. (A) Coomassie stained SDS-PAGE of samples from a COQ8A$^{N\Delta250}$ and COQ8A$^{N\Delta162}$ protein purification. (B) Direct comparison of Coq8p$^{N\Delta41}$ ATPase (Pi) and autophosphorylation activities with or without PC/CL liposomes using [γ-^{32}P]ATP. (C) ADP-Glo assay with Coq8p$^{N\Delta41}$ variants and PKA along with PC/CL liposomes. Error bars represent SD of three technical replicates.

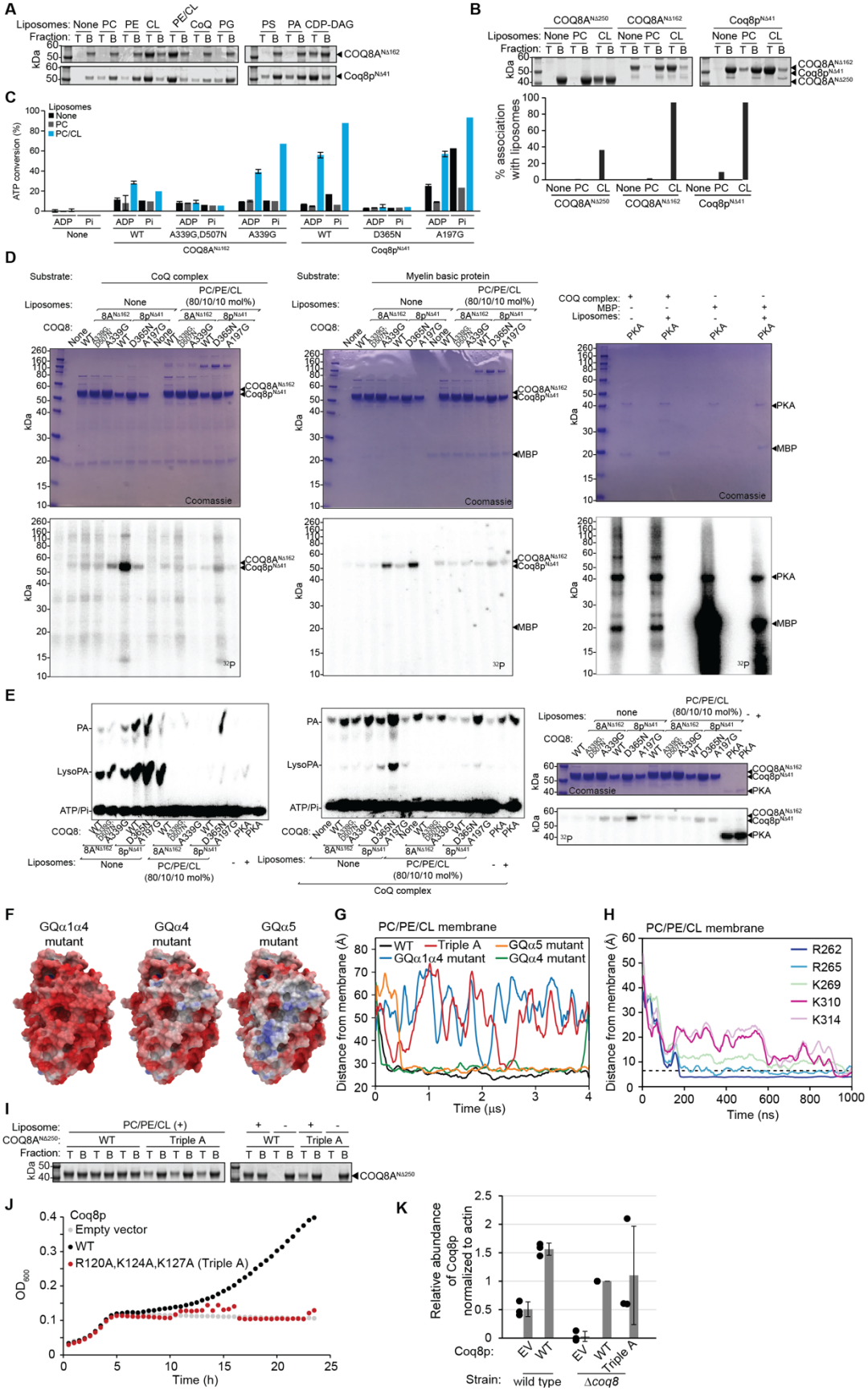
A
Liposomes: None PC PE CL PE/CL CoQ PG PS PA CDP-DAG
Fraction: T B T B T B T B T B T B T B T B
kDa
COQ8A^Δ162
Coq8p^Δ41
B
COQ8A^Δ250 COQ8A^Δ162 Coq8p^Δ41
Liposomes: None PC CL None PC CL None PC CL
Fraction: T B T B T B T B T B T B T B T B
kDa
COQ8A^Δ162
Coq8p^Δ41
COQ8A^Δ250
% association with liposomes
None PC CL None PC CL None PC CL
COQ8A^Δ250 COQ8A^Δ162 Coq8p^Δ41
C
Liposomes
None
PC
PC/CL
ATP conversion (%)
ADP Pi
None
WT
A339G,D507N
A339G
D365N
A197G
COQ8A^Δ162
Coq8p^Δ41
D
Substrate:
CoQ complex
Myelin basic protein
Liposomes:
None
PC/PE/CL (80/10/10 mol%)
COQ8:
COQ complex:
MBP:
PKA
kDa
Coomassie
32P
COQ8A^Δ162
Coq8p^Δ41
MBP
PKA
E
PA
LysoPA
ATP/Pi
COQ8:
Liposomes:
None
PC/PE/CL (80/10/10 mol%)
CoQ complex
Coomassie
32P
F
GQα1α4 mutant
GQα4 mutant
GQα5 mutant
G
PC/PE/CL membrane
WT
Triple A
GQα5 mutant
GQα1α4 mutant
GQα4 mutant
Distance from membrane (Å)
Time (μs)
H
PC/PE/CL membrane
R262
R265
K269
K310
K314
Distance from membrane (Å)
Time (ns)
I
Liposome:
PC/PE/CL (+)
COQ8A^Δ250:
WT
Triple A
Fraction: T B T B T B T B T B T B T B T B
kDa
COQ8A^Δ250
J
Coq8p
Empty vector
WT
R120A,K124A,K127A (Triple A)
OD600
Time (h)
K
Relative abundance of Coq8p normalized to actin
Coq8p:
EV
WT
Triple A
Strain:
wild type
Δcoq8

Figure S4, related to Figure 4. CL Enhances the ATPase Activity of COQ8 and Liposome Binding.

(A) Coomassie-stained SDS-PAGE of the liposome flotation assay in Figure 4A with mature COQ8 and a panel of liposomes. T, top fraction; B, bottom fraction. (B) Coomassie-stained SDS-PAGE of the liposome flotation assay with COQ8 variants and PC/PE/CL liposomes. T, top fraction; B, bottom fraction. (C) ADP-Glo (ADP produced) and [γ-32P]ATP ATPase assay (Pi produced) of COQ8 variants with PC or PC/CL liposomes performed in parallel. (D) Coomassie-stained SDS-PAGE and corresponding phosphorimage of [γ-32P]ATP kinase reactions. The Coq8p D365N mutant looks active because it was overloaded. (E) Phosphorimage of silica TLC from [γ-32P]ATP kinase reactions. (F) Electrostatic maps of COQ8A with the positively charged or polar residues on helices GQα1, GQα4, and GQα5 mutated to alanine [negative (−5 kcal/(mol•e) charge): red, via white, to positive (+5 kcal/(mol•e) charge): blue]. (G) CG-MD simulations of different GQα mutated COQ8A proteins. Time evolution of the distance between the center of mass of the protein and the center of mass of the phosphate heads of the leaflet with which it interacts. Triple A mutant, R262A,R265A,K269A; GQα4 mutant, K310A,K314A; GQα1α4 mutant, R262A,R265A,K269A,K310A,K314A; GQα5 mutant, Q366A,S367A,N369A,S370A,N373A,N374A. (H) Time evolution of the distance between positively charged residues on COQ8A GQα1 and GQα4 and the closest phosphate head. (I) Coomassie-stained SDS-PAGE of top and bottom fraction from the liposome flotation assay in Figure 4G. +, with PC/PE/CL liposomes; -, no liposomes. (J) Representative growth curve of Δcoq8 yeast transformed with WT COQ8 or the Triple A mutant in Ura–, glucose (0.1% w/v) and glycerol (3% w/v) respiratory media. (K) Relative abundance of Coq8p from wild type (WT) or Δcoq8 yeast overexpressing Triple A mutant Coq8p in respiratory growth. Individual data points

are shown on the left of the bars from each immunoblot quantification. Error bars represent SD of three independent experiments. EV, empty vector.

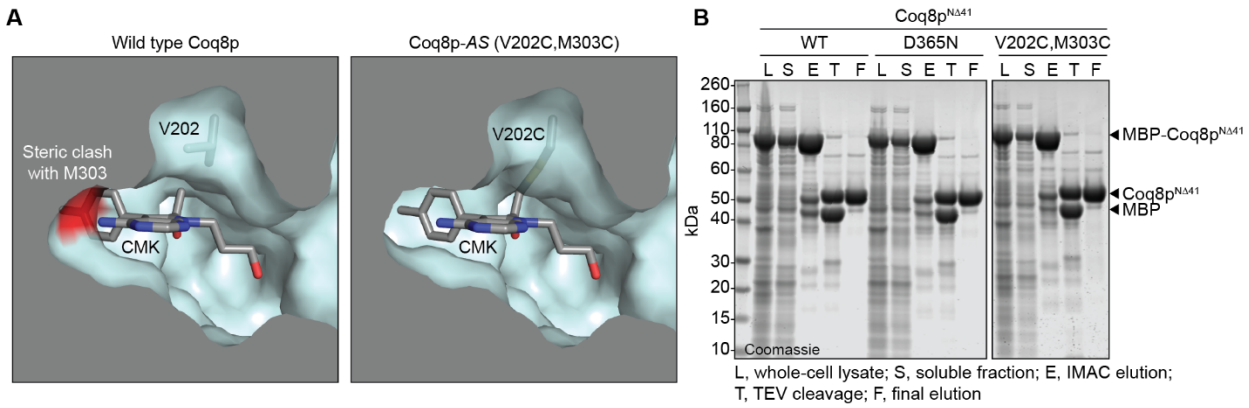

Figure S5, related to Figure 5. Modeling of CMK in the Coq8p Active Site and Purification of Coq8p$^{N\Delta41}$-*AS* (V202C,M303C). (A) Modeling of CMK (lacking the chlorine atom) in the active site of the homology model of Coq8p. The surface of M303 is colored in red demonstrating a steric clash with CMK. Mutation of valine 202 and methionine 303 to cysteine (V202C,M303C) creates a binding pocket for and allows covalent modification by CMK. (B) Coomassie-stained SDS-PAGE of samples from Coq8p$^{N\Delta41}$-*AS* protein purification.

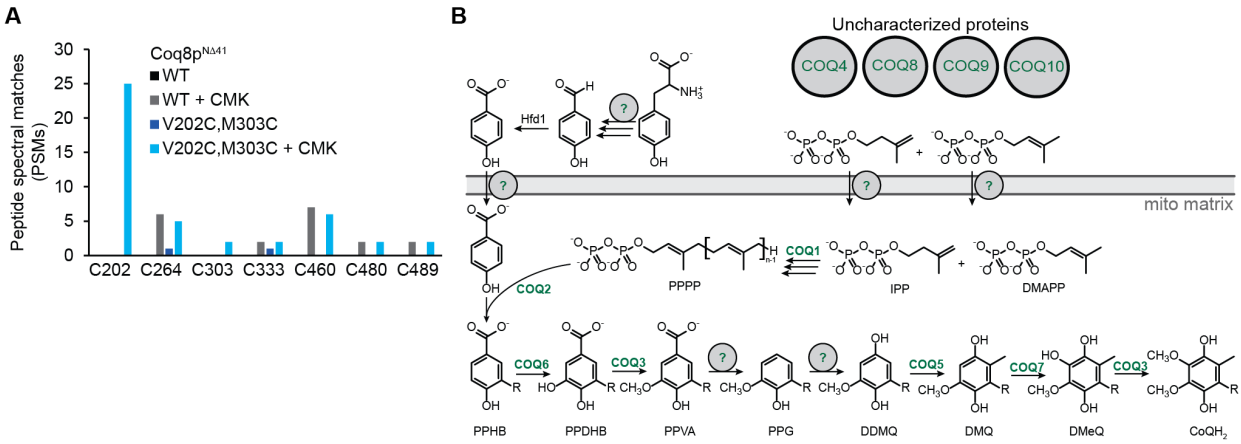

Figure S6, related to Figure 6. CMK Covalently Modifies Coq8p$^{N\Delta41}$-*AS*.

(A) Number of peptide spectral matches (PSMs) observed for CMK-modified cysteine-containing peptides detected by LC-MS/MS analysis of an *in vitro* reaction with Coq8p$^{N\Delta41}$ variants (1 μM) and CMK (20 μM). (B) The eukaryotic CoQ biosynthesis pathway. Proteins in the pathway are highlighted in green. Abbreviations for intermediates are underneath each chemical structure. IPP, isoprenylpyrophosphate; DMAPP, dimethylallylpyrophosphate; PPPP, polyprenyl-pyrophosphate; PPHB, polyprenyl-hydroxybenzoate; PPDHB, polyprenyl-dihydroxybenzoate; PPVA, polyprenyl-vanillic acid; PPG, polyprenyl-guaiacol; DDMQ, demethoxy-demethyl-coenzyme Q; DMQ, demethoxy-coenzyme Q; DMeQ, demethyl-coenzyme Q; $CoQH_2$, reduced coenzyme Q.

Movie S1, related to Figure 4. CG-MD Simulation of COQ8A with PC Bilayer.

4 microseconds of production run of a CG-MD simulation of COQ8A (green) (PDB: 4PED) with PC bilayer (phosphate heads in gray). The positively charged residues R262, R265, K269 are colored blue.

Movie S2, related to Figure 4. CG-MD Simulation of COQ8A with PC/PE/CL Bilayer.

4 microseconds of production run of a CG-MD simulation of COQ8A (green) (PDB: 4PED) with PC/PE/CL bilayer (PC/PE phosphate heads in gray and CL phosphate heads in red). The positively charged residues R262, R265, K269 are colored blue.

Table S1, related to Figure 1. MBP-UbiB$^{C\Delta 47}$ AP-MS Lipidomics Data.

Table S2, related to Figure 1. List of Compounds and Hits from NMR Line-broadening Screen.

Table S3, related to Figures 1-6. Explanation of UbiB Family Member Variants Used in this Study.

Table S4, related to Figures 1-6. Oligonucleotide Primers Used in this Study.

References

1. Leonard, C.J., Aravind, L. & Koonin, E.V. Novel families of putative protein kinases in bacteria and archaea: evolution of the "eukaryotic" protein kinase superfamily. *Genome Res* **8**, 1038-47 (1998).

2. Lundquist, P.K., Davis, J.I. & van Wijk, K.J. ABC1K atypical kinases in plants: filling the organellar kinase void. *Trends Plant Sci* **17**, 546-55 (2012).

3. Wiedemeyer, W.R. et al. Pattern of retinoblastoma pathway inactivation dictates response to CDK4/6 inhibition in GBM. *Proc Natl Acad Sci U S A* **107**, 11501-6 (2010).

4. Simpson, K.J. et al. Identification of genes that regulate epithelial cell migration using an siRNA screening approach. *Nat Cell Biol* **10**, 1027-38 (2008).

5. Do, T.Q., Hsu, A.Y., Jonassen, T., Lee, P.T. & Clarke, C.F. A defect in coenzyme Q biosynthesis is responsible for the respiratory deficiency in Saccharomyces cerevisiae abc1 mutants. *J Biol Chem* **276**, 18161-8 (2001).

6. Poon, W.W. et al. Identification of Escherichia coli ubiB, a gene required for the first monooxygenase step in ubiquinone biosynthesis. *J Bacteriol* **182**, 5139-46 (2000).

7. Mollet, J. et al. CABC1 gene mutations cause ubiquinone deficiency with cerebellar ataxia and seizures. *Am J Hum Genet* **82**, 623-30 (2008).

8. Lagier-Tourenne, C. et al. ADCK3, an ancestral kinase, is mutated in a form of recessive ataxia associated with coenzyme Q10 deficiency. *Am J Hum Genet* **82**, 661-72 (2008).

9. Horvath, R. et al. Adult-onset cerebellar ataxia due to mutations in CABC1/ADCK3. *J Neurol Neurosurg Psychiatry* **83**, 174-8 (2012).

10. Ashraf, S. et al. ADCK4 mutations promote steroid-resistant nephrotic syndrome through CoQ10 biosynthesis disruption. *J Clin Invest* **123**, 5179-89 (2013).

11. Stefely, J.A. et al. Cerebellar Ataxia and Coenzyme Q Deficiency through Loss of Unorthodox Kinase Activity. *Mol Cell* **63**, 608-20 (2016).

12. Stefely, J.A. et al. Mitochondrial ADCK3 employs an atypical protein kinase-like fold to enable coenzyme Q biosynthesis. *Mol Cell* **57**, 83-94 (2015).

13. Ferrer, A., Caelles, C., Massot, N. & Hegardt, F.G. Activation of rat liver cytosolic 3-hydroxy-3-methylglutaryl coenzyme A reductase kinase by adenosine 5'-monophosphate. *Biochem Biophys Res Commun* **132**, 497-504 (1985).

14. Walsh, D.A., Perkins, J.P. & Krebs, E.G. An adenosine 3',5'-monophosphate-dependant protein kinase from rabbit skeletal muscle. *J Biol Chem* **243**, 3763-5 (1968).

15. Takai, Y. et al. Calcium-dependent activation of a multifunctional protein kinase by membrane phospholipids. *J Biol Chem* **254**, 3692-5 (1979).

16. Takai, Y., Kishimoto, A., Kikkawa, U., Mori, T. & Nishizuka, Y. Unsaturated diacylglycerol as a possible messenger for the activation of calcium-activated, phospholipid-dependent protein kinase system. *Biochem Biophys Res Commun* **91**, 1218-24 (1979).

17. Franke, T.F. et al. The protein kinase encoded by the Akt proto-oncogene is a target of the PDGF-activated phosphatidylinositol 3-kinase. *Cell* **81**, 727-36 (1995).

18. Burgering, B.M. & Coffer, P.J. Protein kinase B (c-Akt) in phosphatidylinositol-3-OH kinase signal transduction. *Nature* **376**, 599-602 (1995).

19. Khadria, A.S. et al. A Gly-zipper motif mediates homodimerization of the transmembrane domain of the mitochondrial kinase ADCK3. *J Am Chem Soc* **136**, 14068-77 (2014).

20. Xie, L.X. et al. Expression of the human atypical kinase ADCK3 rescues coenzyme Q biosynthesis and phosphorylation of Coq polypeptides in yeast coq8 mutants. *Biochim Biophys Acta* **1811**, 348-60 (2011).

21. Bishop, A.C. et al. A chemical switch for inhibitor-sensitive alleles of any protein kinase. *Nature* **407**, 395-401 (2000).

22. Cohen, M.S., Zhang, C., Shokat, K.M. & Taunton, J. Structural bioinformatics-based design of selective, irreversible kinase inhibitors. *Science* **308**, 1318-21 (2005).

23. Rodriguez-Molina, J.B., Tseng, S.C., Simonett, S.P., Taunton, J. & Ansari, A.Z. Engineered Covalent Inactivation of TFIIH-Kinase Reveals an Elongation Checkpoint and Results in Widespread mRNA Stabilization. *Mol Cell* **63**, 433-44 (2016).

24. Snead, J.L. et al. A coupled chemical-genetic and bioinformatic approach to Polo-like kinase pathway exploration. *Chem Biol* **14**, 1261-72 (2007).

25. Coudreuse, D. & Nurse, P. Driving the cell cycle with a minimal CDK control network. *Nature* **468**, 1074-9 (2010).

26. Oh, H., Ozkirimli, E., Shah, K., Harrison, M.L. & Geahlen, R.L. Generation of an analog-sensitive Syk tyrosine kinase for the study of signaling dynamics from the B cell antigen receptor. *J Biol Chem* **282**, 33760-8 (2007).

27. Ferreira-Cerca, S. et al. ATPase-dependent role of the atypical kinase Rio2 on the evolving pre-40S ribosomal subunit. *Nat Struct Mol Biol* **19**, 1316-23 (2012).

28. Kanoh, H., Kanaho, Y. & Nozawa, Y. Activation and solubilization by Triton X-100 of membrane-bound phospholipase D of rat brain. *Lipids* **26**, 426-30 (1991).

29. Yoon, S.-H. & Robyt, J.F. Activation and stabilization of 10 starch-degrading enzymes by Triton X-100, polyethylene glycols, and polyvinyl alcohols. *Enzyme and Microbial Technology* **37**, 556-562 (2005).

30. Cullen, J.K. et al. AarF Domain Containing Kinase 3 (ADCK3) Mutant Cells Display Signs of Oxidative Stress, Defects in Mitochondrial Homeostasis and Lysosomal Accumulation. *PLoS One* **11**, e0148213 (2016).

31. Vogtle, F.N. et al. Landscape of submitochondrial protein distribution. *Nat Commun* **8**, 290 (2017).

32. Tauche, A., Krause-Buchholz, U. & Rodel, G. Ubiquinone biosynthesis in Saccharomyces cerevisiae: the molecular organization of O-methylase Coq3p depends on Abc1p/Coq8p. *FEMS Yeast Res* **8**, 1263-75 (2008).

33. Jura, N. et al. Mechanism for activation of the EGF receptor catalytic domain by the juxtamembrane segment. *Cell* **137**, 1293-307 (2009).

34. Calvo, S.E. et al. Comparative Analysis of Mitochondrial N-Termini from Mouse, Human, and Yeast. *Mol Cell Proteomics* **16**, 512-523 (2017).

35. Vogtle, F.N. et al. Global analysis of the mitochondrial N-proteome identifies a processing peptidase critical for protein stability. *Cell* **139**, 428-39 (2009).

36. Horvath, S.E. & Daum, G. Lipids of mitochondria. *Prog Lipid Res* **52**, 590-614 (2013).

37. Zinser, E. et al. Phospholipid synthesis and lipid composition of subcellular membranes in the unicellular eukaryote Saccharomyces cerevisiae. *J Bacteriol* **173**, 2026-34 (1991).

38. de Kroon, A.I., Dolis, D., Mayer, A., Lill, R. & de Kruijff, B. Phospholipid composition of highly purified mitochondrial outer membranes of rat liver and Neurospora crassa. Is cardiolipin present in the mitochondrial outer membrane? *Biochim Biophys Acta* **1325**, 108-16 (1997).

39. Serafimova, I.M. et al. Reversible targeting of noncatalytic cysteines with chemically tuned electrophiles. *Nat Chem Biol* **8**, 471-6 (2012).

40. Niesen, F.H., Berglund, H. & Vedadi, M. The use of differential scanning fluorimetry to detect ligand interactions that promote protein stability. *Nat Protoc* **2**, 2212-21 (2007).

41. Nishizuka, Y. Intracellular signaling by hydrolysis of phospholipids and activation of protein kinase C. *Science* **258**, 607-14 (1992).

42. Gupta, K. et al. The role of interfacial lipids in stabilizing membrane protein oligomers. *Nature* **541**, 421-424 (2017).

43. Moravcevic, K., Oxley, C.L. & Lemmon, M.A. Conditional peripheral membrane proteins: facing up to limited specificity. *Structure* **20**, 15-27 (2012).

44. Yeagle, P.L. Non-covalent binding of membrane lipids to membrane proteins. *Biochim Biophys Acta* **1838**, 1548-59 (2014).

45. Planas-Iglesias, J. et al. Cardiolipin Interactions with Proteins. *Biophys J* **109**, 1282-94 (2015).

46. Claypool, S.M. Cardiolipin, a critical determinant of mitochondrial carrier protein assembly and function. *Biochim Biophys Acta* **1788**, 2059-68 (2009).

47. Gebert, N. et al. Mitochondrial cardiolipin involved in outer-membrane protein biogenesis: implications for Barth syndrome. *Curr Biol* **19**, 2133-9 (2009).

48. Claypool, S.M., Boontheung, P., McCaffery, J.M., Loo, J.A. & Koehler, C.M. The cardiolipin transacylase, tafazzin, associates with two distinct respiratory components providing insight into Barth syndrome. *Mol Biol Cell* **19**, 5143-55 (2008).

49. Pfeiffer, K. et al. Cardiolipin stabilizes respiratory chain supercomplexes. *J Biol Chem* **278**, 52873-80 (2003).

50. Floyd, B.J. et al. Mitochondrial Protein Interaction Mapping Identifies Regulators of Respiratory Chain Function. *Mol Cell* **63**, 621-32 (2016).

51. Mileykovskaya, E. & Dowhan, W. Cardiolipin membrane domains in prokaryotes and eukaryotes. *Biochim Biophys Acta* **1788**, 2084-91 (2009).

52. Fry, M. & Green, D.E. Cardiolipin requirement for electron transfer in complex I and III of the mitochondrial respiratory chain. *J Biol Chem* **256**, 1874-80 (1981).

53. Giustini, M. et al. Influence of cardiolipin on the functionality of the Q(a) site of the photosynthetic bacterial reaction center. *J Phys Chem B* **109**, 21187-96 (2005).

54. Vos, M. et al. Cardiolipin promotes electron transport between ubiquinone and complex I to rescue PINK1 deficiency. *J Cell Biol* **216**, 695-708 (2017).

55. Kar, A. et al. CLD1 Reverses the Ubiquinone Insufficiency of Mutant cat5/coq7 in a Saccharomyces cerevisiae Model System. *PLoS One* **11**, e0162165 (2016).

56. Brough, R. et al. Functional viability profiles of breast cancer. *Cancer Discov* **1**, 260-73 (2011).

57. Martinis, J., Glauser, G., Valimareanu, S. & Kessler, F. A chloroplast ABC1-like kinase regulates vitamin E metabolism in Arabidopsis. *Plant Physiol* **162**, 652-62 (2013).

58. Tan, T., Ozbalci, C., Brugger, B., Rapaport, D. & Dimmer, K.S. Mcp1 and Mcp2, two novel proteins involved in mitochondrial lipid homeostasis. *J Cell Sci* **126**, 3563-74 (2013).

59. Mercier, K.A. et al. FAST-NMR: functional annotation screening technology using NMR spectroscopy. *J Am Chem Soc* **128**, 15292-9 (2006).

60. Fischer, J.J. & Jardetzky, O. Nuclear Magnetic Relaxation Study of Intermolecular Complexes. The Mechanism of Penicillin Binding to Serum Albumin. *J Am Chem Soc* **87**, 3237-44 (1965).

61. Lepre, C.A., Moore, J.M. & Peng, J.W. Theory and applications of NMR-based screening in pharmaceutical research. *Chem Rev* **104**, 3641-76 (2004).

62. Stark, J.L., Eghbalnia, H.R., Lee, W., Westler, W.M. & Markley, J.L. NMRmix: A Tool for the Optimization of Compound Mixtures in 1D (1)H NMR Ligand Affinity Screens. *J Proteome Res* **15**, 1360-8 (2016).

63. Clos, L.J., 2nd, Jofre, M.F., Ellinger, J.J., Westler, W.M. & Markley, J.L. NMRbot: Python scripts enable high-throughput data collection on current Bruker BioSpin NMR spectrometers. *Metabolomics* **9**, 558-563 (2013).

64. Abraham, M.J. et al. GROMACS: High performance molecular simulations through multi-level parallelism from laptops to supercomputers. *SoftwareX* **1–2**, 19-25 (2015).

65. Pronk, S. et al. GROMACS 4.5: a high-throughput and highly parallel open source molecular simulation toolkit. *Bioinformatics* **29**, 845-854 (2013).

66. Marrink, S.J., Risselada, H.J., Yefimov, S., Tieleman, D.P. & de Vries, A.H. The MARTINI force field: coarse grained model for biomolecular simulations. *J Phys Chem B* **111**, 7812-24 (2007).

67. Periole, X., Cavalli, M., Marrink, S.J. & Ceruso, M.A. Combining an Elastic Network With a Coarse-Grained Molecular Force Field: Structure, Dynamics, and Intermolecular Recognition. *J Chem Theory Comput* **5**, 2531-43 (2009).

68. Periole, X., Huber, T., Marrink, S.J. & Sakmar, T.P. G protein-coupled receptors self-assemble in dynamics simulations of model bilayers. *J Am Chem Soc* **129**, 10126-32 (2007).

69. van den Bogaart, G. et al. Membrane protein sequestering by ionic protein-lipid interactions. *Nature* **479**, 552-5 (2011).

70. Stansfeld, P.J., Hopkinson, R., Ashcroft, F.M. & Sansom, M.S. PIP(2)-binding site in Kir channels: definition by multiscale biomolecular simulations. *Biochemistry* **48**, 10926-33 (2009).

71. Schafer, L.V. et al. Lipid packing drives the segregation of transmembrane helices into disordered lipid domains in model membranes. *Proc Natl Acad Sci U S A* **108**, 1343-8 (2011).

72. Daum, G. Lipids of mitochondria. *Biochim Biophys Acta* **822**, 1-42 (1985).

73. Wassenaar, T.A., Ingolfsson, H.I., Bockmann, R.A., Tieleman, D.P. & Marrink, S.J. Computational Lipidomics with insane: A Versatile Tool for Generating Custom Membranes for Molecular Simulations. *J Chem Theory Comput* **11**, 2144-55 (2015).

74. Humphrey, W., Dalke, A. & Schulten, K. VMD: visual molecular dynamics. *J Mol Graph* **14**, 33-8, 27-8 (1996).

75. Abagyan, R., Totrov, M. & Kuznetsov, D. Icm - a New Method for Protein Modeling and Design - Applications to Docking and Structure Prediction from the Distorted Native Conformation. *Journal of Computational Chemistry* **15**, 488-506 (1994).

76. Biasini, M. et al. SWISS-MODEL: modelling protein tertiary and quaternary structure using evolutionary information. *Nucleic Acids Res* **42**, W252-8 (2014).

77. Pettersen, E.F. et al. UCSF Chimera--a visualization system for exploratory research and analysis. *J Comput Chem* **25**, 1605-12 (2004).

78. Crooks, G.E., Hon, G., Chandonia, J.M. & Brenner, S.E. WebLogo: a sequence logo generator. *Genome Res* **14**, 1188-90 (2004).

79. Klock, H.E., Koesema, E.J., Knuth, M.W. & Lesley, S.A. Combining the polymerase incomplete primer extension method for cloning and mutagenesis with microscreening to accelerate structural genomics efforts. *Proteins* **71**, 982-94 (2008).

80. Blommel, P.G., Martin, P.A., Seder, K.D., Wrobel, R.L. & Fox, B.G. Flexi vector cloning. *Methods Mol Biol* **498**, 55-73 (2009).

81. Mumberg, D., Muller, R. & Funk, M. Yeast vectors for the controlled expression of heterologous proteins in different genetic backgrounds. *Gene* **156**, 119-22 (1995).

82. Gietz, R.D. & Woods, R.A. Transformation of yeast by lithium acetate/single-stranded carrier DNA/polyethylene glycol method. *Methods Enzymol* **350**, 87-96 (2002).

83. Liebisch, G. et al. Shorthand notation for lipid structures derived from mass spectrometry. *J Lipid Res* **54**, 1523-30 (2013).

84. Connerth, M. et al. Intramitochondrial transport of phosphatidic acid in yeast by a lipid transfer protein. *Science* **338**, 815-8 (2012).

85. Wessel, D. & Flugge, U.I. A method for the quantitative recovery of protein in dilute solution in the presence of detergents and lipids. *Anal Biochem* **138**, 141-3 (1984).

86. Hebert, A.S. et al. The one hour yeast proteome. *Mol Cell Proteomics* **13**, 339-47 (2014).

87. Wenger, C.D., Phanstiel, D.H., Lee, M.V., Bailey, D.J. & Coon, J.J. COMPASS: a suite of pre- and post-search proteomics software tools for OMSSA. *Proteomics* **11**, 1064-74 (2011).

Chapter 3: CoQ Distribution and Mobilization

Author Contributions: Zachary A. Kemmerer wrote this chapter.

CoQ Distribution

Overview

In the more than 60 years since the discovery of CoQ, most of our efforts have been dedicated to understanding how CoQ is made. Early on, however, it was discovered that CoQ is ubiquitous in living systems—in cells[1], in tissues[2], and across all domains of life[3]. This fact has not been fully appreciated, due to the focus on mitochondrial CoQ and understanding its central role in OxPhos and cellular respiration. Ultimately, the structure and chemical properties of CoQ enable it to perform this canonical function in OxPhos. These same chemical properties have led others to investigate CoQ as a potent lipophilic antioxidant, the only lipid-soluble antioxidant produced by all cells in mammals. CoQ was originally found to inhibit lipid peroxidation *in vitro* using submitochondrial particles[4,5]. Later CoQ was demonstrated to have this effect on all subcellular membranes[6]. Its intramembranous localization, abundant distribution, and capacity to be recycled through cellular reductive mechanisms allow CoQ to be highly effective in mitigating lipid oxidation and cell damage or death[7].

Based on these unique chemical properties, exogenous CoQ has been employed for decades against various malignancies, including cardiomyopathies[8,9], degenerative muscle diseases[10], and general aging[11]. Unfortunately, the results of CoQ supplementation have been inconsistent, likely due to variable bioavailability. This may be explained by CoQ's poor absorption—when taken

orally, an estimated 2-4% reaches circulation[12] and even less CoQ ever reaches the cellular target. Development of improved therapeutics would benefit from a better understanding of how our cells and tissues mobilize CoQ and how that process is regulated.

These ideas highlight major gaps that exist in our understanding of CoQ biology. First, how does CoQ localize to every membrane throughout the cell? What are the cellular factors that are required for this pathway and does more than one pathway exist? Second, why is CoQ found in all cellular membranes? To date, our understanding of how CoQ functions beyond mitochondria is limited. And third, what machinery are involved with exogenous uptake of CoQ, and does this overlap with the endogenous trafficking machinery? Ultimately, this information would help design improved treatments for patients with CoQ-deficiency. Over the past 50 years, some of these questions have been addressed, but many important questions remain unanswered.

Distribution and Mobilization of Subcellular CoQ

Distribution of CoQ within cells has been generally defined by classical fractionation schemes using various tissues and cells[2,13-15]. Mobility has also been assessed by employing heavy and radiolabeled CoQ precursors[16]. Surprising, large concentrations of CoQ were often found outside of mitochondria, highlighting the importance of extra-mitochondrial CoQ pools and supporting the need for mobilization mechanisms. Across various tissues there is significant variability, but CoQ is most abundant in heart, kidney, liver, and muscle tissue[2]. Total CoQ is known to decreases during aging, statin treatment, and is observed in various disease states including cardiomyopathies, liver cancer, and Parkinson's disease[7]. However, the possibility remains that defects in CoQ distribution may also have detrimental consequences that result in

malignancy and disease. Due to our poor understanding of these pathways and of the machineries involved, our ability to intervene is limited.

Synthesized endogenously in the mitochondrial IMM, CoQ is ubiquitous across the cell, but how it navigates to these diverse cellular locations remains unclear (Figure 1). Due to its large molecular size and extreme hydrophobicity, CoQ is unlikely to traverse the aqueous environment of the cell without dedicated machinery. Therefore, two possibilities for how CoQ is derived outside of mitochondria are: 1) mechanisms exist for localized production of CoQ at other organelles, or 2) CoQ is synthesize in mitochondria and mobilized across the cell. In the case of phospholipid biosynthesis, these two approaches are not mutually exclusive[17,18]. It is established that phospholipid biosynthesis depends on a combination of pathway redundancy[19], organelle-specific variants[20-23], dedicated lipid transport proteins[24-26], organelle tethers[27-30], and vesicle-mediated trafficking[17]. These mechanisms result in organelle-specific, non-random phospholipid distribution, but how these processes are regulated are not yet fully understood.

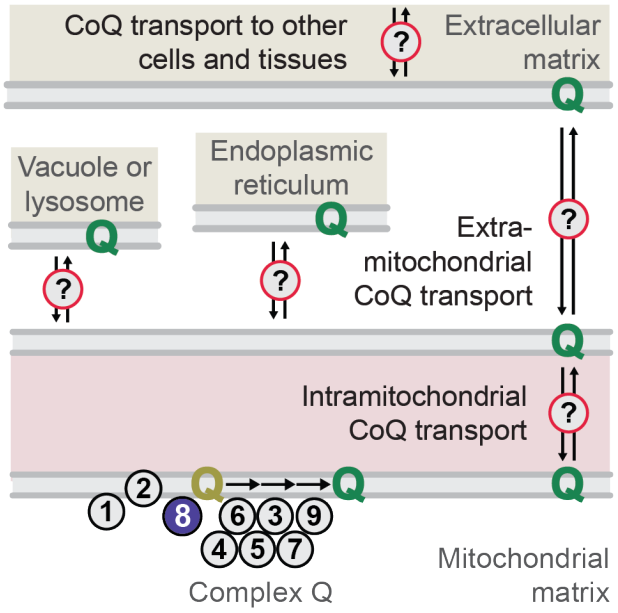

Figure 1. Cellular CoQ Distribution from its Site of Synthesis in Mitochondria. Figure modified from Stefely and Pagliarini, 2017[31]. CoQ is made in the IMM by complex Q before making its way to every membrane throughout the cell. How this occurs is a longstanding mystery in CoQ biology. Transport steps without an assigned enzyme are shown (circled question marks).

The identification of CoQ biosynthetic machinery in other organelles[32,33] has led to speculation that cells may synthesize CoQ locally to negate global distribution challenges. However, only prenyltransferase (COQ2, UbiA) homologs[32-34] have been identified. While it remains possible that local hydroxylases and methylases can perform the necessary headgroup modification, homologous headgroup modifying enzymes have yet to be identified outside of mitochondria. Due to the ubiquity of CoQ in the cell, it seems unlikely that complex Q would be present at all membranes for local biosynthesis. One intriguing possibility is that unidentified machinery exists at the ER-Golgi, where vesicle-mediated transport may enhance CoQ trafficking, under normal or stress conditions. To this effect, [^{14}C]tyrosine precursor labeling experiments in rats showed that microsomal *de novo* CoQ production was higher than in mitochondria, suggesting the presence of ER-localized CoQ biosynthesis[32,35]. Revisiting this work with modern technologies and tools will be required to further address this possibility.

Alternatively, CoQ may be produced exclusively in mitochondria and cellular mechanisms exist for moving CoQ across the cell. Previous work demonstrated treatment of human cells with [^{14}C]4-HB (headgroup precursor) led to the rapid accumulation of [^{14}C]CoQ_{10} in mitochondria, followed by mitochondrial associated membranes, then ER and finally plasma membrane[16]. Importantly, *de novo* CoQ production and exogenously suppled CoQ incorporation were disrupted

by brefeldin A (BFA)[36], a potent inhibitor of the endomembrane trafficking system. This suggests the involvement of the endo-exocytic pathway in the bi-directional cellular mobilization of CoQ. Based on this work, CoQ derived from mitochondria flows to ER where it can then be distributed across the cell via the endomembrane system (Figure 2A). This broad observation raises questions about the identity of specific proteins that impact CoQ mobilization, both amongst the endomembrane system and within mitochondria.

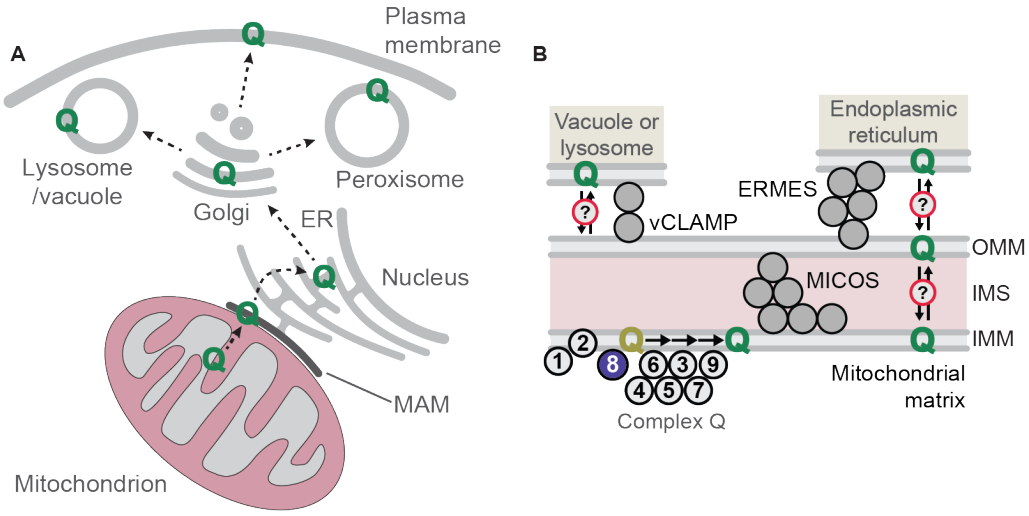

Figure 2. The Putative Pathway for Cellular CoQ Distribution. Figure adapted from Stefely and Pagliarini, 2017[31]. **A,** After synthesis occurs in the IMM, CoQ passes through mitochondrial-associated membranes (MAM) to the ER. Once in the ER, CoQ can enter the endomembrane system and be packaged in the Golgi for widespread distribution across the cell. **B,** Transport from the IMM to the ER may involve large protein complexes (MICOS, ERMES) that can bring multiple membranes together in close proximity to enhance lipid trafficking. MICOS, mitochondrial contact site and cristae organization system; ERMES, ER-mitochondria encounter structure; vCLAMP, vacuolar and mitochondrial patch.

For mitochondria, membrane organization and orchestration of inter-organellar contact sites may be critical for the mobilization of CoQ synthesized at the IMM (Figure 2B). Over the past decade, contact site biology has become central to our understanding of cellular communication, metabolism, and maintenance[37,38]. As a double membrane organelle, mitochondria have both intra- and inter-organellar contact sites that may participate in the mobilization of CoQ. Within mitochondria, structural integrity and organization of the highly folded inner membrane is regulate by the mitochondrial contact site and cristae organization system (MICOS)[39]. MICOS is comprised of seven protein subunits, conserved across eukaryotes, and is crucial for maintaining mitochondrial morphology, protein import, respiratory chain organization, and nucleoid segregation in mitochondria. At the outer mitochondrial membrane (OMM), functional contact sites have been identified for a growing list of organelles[38]. The first and most extensively studied contact site is the yeast ER-mitochondria encounter structure (ERMES), a multimeric protein complex that tethers ER to mitochondria[40]. ERMES enables proper cation and lipid exchange between organelles, and has been shown to influence mitochondrial morphology and biogenesis. Although ERMES is not conserved in higher eukaryotes, these essential functions are thought to be driven by other organelle contact sites[41,42]. In the absence of ERMES, a redundant protein tether call the vacuolar and mitochondrial patch (vCLAMP) appears to support similar functions[43,44]. Numerous other mitochondrial contact site exist and proteins tethers have recently been identified for peroxisome, lipid droplets, and the plasma membrane[41]. It has become clear that the cellular environment has an astounding degree of interconnectedness, and mitochondria are seemingly at the center of this complicated organelle web.

To date, no protein has been assigned to cellular CoQ mobilization from mitochondria. Previous reports suggested that saposin B binds and transports CoQ_{10}[45,46], but this protein is localized exclusively in lysosomes and this work has not been independently confirmed. Considering how CoQ would get from its site of synthesis in the IMM to the ER, it must traverse the IMS, the OMM, and the cytosol before arriving at the ER lumen (or other organelle membranes). As such, we expect that a collection of proteins will be involved in moving CoQ beyond the IMM (Figure 2B). One possibility is that mitochondrial contact sites juxtapose membranes in close proximity for non-vesicle mediated lipid transfer (NVM)[18]. Some examples of NVM lipid transfer include the formation of a hydrophobic conduit (e.g., ERMES), lipid transport proteins (e.g., Ups1/2 for phosphatidic acid and phosphatidylserine, respectively[26]), and transient membrane hemifusion. In support of this hypothesis, recent work in yeast revealed that MICOS subcomplexes assemble in proximity to ER at ERMES contact sites[47]. Further, overexpression of Vps39, which induces mitochondria-vacuole contact sites, caused one MICOS subcomplex to reorganize to vacuolar contact sites (vCLAMP). Together, this hints that MICOS may has a functional association with these contact sites tethers, perhaps to support proper cristae structure or metabolite transfer. In two recent yeast studies, submitochondrial fluorescent co-localization demonstrated that complex Q is also proximal to ERMES[48,49], suggesting a tight juxtaposition of these three membranes. Based on these observations, it appears the membrane organization within and beyond mitochondria are well positioned to minimize hydrophobic barriers associated with CoQ transport (Figure 2B). Moving forward, screening approaches and detailed biochemistry will be needed to identify the mitochondrial machinery responsible for mobilizing CoQ across the cell.

Cellular CoQ Uptake

Efficacy of CoQ supplementation is often hard to predict in human patients, due to its poor absorption rates and limited bioavailability. Moreover, our understanding of the cellular CoQ uptake pathway and mechanisms are severely lacking. Identification of factors involved in this pathway would help in the development of better delivery strategies, which are needed for a host of disease states involving CoQ deficiency[8-11].

Recent work in yeast investigated what cellular machinery might play a role in CoQ uptake. Using a Δ*coq3* respiratory deficient strain, four genes involved in the endocytic pathway—Erg2, Pep12, Tlg2, and Vps45—were shown to ablate CoQ_6 uptake rescue[50]. Another study used a similar strategy, generating 40 Δ*coq2* double knockout yeast strains with genes predicted to be involved with CoQ uptake[51], including the four previously identified endocytosis genes. Of these, 17 showed diminished growth during CoQ_6 uptake rescue and five strains displayed greater rescue by CoQ_2 than CoQ_6. Together, these studies provide evidence in yeast of the involvement of the endomembrane system in moving CoQ across the cells. Using targeted methods against the human orthologs will be of interest to determine whether these effects are conserved in humans. In the future, genome-wide and mitochondrial-specific screens will be needed to uncover mitochondrial machinery and other cellular components essential for CoQ uptake, as well as CoQ mobilization.

Significance—A Recent Example of Extra-mitochondrial CoQ Function

CoQ functions as a potent antioxidant exclusively in its reduced state, $CoQH_2$[52]. Cellular reduction, either by a protein reductase or other reducing equivalent in the cell, is required to regenerate and maintain this reductive state[53]. A number of proteins have been demonstrated to reduce CoQ, including mitochondrial OxPhos complexes, DHODH, ETFDH, and GPDH[54].

Beyond mitochondria, other reductases have been identified, namely plasma membrane NAD(P)H:quinone reductase 1 (NQO1, formerly DT-diaphorase) and NADH-cytochrome b_5, placing CoQ at the center of an important cellular boundary redox system[55]. A similar system exists in yeast as demonstrated by Δ*coq3* yeast having diminished NADH-reductase activity at the plasma membrane[56]. This activity was restored upon replacement of the *Coq3* gene or CoQ supplementation.

In 2019, two groups simultaneously identified a new NADH-oxidoreductase that catalyzes FAD-dependent CoQ reduction at the plasma membrane[57,58]. Published in Nature, this work details how FSP1-dependent CoQ reduction prevents toxic lipid peroxidation and consequently ferroptosis, a type of regulated cell death[59]. NQO1 was examined by both groups to determine if other reductases could support this same function. Deletion of *NQO1* did not affect cells treated with RSL3 (GPX4 inhibitor, ferroptosis inducer) and plasma membrane targeted NQO1-GFP could not rescue cells lacking *FSP1*[57]. Differences in kinetic parameters may explain this observation, with FSP1 having a significantly higher maximum rate of reaction than NQO1 (FSP1 V_{max} = 4.1x10^{-7} Ms^{-1}; NQO1 V_{max} = 6.1x10^{-9} Ms^{-1})[58]. Together, these data indicate that FSP1 has a unique ability to utilize plasma membrane CoQ pools to suppress ferroptosis, an important regulatory pathway for proper cellular function.

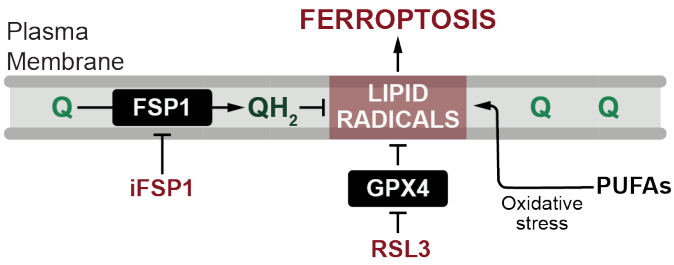

Figure 3. CoQ Mitigates Ferroptosis at the Plasma Membrane. Schematic of CoQ-dependent prevention of ferroptosis by plasma membrane oxidoreductase FSP1. In the absence of GPX4 (glutathione peroxidase 4) activity, lipid oxidative stress accumulates and leads to ferroptotic cell death. Reduced $CoQH_2$ generated by FSP1 functions as an orthogonal system in human cells to maintain lipid homeostasis. RSL3, small-molecule GPX4 inhibitor; iFSP1, small-molecule FSP1 inhibitor.

Recent work suggest that activation and inhibition of the ferroptosis pathway has clear implications for combatting human disease[60]. Thus, significant efforts are being dedicated to fully elucidate the biological networks impacting ferroptosis[61]. These discoveries highlights the necessity and importance of investigating CoQ distribution and mobilization. Understanding how CoQ exits mitochondria en route to other cellular locations may afford new opportunities for clinical intervention[60].

References

1. Sastry, P.S., Jayaraman, J. & Ramasarma, T. Distribution of coenzyme Q in rat liver cell fractions. *Nature* **189**, 577 (1961).

2. Aberg, F., Appelkvist, E.L., Dallner, G. & Ernster, L. Distribution and redox state of ubiquinones in rat and human tissues. *Arch Biochem Biophys* **295**, 230-4 (1992).

3. Lester, R.L. & Crane, F.L. The natural occurrence of coenzyme Q and related compounds. *J Biol Chem* **234**, 2169-75 (1959).

4. Mellors, A. & Tappel, A.L. The inhibition of mitochondrial peroxidation by ubiquinone and ubiquinol. *J Biol Chem* **241**, 4353-6 (1966).

5. Takayanagi, R., Takeshige, K. & Minakami, S. NADH- and NADPH-dependent lipid peroxidation in bovine heart submitochondrial particles. Dependence on the rate of electron flow in the respiratory chain and an antioxidant role of ubiquinol. *Biochem J* **192**, 853-60 (1980).

6. Ernster, L. & Dallner, G. Biochemical, physiological and medical aspects of ubiquinone function. *Biochim Biophys Acta* **1271**, 195-204 (1995).

7. Bentinger, M., Tekle, M. & Dallner, G. Coenzyme Q--biosynthesis and functions. *Biochem Biophys Res Commun* **396**, 74-9 (2010).

8. Ayer, A., Macdonald, P. & Stocker, R. CoQ(1)(0) Function and Role in Heart Failure and Ischemic Heart Disease. *Annu Rev Nutr* **35**, 175-213 (2015).

9. Martelli, A., Testai, L., Colletti, A. & Cicero, A.F.G. Coenzyme Q10: Clinical Applications in Cardiovascular Diseases. *Antioxidants (Basel)* **9**(2020).

10. Trevisson, E., DiMauro, S., Navas, P. & Salviati, L. Coenzyme Q deficiency in muscle. *Curr Opin Neurol* **24**, 449-56 (2011).

11. Diaz-Casado, M.E. et al. The Paradox of Coenzyme Q10 in Aging. *Nutrients* **11**(2019).

12. Zhang, Y., Aberg, F., Appelkvist, E.L., Dallner, G. & Ernster, L. Uptake of dietary coenzyme Q supplement is limited in rats. *J Nutr* **125**, 446-53 (1995).

13. Zhang, Y., Turunen, M. & Appelkvist, E.L. Restricted uptake of dietary coenzyme Q is in contrast to the unrestricted uptake of alpha-tocopherol into rat organs and cells. *J Nutr* **126**, 2089-97 (1996).

14. Saito, Y. et al. Characterization of cellular uptake and distribution of coenzyme Q10 and vitamin E in PC12 cells. *J Nutr Biochem* **20**, 350-7 (2009).

15. Takahashi, T., Okamoto, T., Mori, K., Sayo, H. & Kishi, T. Distribution of ubiquinone and ubiquinol homologues in rat tissues and subcellular fractions. *Lipids* **28**, 803-9 (1993).

16. Fernandez-Ayala, D.J., Brea-Calvo, G., Lopez-Lluch, G. & Navas, P. Coenzyme Q distribution in HL-60 human cells depends on the endomembrane system. *Biochim Biophys Acta* **1713**, 129-37 (2005).

17. Vance, J.E. Phospholipid synthesis and transport in mammalian cells. *Traffic* **16**, 1-18 (2015).

18. Prinz, W.A. Lipid trafficking sans vesicles: where, why, how? *Cell* **143**, 870-4 (2010).

19. Vance, J.E. & Tasseva, G. Formation and function of phosphatidylserine and phosphatidylethanolamine in mammalian cells. *Biochim Biophys Acta* **1831**, 543-54 (2013).

20. Shiao, Y.J., Lupo, G. & Vance, J.E. Evidence that phosphatidylserine is imported into mitochondria via a mitochondria-associated membrane and that the majority of mitochondrial phosphatidylethanolamine is derived from decarboxylation of phosphatidylserine. *J Biol Chem* **270**, 11190-8 (1995).

21. Kainu, V., Hermansson, M., Hanninen, S., Hokynar, K. & Somerharju, P. Import of phosphatidylserine to and export of phosphatidylethanolamine molecular species from mitochondria. *Biochim Biophys Acta* **1831**, 429-37 (2013).

22. Trotter, P.J. & Voelker, D.R. Identification of a non-mitochondrial phosphatidylserine decarboxylase activity (PSD2) in the yeast Saccharomyces cerevisiae. *J Biol Chem* **270**, 6062-70 (1995).

23. Kannan, M., Riekhof, W.R. & Voelker, D.R. Transport of phosphatidylserine from the endoplasmic reticulum to the site of phosphatidylserine decarboxylase2 in yeast. *Traffic* **16**, 123-34 (2015).

24. Connerth, M. et al. Intramitochondrial transport of phosphatidic acid in yeast by a lipid transfer protein. *Science* **338**, 815-8 (2012).

25. Aaltonen, M.J. et al. MICOS and phospholipid transfer by Ups2-Mdm35 organize membrane lipid synthesis in mitochondria. *J Cell Biol* **213**, 525-34 (2016).

26. Tatsuta, T. & Langer, T. Intramitochondrial phospholipid trafficking. *Biochim Biophys Acta Mol Cell Biol Lipids* **1862**, 81-89 (2017).

27. Osman, C., Voelker, D.R. & Langer, T. Making heads or tails of phospholipids in mitochondria. *J Cell Biol* **192**, 7-16 (2011).

28. Scharwey, M., Tatsuta, T. & Langer, T. Mitochondrial lipid transport at a glance. *J Cell Sci* **126**, 5317-23 (2013).

29. Tamura, Y., Sesaki, H. & Endo, T. Phospholipid transport via mitochondria. *Traffic* **15**, 933-45 (2014).

30. Dimmer, K.S. & Rapaport, D. Mitochondrial contact sites as platforms for phospholipid exchange. *Biochim Biophys Acta Mol Cell Biol Lipids* **1862**, 69-80 (2017).

31. Stefely, J.A. & Pagliarini, D.J. Biochemistry of Mitochondrial Coenzyme Q Biosynthesis. *Trends Biochem Sci* **42**, 824-843 (2017).

32. Kalen, A., Appelkvist, E.L., Chojnacki, T. & Dallner, G. Nonaprenyl-4-hydroxybenzoate transferase, an enzyme involved in ubiquinone biosynthesis, in the endoplasmic reticulum-Golgi system of rat liver. *J Biol Chem* **265**, 1158-64 (1990).

33. Mugoni, V. et al. Ubiad1 is an antioxidant enzyme that regulates eNOS activity by CoQ10 synthesis. *Cell* **152**, 504-18 (2013).

34. Teclebrhan, H., Olsson, J., Swiezewska, E. & Dallner, G. Biosynthesis of the side chain of ubiquinone:trans-prenyltransferase in rat liver microsomes. *J Biol Chem* **268**, 23081-6 (1993).

35. Kalen, A., Norling, B., Appelkvist, E.L. & Dallner, G. Ubiquinone biosynthesis by the microsomal fraction from rat liver. *Biochim Biophys Acta* **926**, 70-8 (1987).

36. Misumi, Y. et al. Novel blockade by brefeldin A of intracellular transport of secretory proteins in cultured rat hepatocytes. *J Biol Chem* **261**, 11398-403 (1986).

37. Murley, A. & Nunnari, J. The Emerging Network of Mitochondria-Organelle Contacts. *Mol Cell* **61**, 648-653 (2016).

38. Eisenberg-Bord, M. & Schuldiner, M. Mitochatting - If only we could be a fly on the cell wall. *Biochim Biophys Acta Mol Cell Res* **1864**, 1469-1480 (2017).

39. Rampelt, H., Zerbes, R.M., van der Laan, M. & Pfanner, N. Role of the mitochondrial contact site and cristae organizing system in membrane architecture and dynamics. *Biochim Biophys Acta Mol Cell Res* **1864**, 737-746 (2017).

40. Kornmann, B. et al. An ER-mitochondria tethering complex revealed by a synthetic biology screen. *Science* **325**, 477-81 (2009).

41. Lackner, L.L. The Expanding and Unexpected Functions of Mitochondria Contact Sites. *Trends Cell Biol* **29**, 580-590 (2019).

42. Harper, C.S., White, A.J. & Lackner, L.L. The multifunctional nature of mitochondrial contact site proteins. *Curr Opin Cell Biol* **65**, 58-65 (2020).

43. Honscher, C. et al. Cellular metabolism regulates contact sites between vacuoles and mitochondria. *Dev Cell* **30**, 86-94 (2014).

44. Elbaz-Alon, Y. et al. A dynamic interface between vacuoles and mitochondria in yeast. *Dev Cell* **30**, 95-102 (2014).

45. Jin, G. et al. Saposin B is a human coenzyme q10-binding/transfer protein. *J Clin Biochem Nutr* **42**, 167-74 (2008).

46. Kashiba, M. et al. Prosaposin regulates coenzyme Q10 levels in HepG2 cells, especially those in mitochondria. *J Clin Biochem Nutr* **55**, 85-9 (2014).

47. Tirrell, P.S., Nguyen, K.N., Luby-Phelps, K. & Friedman, J.R. MICOS subcomplexes assemble independently on the mitochondrial inner membrane in proximity to ER contact sites. *J Cell Biol* **219**(2020).

48. Subramanian, K. et al. Coenzyme Q biosynthetic proteins assemble in a substrate-dependent manner into domains at ER-mitochondria contacts. *J Cell Biol* **218**, 1353-1369 (2019).

49. Eisenberg-Bord, M. et al. The Endoplasmic Reticulum-Mitochondria Encounter Structure Complex Coordinates Coenzyme Q Biosynthesis. *Contact (Thousand Oaks)* **2**, 2515256418825409 (2019).

50. Padilla-Lopez, S. et al. Genetic evidence for the requirement of the endocytic pathway in the uptake of coenzyme Q6 in Saccharomyces cerevisiae. *Biochim Biophys Acta* **1788**, 1238-48 (2009).

51. Fernandez-Del-Rio, L. et al. Genes and lipids that impact uptake and assimilation of exogenous coenzyme Q in Saccharomyces cerevisiae. *Free Radic Biol Med* **154**, 105-118 (2020).

52. Bentinger, M., Brismar, K. & Dallner, G. The antioxidant role of coenzyme Q. *Mitochondrion* **7 Suppl**, S41-50 (2007).

53. Turunen, M., Olsson, J. & Dallner, G. Metabolism and function of coenzyme Q. *Biochim Biophys Acta* **1660**, 171-99 (2004).

54. Alcazar-Fabra, M., Navas, P. & Brea-Calvo, G. Coenzyme Q biosynthesis and its role in the respiratory chain structure. *Biochim Biophys Acta* **1857**, 1073-1078 (2016).

55. Navas, P., Villalba, J.M. & de Cabo, R. The importance of plasma membrane coenzyme Q in aging and stress responses. *Mitochondrion* **7 Suppl**, S34-40 (2007).

56. Santos-Ocana, C. et al. Genetic evidence for coenzyme Q requirement in plasma membrane electron transport. *J Bioenerg Biomembr* **30**, 465-75 (1998).

57. Bersuker, K. et al. The CoQ oxidoreductase FSP1 acts parallel to GPX4 to inhibit ferroptosis. *Nature* **575**, 688-692 (2019).

58. Doll, S. et al. FSP1 is a glutathione-independent ferroptosis suppressor. *Nature* **575**, 693-698 (2019).

59. Dixon, S.J. et al. Ferroptosis: an iron-dependent form of nonapoptotic cell death. *Cell* **149**, 1060-72 (2012).

60. Conrad, M. & Pratt, D.A. The chemical basis of ferroptosis. *Nat Chem Biol* **15**, 1137-1147 (2019).

61. Friedmann Angeli, J.P., Krysko, D.V. & Conrad, M. Ferroptosis at the crossroads of cancer-acquired drug resistance and immune evasion. *Nat Rev Cancer* **19**, 405-414 (2019).

Chapter 4. UbiB Proteins Regulate Cellular CoQ Distribution

Zachary A. Kemmerer[1], Kyle P. Robinson[1], Jonathan M. Schmitz, Brett R. Paulson, Adam Jochem, Paul D. Hutchins, Joshua J. Coon, and David J. Pagliarini

[1]These authors contributed equally to this work.

This chapter was submitted to *Nature Communications* for publication and is currently under review. It has also been published as an article at *bioRxiv* (2020, doi:10.1101/2020.12.09.418202) by the authors listed above.

Author Contributions

Z.A.K., K.P.R., and D.J.P. conceived of the project and its design. Z.A.K. and K.P.R. conducted experiments and performed data analysis. J.M.S. purified and characterized GFP nanobody. B.R.P. and P.D.H. performed and analyzed mass spectrometry experiments. A.J. contributed to new reagents (cloning). All authors edited the manuscript. Z.A.K., K.P.R., and D.J.P. wrote the manuscript. D.J.P. supervised the project.

Abstract

Coenzyme Q (CoQ, or ubiquinone) is a redox-active lipid essential for many core metabolic processes in mitochondria, including oxidative phosphorylation[1-3]. While lesser appreciated, CoQ also serves as a key membrane-embedded antioxidant throughout the cell[4]. However, how CoQ is mobilized from its site of synthesis on the inner mitochondrial membrane to other sites of action remains a longstanding mystery. Here, using a combination of yeast genetics, biochemical fractionation, and lipid profiling, we identify two highly conserved but poorly characterized mitochondrial proteins, Ypl109c (Cqd1) and Ylr253w (Cqd2), that reciprocally regulate this process. Loss of Cqd1 skews cellular CoQ distribution away from mitochondria, resulting in markedly enhanced resistance to oxidative stress caused by exogenous polyunsaturated fatty acids (PUFAs), whereas loss of Cqd2 promotes the opposite effects. The activities of both proteins rely on their atypical kinase/ATPase domains, which they share with Coq8—an essential auxiliary protein for CoQ biosynthesis. Overall, our results reveal new protein machinery central to CoQ trafficking in yeast and lend new insights into the broader interplay between mitochondrial and cellular processes.

Results

Extramitochondrial CoQ combats oxidative stress

To our knowledge, no proteins have yet been directly associated with cellular CoQ trafficking from mitochondria, but the extreme hydrophobicity of CoQ suggests that this process likely requires dedicated machinery. We sought to identify such proteins by exploiting CoQ's extramitochondrial antioxidant role. Budding yeast (*Saccharomyces cerevisiae*) lacking CoQ or phospholipid hydroperoxide glutathione peroxidases (PHGPx) are sensitive to the oxidative stress conferred by exogenous polyunsaturated fatty acids (PUFAs), such as linolenic acid (18:3)[5,6]. To force cells into relying more heavily on the antioxidant properties of CoQ, we deleted all three PHGPx genes in W303 *S. cerevisiae* (Δ*gpx1*Δ*gpx2*Δ*gpx3,* hereafter referred to as Δ*gpx1/2/3*). We validated that this strain is sensitized to 18:3 treatment and demonstrated that this sensitivity is dampened when cellular CoQ levels are augmented through supplementation with the soluble CoQ precursor 4-hydroxybenzoate (4-HB) (Fig. 1a-b). Importantly, the CoQ analog decylubiquinone was markedly more effective at protecting against PUFA stress than its mitochondria-targeted counterpart, mitoquinone, suggesting that extramitochondrial CoQ is the predominant mediator of PUFA resistance (Fig. 1c). This is consistent with previous data showing that exogenous PUFAs are incorporated into endogenous membranes slowly, and therefore, populate non-mitochondrial membranes first[6]. Thus, we established a strain whose survival in the presence of PUFAs is especially dependent on extramitochondrial CoQ.

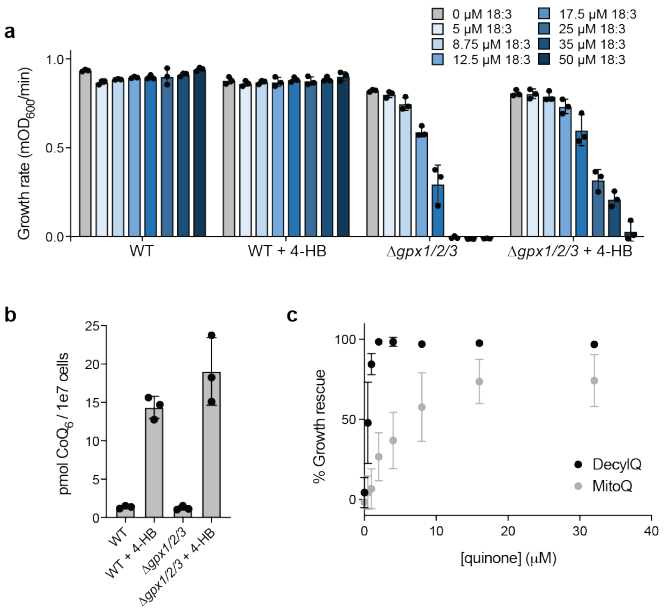

Figure 1. Extramitochondrial CoQ combats oxidative stress. a, Growth rate of wild type (WT) and Δ*gpx1/2/3* yeast in synthetic complete media minus para-aminobenzoate (*p*ABA–) containing 2% (w/v) glucose (mean ± SD, n = 3) and the indicated additives. 4-hydroxybenzoate, 4-HB; linolenic acid (PUFA), 18:3. **b**, Total CoQ from WT and Δ*gpx1/2/3* yeast described in **a** (mean ± SD, n = 3). **c**, Rescue assay under the conditions described in **a** comparing the ability of decylubiquinone (DecylQ) and mitoquinone (MitoQ) to restore growth of Δ*gpx1/2/3* yeast treated with 35 μM 18:3 (mean ± SD, n = 3).

Loss of Cqd1 confers PUFA resistance

We reasoned that suppressor mutations that increase extramitochondrial CoQ levels would enhance PUFA resistance in this strain, so we performed a forward-genetic suppressor screen (Fig. 2a). We randomly mutagenized Δ*gpx1/2/3* yeast with ethyl methanesulfonate (EMS) and isolated colonies tolerant of 18:3 treatment. From ~20,000 unique mutant colonies, we obtained four hit strains with substantial PUFA resistance (Fig. 2b). We then performed whole-genome sequencing that revealed non-synonymous mutations in 442 unique genes across these four strains (Extended

Data Table 1). These mutants were ranked using PROVEAN (Protein Variation Effect Analyzer), a software tool for predicting deleterious protein changes[7]. PROVEAN assigns a disruption score (D-Score) that reflects the likelihood that a given mutation is deleterious. In our collective dataset, 99 genes achieved a D-Score below the strict threshold of -4.1 (Fig. 2c; Extended Data Table 1). Given the overall limited overlap in hits between mutant strains, it is likely that our dataset includes multiple genes that contribute to an enhanced PUFA resistance phenotype.

We chose to focus on mitochondrial proteins for further examination since, to our knowledge, trafficking machinery at the site of CoQ synthesis in mitochondria has yet to be identified. Of the nine mitochondrial proteins harboring likely deleterious mutations, one, Cqd1 (Ypl109c), is an uncharacterized protein that resides on the inner mitochondrial membrane (IMM), making it an attractive candidate for further study (Fig. 2c; Extended Data Fig. 1a). Moreover, Cqd1 possesses the same UbiB atypical kinase/ATPase domain as Coq8, an essential protein for CoQ synthesis that resides on the matrix face of the IMM[8-11]. Our recent work suggests that Coq8 ATPase activity may be coupled to the extraction of hydrophobic CoQ precursors from the IMM for subsequent processing by membrane-associated matrix enzymes[12]. Cqd1 resides on the opposite side of the IMM, facing the intermembrane space[9,13] (Extended Data Fig. 1b), physically separated from the other CoQ-related enzymes but still positioned for direct access to membrane-embedded CoQ precursors and mature CoQ. Furthermore, a recent study reported that haploinsufficiency of human *CQD1* ortholog *ADCK2* led to aberrant mitochondrial lipid oxidation and myopathy associated with CoQ deficiency[14].

In our screen, mutant C (mutC) contains an early stop codon in *CQD1* (Fig. 2c, Extended Data Fig. 1c). To test whether this mutation is important for mutC's phenotype, we reintroduced WT *CQD1* into this strain under its endogenous promoter. Indeed, this reintroduction re-conferred

PUFA sensitivity (Fig. 2d). Furthermore, deletion of *CQD1* in the parent Δ*gpx1/2/3* strain, which lacks all other mutC mutations, was sufficient to enhance PUFA resistance (Fig. 2e-f). Collectively, these data demonstrate that disruption of *CQD1* is at least partially causative for mutC's PUFA-resistant phenotype.

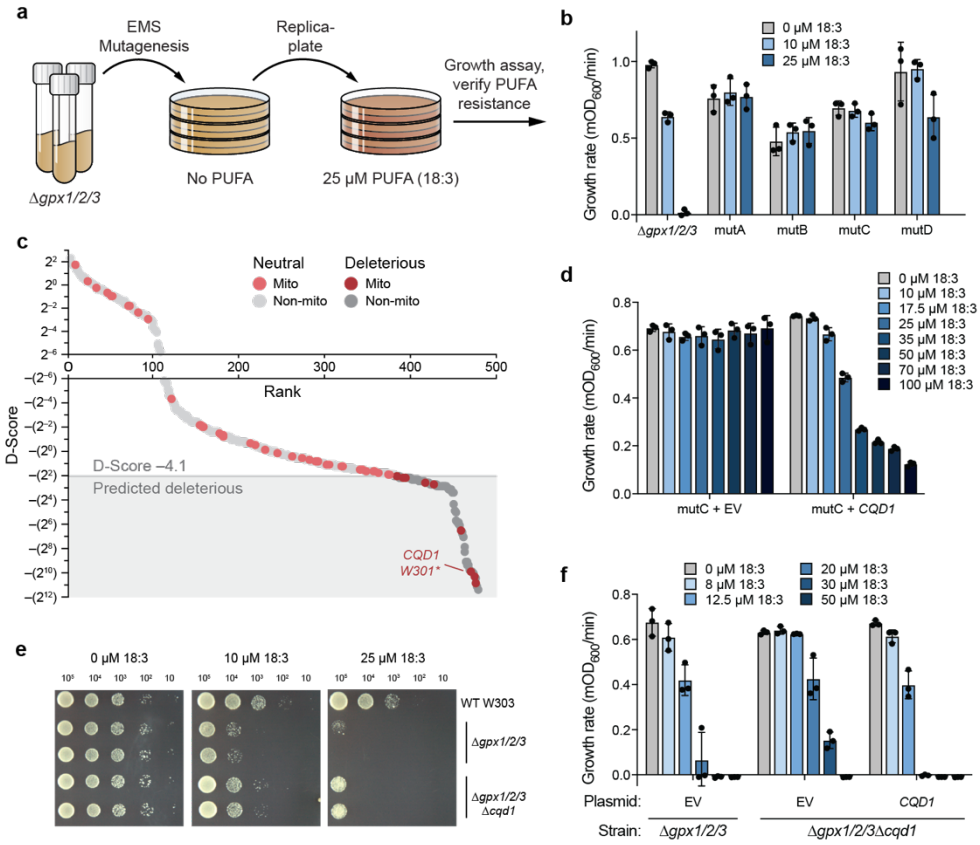

Figure 2. Genome-wide screen for CoQ trafficking genes identifies uncharacterized UbiB protein Cqd1. a, Schematic of forward-genetic yeast screen for genes involved in CoQ trafficking. **b**, Growth rates of Δ*gpx1/2/3* and four mutant strains resistant to 18:3 treatment (mutA-D). Yeast were assayed in *p*ABA– media containing 2% (w/v) glucose with 0-25 μM 18:3 (mean ± SD, n = 3). **c**, Mutant strains mutA-D were submitted for whole-genome sequencing to identify non-synonymous mutations (total = 442). Mutations were analyzed with PROVEAN to filter for likely

deleterious changes (D-score ≤ -4.1, shaded box). Gray, all genes; red, mitochondrial genes. Light, predicted neutral; dark, predicted deleterious. **d**, Growth rate of mutC yeast expressing empty vector (EV) or endogenous *CQD1* (mean ± SD, n = 3). Yeast were assayed under the conditions described in **b** with 0-100 μM 18:3. **e,** Drop assay of WT, Δ*gpx1/2/3*, and Δ*gpx1/2/3*Δ*cqd1* yeast grown for 3 days on solid *p*ABA– medium containing 2% (w/v) glucose, 0.5% (w/v) ethanol (EtOH), and 0-25 μM 18:3. **f**, Growth rates of Δ*gpx1/2/3* and Δ*gpx1/2/3*Δ*cqd1* yeast expressing EV or endogenous *CQD1* (mean ± SD, n = 3). Yeast were assayed under the conditions described in **b** with 0-50 μM 18:3. Source data for panel **c** is provided as a Source Data file.

Cqd1 affects CoQ distribution

Our results above suggest that loss of *CQD1* confers cellular resistance to PUFA-mediated oxidative stress by increasing extramitochondrial CoQ. We reasoned that this was likely rooted either in a general increase in CoQ production or in its redistribution. To test these models, we first measured total levels of CoQ and its early mitochondrial precursor polyprenyl-4-hydroxybenzoate (PPHB) in cells lacking *CQD1* or control genes (Fig. 3a-c). As expected, disruption of *HFD1*, which encodes the enzyme that produces the soluble CoQ precursor 4-HB, led to loss of CoQ and PPHB, while disruption of *COQ8* caused complete loss of CoQ with the expected buildup of the PPHB precursor. However, we found no significant change in CoQ or PPHB levels in the Δ*cqd1* strain, demonstrating that Cqd1 is essential neither for CoQ biosynthesis nor the import of CoQ precursors under the conditions of our analyses.

To next examine CoQ distribution, we fractionated yeast and measured CoQ levels (Fig. 3d; Extended Data Fig. 2a). We observed that Δ*cqd1* yeast had a significant increase in CoQ from the non-mitochondrial (NM) fraction, consisting of organelles and membranes that do not pellet

with mitochondria, and a corresponding decrease in mitochondrial (M) CoQ. Deletion of the tricarboxylic acid (TCA) cycle enzyme Kgd1 had no effect on relative CoQ levels (Fig. 3d) despite causing a deficiency in respiratory growth (Fig. 3e), indicating that general mitochondrial dysfunction does not perturb CoQ distribution. The increased extramitochondrial CoQ in Δ*cqd1* yeast is consistent with the observation that deleting *CQD1* increases PUFA resistance (Fig. 2e-f).

To our knowledge, this is the first example of a genetic disruption leading to altered cellular distribution of endogenous CoQ. To further validate this finding, we examined growth in glycerol, a non-fermentable carbon source, which requires an intact mitochondrial electron transport chain. We reasoned that a decrease in mitochondrial CoQ would disrupt respiratory growth in media depleted of CoQ precursors. Indeed, deletion of *CQD1* significantly reduced respiratory growth rate in this medium (Fig. 3e). To confirm that this defect is caused by CoQ depletion, we rescued growth with CoQ of different isoprene tail lengths (CoQ_2 and CoQ_4) and with CoQ precursors, which are more readily delivered due to their solubility (Fig. 3f). Endogenous expression of *CQD1* rescued respiratory growth without affecting total CoQ levels (Fig. 3g, Extended Data Fig. 2b), further supporting the hypothesis that CoQ distribution, not biosynthesis, is perturbed in Δ*cqd1* yeast.

We next sought to begin understanding how Cqd1 functions in CoQ distribution. Our recent work on Cqd1's UbiB homolog COQ8 (yeast Coq8 and human/mouse COQ8A) revealed that it possesses an atypical protein kinase-like (PKL) fold that endows ATPase activity but occludes larger proteinaceous substrates from entering the active site[11,15] (Extended Data Fig. 2c-e). Unlike COQ8, Cqd1 is recalcitrant to recombinant protein purification; therefore, in lieu of direct in vitro activity assays, we examined the ability of Cqd1 point mutants to rescue the respiratory growth defect of Δ*cqd1* yeast. Similar to Coq8[11,12,15], the ability of Cqd1 to rescue the

Δ*cqd1* respiratory growth deficiency depended on its core protein kinase-like (PKL) family residues[16] required for phosphoryl transfer (Fig. 3g) and on quintessential UbiB motif residues (Extended Data Fig. 2e-h). Further biochemical work is required to prove Cqd1's enzymatic activity; however, these data support a model whereby its ability to promote CoQ distribution relies on atypical kinase/ATPase activity (Fig. 3h).

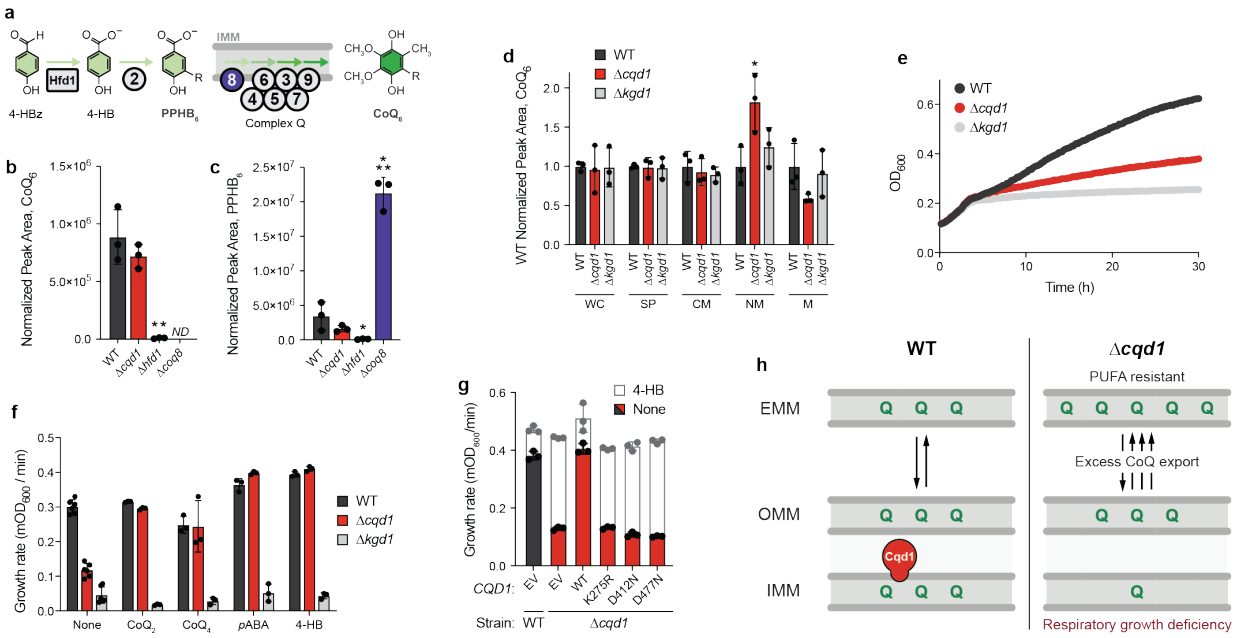

Figure 3. Cqd1 influences cellular CoQ distribution. a, Schematic of CoQ biosynthesis pathway. Polyprenyl hydroxybenzoate (PPHB) is an early precursor that undergoes a series of head group modifications by IMM-associated Coq enzymes (complex Q) to produce CoQ. Hfd1 is essential for PPHB synthesis, while Coq8 is required for production of CoQ. **b**, Total CoQ and **c**, polyprenyl-4-hydroxybenzoate (PPHB) from WT, Δ*cqd1*, Δ*hfd1*, and Δ*coq8* yeast (mean ± SD, n = 3); not detected, ND. **d**, CoQ from subcellular fractions derived from WT, Δ*cqd1*, and Δ*kgd1* yeast (mean ± SD, n = 3). Spheroplast, SP; crude mitochondria, CM; non-mitochondrial fraction, NM; enriched mitochondria, M. **e**, Growth assay of WT, Δ*cqd1*, and Δ*kgd1* yeast in *p*ABA– media

containing 0.1% (w/v) glucose and 3% (w/v) glycerol (mean, n = 6). Yeast enter the respiratory phase of growth after ~4 hours in this growth condition. **f**, Growth rate of WT, Δ*cqd1*, and Δ*kgd1* yeast assayed under conditions described in d (mean ± SD; none n = 6, all others n = 3). Yeast were grown in the presence and absence of 100 μM CoQ analogs (CoQ_2, CoQ_4) and 1 μM CoQ precursors (*p*ABA, 4-HB). **g**, Growth rate of WT and Δ*cqd1* yeast transformed with the indicated plasmids (EV, *CQD1* or *CQD1* point mutants) and grown in Ura–, *p*ABA– media containing 0.1% (w/v) glucose and 3% (w/v) glycerol (mean ± SD, n = 3). Yeast were treated with 0 (colored bars) or 1 μM 4-HB (white bars, superimposed) to determine rescue of respiratory growth. **h**, Model for Cqd1's putative role in cellular CoQ distribution. Significance calculated by a two-tailed Student's *t*-test; * = $p < 0.05$, ** = $p < 0.01$, *** = $p < 0.001$.

Cqd2 counteracts Cqd1 function

Beyond Coq8 and Cqd1, *S. cerevisiae* have just one other member of the UbiB family—Cqd2 (aka Mcp2 or Ylr253w). Cqd2 is also poorly characterized and resides in the same location as Cqd1, on the outer face of the IMM[9,13,17] (Extended Data Fig. 1b). Previous studies have identified genetic and physical interactions connecting Cqd2 to mitochondrial lipid homeostasis, but not to a specific pathway[17-19]. Given the similarity between these three proteins (Extended Data Fig. 2d-e), we anticipated that Cqd2 might also be connected to CoQ biology.

To test this hypothesis, we disrupted *CQD2* in Δ*gpx1/2/3* yeast and subjected this strain to PUFA-mediated stress. Surprisingly, Δ*gpx1/2/3*Δ*cqd2* yeast exhibited an enhanced sensitivity to PUFA treatment—the opposite phenotype to that of Δ*gpx1/2/3*Δ*cqd1* (Fig. 4a; Extended Data Fig. 3a). Furthermore, Δ*gpx1/2/3*Δ*cqd1*Δ*cqd2* yeast phenocopied the parental (Δ*gpx1/2/3*) strain (Fig. 4a; Extended Data Fig. 3a). Under respiratory conditions, Δ*cqd2* yeast exhibited no detectable

change in growth. However, deleting *CQD2* from Δ*cqd1* yeast (Δ*cqd1*Δ*cqd2*) restored this strain's impaired respiratory growth rate to WT levels (Fig. 4b-c). Conversely, reintroduction of *CQD2* into the Δ*cqd1*Δ*cqd2* strain recapitulated the respiratory growth deficiency of Δ*cqd1* (Fig. 4d). Total cellular CoQ levels remained unchanged (Extended Data Fig. 3b), again suggesting these CoQ-related phenotypes are unrelated to CoQ biosynthesis. Similar to Cqd1 (Fig. 3g), Cqd2 function was dependent on intact canonical PKL and UbiB-specific residues (Fig. 4d, Extended Data Fig. 3c-e), suggesting that all three UbiB family proteins in yeast are active phosphoryl transfer enzymes.

The analyses above, coupled with the submitochondrial location of Cqd1 and Cqd2, suggest a model whereby these enzymes may reciprocally regulate the amount of CoQ within the IMM. To test this directly, we used the amphipathic polymer styrene maleic acid (SMA) to solubilize integral membrane proteins into detergent-free SMA lipid particles (SMALPs)[20] from yeast harboring an endogenously-tagged subunit of mitochondrial complex II (Sdh4-GFP). We reasoned that purifying lipid patches containing Sdh4, which directly interacts with CoQ to facilitate succinate dehydrogenase (Complex II) activity[21], would yield a suitable lipid microenvironment to measure IMM-localized CoQ. After solubilization (Extended Data Fig. 3f), we isolated native IMM patches that possessed Sdh4-GFP using a recombinantly purified His-tagged GFP nanobody (Fig. 4e; Extended Data Fig. 3g-h). We show that purified Sdh4-GFP IMM patches are largely void of extramitochondrial and outer mitochondrial membrane (OMM) protein contamination (Fig. 4f), making this an attractive approach for assessing IMM CoQ abundance.

We generated a panel of deletion strains in the Sdh4-GFP background to investigate how loss of Cqd1 and Cqd2 impact CoQ abundance in this IMM microenvironment. These yeast strains exhibited the same respiratory phenotypes as the W303 background strains and had similar levels

of whole-cell CoQ (Extended Data Fig. 3i-j). After solubilization and affinity enrichment (Extended Data Fig. 3k-l), Sdh4-GFP IMM patch lipids were extracted for targeted CoQ measurements. Consistent with our respiratory growth observations, Δ*cqd1* yeast had significantly lower levels of IMM patch CoQ. Conversely, the Δ*cqd2* yeast had elevated IMM patch CoQ, while Δ*cqd1*Δ*cqd2* yeast had levels similar to the parental strain (Fig. 4g). These data provide direct evidence of protein-dependent changes in CoQ distribution, corroborating our phenotypic observations. Taken together, our results suggest that Cqd1 and Cqd2 reciprocally regulate the levels of IMM CoQ and support a model wherein proper cellular CoQ distribution is dependent on the balance of their activities (Fig. 4h).

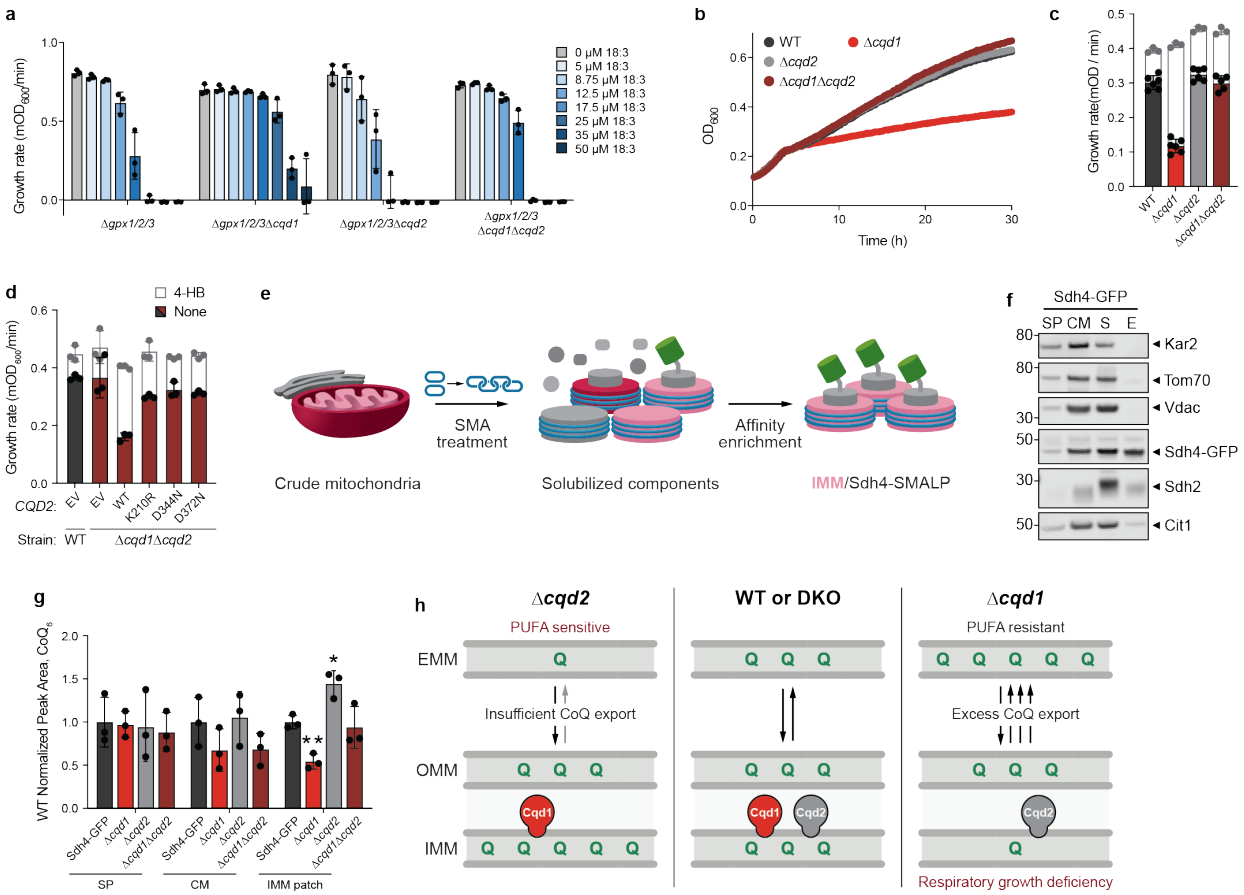

Figure 4. Cqd2 function opposes Cqd1 control of CoQ distribution. a, Growth rate of Δ*gpx1/2/3* and the described yeast strains in *p*ABA– media containing 2% (w/v) glucose and the indicated additives (mean ± SD, n = 3). **b**, Growth assay of WT, Δ*cqd1*, Δ*cqd2*, and Δ*cqd1*Δ*cqd2* yeast in *p*ABA– media containing 0.1% (w/v) glucose and 3% (w/v) glycerol (mean ± SD, n = 6). **c**, Growth rate of yeast strains in b treated with 0 (colored bars) or 1 μM 4-HB (white bars, superimposed) (mean ± SD; 0 μM 4-HB n = 6, 1 μM 4-HB n = 3). **d,** Growth rate of WT and Δ*cqd1*Δ*cqd2* yeast transformed with the indicated plasmids (EV, *CQD2* or *CQD2* point mutants) and grown in Ura–, pABA– media containing 0.1% (w/v) glucose and 3% (w/v) glycerol (mean ± SD, n = 3). Yeast were treated with 0 (colored bars) or 1 μM 4-HB (white bars, superimposed) to determine recapitulation of respiratory growth defect. **e**, Schematic of Sdh4-GFP styrene maleic acid (SMA) lipid particle (SMALP) isolation. **f**, Western blot to assess purity of SMALP isolation samples from endogenously tagged Sdh4-GFP yeast. Spheroplast, SP; crude mitochondria, CM; soluble, S; elution, E (or IMM patch). Kar2, endoplasmic reticulum; Tom70, outer mitochondrial membrane (OMM); Vdac, OMM; Sdh4-GFP, SMALP target/IMM; Sdh2, IMM; Cit1, mitochondrial matrix. **g**, CoQ from subcellular fractions derived from SMALP isolation described in **f** for the indicated strains (mean ± SD, n = 3). **h**, Summary model depicting opposing roles for yeast UbiB family proteins in cellular distribution of CoQ. Significance calculated by a two-tailed Student's *t*-test; * = $p < 0.05$, ** = $p < 0.01$, *** = $p < 0.001$.

Discussion

Our work demonstrates that two previously uncharacterized UbiB family proteins influence the cellular distribution of mitochondria-derived CoQ. To our knowledge, Cqd1 and Cqd2 are the first proteins implicated in this process, which is essential for providing membranes throughout the cell

with the CoQ necessary for enzymatic reactions and antioxidant defense. Further efforts are needed to establish how these proteins support CoQ distribution mechanistically; however, their similarity to Coq8 and the requirement for canonical PKL residues in their active sites suggests that Cqd1 and Cqd2 may couple ATPase activity to the selective extraction/deposition of CoQ from/to the IMM.

Once extracted from the IMM, we expect that subsequent steps would be required to deliver CoQ throughout the cell. The multimeric ER-mitochondrial encounter structure (ERMES) and mitochondrial contact site and cristae organizing system (MICOS) complexes facilitate interorganellar lipid and metabolite transfer[22,23]. Recent work has revealed that CoQ biosynthetic machinery and MICOS subcomplexes often colocalize with ERMES[24-26], suggesting that these sites could serve as conduits for CoQ transport. Additionally, COQ9 is a lipid binding protein that likely delivers CoQ precursors to matrix enzymes[27], suggesting that other lipid binding proteins may exist to shuttle CoQ from mitochondria to other membranes. Our genetic screen has nominated several extramitochondrial and cytosolic proteins as promising leads for these processes.

Our investigations here focused on CoQ; however, it is possible that Cqd1 and Cqd2 (aka Mcp2) influence lipid transport and homeostasis more broadly. Previous work has identified an array of genetic interactions for Cqd1 and Cqd2 with lipid biosynthesis and homeostasis genes[19,28]. Notably, Cqd2 has negative genetic interactions with all five subunits of ERMES, while Cqd1 and Cqd2 have inverse genetic relationships with Psd1 and Ups1. Indeed, Cqd2 was previously identified as a high-copy suppressor of a growth defect caused by loss of the ERMES subunit Mdm10[17]. More recently, three conserved Cqd2 active site residues were shown to mitigate rescue

of Δ*mdm10* yeast growth[18], results that we confirm (Cqd2 K210R) and expand upon with six additional residue mutations.

Finally, UbiB family proteins are found across all domains of life[29]. UbiB homologs in plants are abundant, with 17 ABC1K proteins found in *Arabidopsis*[30]. Many of these ABC1K proteins are localized to plastoglobules, and recent work suggests that ABC1K1 and ABC1K3 may affect the mobility and exchange of subcellular plastoquinone-9 pools[31], suggesting UbiB proteins might function in quinone distribution across species. In humans, five UbiB proteins have been identified, ADCK1-5. While COQ8A (ADCK3) and COQ8B (ADCK4) have established roles in CoQ biosynthesis and human disease[11,32,33], the biological roles of other ADCK proteins remain elusive. Genome-wide knockdown studies have implicated these uncharacterized *ADCK* genes in several cancer disease states[34-37]. As novel targets for human disease intervention, it will be important to determine if functional conservation exists between Cqd1 and Cqd2 and their human orthologs, ADCK2 and ADCK1/5, respectively. Recently, a crucial new role for extramitochondrial CoQ was identified in mitigating ferroptosis, a type of cell death stemming from a buildup of toxic lipid peroxides, suggesting that manipulating CoQ distribution could provide therapeutic benefits[38,39]. Notably, small-molecule modulators have been developed for Coq8[12] and COQ8A[40], indicating that UbiB proteins are promising druggable targets.

Collectively, our work to de-orphanize these poorly characterized mitochondrial proteins represents the first step in addressing enduring questions regarding endogenous cellular CoQ distribution and unlocking the therapeutic potential of controlling this pathway.

Methods

Yeast Strains and Cultures

Unless otherwise described, *Saccharomyces cerevisiae* haploid W303 (MATa his3 leu2 met15 trp1 ura3) yeast were used. For SMA-derived lipid nanodisc work, endogenous GFP-tagged BY4741 (MATa his3Δ1 leu2Δ0 met15Δ0 ura3Δ0) yeast strains[41] were used. Yeast deletion strains were generated using standard homologous recombination or CRISPR-mediated methods. For homologous recombination, open reading frames were replaced with the KanMX6, HygMX6, or NatMX6 cassette as previously described[42]. Cassette insertion was confirmed by a PCR assay and DNA sequencing. CRISPR-mediated deletions were performed as described in[43]. 20-mer guide sequences were designed with the ATUM CRISPR gRNA design tool (https://www.atum.bio/eCommerce/cas9/input) and cloned into pRCC-K, and 500 ng of the guide-inserted pRCC-K was used per yeast transformation. Donor DNA was 300 pmol of an 80-nt Ultramer consisting of 40 bp upstream and 40 bp downstream of the ORF (for scarless deletions) or ~6 µg of PCR-amplified Longtine cassette with flanking homology 40 bp upstream and 40 bp downstream of the ORF (for cassette-replacement deletions).

Synthetic complete (and dropout) media contained drop-out mix (US Biological), yeast nitrogen base (with ammonium sulfate and without amino acids) (US Biological), and the indicated carbon source. *p*ABA$^-$ (and dropout) media contained Complete Supplement Mixture (Formedium), Yeast Nitrogen Base without amino acids and without *p*ABA (Formedium), and the indicated carbon source. All media were sterilized by filtration (0.22 µm pore size).

Yeast Growth Assay and Drop Assay

PUFA Growth Assays

To assay yeast growth in liquid media, individual colonies were used to inoculate synthetic complete (or synthetic complete dropout) media (2% glucose, w/v) starter cultures, which were incubated overnight (30 °C, 230 rpm). Yeast were diluted to 1.1×10^6 cells/mL in *p*ABA$^-$ (or *p*ABA$^-$ dropout) media (2% glucose, w/v) and incubated until early log phase (30 °C, 7-8 h, 230 rpm). Yeast were swapped into fresh *p*ABA$^-$ media (2% glucose, w/v) at an initial density of 5×10^6 cells/mL with indicated additives. The cultures were incubated (30 °C, 1140 rpm) in an Epoch2™ plate reader (BioTek®) in a sterile 96 well polystyrene round bottom microwell plate (Thermo) with a Breathe-Easy® cover seal (Diversified Biotech). Optical density readings (A_{600}) were obtained every 10 minutes, and growth rates were calculated with Gen5 v3.02.2 software (BioTek®), excluding timepoints from stationary phase.

Respiratory Growth Assays

Individual colonies of *S. cerevisiae* were used to inoculate synthetic complete media (2% glucose, w/v) starter cultures, which were incubated overnight (30 °C, 230 rpm). For transformed yeast strains, the corresponding Ura$^-$ media was used. Yeast were diluted to 1×10^6–1.33×10^6 cells/mL in *p*ABA$^-$ media (2% glucose, w/v) and incubated until early log phase (30 °C, 7-8 h, 230 rpm). Yeast were swapped into *p*ABA$^-$ media with glucose (0.1%, w/v) and glycerol (3%, w/v) at an initial density of 5×10^6 cells/mL with indicated additives. The cultures were incubated (30 °C, 1140 rpm) in an Epoch2 plate reader (BioTek) in a sterile 96 well polystyrene round bottom microwell plate (Thermo) with a Breathe-Easy cover seal (Diversified Biotech). Optical density readings (A_{600}) were obtained every 10 minutes, and growth rates were calculated with Gen5 v3.02.2 software (BioTek), excluding timepoints before the diauxic shift and during stationary phase growth.

Drop Assays

Individual colonies of yeast were used to inoculate *p*ABA-limited media (2% w/v glucose, 100 nM *p*ABA) starter cultures, which were incubated overnight (30 °C, 230 rpm). Cells were spun down (21,000 x *g*, 2 min) and resuspended in water. Serial dilutions of yeast (10^5, 10^4, 10^3, 10^2, or 10 cells) were dropped onto *p*ABA$^-$ media (2% glucose and 1% EtOH, w/v) agar plates with indicated additives and incubated (30 °C, 2-3 d).

Forward-genetic Screen

Individual colonies of Δ*gpx1/2/3* yeast were used to inoculate YEPD starter cultures, which were incubated overnight. 1.0×10^8 cells were pelleted, washed once with sterile water, and resuspended in 2.5 mL of 100 mM sodium phosphate buffer, pH 7.0. Ethyl methanesulfonate (EMS) (80 µL) was added, and cells were incubated (90 min, 30 °C, 230 rpm). Cells were washed thrice with sodium thiosulfate (5% w/v) to inactivate EMS. Cells were resuspended in water, and 1.0×10^4 cells were plated on *p*ABA-limited (2% w/v glucose, 100 nM *p*ABA) agar plates. After 3 days, cells were replica-plated onto *p*ABA$^-$ (2% glucose, w/v) plates with 0 µM or 25 µM linolenic acid (C18:3, Sigma). Colonies that grew on 25 µM linolenic acid were picked into YEPD overnight cultures and struck on YEPD plates, and PUFA resistance phenotypes were confirmed with plate reader growth assays. For mutant strains that grew in the presence of 25 µM linolenic acid, genomic DNA was isolated with the MasterPure™ Yeast DNA Purification Kit (Lucigen) and submitted to GENEWIZ for whole-genome sequencing. *S. cerevisiae* genome assembly and variation calling were performed with SeqMan NGen 14 and ArrayStar 14 (DNASTAR Lasergene

suite). Variant D-Score predictions were obtained using the PROVEAN v1.1.3 web server (http://provean.jcvi.org/seq_submit.php).

Plasmid Cloning

Expression plasmids were cloned with standard restriction enzyme cloning methods. ORF specific primers were used to amplify Cqd1 (Ypl109c) and Cqd2 (Ylr253w) from W303 yeast genomic DNA. Amplicons were treated with DpnI to degrade genomic DNA and ligated into the digested p416 GPD plasmid (Addgene). Cloning products were then transformed into *E. coli* 10G chemically competent cells (Lucigen). Plasmids were isolated from transformants and Sanger sequencing was used to identify those containing the correct insertion.

Constructs containing Cqd1 and Cqd2 were digested with SalI and BamHI or HindIII to liberate the GPD promoter. Digested backbones were then combined with amplified endogenous promoter regions (1000 bases upstream for Cqd1, 500 bases upstream for Cqd2) and ligated to generate endogenous promoter vectors for Cqd1 and Cqd2.

Site-Directed Mutagenesis

Point mutants were constructed as described in the Q5® Site-Directed Mutagenesis Kit (New England Biolabs) and were confirmed via Sanger sequencing. Yeast were transformed as previously described[44] with plasmids encoding Cqd1 and Cqd2 variants with their endogenous promoters and grown on uracil drop-out (Ura^-) synthetic media plates containing glucose (2%, w/v).

Homology Model Generation

Amino acid sequences of Cqd1 and Cqd2 were threaded through COQ8A apo crystal structure (PDB:4PED) via the online iTASSER webserver[45]. Superimposed homology models were visualized in the PyMOL Molecular Graphics System (Version 2.0, Schrödinger, LLC). Color schemes depicting protein domain organization were chosen according to previous work[15].

Subcellular Fractionation

Individual colonies of *S. cerevisiae* were used to inoculate synthetic complete media (2% glucose, w/v) starter cultures, which were incubated overnight (30 °C, 230 rpm). Yeast were diluted to 1.2×10^6 cells/mL in 50 mL *p*ABA$^-$ media (2% glucose, w/v) and incubated until early log phase (30 °C, 12 h, 230 rpm). Yeast were swapped into 2 L of *p*ABA$^-$ media with glucose (0.1%, w/v) and glycerol (3%, w/v) at an initial density of 5×10^4 cells/mL and incubated until early log phase (30 °C, 20 h, 230 rpm). $1x10^8$ cells were collected for whole-cell (WC) analyses. The remaining culture was pelleted by centrifugation (4,500 x g, 7 min) and weighed (5-6 g). Pellets were then fractionated using previously described methods[46]. To isolate crude mitochondria, samples were pelleted by centrifugation (15,000 x g, 10 min, 4 °C). Crude mitochondria were resuspended in SEM buffer (10 mM MOPS/KOH pH 7.2, 250 mM sucrose, 1 mM EDTA) containing 10 µg trypsin (sequencing grade, Promega) and rotated end-over-end overnight (12 h, 4 °C) to disrupt proteinaceous organelle contact tethers[47]. Digested samples were pelleted by centrifugation (12,000 x g, 10 min, 4 °C) and the supernatant was collected. Pelleted material was resuspended in 900 µL SEM buffer containing 1 mM phenylmethylsulfonyl fluoride (SEM+PMSF) to deactivate trypsin. Resuspended material was pelleted (12,000 x g, 10 min, 4 °C) and the supernatant was collected. This was repeated once more and supernatant material was pooled (2.7 mL). To this, SEM buffer was added up to 10 mL before ultracentrifugation (106,000 x g, 1 h, 4

°C) to collect microsomes (non-mitochondrial fraction; NM). Pelleted crude mitochondria were resuspended in 700 µL SEM+PMSF and then added to a freshly prepared sucrose gradient (bottom to top: 1.5 mL 60% sucrose, 4 mL 32% sucrose, 1.5 mL 23% sucrose, and 1.5 mL 15% sucrose) for separation by ultracentrifugation (134,000 x g, 1 h, 4 °C). Enriched mitochondrial samples were recovered at the 32-60% interface and diluted with 30 mL SEM. Mitochondria were pelleted (15,000 x g, 10 min, 4 °C) and resuspended in fresh SEM (150 µL total). The protein concentration of all subcellular fractions (spheroplasts, SP; crude mitochondria, CM; non-mitochondrial fraction, NM; enriched mitochondria, M) was determined using the Pierce™ BCA Protein Assay Kit (Thermo) before Western blot (5 µg) analyses and lipid extractions.

GFP Nanobody

Recombinant Purification

pCA528-His-SUMO-GFP nanobody (GFPnb) constructs were transformed into RIPL competent *E. coli* cells for protein expression. GFPnb was overexpressed in *E. coli* by autoinduction overnight[48] (37 °C, 4 h; 20°C, 20 h). Cells were isolated by centrifugation (4,500 x *g*, 12 min, RT), flash frozen in N_2(l) dropwise, and stored at -80 °C. For protein purification, cells were added to a Retsch® mixer mill MM 400 screw-top grinding jar pre-equilibrated with N_2(l). The cells were lysed by cryogenic grinding (-196 °C, 30 Hz, 120 s x 3). Ground cell pellet was collected and resuspended end-over-end for 1 h in lysis buffer (160 mM HEPES pH 7.5, 400 mM NaCl, 0.25 mM PMSF, 1 Roche cOmplete™ Protease Inhibitor Cocktail tablet, 500 U Benzonase® Nuclease) at 4 °C. The lysate was clarified by centrifugation (15,000 x *g*, 30 min, 4 °C). Clarified lysate was added to pre-equilibrated TALON® cobalt resin (Takara Bio) and incubated end-over-end for 1 h at 4 °C. TALON® resin was pelleted by centrifugation (700 x *g*, 2 min, 4 °C) and washed twice

with equilibration buffer (160 mM HEPES pH 7.5, 400 mM NaCl, 0.25 mM PMSF) and twice with wash buffer (160 mM HEPES pH 7.5, 400 mM NaCl, 0.25 mM PMSF, 20 mM imidazole). His-tagged protein was eluted with elution buffer (160 mM HEPES (pH 7.5), 400 mM NaCl, 0.25 mM PMSF, 400 mM imidazole). The eluted protein was concentrated to ~600 µL with an Amicon® Ultra Centrifugal Filter (10 kDa MWCO) and exchanged into equilibration buffer. Concentrated protein elution was centrifuged (15,000 x *g*, 5 min, 4 °C) to pellet precipitate and filtered through a 0.22 µM syringe filter. Concentrated protein elution was separated via size exclusion chromatography on a HiLoad™ 16/600 Superdex™ 75 pg. Fractions from the size exclusion chromatography were analyzed by SDS-PAGE, and the fractions containing GFPnb were pooled and concentrated to ~1 mL. The concentration of GFPnb was determined by Bradford assay (Bio-Rad Protein Assay Kit II) and was diluted with equilibration buffer and glycerol to a final concentration of 20 mg/mL protein (160 mM HEPES pH 7.5, 400 mM NaCl, 10% glycerol). The final protein was aliquoted, flash frozen in N_2(l) and stored at -80 °C. Fractions from the protein preparation were analyzed by SDS-PAGE.

Differential Scanning Fluorimetry

The differential scanning fluorimetry method (thermal shift assay) was performed as described previously[49]. Purified recombinant GFPnb was diluted to a final concentration of 4 µM with DSF buffer (100 mM HEPES pH 7.5, 150mM NaCl) and 1:1250 SYPRO® Orange Dye (Life Tech). Thermal shift data was collected with QuantStudio Real-Time PCR v1.2 software and analyzed with Protein Thermal Shift v1.3 software.

Native Nanodisc Isolation

Individual colonies of *S. cerevisiae* (BY4741) were used to inoculate synthetic complete media (2% glucose, w/v) starter cultures, which were incubated overnight (30 °C, 230 rpm). Yeast were diluted to 5×10^6 cells/mL in 50 mL *p*ABA$^-$ media (2% glucose, w/v) and incubated until late log phase (30 °C, 16 h, 230 rpm). Yeast were swapped into 2 L of *p*ABA$^-$ media with glucose (0.1%, w/v) and glycerol (3%, w/v) at an initial density of 2.5×10^6 cells/mL and incubated until early log phase (30 °C, 16 h, 230 rpm). Yeast cultures were pelleted by centrifugation (4,500 x g, 7 min) and weighed (2–3 g). Pellets were then fractionated using previously described methods[46]. For preparative scale affinity purification, crude mitochondria were resuspended in 50 µL BB7.4 (0.6 M sorbitol, 20 mM HEPES-KOH pH 7.4), diluted in 950 µL ice cold BB7.S (20 mM HEPES-KOH pH 7.4), vortexed for 10 sec (medium setting 8, Vortex Genie), and incubated on ice for 30 minutes. Swollen mitochondria were then sonicated briefly (⅛'' tip, 20% amplitude) for 2 - 5 second pulses with 60 seconds between pulses. Mitoplasts with osmotically ruptured outer membranes were recovered by centrifugation at (20,000 × *g*, 10 min, 4 °C). After removing the supernatant, each pellet was resuspended with 1 mL of Buffer B (20 mM HEPES-KOH pH 8.0, 200 mM NaCl) containing 2% (w/v) styrene maleic acid copolymer (SMA, Polyscope SMALP® 25010P) by repeat pipetting and rotated end-over-end (4 h, 4 °C). Soluble SMA extracts were separated from non-extracted material by centrifugation at 21,000 × *g* for 10 min at 4 °C. Soluble material was then were added to NTA nickel resin (400 µL slurry, Qiagen), which was pre-charged (overnight at 4 °C, end-over-end) with recombinant His-tagged GFPnb (12.5 µL, 20 mg/mL). This mixture of soluble SMA extracts and charged nickel resin was rotated end-over-end (24 h, 4 °C).

Nickel resin was pelleted by centrifugation (700 x *g*, 2 min, 4 °C) and the supernatant fraction was carefully collected. Nickel resin was washed twice with Buffer B and twice with 500 µL Wash Buffer [Buffer B containing 20 mM imidazole]. Native nanodiscs bound to His-GFPnb

were eluted with Buffer B containing 250 mM imidazole by rotating end-over-end for 20 min at 4 °C. Due to the presence of GFP nanobody in the elution samples, relative target abundance was determined by Western analysis and anti-GFP band quantification. Protein concentrations of all other samples were quantified by Pierce™ BCA Protein Assay Kit (Thermo).

Lipid Extraction

$CHCl_3$:MeOH Extraction

$1x10^8$ yeast cells were harvested by centrifugation (4,000 *g*, 5 min, 4 °C). The supernatant was removed, and the cell pellet was flash frozen in N_2 (l) and stored at -80 C. (l) and stored at −80 °C. Frozen yeast pellets were thawed on ice and resuspended in 100 µL cold water. To this, 100 µL of glass beads (0.5 mm; RPI) and CoQ_{10} internal standard (10 µL, 10 µM) were added and bead beat (2 min, 4 °C). 900 µL extraction solvent (1:1 $CHCl_3$/MeOH, 4 °C) was added and samples were vortexed briefly. To complete phase separation, samples were acidified with 85 µL 6 M HCl (4 °C), vortexed (2 x 30 s, 4 °C), and centrifuged (5,000 *g*, 2 min, 4 °C). The resulting aqueous layer (top) was removed and 400 µL of the organic layer (bottom) was transferred to a clean tube and dried under $Ar_{(g)}$. Dried organic matter (lipids) were reconstituted in ACN/IPA/H_2O (65:30:5, v/v/v, 100 µL) by vortexing (2 x 30 s, RT) and transferred to an amber vial (Sigma; QSertVial™, 12 x 32 mm, 0.3 mL) for LC–MS analysis.

Petroleum Ether:MeOH Extraction

For yeast whole-cell measurements, 1 $x10^8$ cells were collected by centrifugation (4,000 x *g*, 5 min) and layered with 100 µL of glass beads (0.5 mm; RPI). Whole-cell samples and all other fractions were then suspended in ice-cold methanol (500 µL; with 1 µM CoQ_8 internal standard)

and vortexed (10 min, 4 °C). ~500 µL of petroleum ether was added to extract lipids, and samples were vortexed (3 min, 4 °C) and centrifuged (17,000 x *g*, 1 min) to separate phases. The petroleum ether (upper) layer was collected, and the extraction was repeated with another round of petroleum ether (500 µL), vortexing (3 min, 4 °C), and centrifugation (17,000 x *g*, 1 min). The petroleum ether layers were pooled and dried under argon. Lipids were resuspended in 2-propanol (15 µL) and transferred to amber glass vials (Sigma; QSertVial™, 12 x 32 mm, 0.3 mL). Sodium borohydride (15 µL of 10 mM in 2-propanol) was added to reduce quinones, and samples were vortexed briefly and incubated (5-10 min). Methanol (20 µL) was added to remove excess sodium borohydride, and samples were vortexed briefly and incubated (5-10 min). Samples were briefly flushed with nitrogen gas.

Lipidomic Analysis

Targeted LC-MS for Yeast CoQ_6 and $PPHB_6$

LC-MS analysis was performed on an Acquity CSH C18 column held at 50 °C (100 mm x 2.1 mm x 1.7 µm particle size; Waters) using a Vanquish Binary Pump (400 µL/min flow rate; Thermo Scientific). Mobile phase A consisted of 10 mM ammonium acetate and 250 µL/L acetic acid in ACN:H2O (70:30, v/v). Mobile phase B consisted of IPA:ACN (90:10, v/v) also with 10 mM ammonium acetate and 250 µL/L acetic acid. Mobile phase B was initially held at 50% for 1.5 min and then increased to 99% over 7.5 min and held there for 2 min. The column was equilibrated for 2.5 min before the next injection. 10 µL of each extract was injected by a Vanquish Split Sampler HT autosampler (Thermo Scientific) in a randomized order.

The LC system was coupled to a Q Exactive Orbitrap mass spectrometer (MS) through a heated electrospray ionization (HESI II) source (Thermo Scientific). Source conditions were as follow: HESI II and capillary temperature at 350 °C, sheath gas flow rate at 25 units, aux gas flow rate at 15 units, sweep gas flow rate at 5 units, spray voltage at +3.5 kV/-3.5 kV, and S-lens RF at 90.0 units. The MS was operated in a polarity switching mode acquiring positive and negative full MS and MS2 spectra (Top2) within the same injection. Acquisition parameters for full MS scans in both modes were 17,500 resolution, 1×10^6 automatic gain control (AGC) target, 100 ms ion accumulation time (max IT), and 200 to 1600 m/z scan range. MS2 scans in both modes were then performed at 17,500 resolution, 1×10^5 AGC target, 50 ms max IT, 1.0 m/z isolation window, stepped normalized collision energy (NCE) at 20, 30, 40, and a 10.0 s dynamic exclusion.

Parallel Reaction Monitoring (PRM) in positive polarity mode was utilized to monitor for two primary adducts, $[M+H]^+$ and $[M+NH^4]^+$, of each CoQ species. For CoQ_6, we targeted the mass to charge ratio of 592.449 and 609.475; for CoQ_8, 728.574 and 745.601; and for CoQ_{10}, 864.7 and 881.727. PRM MS settings were: Automatic gain control (AGC) target at $5x10^5$, Maximum IT at 100 ms, resolving power at 35,000, loop count at 2, isolation window at 3.0 *m/z,* and collision energy at 35. Another experiment performed in tandem with PRM used targeted single ion monitoring (t-SIM) in negative mode to determine the primary adduct, $[M-H]^-$, of CoQ intermediates. For $PPHB_6$, we targeted the mass to charge ratio of 544.908 and used the following t-SIM MS settings: AGC target at $5x10^5$, Maximum IT at 100 ms, and resolving power at 140,000 with an isolation window of 4.0 *m/z*.

Data Analysis

The resulting LC-MS data was manually processed using a custom TraceFinder 4.1 (Thermo Scientific) method using a mass precision of 4 and mass tolerance of 10 ppm to detect and identify the different species and adducts of CoQ_6 and CoQ_8 and intermediates.

Targeted HPLC-ECD for Yeast CoQ_6

For yeast whole-cell measurements, 5 $x10^8$ cells were collected by centrifugation (4,000 x *g*, 5 min) and layered with 100 µL of glass beads (0.5 mm; RPI). Lipids from whole-cell samples and other fractions were extracted according to the "*Petroleum Ether:MeOH Extraction*" section above. Samples were analyzed by reverse-phase high-pressure liquid chromatography with electrochemical detection (HPLC-ECD) using a C18 column (Thermo Scientific, Betasil C18, 100 x 2.1 mm, particle size 3 µm) at a flow rate of 0.3 mL/min with a mobile phase of 75% methanol, 20% 2-propanol, and 5% ammonium acetate (1 M, pH 4.4). After separation on the column, the $NaBH_4$-reduced quinones were quantified on ECD detector (Thermo Scientific ECD3000-RS) equipped with 6020RS omni Coulometric Guarding Cell "E1", and 6011RS ultra Analytical Cell "E2" and "E3". To prevent premature quinone oxidation, the E1 guarding electrode was set to −200 mV. Measurements were made using the analytical E2 electrode operating at 600 mV after complete oxidation of the quinone sample and E3 electrode (600 mV) was used to ensure that total signal was recorded on the E2 cell. For each experiment, a CoQ_6 standard in 2-propanol was also prepared with sodium borohydride and methanol treatment, and different volumes were injected to make a standard curve. Quinones were quantified by integrating respective peaks using the Chromeleon 7.2.10 software (Thermo) and normalized to CoQ_8 internal standard.

Antibodies and Western Blots

Antibodies

Primary antibodies used in this study include anti-Kar2 (SCBT sc-33630, 1:5000; RRID: AB_672118), anti-Cit1[50] (Biomatik, 1:4000), anti-β-actin (Abcam ab8224, 1:1000; RRID: AB_449644), anti-Tom70[51] (1:1000, a gift from Nora Vogtle, University of Freiburg), anti-Vdac (Abcam ab110326, 1:2000; RRID: AB_10865182); anti-GFP (SCBT sc-9996, 1:1000; RRID: AB_627695), anti-Sdh2[52] (1:5000, a gift from Oleh Khalimonchuk, University of Nebraska). Secondary antibodies include goat anti-mouse (LI-COR 926-32210, 1:15000; RRID: AB_621842) and goat anti-rabbit (LI-COR 926-32211, 1:15000; RRID: AB_621843).

SMA Solubility Western Blot

Mitoplasts were recovered and solubilized in styrene maleic acid containing buffer as described above in "*Native Nanodisc Isolation.*" To determine the extent of GFP target solubilization, equal amounts of "input" (IP) and soluble supernatant (S) were obtained, along with the total pellet (insoluble, IS). 75 µL of the input sample was collected immediately after SMA solubilization. After separating soluble SMA extracts from non-extracted material via centrifugation (21,000 × *g*, 10 min, 4 °C), the supernatant was transferred to a clean tube for an additional 5 minute spin. 75 µL of soluble sample was then transferred to a new tube. The resulting pellet was washed with 1 mL of Buffer B and centrifuged (21,000 × *g* for 5 min at 4 °C). The resulting supernatant was aspirated and 75 µL of Buffer B was added to the insoluble (IS) fraction. From each sample, proteins were extracted by standard chloroform-methanol procedures. Precipitated protein was reconstituted in 75 µL 0.1 M NaOH. 25 µL 4X LDS sample buffer containing beta-mercaptoethanol (BME) was added and samples were incubated (95 °C, ~10 min). Proteins were analyzed with 4–12% Novex NuPAGE Bis-Tris SDS-PAGE (Invitrogen) gels (1 h, 150 V). The

gel was transferred to PVDF membrane at 100 V for 1 h with transfer buffer (192 mM glycine, 25 mM Tris, 20% methanol [v/v]). The membrane was blocked with 5% nonfat dry milk (NFDM) in TBST (20 mM Tris pH 7.4, 150 mM NaCl, 0.05% Tween 20 [v/v]) (1 h with agitation). Antibodies were diluted in 1% NFDM in TBST and incubated with the PVDF (overnight, 4 °C with agitation). The PVDF was washed three times in TBST and the secondary antibodies were diluted 1:15,000 in 1% NFDM in TBST (1.5 h, r.t.). The membrane was washed three times in TBST and imaged on a LI-COR Odyessey CLx using Image Studio v5.2 software.

SMALP Fractionation Western Blot

Fractions described above in "*Native Nanodisc Isolation*" and "*SMA Solubility Western Blot*" were collected and used for western blot analysis. 4 μg of spheroplasts (SP) and crude mitochondria (CM) were loaded, along with equal volumes of extracted soluble (S) and final elution (E) samples. Western blots were performed as described above.

Statistical Analysis

All experiments were performed in at least biological triplicate, unless stated otherwise. In all cases, "mean" refers to arithmetic mean, and "SD" refers to sample standard deviation. Statistical analyses were performed using Microsoft Excel. *p*-values were calculated using an unpaired, two-tailed, Student's *t*-test. In all cases, *n* represents independent replicates of an experiment.

Additional Information

Code Availability

No coding was used or generated for the completion of this study.

Reporting Summary

Further information on research design is available in the Nature Research Reporting Summary linked to this article.

Data availability

Next generation sequencing data (Fig. 2, Extended Data Fig 1) have been deposited to NCBI SRA (BioProject ID PRJNA679831; SRA accession SRP293543). Additional source data for Fig. 1-4 and Extended Data 1-3 are provided with the paper. All other data supporting the finding of this study are available from the corresponding authors on reasonable request.

Acknowledgements

We thank Jared Rutter and Jodi Nunnari for providing the parental yeast strains used in our studies, Steven Claypool for consultation on SMALP generation, Adam Frost for providing the plasmid containing GFP nanobody, Nora Vogtle and Oleh Khalimonchuk for providing mitochondrial antibodies, Matt Stefely for assistance with figure generation, and current and former members of the Pagliarini Laboratory for their feedback. This work was supported by NIH R35GM131795 and R01 GM112057 (to D.J.P.), NIH T32DK007665, William H. Peterson Fellowship, Washburn Wharton Fellowship, and University of Wisconsin Biochemistry Funding (to Z.A.K.), a National Science Foundation Graduate Research Fellowship DGE-1747503 (to K.P.R.), and P41GM108538 (to J.J.C. and D.J.P.).

Affiliations

Morgridge Institute for Research, Madison, WI, USA.

Zachary A. Kemmerer, Kyle P. Robinson, Jonathan M. Schmitz, Adam Jochem, and David J. Pagliarini

Department of Biochemistry, University of Wisconsin-Madison, Madison, WI, USA.

Zachary A. Kemmerer, Kyle P. Robinson, Jonathan M. Schmitz, Adam Jochem, and David J. Pagliarini

Genome Center of Wisconsin, Madison, Wisconsin, USA.

Joshua J. Coon

Department of Chemistry, University of Wisconsin-Madison, Madison, WI, USA.

Brett R. Paulson, Paul D. Hutchins, and Joshua J. Coon

Department of Biomolecular Chemistry, University of Wisconsin-Madison, Madison, WI, USA.

Joshua J. Coon

Departments of Cell Biology and Physiology; Biochemistry and Molecular Biophysics; and Genetics, Washington University School of Medicine, St. Louis, MO, USA

David J. Pagliarini

Corresponding Author

Correspondence and requests for materials should be addressed to D.J.P. (pagliarini@wustl.edu).

Ethics Declaration

Competing interests

J.J.C. is a consultant for Thermo Fisher Scientific.

Extended Data

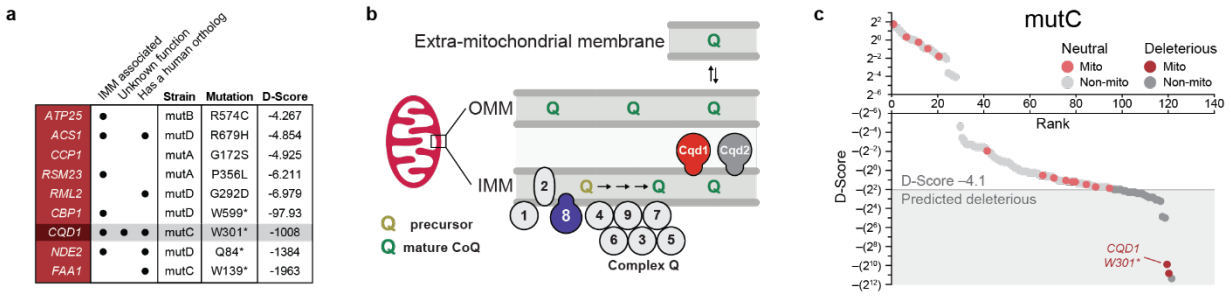

Extended Data Figure 1. Genome-wide screen for CoQ trafficking genes identifies uncharacterized UbiB protein Cqd1. a, Criteria for nine mitochondrial candidates used to nominate genes for additional investigation. Submitochondrial localization was confirmed by comparison to previous submitochondrial profiling datasets[9], while protein function and human ortholog criteria were determined with existing database mining (UniProt and PhylomeDB, respectively). **b,** Schematic showing the submitochondrial localization of UbiB family proteins Coq8 (purple), Cqd1 (red), and Cqd2 (gray). Coq8 is essential for CoQ biosynthesis in concert with other Coq proteins (Coq1-9). **c**, Non-synonymous mutations identified using whole-genome sequencing for strain mutC were analyzed with PROVEAN to filter for likely deleterious changes (D-score ≤ -4.1, shaded box). Gray, all genes; red, mitochondrial genes. Light, predicted neutral; dark, predicted deleterious.

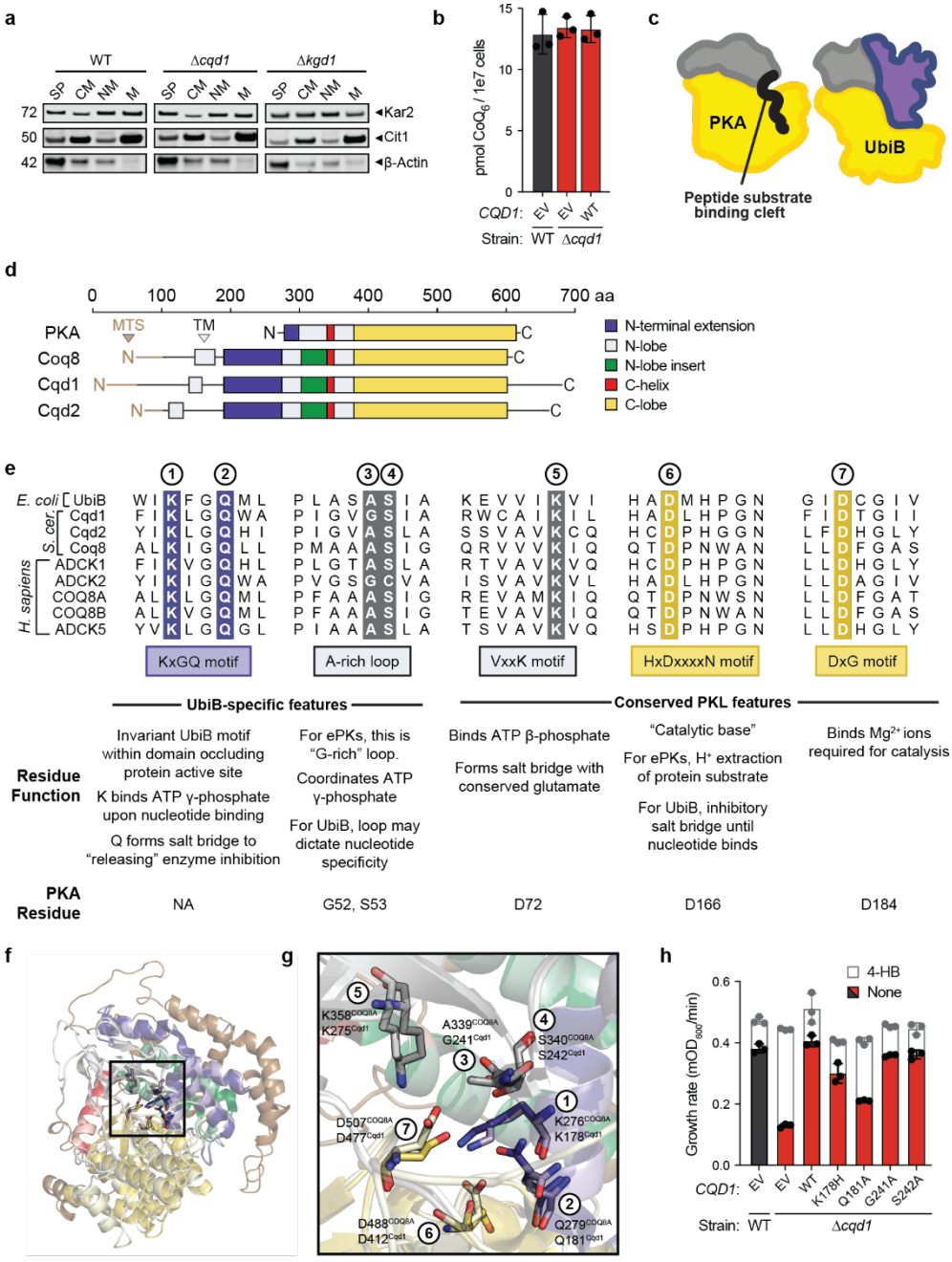

Extended Data Figure 2. Cqd1 influences cellular CoQ distribution. a, Western blot of subcellular samples derived from fractionated WT, Δ*cqd1*, and Δ*kgd1* yeast. Spheroplast, SP; crude mitochondria, CM; non-mitochondrial fraction, NM; enriched mitochondria, M. Kar2, endoplasmic reticulum; Cit1, mitochondria; β-actin, cytoplasm. **b**, Total CoQ from WT and Δ*cqd1* yeast transformed with the indicated plasmids and grown in Ura–, *p*ABA– media containing 0.1%

(w/v) glucose and 3% (w/v) glycerol (mean ± SD, n = 3). **c**, Cartoon of canonical protein kinase A (PKA; 1ATP) and human COQ8A (4PED) showing protein domain organization. Protein kinases often contain a β-sheet rich N-terminal domain (gray) and a helical C-terminal domain (yellow). COQ8A contains a unique N-terminal extension (purple) containing the invariant UbiB-specific 'KxGQ' motif. **d**, Domain alignment of PKA and yeast UbiB proteins. Mitochondrial targeting sequence, MTS; transmembrane domain, TM. **e**, UbiB family sequence alignment of UbiB-specific and conserved protein kinase-like (PKL) features. Residue functions within the canonical protein kinase or UbiB architecture are described below. The three conserved PKL residues shown are essential for phosphoryl transfer activity. **f**, Homology model for Cqd1 (light) aligned with COQ8A (4PED, dark). The model was threaded using I-TASSER[45] and COQ8A structure to guide modeling. Boxed and outlined in black are residues described in **g**, and unmodeled regions are colored in brown. **i**, Zoomed in view of conserved PKL and UbiB-specific residues. **h**, Growth rate of WT and Δ*cqd1* yeast transformed with the indicated plasmids (EV, *CQD1* or *CQD1* point mutants*)* and grown in Ura–, *p*ABA– media containing 0.1% (w/v) glucose and 3% (w/v) glycerol (mean ± SD, n = 3). Yeast were treated with 0 (colored bars) or 1 μM 4-HB (white bars, superimposed) to determine rescue of respiratory growth.

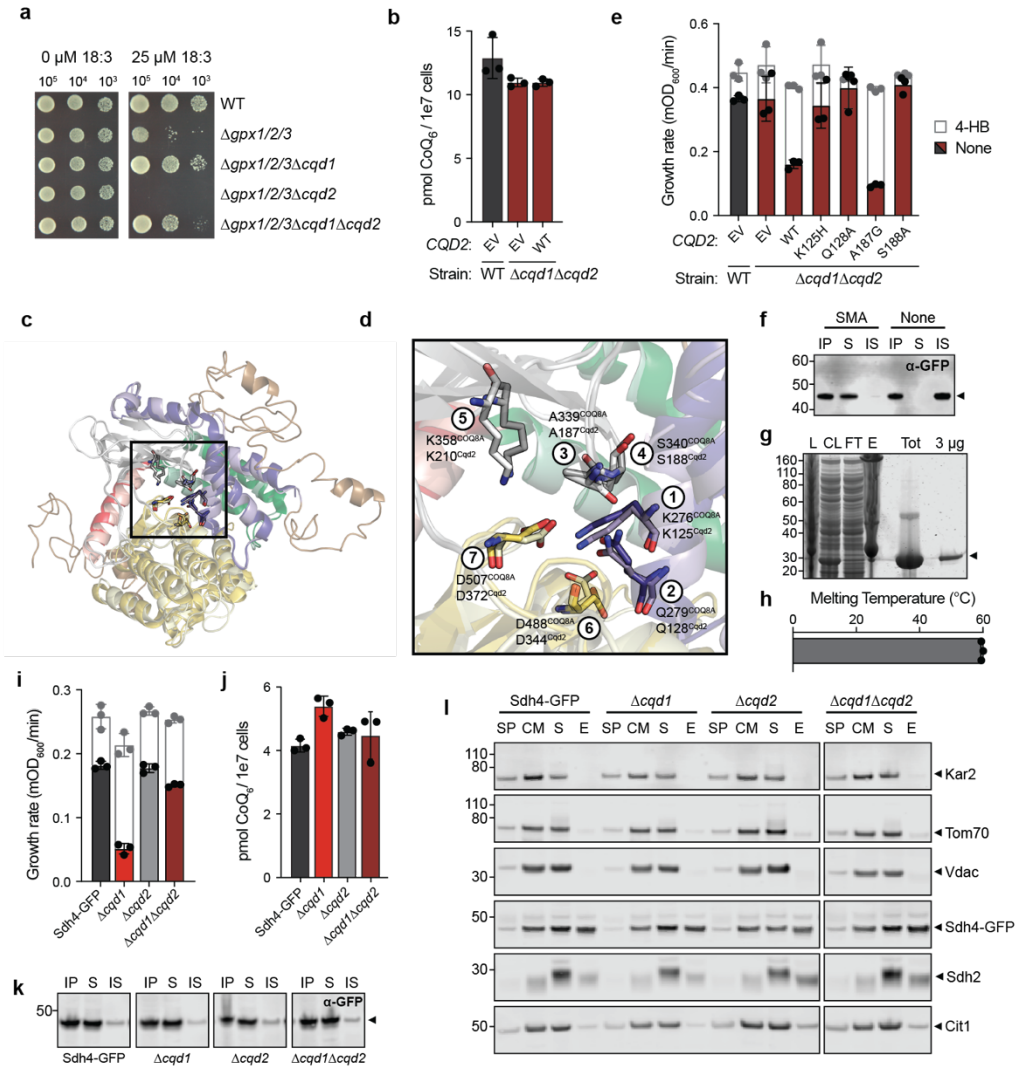

Extended Data Figure 3. Cqd2 function opposes Cqd1 control of CoQ distribution.

a, Serial dilution drop assay of indicated yeast strains grown for 3 days on solid *p*ABA– medium containing 2% (w/v) glucose, 0.5% (w/v) ethanol (EtOH), and 0-25 µM 18:3. **b**, Total CoQ from WT and Δ*cqd1*Δ*cqd2* yeast transformed with EV or endogenous *CQD2* and grown in Ura–, *p*ABA– media containing 0.1% (w/v) glucose and 3% (w/v) glycerol (mean ± SD, n = 3). **c**, Homology model for Cqd2 (light) aligned with COQ8A (4PED, dark). The model was threaded using I-TASSER[45] and COQ8A structure to guide modeling. Boxed and outlined in black are residues described previously (**Extended Data Fig. 2f**) and unmodeled regions are colored in

brown. **d**, Zoomed in view of conserved PKL and UbiB-specific residues described previously. **e**, Growth rate of WT and Δ*cqd1*Δ*cqd2* yeast transformed with the indicated plasmids and grown in Ura–, *p*ABA– media containing 0.1% (w/v) glucose and 3% (w/v) glycerol (mean ± SD, n = 3). Yeast were treated with 0 (colored bars) or 1 μM 4-HB (white bars, superimposed) to determine recapitulation of respiratory growth defect. **f**, Western blot to determine solubility of Sdh4-GFP target in the presence and absence of 2% (w/v) SMA. Input, IP; soluble, S; insoluble, IS. **g**, Recombinant purification of His-tagged GFP nanobody (GFPnb) via nickel resin enrichment and size-exclusion isolation. Lysate, L; clarified lysate, CL; flow-through, FT; elution, E; size-exclusion chromatography, SEC. **h**, Differential scanning fluorimetry of recombinant GFPnb to determine protein melting temperature. **i**, Growth rate of Sdh4-GFP yeast and indicated deletion strains assayed in *p*ABA– media containing 0.1% (w/v) glucose and 3% (w/v) glycerol and treated with 0 (colored bars) or 1 μM 4-HB (white bars, superimposed) (mean ± SD, n = 3). **j**, Total CoQ from yeast strains described in **i. k**, Western blot to determine solubility of Sdh4-GFP target during SMALP preparation from the indicated yeast strains. Input, IP; soluble, S; insoluble, IS. **l**, Western blot of SMALP isolation samples derived from the indicated yeast. Spheroplast, SP; crude mitochondria, CM; soluble, S; elution, elution, E (or IMM patch). Kar2, endoplasmic reticulum; Tom70, OMM; Vdac, OMM; Sdh4-GFP, SMALP target/IMM; Sdh2, IMM; Cit1, mitochondrial matrix.

References

1. Hatefi, Y., Haavik, A.G., Fowler, L.R. & Griffiths, D.E. Studies on the electron transfer system. XLII. Reconstitution of the electron transfer system. *J Biol Chem* **237**, 2661-2669 (1962).

2. Frerman, F.E. Acyl-CoA dehydrogenases, electron transfer flavoprotein and electron transfer flavoprotein dehydrogenase. *Biochem Soc Trans* **16**, 416-418 (1988).

3. Jones, M.E. Pyrimidine nucleotide biosynthesis in animals: genes, enzymes, and regulation of UMP biosynthesis. *Annu Rev Biochem* **49**, 253-279 (1980).

4. Bentinger, M., Brismar, K. & Dallner, G. The antioxidant role of coenzyme Q. *Mitochondrion* **7 Suppl**, S41-50 (2007).

5. Do, T.Q., Schultz, J.R. & Clarke, C.F. Enhanced sensitivity of ubiquinone-deficient mutants of Saccharomyces cerevisiae to products of autoxidized polyunsaturated fatty acids. *Proc Natl Acad Sci U S A* **93**, 7534-7539 (1996).

6. Avery, A.M. & Avery, S.V. Saccharomyces cerevisiae expresses three phospholipid hydroperoxide glutathione peroxidases. *J Biol Chem* **276**, 33730-33735 (2001).

7. Choi, Y., Sims, G.E., Murphy, S., Miller, J.R. & Chan, A.P. Predicting the functional effect of amino acid substitutions and indels. *PLoS One* **7**, e46688 (2012).

8. Tauche, A., Krause-Buchholz, U. & Rodel, G. Ubiquinone biosynthesis in Saccharomyces cerevisiae: the molecular organization of O-methylase Coq3p depends on Abc1p/Coq8p. *FEMS Yeast Res* **8**, 1263-1275 (2008).

9. Vogtle, F.N. *et al.* Landscape of submitochondrial protein distribution. *Nat Commun* **8**, 290 (2017).

10. Rhee, H.W. *et al.* Proteomic mapping of mitochondria in living cells via spatially restricted enzymatic tagging. *Science* **339**, 1328-1331 (2013).

11. Stefely, J.A. *et al.* Cerebellar Ataxia and Coenzyme Q Deficiency through Loss of Unorthodox Kinase Activity. *Mol Cell* **63**, 608-620 (2016).

12. Reidenbach, A.G. *et al.* Conserved Lipid and Small-Molecule Modulation of COQ8 Reveals Regulation of the Ancient Kinase-like UbiB Family. *Cell Chem Biol* **25**, 154-165 e111 (2018).

13. Morgenstern, M. *et al.* Definition of a High-Confidence Mitochondrial Proteome at Quantitative Scale. *Cell Rep* **19**, 2836-2852 (2017).

14. Vazquez-Fonseca, L. *et al.* ADCK2 Haploinsufficiency Reduces Mitochondrial Lipid Oxidation and Causes Myopathy Associated with CoQ Deficiency. *J Clin Med* **8** (2019).

15. Stefely, J.A. *et al.* Mitochondrial ADCK3 employs an atypical protein kinase-like fold to enable coenzyme Q biosynthesis. *Mol Cell* **57**, 83-94 (2015).

16. Kannan, N., Taylor, S.S., Zhai, Y., Venter, J.C. & Manning, G. Structural and functional diversity of the microbial kinome. *PLoS Biol* **5**, e17 (2007).

17. Tan, T., Ozbalci, C., Brugger, B., Rapaport, D. & Dimmer, K.S. Mcp1 and Mcp2, two novel proteins involved in mitochondrial lipid homeostasis. *J Cell Sci* **126**, 3563-3574 (2013).

18. Odendall, F. *et al.* The mitochondrial intermembrane space-facing proteins Mcp2 and Tgl2 are involved in yeast lipid metabolism. *Mol Biol Cell* **30**, 2681-2694 (2019).

19. Costanzo, M. *et al.* A global genetic interaction network maps a wiring diagram of cellular function. *Science* **353** (2016).

20. Lee, S.C. *et al.* A method for detergent-free isolation of membrane proteins in their local lipid environment. *Nat Protoc* **11**, 1149-1162 (2016).

21. Oyedotun, K.S. & Lemire, B.D. The Quinone-binding sites of the Saccharomyces cerevisiae succinate-ubiquinone oxidoreductase. *J Biol Chem* **276**, 16936-16943 (2001).

22. Murley, A. & Nunnari, J. The Emerging Network of Mitochondria-Organelle Contacts. *Mol Cell* **61**, 648-653 (2016).

23. Tamura, Y., Kawano, S. & Endo, T. Organelle contact zones as sites for lipid transfer. *J Biochem* **165**, 115-123 (2019).

24. Subramanian, K. *et al.* Coenzyme Q biosynthetic proteins assemble in a substrate-dependent manner into domains at ER-mitochondria contacts. *J Cell Biol* **218**, 1353-1369 (2019).

25. Eisenberg-Bord, M. *et al.* The Endoplasmic Reticulum-Mitochondria Encounter Structure Complex Coordinates Coenzyme Q Biosynthesis. *Contact (Thousand Oaks)* **2**, 2515256418825409 (2019).

26. Tirrell, P.S., Nguyen, K.N., Luby-Phelps, K. & Friedman, J.R. MICOS subcomplexes assemble independently on the mitochondrial inner membrane in proximity to ER contact sites. *J Cell Biol* **219** (2020).

27. Lohman, D.C. *et al.* An Isoprene Lipid-Binding Protein Promotes Eukaryotic Coenzyme Q Biosynthesis. *Mol Cell* **73**, 763-774 e710 (2019).

28. Hoppins, S. *et al.* A mitochondrial-focused genetic interaction map reveals a scaffold-like complex required for inner membrane organization in mitochondria. *J Cell Biol* **195**, 323-340 (2011).

29. Leonard, C.J., Aravind, L. & Koonin, E.V. Novel families of putative protein kinases in bacteria and archaea: evolution of the "eukaryotic" protein kinase superfamily. *Genome Res* **8**, 1038-1047 (1998).

30. Lundquist, P.K., Davis, J.I. & van Wijk, K.J. ABC1K atypical kinases in plants: filling the organellar kinase void. *Trends Plant Sci* **17**, 546-555 (2012).

31. Pralon, T. *et al.* Mutation of the Atypical Kinase ABC1K3 Partially Rescues the PROTON GRADIENT REGULATION 6 Phenotype in Arabidopsis thaliana. *Front Plant Sci* **11**, 337 (2020).

32. Ashraf, S. *et al.* ADCK4 mutations promote steroid-resistant nephrotic syndrome through CoQ10 biosynthesis disruption. *J Clin Invest* **123**, 5179-5189 (2013).

33. Lagier-Tourenne, C. *et al.* ADCK3, an ancestral kinase, is mutated in a form of recessive ataxia associated with coenzyme Q10 deficiency. *Am J Hum Genet* **82**, 661-672 (2008).

34. Wiedemeyer, W.R. *et al.* Pattern of retinoblastoma pathway inactivation dictates response to CDK4/6 inhibition in GBM. *Proc Natl Acad Sci U S A* **107**, 11501-11506 (2010).

35. Brough, R. *et al.* Functional viability profiles of breast cancer. *Cancer Discov* **1**, 260-273 (2011).

36. Simpson, K.J. *et al.* Identification of genes that regulate epithelial cell migration using an siRNA screening approach. *Nat Cell Biol* **10**, 1027-1038 (2008).

37. Qiu, M. *et al.* aarF domain containing kinase 5 gene promotes invasion and migration of lung cancer cells through ADCK5-SOX9-PTTG1 pathway. *Exp Cell Res* **392**, 112002 (2020).

38. Bersuker, K. *et al.* The CoQ oxidoreductase FSP1 acts parallel to GPX4 to inhibit ferroptosis. *Nature* **575**, 688-692 (2019).

39. Doll, S. *et al.* FSP1 is a glutathione-independent ferroptosis suppressor. *Nature* **575**, 693-698 (2019).

40. Asquith, C.R.M., Murray, N.H. & Pagliarini, D.J. ADCK3/COQ8A: the choice target of the UbiB protein kinase-like family. *Nat Rev Drug Discov* **18**, 815 (2019).

41. Huh, W.K. *et al.* Global analysis of protein localization in budding yeast. *Nature* **425**, 686-691 (2003).

42. Baudin, A., Ozier-Kalogeropoulos, O., Denouel, A., Lacroute, F. & Cullin, C. A simple and efficient method for direct gene deletion in Saccharomyces cerevisiae. *Nucleic Acids Res* **21**, 3329-3330 (1993).

43. Generoso, W.C., Gottardi, M., Oreb, M. & Boles, E. Simplified CRISPR-Cas genome editing for Saccharomyces cerevisiae. *J Microbiol Methods* **127**, 203-205 (2016).

44. Gietz, R.D. & Woods, R.A. Transformation of yeast by lithium acetate/single-stranded carrier DNA/polyethylene glycol method. *Methods Enzymol* **350**, 87-96 (2002).

45. Yang, J. *et al.* The I-TASSER Suite: protein structure and function prediction. *Nat Methods* **12**, 7-8 (2015).

46. Meisinger, C., Pfanner, N. & Truscott, K.N. Isolation of yeast mitochondria. *Methods Mol Biol* **313**, 33-39 (2006).

47. Forner, F., Arriaga, E.A. & Mann, M. Mild protease treatment as a small-scale biochemical method for mitochondria purification and proteomic mapping of cytoplasm-exposed mitochondrial proteins. *J Proteome Res* **5**, 3277-3287 (2006).

48. Fox, B.G. & Blommel, P.G. Autoinduction of protein expression. *Curr Protoc Protein Sci* **Chapter 5**, Unit 5 23 (2009).

49. Niesen, F.H., Berglund, H. & Vedadi, M. The use of differential scanning fluorimetry to detect ligand interactions that promote protein stability. *Nat Protoc* **2**, 2212-2221 (2007).

50. Guo, X. *et al.* Ptc7p Dephosphorylates Select Mitochondrial Proteins to Enhance Metabolic Function. *Cell Rep* **18**, 307-313 (2017).

51. Vogtle, F.N. *et al.* Mutations in PMPCB Encoding the Catalytic Subunit of the Mitochondrial Presequence Protease Cause Neurodegeneration in Early Childhood. *Am J Hum Genet* **102**, 557-573 (2018).

52. Bohovych, I. *et al.* Metalloprotease OMA1 Fine-tunes Mitochondrial Bioenergetic Function and Respiratory Supercomplex Stability. *Sci Rep* **5**, 13989 (2015).

Chapter 5: Conclusions and Future Directions

Author Contributions: Zachary A. Kemmerer wrote this chapter.

Conclusions

Summary

Coenzyme Q (CoQ, or ubiquinone) is a redox-active lipid essential for many core metabolic processes in mitochondria, including oxidative phosphorylation[1], fatty acid oxidation[2], and nucleotide biosynthesis[3]. CoQ also serves as a key membrane-embedded antioxidant throughout the cell[4]. Despite discovering CoQ more than 60 years ago, our understanding of CoQ biosynthesis is incomplete and how CoQ is mobilized from its site of synthesis on the IMM to other sites of action remains a longstanding mystery[5]. COQ8, a member of the highly conserved, UbiB family of atypical kinases[6,7], is an essential gene for CoQ production. Importantly, human UbiB proteins are connected to human disease, but lack effective treatment options.

The work presented in this thesis has advanced our understanding of (1) COQ8 biochemical function by characterizing robust ATPase activity, identifying small-molecule modulators, and generating a new tool for *in vivo* studies[8] and (2) identifying and characterizing previously uncharacterized UbiB yeast homologs Cqd1 (Ypl109c) and Cqd2 (Ylr253w) as reciprocal regulators of cellular CoQ distribution (Kemmerer, Robinson submitted). Collectively, this work has created a foundation on which to study the molecular function of UbiB proteins in both CoQ biosynthesis and CoQ mobilization.

Small-molecule and Lipid Regulation of COQ8

Activity of protein and small-molecule kinases are often regulated by endogenous small-molecules. Therefore, we wanted to investigate small-molecule modulation of COQ8 ATPase activity using unbiased and targeted means. Previously, we identified OHB (octaprenyl hydroxybenzoate) and OPP (octaprenylphenol) as two top hits for co-purifying lipids from yeast COQ8. Repeating this work with bacterial UbiB, affinity purification mass spectrometry was used in collaboration with Joshua Coon's laboratory to determine OHB and OPP are also highly enriched lipids, highlighting a conserved preference for UbiB proteins to bind early CoQ pathway intermediates. Using an orthogonal unbiased approach, one dimensional ^{1}H nuclear magnetic resonance ligand discovery was used to identify additional phenol derivatives resembling OHB and OPP. Considering that binding of these early intermediates may stimulate COQ8 ATPase activity, we then tested small-molecule mimics *in vitro*. Consistently, 2-allylphenol and 2-propylphenol increased activity, which was further enhanced in the presence of Triton X-100. This hinted that membrane association *in vivo* may be important for activation of COQ8 by CoQ intermediates.

COQ8 contains a transmembrane (TM) domain, is membrane-associated, and performs its functions at the IMM surface, suggesting that lipids could modulate its activity. *In vitro* assays were used to determine liposomes binding and ATPase activity were dramatically enhance by the presence of COQ8's TM domain. Interestingly, liposome binding only occurred in the presence of cardiolipin (CL), an important mitochondrial lipid. To identify residues important for membrane binding, we first employed *in silico* modeling (coarse-grained molecular dynamics) in collaboration with Matteo Dal Perraro's laboratory. We confirmed these results *in vitro*,

demonstrating that mutations significantly reduced liposome binding, as well as COQ8 function *in vivo*.

Since chemical tools for probing COQ8 function *in vivo* are lacking, we developed an "analog-sensitive" Coq8 variant (Coq8-*AS*) that could be acutely inhibited by halomethyl ketone inhibitors. Using differential scanning fluorimetry, we demonstrated a highly specific interaction between Coq8-*AS* and our inhibitor 3-MB-PPI *in vitro.* Next, we showed Coq8-*AS* can fully rescue Δ*coq8* yeast, suggesting intact protein function. Then, we showed that yeast expressing Coq8-*AS*, not WT, were inhibited by 3-MB-PPI, suggesting protein-specific inhibition *in vivo*. To understand how CoQ biosynthesis is impacted during acute Coq8-*AS* inhibition, *de novo* CoQ production was measured using quantitative mass spectrometry (Joshua Coon laboratory). Inhibition of Coq8-*AS* led to a rapid decrease in heavy CoQ and buildup of early precursor PPHB. Notably, COQ8 represented the first UbiB family kinase, as well as the first mitochondrial protein, to be targeted using the analog-sensitive system. Collectively, this work determined important *in vivo* small-molecule regulators of COQ8 activity and developed the first acute inhibition system for subsequent *in vivo* investigations of COQ8 function and the CoQ biosynthesis pathway. These observations will be fundamentally important for the biochemical exploration of other UbiB family atypical kinases.

UbiB Proteins Regulate CoQ Distribution

CoQ serves as a key membrane-embedded antioxidant throughout the cell, yet how CoQ is mobilized from its site of synthesis on the IMM to other sites of action is unknown. To address this gap in knowledge, we designed a genome-wide screen to identify mitochondrial machinery involved in mobilizing CoQ. Elimination of endogenous genes involved in mitigating oxidative

lipid stress (Δ*gpx1/2/3*) and supplementing media with polyunsaturated fatty acids (PUFAs) required yeast to increase their extramitochondrial CoQ pools in order to survive. After inducing random mutagenesis with ethyl methanesulfonate (EMS), surviving colonies were submitted for next-generation sequencing and the results were filtered for likely deleterious mutations. Our analyses yielded nine mitochondrial hits, of which only one was uncharacterized, Cqd1 (CoQ distribution protein 1, Ypl109c). We validated this hit by reintroducing *CQD1* into the mutant strain (mutC) which restored mutC's PUFA sensitivity. Further, targeted deletion of *CQD1* and subsequent reintroduction into WT yeast recapitulated these results, suggesting that deletion of *CQD1* either increases total CoQ levels or alters cellular CoQ distribution.

We found that deletion of *CQD1* had no effect on total CoQ levels, suggesting subcellular distribution may be altered. To test this, we fractionated cells and found altered CoQ distribution in Δ*cqd1* yeast—decreased CoQ in mitochondria and increased CoQ in the microsomal fraction. To validate this altered CoQ profile, we examined respiratory growth. Indeed, we found Δ*cqd1* yeast were respiratory deficient and growth was restored by supplementing with CoQ, as well as headgroup precursors. Respiratory growth was dependent on conserved kinase motifs as well as UbiB-specific residues, suggesting Cqd1 may possess phosphoryl transfer activity.

Given the similarity between Coq8, Cqd1, and Cqd2 (Ylr253w, Mcp2), we anticipated that Cqd2 might also be connected to CoQ biology. To test this hypothesis, we disrupted *CQD2* and subjected single (Δ*cqd1* or Δ*cqd2*) and double (Δ*cqd1*Δ*cqd2*) knockout strains to the previously employed PUFA-stress and respiratory growth assays. Consistent with a model in which Cqd1 and Cqd2 work in opposition, Δ*cqd2* yeast were sensitized to PUFA stress and had no respiratory growth defects. Interestingly, Δ*cqd1*Δ*cqd2* showed an intermediate phenotype against PUFA stress, and restored Δ*cqd1* respiratory growth, suggesting altered mitochondrial CoQ distribution.

Importantly, these *CQD2* phenotypes were again dependent on conserved residues, suggesting UbiB family proteins in yeast are all active phosphoryl transfer enzymes. Finally, we optimized a method for isolating native nanodiscs to probe IMM CoQ pools directly. Consistent with our previous results and model, IMM CoQ was down in Δ*cqd1*, up in Δ*cqd2*, and unchanged in Δ*cqd1*Δ*cqd2* yeast. Overall, our results reveal new protein machinery central to CoQ trafficking in yeast and lend new insights into the broader interplay between mitochondrial and cellular processes.

Future Directions

COQ8 Function and Mechanism of Action

Through this work, fundamental questions have been addressed about how COQ8 supports CoQ biosynthesis. Our work highlights essential facets of this COQ8 activity, including proximity to the membrane, an intact TM domain, the presence of CL in the membrane, and early CoQ intermediates. Stitching these observations together, we can hypothesize about COQ8's function and how this might happen *in vivo*, but the mechanistic underpinnings of this process remain unclear. Conformational changes in COQ8 during ATP hydrolysis are likely linked to either the extraction of early CoQ intermediates (e.g., PPHB) or assembly of other biosynthetic machinery (complex Q). Extraction of PPHB from the IMM may itself catalyze the assembly of complex Q as a lipid anchor, or this assembly may be driven by a second ATP hydrolysis event. Structural work supporting this idea[9] has only examined the globular domain of COQ8 (truncation of the TM domain), so it is unclear what changes might occur in the TM domain region during hydrolysis. Changes in the enzyme core may be propagated to the TM domain, and these changes might enable

lipid extraction. Changes in the globular domain may also create a favorable protein-protein interaction surface for enzyme recruitment.

To address some of these gaps, full length yeast ($Coq8^{N\Delta41}$) and human ($COQ8A^{N\Delta162}$) proteins should be reexamined using deuterium-exchange mass spectrometry (DXMS) in the presence of liposomes. Determining how the full-length protein behaves on a liposome membrane in response to different phospholipid compositions (CL content), substrates (nucleotides), and activators (CoQ mimics 2-allylphenol and 2-propylphenol) would yield important information about TM-domain flexibility. This experiment could be advanced one step further by making liposomes that contain PPHB, which may drive additional conformational changes that can be detected by DMXS analyses.

COQ8 Activity is Influenced by Small-molecules and its TM Domain

We now recognize specific small-molecule interactions and unique structural elements are important in modulating COQ8 activity. Our work demonstrates that these different layers of regulation are highly conserved from humans to bacteria. However, many unresolved questions remain regarding CoQ intermediate, CL, and TM domain modulation of COQ8 activity. CoQ intermediate binding was first identified in a co-immunoprecipitation (co-IP) experiment where overexpressed yeast Coq8 was purified from bacteria. Although conserved kinase and UbiB-specific residues have been implicated in this binding event, where CoQ intermediates actually binds to COQ8 is unclear. Determining whether these residues are directly involved will be important for understanding how COQ8 functions and how to perturb its activity. Structural investigations in the presence with CoQ analogs and intermediates will be important for achieving this. Chemical[10,11] and biological[12,13] means are available for obtaining bona fide CoQ

intermediates, but new approaches and tools will likely be needed to collect them efficiently, in high purity, and in a soluble state ready for protein incorporation and subsequent structural analyses. Further, important technological and method-based advances have made similar co-IP experiments in yeast and human systems more tractable[14-17]. Unbiased lipidomic and metabolomic analyses of these samples has the potential to reveal additional small-molecule interactions that may not yet be appreciated.

CL is the defining membrane constituent of the mitochondria[18], and it has been shown to enhance both COQ8 liposome binding and ATPase activity *in vitro*. However, how CL impacts COQ8 organization and activity *in vivo* is unknown. CL is a curvature inducing lipid that makes up roughly 20% of the IMM[19], a protein-dense and extensively folded environment that houses large protein complexes important for energy production and mitochondria architecture. CL is required for the assembly of respiratory supercomplexes in yeast and mammals[20-23], influences the binding and stability of MICOS subunits[24-26], as well as the organization and recruitment of DRP1/Dnm1 during mitochondrial fission[27,28]. It is possible that CL plays a similar role in regulating complex Q and CoQ biosynthesis via COQ8 localization and activity modulation. Tuning CL levels in mitochondria could function as a rheostat for COQ8 activity. More intriguingly, CL microenvironments have been proposed in seeding protein complexes, suggesting that spatial organization of IMM lipids may play an important role in organizing COQ8/complex Q and regulation CoQ production. Testing these models *in vivo* will be necessary for determining what extent CL influences COQ8 activity. This may rely on cutting-edge microscopy techniques capable of super-resolution imaging of co-localized mitochondrial CL and COQ8. Impressive work from the Lippincott-Schwartz laboratory has pioneered new microscopic applications[29,30] and demonstrated the ability to track single protein particles across organelle networks over time[31].

Pairing organelle-specific lipid labeling and protein tagging may enable tracking of CL-dependent COQ8 localization/movement within mitochondria Understanding the CL-COQ8 dynamic may inspire new treatments for CoQ deficiency. For example, increasing CL abundance may increase CoQ production via enhanced COQ8 activity. This work is likely to provide new insights into the regulated nature of submitochondrial lipid and protein organization[32].

Similar to COQ8, homologs in yeast and humans all have predicted TM domains. However, important questions regarding the orientation of COQ8's TM domain have yet to be addressed. Examination of endogenous COQ8 from yeast and human cells show that it is a peripherally-associated membrane-protein[33-35]. By itself, the human COQ8A TM domain has been shown to dimerize[36], and this association is driven by the presence of a GAS_{right} motif[37]. Coq8 dimers have also been identified from yeast[35], causing confusion over how COQ8 is oriented *in vivo*. If the COQ8 TM domain is fully inserted, there would be 30-40 N-terminal residues located within the IMS. This segment may form one or more helices that could interact with additional protein machinery for regulatory purposes. If this is true, previous submitochondrial analyses may support the existence of two COQ8 pools—some inserted and some merely membrane-associated. Alternatively, if COQ8 exists as a peripherally-associated protein, it is likely that this domain is partially inserted into the membrane to interact with CoQ intermediates, similar to the amphipathic helix of COQ9[38]. Here, the N-terminal residues would have the ability to interface with matrix proteins, possibly mediating complex Q formation through these interactions. Regardless, it is intriguing to consider the COQ8 TM domain a membrane-associated "sensor," integral to the process of CoQ intermediate extraction and/or complex Q assembly. Targeted mutagenesis of these N-terminal residues and those found in the TM domain are underway, and should shed light on what amino acids and motifs are necessary *in vivo*. To address this in more detail, creating a

COQ8 chimera protein with the COQ9 amphipathic helix would help infer the TM domain function. Alternatively, native nanodiscs containing COQ8 could be isolated for subsequent structural analyses to determine the precise orientation of this protein on a native membrane patch. In addition to these experiments, future studies should focus on determining the existence and functional requirement of COQ8 dimerization *in vivo*, with itself or with other UbiB homologs. Collectively, this knowledge will serve as a foundation for future investigations of regulatory elements that may influence general behavior, activity, or localized of other UbiB homologs.

Recent Advances in Understanding COQ8's Role

Beyond the questions and gaps described above, two collaborative projects involving our lab have used and generated additional chemical tools for COQ8 studies. In collaboration with Jodi Nunnari's laboratory, fluorescence co-localization of submitochondrial compartments in yeast was done to explore how Coq8's activity influences complex Q domain formation and pathway flux[39]. In this study, it was determined that headgroup modifying enzymes (complex Q) formed discrete foci within mitochondria, and certain proteins (Coq8, 1, 2, and 10) were not included. Overexpression and acute inhibition of Coq8-*AS* (tool described in Chapter 2) resulted in a near ablation of domain formation and rapid shut down (30 min) of *de novo* CoQ biosynthesis. These results further support a model where COQ8 lipid interactions are essential for the formation and stability of complex Q. This also represented the first application of our acute inhibition system, paving the way for future COQ8 investigations and discoveries *in vivo*.

In a separate collaboration, a selective and potent inhibitor for endogenous COQ8A was characterized[40], representing the second inhibitor available for the UbiB family. This tool will be extremely valuable in teasing apart COQ8A and COQ8B function *in vivo*, as they are believed to

have similar or redundant functions. Having both chemical and genetic perturbation options available will accelerate future investigations of these two human proteins, in terms of their tissue-specific functions, as well as mechanistic details about their active site architecture and catalytic properties. Overall, this work suggests that UbiB family proteins are amenable to chemical inhibition. Developing similar tools for other UbiB proteins would significantly improve our ability to study these uncharacterized proteins *in vivo*, as *in vitro* biochemistry is not yet accessible.

CoQ Distribution—A New Frontier

Despite knowing that CoQ is localized ubiquitously across the cell for almost 60 years[41], the molecular details of CoQ's mobilization have remained unresolved. Two competing models exist for explaining the widespread distribution of CoQ—means of trafficking or local production must be present. Although evidence exists to support the ladder[42,43], the distribution model is substantially stronger, in part because most CoQ biosynthetic machinery has been localized exclusively to mitochondria across a host of eukaryotic systems. Previous labelling experiments[44] support a model where CoQ is synthesized in mitochondria, makes it way to the ER via connective MAMs, and enters the endomembrane system for widespread cellular distribution. Within this model, several genes have been implicated in the terminal endomembrane system[44-46], which has been suggested to function in both CoQ distribution and uptake. However, no other genes had been connected to CoQ distribution, including steps that occur in mitochondria after its synthesis. Addressing this gap, our work identified yeast Cqd1 and Cqd2, two previously uncharacterized IMM localized UbiB proteins that reciprocally regulate CoQ distribution across the cell. However, it is unclear how exactly these proteins are involved in CoQ distribution and how they function mechanistically. Further, we predict that other protein machinery is required to facilitate CoQ

mobilization from the IMM to the ER, but the identity of these additional factors is currently unknown.

Possible Mechanism of Action for Cqd1 and Cqd2

Cqd1 and Cqd2 only share limited sequence identity with Coq8, but they contain all of the conserved catalytic kinase residues, most UbiB-specific motifs, the large N-terminal extension (KxGQ domain), and a predicted TM domain. Using predictive threading algorithms (iTASSER)[47], homolog models for Cqd1 and Cqd2 reveal that catalytic residues are similarly oriented when compared to COQ8A (PDB: 4PED). Like COQ8, mutating conserved kinase residues and UbiB-specific motifs generally ablates respiratory growth phenotypes, suggesting that Cqd1 and Cqd2 are likely phosphoryl transfer enzymes with similar structural features to COQ8.

Based on these similarities, a few models can be proposed for how Cqd1 and Cqd2 function. It's possible that Cqd1 and Cqd2 function identically to Coq8, as CoQ handling proteins that extract or deposit mature CoQ at the IMM. Lipid binding has not yet been tested for Cqd1 and Cqd2, but it is reasonable to predict one or both proteins bind CoQ (or CoQ intermediates). In the absence of *CQD1*, CoQ is skewed away from mitochondria to extramitochondrial compartments, which could be explained by unregulated Cqd2 extraction from the IMM. Similar to the model where Coq8 presents intermediates to complex Q, we predict that Cqd2 functions in complex with other IMS proteins, potentially a larger complex such as MICOS. Previous work has identified a physical interaction for Cqd2 with Mic60 (MICOS subunit)[48], as well as its human orthologs ADCK1 and 5[14] (Figure 1A-B). MICOS has well-established roles in maintaining mitochondrial cristae structures and lipid homeostasis[49], and has recently been co-localized to ER-mitochondria

contact sites[50], making this an intriguing candidate for further investigations. Targeted analyses will be needed to determine if Cqd proteins can bind CoQ and if other IMS proteins are required for proper CoQ distribution.

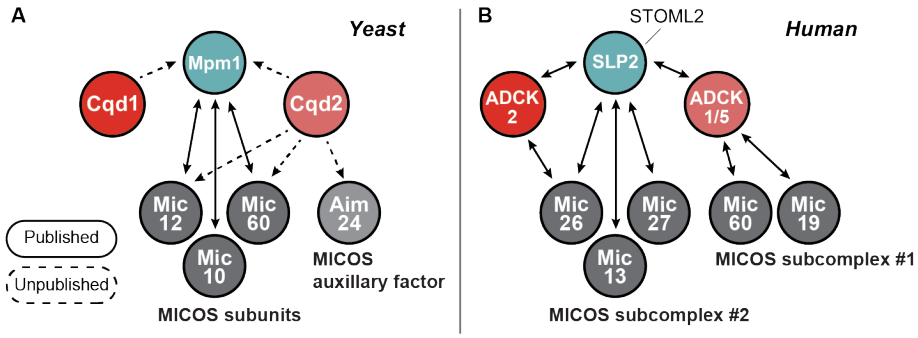

Figure 1. Protein Interaction Network Suggests a Possible Connection to Mpm1, MICOS. Figure was generated using information from the BioGRID database (v4.2.192), as well as unpublished data from our lab and Jared Rutter's Laboratory. **A,** Co-immunoprecipitation data from yeast reveals a strong interaction between Cqd proteins and uncharacterized IMS protein, Mpm1. A network of interactions is also present with various MICOS subunits. **B,** Protein interaction network for human orthologs ADCK1, 2, and 5 also includes MICOS subunits, as well as IMS/IMM protein STOML2 (SLP2).

Notably, unpublished work from our lab and Jared Rutter's Laboratory identified a strong interaction between Cqd proteins and uncharacterized IMS protein Mpm1 (mitochondrial peculiar membrane protein 1) (Figure 1A). Nothing is known about the biological role of Mpm1, but it was initially isolated from the insoluble fraction of a yeast cell lysate using Triton X-100[51], suggesting that Mpm1 is either membrane-associated or tightly associated with membrane-bound proteins. Mpm1 also physically interacts with multiple MICOS subunits[48,52], as well as Mdm10[53], the

mitochondrial subunit of ERMES. Connecting these observations, Mpm1 emerges as a strong candidate to interface with Cqd proteins, MICOS, and potentially ERMES to enable IMM to ER CoQ transfer. Although there is no obvious relationship with Mpm1, STOML2 (SLP-2) is an interesting human protein that appears similarly fitting in terms of its physical interactions and submitochondrial localization (Figure 1B). STOML2 is an IMM/IMS protein that binds CL-rich microdomains in the IMM, stabilizes proteins such as prohibitins, and has been implicated in regulating mitochondrial biogenesis and energetic activity[54]. Further, STOML2 was originally discovered and characterized as an Mfn2 binding partner[55], suggesting a connection to eukaryotic ER-mitochondria crosstalk. Together, this collection of mitochondrial proteins from yeast and humans warrant additional studies to determine if they participate in the CoQ distribution pathway.

Proposing a model for Cqd1 is more difficult because it likely functions in a different way than Cqd2. With the vast majority of CoQ synthesize in the IMM, active CoQ import/insertion seems inefficient for "balancing" Cqd2-driven export. Instead, a model whereby Cqd1 directly or indirectly regulates Cqd2 activity is better supported by our work and other previous observations. A physical interaction between Coq1 and Coq2 has not yet been identified, but each have a strong interaction with Mpm1, potentially representing the functional conduit between these two proteins. As mentioned above, Mpm1 and Cqd2 have extensive interactions with MICOS, so Cqd1 could influence protein-protein interactions via conformational changes during nucleotide hydrolysis.

Interestingly, nucleotide specificity may also influence the activities of Cqd1 and Cqd2. *In vitro* nucleotide binding assays for COQ8 have shown its unique alanine-rich nucleotide binding loop ('AAAS') flips its preference from ATP to ADP. Cdq1 has a more traditional G-rich loop motif GVGS, while Cqd2 has a mixed motif GVAS. Investigating each of these COQ8 residues with A-to-G mutations, it was determined that A339G (underlined) led to an a 6-fold increase in

selectivity for ATP over ADP, while A337G did not flip nucleotide specificity[56] . Based on these results, Cqd1 is predicted to bind ATP, while Cqd2 may prefer to bind ADP, similar to Coq8. This difference in substrate preference has the potential of influencing enzyme activity to regulate CoQ distribution under varying energetic states. This hypothesis will need to be tested and validated using multiple *in vitro* and *in vivo* approaches.

One major caveat that is difficult to explain is why CoQ distribution in the absence of both *cqd* genes (Δ*cqd1*Δ*cqd2*) is similar to WT conditions. If Cqd2 does facilitate CoQ export and Cqd1 functions to tune Cqd2-mediated distribution, mitochondrial CoQ levels in Δ*cqd1*Δ*cqd2* should resemble Δ*cqd2* yeast. One possible explanation is that a redundant CoQ distribution mechanism is activated in the absence of the Cqd1-Cqd2 system. Deletion of these genes could invoke a stress-like response that effectively circumvents this part of the pathway. Alternatively, Cqd1 may in fact facilitate active import of CoQ in the absence of *cqd2*, which is not observed in the Δ*cqd1*Δ*cqd2* strain. If this is true, it would appear that Cqd1 and Cqd2 are likely required to respond to specific stimuli or acute stress. Investigation of temporal changes in CoQ distribution in response to different stress (e.g., PUFA supplementation) will be essential to addressing these possibilities. Revisiting previous proteomic datasets and designing new proteomic experiments that incorporate these stress conditions should provide clues about this pathway.

Definitive validation of this will require recombinant protein purification, *in vitro* biochemistry, and structural analyses. These experiments are not yet accessible due to our inability to purify other UbiB proteins. These proteins have putative TM domains and are closely associated with the membrane, making them highly insoluble targets. Efforts to reconstitute insoluble protein from the pellet using a more extensive panel of detergents may prove useful. Alternatively, Cqd1 and Cqd2 purification may require the isolation of native nanodiscs (SMALPs; SMA lipid

particles), an approach that preserves the native lipid environment to enhance protein stability (Lee 2016). Work described in Chapter 4 pioneered a new method for collecting native nanodiscs containing a GFP-tagged protein (Figure 2A). Importantly, GFP-tagged Cqd1 and Cqd2 protein obtained via this method could still be used in our lipid-compatible activity assays (discussed in Chapter 2). This approach is more low-throughput than standard protein purification, but is still amenable to point mutant analyses. Further, this approach is likely to improve the chances of collecting stable, functional protein by (1) isolating protein from its endogenous environment thus eliminating any predictive/damaging truncations, (2) removing the need for structure/function disrupting chemicals like detergents, and (3) isolating a native patch of membrane to enhance protein stability, especially for integral membrane proteins. Future efforts should be directed at the purification or endogenous collection of Cqd1 and Cqd2 to enable *in vitro* biochemistry and structure elucidation studies (Figure 2B).

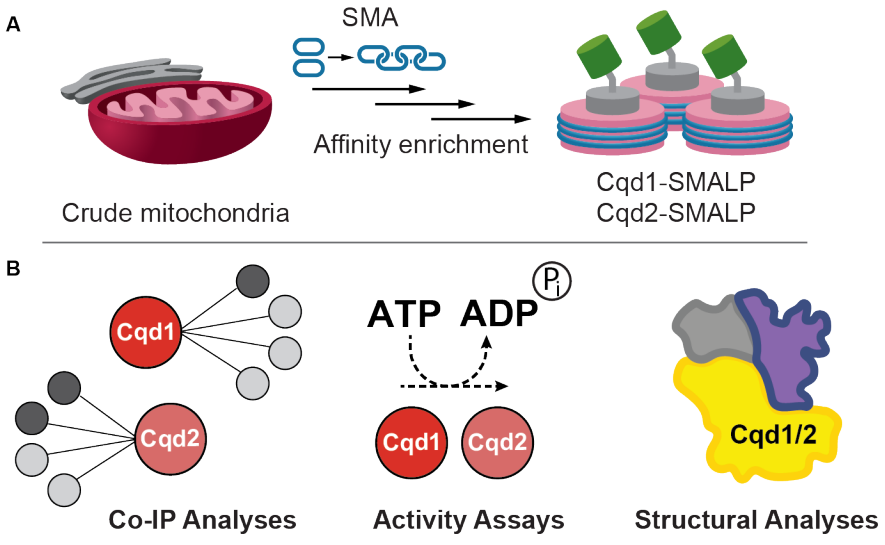

Figure 2. Using Cqd1 and Cqd2 SMALPs for *In Vitro* Biochemistry. A, Native nanodiscs containing endogenously tagged or overexpressed Cqd1/2-GFP can be isolated using methods

described in Chapter 4. **B,** Isolated protein can be used to determine co-purifying proteins and lipids, ATPase activity in the presence of different small-molecules, and structural information.

Other Machinery that might be Involved

We predict that other protein machinery is required to facilitate CoQ mobilization from the IMM to the ER, including Mpm1, MICOS, and ERMES. However, there could be additional machinery involved that cannot be anticipated. Importantly, our screen has identified 8 other candidate mitochondrial genes that require targeted validation. One of these genes, *FAA1*, is a long chain-fatty acyl-CoA synthetase that was previously identified in mitochondria[57], but have since been localized to ER and lipid droplets[58,59]. Previous work showed that the altered lipid profile of Δ*faa1*Δ*faa4* yeast can be rescued by a number of human ACSL proteins, including ACSL4[60]. ACSL4 is a key driver in ferroptosis, and deletion of this gene prevents cells from accumulating oxidative lipid stress[61]. Based on this, it may follow that deletion of *FAA1* is protective during PUFA supplementation. *NDE2*, another intriguing hit, is a NADH dehydrogenase that is capable of converting oxidized CoQ to the reduced form[62]. Although no yeast homolog has yet been identified, Nde2 (and Nde1) are candidate orthologs of human FSP1, the plasma membrane oxidoreductase involved in preventing ferroptosis[63,64].

In addition to the mitochondrial hits, there are 90 extramitochondrial genes that were identified that we did not explore. These hits are localized to a wide range of organelles and may function in organelle-specific import or handling of CoQ. These may also represent hits involved in dampening cellular lipid stress toxicity that would be beneficial for survival. Although ferroptosis has not been described in yeast, they appear to possess the necessary machinery to

combat such cellular assaults. Targeted validation and future investigations of genes identified from our screen will likely be fruitful for understanding how cells combat acute lipid toxicity.

Further, it should be noted that our screen was designed to identify suppressor mutations that release excessive amounts of CoQ to enable survival. This effectively identifies genes that retain CoQ in mitochondria. An exciting prospect will be exploring the opposite pathway direction by designing a screen for genes tasked with moving CoQ out of mitochondria. Using a parental strain with disrupted CoQ production (e.g., Coq2 activity impaired mutant[65]), respiratory growth could be save by the deletion of CoQ mobilization genes. In this hypothetical screen, you would expect to find *CQD2*, as well as some of the predicted proteins described above (*MPM1*, *MICOS* and *ERMES* subunits). The challenge in designing this screen would be tuning CoQ levels such that the parental strain has sufficiently low CoQ levels to impair respiratory growth, and deletions rescue well enough to be identified. Alternatively, Δ*gpx1/2/3* yeast could be treated with a mitochondria-specific or genome-wide CRISPRa (CRISPR activation) library to determine what overexpressed genes improve cell survival in the presence of PUFA, identifying genes that enhance CoQ export from mitochondria. Collectively, our work outlines important next steps for identifying additional machinery required for cellular CoQ distribution.

Cqd1 and Cqd2 Orthologs in Human Disease

In humans, five UbiB proteins have been identified, ADCK1-5[66]. While COQ8A (ADCK3) and COQ8B (ADCK4) have established roles in CoQ biosynthesis and human disease[9,67,68], the biological roles of other ADCK proteins remain elusive. Genome-wide knockdown studies have implicated these uncharacterized *ADCK* genes in several cancer disease states[69-72]. As novel targets for human disease intervention, it will be vital to determine if functional conservation exists

between Cqd1 and Cqd2 and their putative human orthologs, ADCK2 and ADCK1 and 5 respectively (Figure 3A). A recent attempt to measure plasma membrane CoQ in CRISPR-mediated *ADCK2* knockdown cells was unsuccessful (unpublished data) (Figure 3B). However, using H460 (human lung cancer) cells[63], we have seen *ADCK*-dependent changes in cell survival during co-treatment with RSL3 and iFSP1 (induction of ferroptosis), but attempts to replicate the data have failed (unpublished data) (Figure 3B). It is possible that our system is not sensitized sufficiently, or the difference between strains/conditions is not large enough to detect. Alternatively, these proteins—in yeast and/or humans—may influence lipid transport and homeostasis more broadly, beyond CoQ. Determining functional conservation in humans should be a main priority for this project moving forward. UbiB proteins appear to be promising druggable targets, demonstrated by recent work employing small-molecule inhibitors against COQ8[8,40]. Therefore, having a better understanding of ADCK1, 2, and 5's biological function will assist in chemically targeting these proteins in human disease.

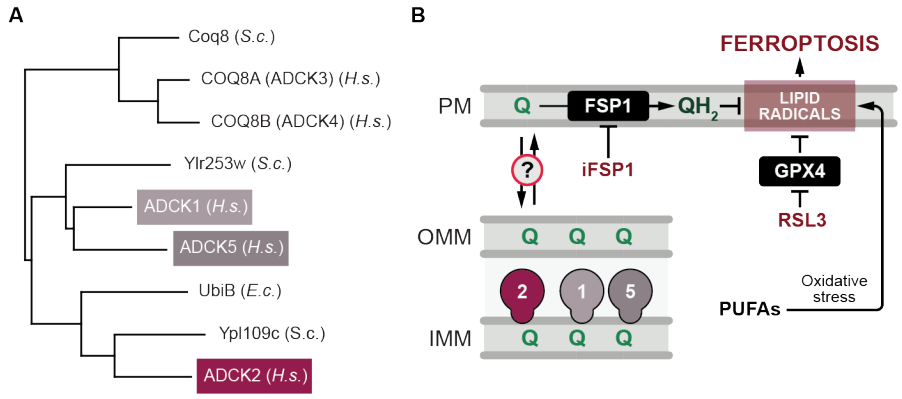

Figure 3. Human Orthologs and Determining Functional Conservation. A, Phylogenetic tree of UbiB family proteins from humans, yeast, and bacteria. Highlighted in colored boxes are the putative human orthologs of Cqd1 (ADCK2) and Cqd2 (ADCK1 and 5). **B,** To test for functional

conservation in these human orthologs, we performed knockdown studies of ADCK genes and attempted to monitor changes in CoQ at the plasma membrane, both directly via fractionation experiments and indirectly via a ferroptosis-dependent cell viability assay. These experiments were inconclusive, but warrant a deeper investigation.

Tool Development

Other UbiB proteins have been recalcitrant to recombinant purification efforts, so new tools and approaches will be needed to effectively investigate CoQ distribution. Clever screens, refined purification schemes, and improved approaches for defining *in vivo* interactions will all be useful in defining UbiB protein function. However, development of new tools will likely be necessary to fully understand and appreciate the endogenous organization and regulation of CoQ distribution. Specifically, the ability to track endogenous CoQ, either visually or enzymatically, would enhance our ongoing investigation immensely.

Recent innovations in synthetic chemistry have provided new chemical approaches for labeling a variety of lipids *in vivo*[73]. Bifunctional lipids, or clickable and photoactivatable lipid analogues, are emerging as key chemical tools that enable global profiling of lipid-protein interactions, as well as lipid tracking. Paired with advancing microscopic platforms, it is possible to track lipid species in particular parts of the cell in real-time. One major hurdle is designing a fluorescent lipid probe without perturbing its endogenous function. Fluorescent tags are often large and bulky moieties can displace a lipid or disrupt endogenous interactions. For some lipids, such as cholesterol and sphingolipids, fluorescent probes exist that are tolerable[73]. However, this has been more challenging for CoQ since it exists within the lipid bilayer and its quinone moiety is

essential for is function, likely through protein interfacing. Application of a smaller, hydrophobic probe to the prenyl tail may be the most promising approach in this regard.

An alternative approach that is gaining traction is Raman scattering microscopy (Coherent anti-strokes and stimulated; CARS and SRS)[74]. These are non-invasive approaches that selectively image the vibration pattern of endogenous chemical groups, enabling high-resolution and three-dimensional imaging of these *in vivo* molecules[75]. In 2008, SRS was used to track retinoic acid (RA) penetration of mouse epidermis[76], and RA is structurally similar to CoQ. Intriguingly, RA was tracked via the conjugated C=C bonds in its di-prenyl tail, suggesting that the polyprenyl tail of CoQ may have a unique Raman signature that can also be tracked *in vivo*. With improved instrumental advances, CARS and SRS are now amenable for high-throughput screening in transparent biological samples, such as human tissue culture and worms[77]. These approaches support long-term sample analyses due to the absence of photobleaching[78], but can be paired with traditional fluorescent analyses if needed[79]. Overall, Raman scattering microscopy is a promising option for visualizing endogenous CoQ that should be explored for future studies.

Finally, having an enzymatic or functional CoQ "sensor" would also be useful, potentially for organelle-specific investigations. Several proteins have been shown to bind CoQ to perform their endogenous function, such as mitochondrial DHODH (dihydroorotate dehydrogenase)[3]. Due to mitochondrial permeability of both substrate and product, DHODH can be localized to other organelle surfaces across the cell without impacting cell viability. As such, DHODH could function as a CoQ-sensor at different organelles (e.g., ER, Golgi) by reading out DHODH activity from those specific compartments. This may require extensive cell fractionation and there might be concerns about indirect effects from altered nucleotide biosynthesis. Another option is the bacterial ArcA/ArcB two component signaling system, which senses quinone redox state via

autophosphorylation[80]. Preliminary exploration of these two ideas are ongoing in our lab. Beyond an engineered CoQ sensor, identification of extramitochondrial phenotypes would also be useful to incorporate into our studies. Recent work has shown that changes in lysosomal CoQ distribution results in altered organelle pH[81], which could be leveraged as an extramitochondrial readout under certain conditions. The creation of new tools and approaches for studying CoQ endogenously are needed to explore important facets of CoQ distribution, such as its spatial and temporal regulation across the cell. Collectively, our work suggests that UbiB family proteins may function generally to manage quinone biology, an exciting new frontier where scientific discoveries and technological innovation will likely progress in parallel.

References

1. Hatefi, Y., Haavik, A.G., Fowler, L.R. & Griffiths, D.E. Studies on the electron transfer system. XLII. Reconstitution of the electron transfer system. *J Biol Chem* **237**, 2661-9 (1962).

2. Frerman, F.E. Acyl-CoA dehydrogenases, electron transfer flavoprotein and electron transfer flavoprotein dehydrogenase. *Biochem Soc Trans* **16**, 416-8 (1988).

3. Jones, M.E. Pyrimidine nucleotide biosynthesis in animals: genes, enzymes, and regulation of UMP biosynthesis. *Annu Rev Biochem* **49**, 253-79 (1980).

4. Bentinger, M., Brismar, K. & Dallner, G. The antioxidant role of coenzyme Q. *Mitochondrion* **7 Suppl**, S41-50 (2007).

5. Stefely, J.A. & Pagliarini, D.J. Biochemistry of Mitochondrial Coenzyme Q Biosynthesis. *Trends Biochem Sci* **42**, 824-843 (2017).

6. Leonard, C.J., Aravind, L. & Koonin, E.V. Novel families of putative protein kinases in bacteria and archaea: evolution of the "eukaryotic" protein kinase superfamily. *Genome Res* **8**, 1038-47 (1998).

7. Kannan, N., Taylor, S.S., Zhai, Y., Venter, J.C. & Manning, G. Structural and functional diversity of the microbial kinome. *PLoS Biol* **5**, e17 (2007).

8. Reidenbach, A.G. et al. Conserved Lipid and Small-Molecule Modulation of COQ8 Reveals Regulation of the Ancient Kinase-like UbiB Family. *Cell Chem Biol* **25**, 154-165 e11 (2018).

9. Stefely, J.A. et al. Cerebellar Ataxia and Coenzyme Q Deficiency through Loss of Unorthodox Kinase Activity. *Mol Cell* **63**, 608-20 (2016).

10. Barkovich, R.J. et al. Characterization of the COQ5 gene from Saccharomyces cerevisiae. Evidence for a C-methyltransferase in ubiquinone biosynthesis. *J Biol Chem* **272**, 9182-8 (1997).

11. Lu, T.T., Lee, S.J., Apfel, U.P. & Lippard, S.J. Aging-associated enzyme human clock-1: substrate-mediated reduction of the diiron center for 5-demethoxyubiquinone hydroxylation. *Biochemistry* **52**, 2236-44 (2013).

12. Aussel, L. et al. Biosynthesis and physiology of coenzyme Q in bacteria. *Biochim Biophys Acta* **1837**, 1004-11 (2014).

13. Xie, L.X. et al. Overexpression of the Coq8 kinase in Saccharomyces cerevisiae coq null mutants allows for accumulation of diagnostic intermediates of the coenzyme Q6 biosynthetic pathway. *J Biol Chem* **287**, 23571-81 (2012).

14. Floyd, B.J. et al. Mitochondrial Protein Interaction Mapping Identifies Regulators of Respiratory Chain Function. *Mol Cell* **63**, 621-32 (2016).

15. Lee, S.C. et al. A method for detergent-free isolation of membrane proteins in their local lipid environment. *Nat Protoc* **11**, 1149-62 (2016).

16. Gupta, K. et al. The role of interfacial lipids in stabilizing membrane protein oligomers. *Nature* **541**, 421-424 (2017).

17. Chen, W.W., Freinkman, E., Wang, T., Birsoy, K. & Sabatini, D.M. Absolute Quantification of Matrix Metabolites Reveals the Dynamics of Mitochondrial Metabolism. *Cell* **166**, 1324-1337 e11 (2016).

18. Ren, M., Phoon, C.K. & Schlame, M. Metabolism and function of mitochondrial cardiolipin. *Prog Lipid Res* **55**, 1-16 (2014).

19. Horvath, S.E. & Daum, G. Lipids of mitochondria. *Prog Lipid Res* **52**, 590-614 (2013).

20. Althoff, T., Mills, D.J., Popot, J.L. & Kuhlbrandt, W. Arrangement of electron transport chain components in bovine mitochondrial supercomplex I1III2IV1. *EMBO J* **30**, 4652-64 (2011).

21. Pfeiffer, K. et al. Cardiolipin stabilizes respiratory chain supercomplexes. *J Biol Chem* **278**, 52873-80 (2003).

22. Schagger, H. & Pfeiffer, K. The ratio of oxidative phosphorylation complexes I-V in bovine heart mitochondria and the composition of respiratory chain supercomplexes. *J Biol Chem* **276**, 37861-7 (2001).

23. Zhang, M., Mileykovskaya, E. & Dowhan, W. Gluing the respiratory chain together. Cardiolipin is required for supercomplex formation in the inner mitochondrial membrane. *J Biol Chem* **277**, 43553-6 (2002).

24. Friedman, J.R., Mourier, A., Yamada, J., McCaffery, J.M. & Nunnari, J. MICOS coordinates with respiratory complexes and lipids to establish mitochondrial inner membrane architecture. *Elife* **4**(2015).

25. Rampelt, H. et al. Assembly of the Mitochondrial Cristae Organizer Mic10 Is Regulated by Mic26-Mic27 Antagonism and Cardiolipin. *J Mol Biol* **430**, 1883-1890 (2018).

26. Weber, T.A. et al. APOOL is a cardiolipin-binding constituent of the Mitofilin/MINOS protein complex determining cristae morphology in mammalian mitochondria. *PLoS One* **8**, e63683 (2013).

27. Macdonald, P.J. et al. A dimeric equilibrium intermediate nucleates Drp1 reassembly on mitochondrial membranes for fission. *Mol Biol Cell* **25**, 1905-15 (2014).

28. Montessuit, S. et al. Membrane remodeling induced by the dynamin-related protein Drp1 stimulates Bax oligomerization. *Cell* **142**, 889-901 (2010).

29. Guo, Y. et al. Visualizing Intracellular Organelle and Cytoskeletal Interactions at Nanoscale Resolution on Millisecond Timescales. *Cell* **175**, 1430-1442 e17 (2018).

30. Hoffman, D.P. et al. Correlative three-dimensional super-resolution and block-face electron microscopy of whole vitreously frozen cells. *Science* **367**(2020).

31. Omari, S. et al. Mechanisms of procollagen and HSP47 sorting during ER-to-Golgi trafficking. *Matrix Biol* **93**, 79-94 (2020).

32. Acoba, M.G., Senoo, N. & Claypool, S.M. Phospholipid ebb and flow makes mitochondria go. *J Cell Biol* **219**(2020).

33. Cullen, J.K. et al. AarF Domain Containing Kinase 3 (ADCK3) Mutant Cells Display Signs of Oxidative Stress, Defects in Mitochondrial Homeostasis and Lysosomal Accumulation. *PLoS One* **11**, e0148213 (2016).

34. He, C.H., Xie, L.X., Allan, C.M., Tran, U.C. & Clarke, C.F. Coenzyme Q supplementation or over-expression of the yeast Coq8 putative kinase stabilizes multi-subunit Coq polypeptide complexes in yeast coq null mutants. *Biochim Biophys Acta* **1841**, 630-44 (2014).

35. Tauche, A., Krause-Buchholz, U. & Rodel, G. Ubiquinone biosynthesis in Saccharomyces cerevisiae: the molecular organization of O-methylase Coq3p depends on Abc1p/Coq8p. *FEMS Yeast Res* **8**, 1263-75 (2008).

36. Khadria, A.S. et al. A Gly-zipper motif mediates homodimerization of the transmembrane domain of the mitochondrial kinase ADCK3. *J Am Chem Soc* **136**, 14068-77 (2014).

37. Walters, R.F. & DeGrado, W.F. Helix-packing motifs in membrane proteins. *Proc Natl Acad Sci U S A* **103**, 13658-63 (2006).

38. Lohman, D.C. et al. An Isoprene Lipid-Binding Protein Promotes Eukaryotic Coenzyme Q Biosynthesis. *Mol Cell* **73**, 763-774 e10 (2019).

39. Subramanian, K. et al. Coenzyme Q biosynthetic proteins assemble in a substrate-dependent manner into domains at ER-mitochondria contacts. *J Cell Biol* **218**, 1353-1369 (2019).

40. Asquith, C.R.M., Murray, N.H. & Pagliarini, D.J. ADCK3/COQ8A: the choice target of the UbiB protein kinase-like family. *Nat Rev Drug Discov* **18**, 815 (2019).

41. Sastry, P.S., Jayaraman, J. & Ramasarma, T. Distribution of coenzyme Q in rat liver cell fractions. *Nature* **189**, 577 (1961).

42. Kalen, A., Appelkvist, E.L., Chojnacki, T. & Dallner, G. Nonaprenyl-4-hydroxybenzoate transferase, an enzyme involved in ubiquinone biosynthesis, in the endoplasmic reticulum-Golgi system of rat liver. *J Biol Chem* **265**, 1158-64 (1990).

43. Mugoni, V. et al. Ubiad1 is an antioxidant enzyme that regulates eNOS activity by CoQ10 synthesis. *Cell* **152**, 504-18 (2013).

44. Fernandez-Ayala, D.J., Brea-Calvo, G., Lopez-Lluch, G. & Navas, P. Coenzyme Q distribution in HL-60 human cells depends on the endomembrane system. *Biochim Biophys Acta* **1713**, 129-37 (2005).

45. Padilla-Lopez, S. et al. Genetic evidence for the requirement of the endocytic pathway in the uptake of coenzyme Q6 in Saccharomyces cerevisiae. *Biochim Biophys Acta* **1788**, 1238-48 (2009).

46. Fernandez-Del-Rio, L. et al. Genes and lipids that impact uptake and assimilation of exogenous coenzyme Q in Saccharomyces cerevisiae. *Free Radic Biol Med* **154**, 105-118 (2020).

47. Yang, J. et al. The I-TASSER Suite: protein structure and function prediction. *Nat Methods* **12**, 7-8 (2015).

48. von der Malsburg, K. et al. Dual role of mitofilin in mitochondrial membrane organization and protein biogenesis. *Dev Cell* **21**, 694-707 (2011).

49. Rampelt, H., Zerbes, R.M., van der Laan, M. & Pfanner, N. Role of the mitochondrial contact site and cristae organizing system in membrane architecture and dynamics. *Biochim Biophys Acta Mol Cell Res* **1864**, 737-746 (2017).

50. Tirrell, P.S., Nguyen, K.N., Luby-Phelps, K. & Friedman, J.R. MICOS subcomplexes assemble independently on the mitochondrial inner membrane in proximity to ER contact sites. *J Cell Biol* **219**(2020).

51. Inadome, H., Noda, Y., Adachi, H. & Yoda, K. A novel protein, Mpm1, of the mitochondria of the yeast Saccharomyces cerevisiae. *Biosci Biotechnol Biochem* **65**, 2577-80 (2001).

52. Hoppins, S. et al. A mitochondrial-focused genetic interaction map reveals a scaffold-like complex required for inner membrane organization in mitochondria. *J Cell Biol* **195**, 323-40 (2011).

53. Gavin, A.C. et al. Functional organization of the yeast proteome by systematic analysis of protein complexes. *Nature* **415**, 141-7 (2002).

54. Christie, D.A. et al. Stomatin-like protein 2 binds cardiolipin and regulates mitochondrial biogenesis and function. *Mol Cell Biol* **31**, 3845-56 (2011).

55. Hajek, P., Chomyn, A. & Attardi, G. Identification of a novel mitochondrial complex containing mitofusin 2 and stomatin-like protein 2. *J Biol Chem* **282**, 5670-81 (2007).

56. Stefely, J.A. et al. Mitochondrial ADCK3 employs an atypical protein kinase-like fold to enable coenzyme Q biosynthesis. *Mol Cell* **57**, 83-94 (2015).

57. Zahedi, R.P. et al. Proteomic analysis of the yeast mitochondrial outer membrane reveals accumulation of a subclass of preproteins. *Mol Biol Cell* **17**, 1436-50 (2006).

58. Natter, K. et al. The spatial organization of lipid synthesis in the yeast Saccharomyces cerevisiae derived from large scale green fluorescent protein tagging and high resolution microscopy. *Mol Cell Proteomics* **4**, 662-72 (2005).

59. Hariri, H. et al. Lipid droplet biogenesis is spatially coordinated at ER-vacuole contacts under nutritional stress. *EMBO Rep* **19**, 57-72 (2018).

60. Nakahara, K. et al. The Sjogren-Larsson syndrome gene encodes a hexadecenal dehydrogenase of the sphingosine 1-phosphate degradation pathway. *Mol Cell* **46**, 461-71 (2012).

61. Doll, S. et al. ACSL4 dictates ferroptosis sensitivity by shaping cellular lipid composition. *Nat Chem Biol* **13**, 91-98 (2017).

62. Overkamp, K.M. et al. In vivo analysis of the mechanisms for oxidation of cytosolic NADH by Saccharomyces cerevisiae mitochondria. *J Bacteriol* **182**, 2823-30 (2000).

63. Bersuker, K. et al. The CoQ oxidoreductase FSP1 acts parallel to GPX4 to inhibit ferroptosis. *Nature* **575**, 688-692 (2019).

64. Doll, S. et al. FSP1 is a glutathione-independent ferroptosis suppressor. *Nature* **575**, 693-698 (2019).

65. Desbats, M.A. et al. The COQ2 genotype predicts the severity of coenzyme Q10 deficiency. *Hum Mol Genet* **25**, 4256-4265 (2016).

66. Manning, G., Whyte, D.B., Martinez, R., Hunter, T. & Sudarsanam, S. The protein kinase complement of the human genome. *Science* **298**, 1912-34 (2002).

67. Lagier-Tourenne, C. et al. ADCK3, an ancestral kinase, is mutated in a form of recessive ataxia associated with coenzyme Q10 deficiency. *Am J Hum Genet* **82**, 661-72 (2008).

68. Ashraf, S. et al. ADCK4 mutations promote steroid-resistant nephrotic syndrome through CoQ10 biosynthesis disruption. *J Clin Invest* **123**, 5179-89 (2013).

69. Wiedemeyer, W.R. et al. Pattern of retinoblastoma pathway inactivation dictates response to CDK4/6 inhibition in GBM. *Proc Natl Acad Sci U S A* **107**, 11501-6 (2010).

70. Brough, R. et al. Functional viability profiles of breast cancer. *Cancer Discov* **1**, 260-73 (2011).

71. Simpson, K.J. et al. Identification of genes that regulate epithelial cell migration using an siRNA screening approach. *Nat Cell Biol* **10**, 1027-38 (2008).

72. Qiu, M. et al. aarF domain containing kinase 5 gene promotes invasion and migration of lung cancer cells through ADCK5-SOX9-PTTG1 pathway. *Exp Cell Res* **392**, 112002 (2020).

73. Haberkant, P. & Holthuis, J.C. Fat & fabulous: bifunctional lipids in the spotlight. *Biochim Biophys Acta* **1841**, 1022-30 (2014).

74. Hu, F., Shi, L. & Min, W. Biological imaging of chemical bonds by stimulated Raman scattering microscopy. *Nat Methods* **16**, 830-842 (2019).

75. Yu, Y., Ramachandran, P.V. & Wang, M.C. Shedding new light on lipid functions with CARS and SRS microscopy. *Biochim Biophys Acta* **1841**, 1120-9 (2014).

76. Freudiger, C.W. et al. Label-free biomedical imaging with high sensitivity by stimulated Raman scattering microscopy. *Science* **322**, 1857-61 (2008).

77. Wang, M.C., Min, W., Freudiger, C.W., Ruvkun, G. & Xie, X.S. RNAi screening for fat regulatory genes with SRS microscopy. *Nat Methods* **8**, 135-8 (2011).

78. Evans, C.L. et al. Chemical imaging of tissue in vivo with video-rate coherent anti-Stokes Raman scattering microscopy. *Proc Natl Acad Sci U S A* **102**, 16807-12 (2005).

79. Nan, X., Potma, E.O. & Xie, X.S. Nonperturbative chemical imaging of organelle transport in living cells with coherent anti-stokes Raman scattering microscopy. *Biophys J* **91**, 728-35 (2006).

80. Georgellis, D., Kwon, O. & Lin, E.C. Quinones as the redox signal for the arc two-component system of bacteria. *Science* **292**, 2314-6 (2001).

81. Heaton, R.A., Heales, S., Rahman, K., Sexton, D.W. & Hargreaves, I. The Effect of Cellular Coenzyme Q10 Deficiency on Lysosomal Acidification. *J Clin Med* **9**(2020).